# BIOPHYSICAL MODELS AS TOOLS TO IMPROVE UNDERSTANDING OF ENDOTHERM RESPONSES TO ENVIRONMENTAL CHANGE

By

Paul D. Mathewson

A dissertation submitted in partial fulfillment of

the requirements for the degree of

Doctor of Philosophy

(Zoology)

At the

UNIVERSITY OF WISCONSIN-MADISON

2018

Date of final oral examination: 12/12/2018

The dissertation is approved by the following member of the Final Oral Committee:

Warren P. Porter, Professor, Integrative Biology
Ellen I. Damschen, Associate Professor, Integrative Biology
William H. Karasov, Professor, Forest & Wildlife Ecology
Jonathan N. Pauli, Associate Professor, Forest & Wildlife Ecology
Benjamin Zuckerberg, Associate Professor, Forest & Wildlife Ecology

# TABLE OF CONTENTS

ABSTRACT

A fundamental challenge for animal survival is the maintenance of a positive energy balance. Important threats facing wildlife including climate change, habitat transformation, and pollution can alter an animal's thermal relationship with its surroundings, affecting its ability to maintain its energetic balance. I explore how using bioenergetics models, which provide insight into the thermal consequences of the interaction between a species' functional traits and its surrounding environment, can be valuable tools for endotherm conservation and management. Specifically, I focus on endotherms because modeling for endotherms has lagged behind that for ectotherms due to the less direct relationship between environmental conditions and animal performance for endotherms. First, I use the bioenergetics model Niche Mapper™ to illustrate a generic approach to incorporate more mechanism into species distribution modeling in order to provide insight into responses to climate change. I compare predictions from species distribution models that are informed by correlations with macroclimate variables ("correlative models") to models that are informed by species-specific outputs related to thermal stress from Niche Mapper ("hybrid models") for two species, the American pika (*Ochotona princeps*) and the vervet monkey (*Chlorocebus pygerythrus*). The two models performed similarly under current climate conditions but produced divergent predictions when applied to other conditions. The hybrid model predicted more suitable climate space remaining in the future and there is evidence that the hybrid model may more accurately capture the species' ability to tolerate warming temperatures. Second, I present a novel use of Niche Mapper: estimating thermoregulatory impacts of oiling, using data from Double-crested Cormorants (*Phalacrocorax auritus*) experimentally exposed to oil. Niche Mapper accurately predicted surface temperatures and metabolic rates for unoiled and oiled cormorants and predicted increased daily energetic

demands due to increased thermoregulatory costs of oiling, consistent with observed increased food consumption by oiled cormorants. I show that Niche Mapper can provide insight into sublethal oiling effects by quantifying the extent to which thermoregulatory costs divert energy resources away from important life processes like reproduction and migration. These applications illustrate how bioenergetics models can provide valuable predictions about how animals might respond to a world being rapidly altered by human activities.

ACKNOWLEDGEMENTS

I would like to thank my advisor, Warren Porter, for his guidance, encouragement and enthusiasm throughout this work, as well as the entire Porter lab, particularly Megan Fitzpatrick, with whom many hours were spent debugging program code. Thanks to my graduate committee—Warren, Ellen, Bill, Jon and Ben—for insightful suggestions and constructive critiques. Many thanks to all collaborators listed in individual chapters; in particular, Erik Beever, Richard McFarland, Brian Dorr and Katie Hanson-Dorr for sharing real world animal data against which to test Niche Mapper predictions. Thanks to Lee Attix for my first "real world" experience as a biologist and two memorable seasons working with loons. A very special thanks to all family and friends whose support, encouragement, and inspiration helped me to complete this, in particular Mom and Dad for encouraging a fascination with the natural world as far back as I can remember. To Steph, I promise to make up for the nights and weekends spent writing this dissertation; to Evie and Clara, I promise to make up for the lost play time.

# GENERAL INTRODUCTION

The objective of this dissertation is to explore how biophysical models, which provide insight into the thermal consequences of the interaction between a species' functional traits and its surrounding environment, can be valuable tools for endotherm conservation and management. Some of the most important threats currently facing wildlife, including climate change, habitat conversion, and pollution, can alter an animal's thermal relationship with its surroundings. Better understanding of the consequences of the thermal stresses resulting from these threats can enable more informed efforts to protect and manage animals in a world being rapidly altered by human activities.

This introduction surveys the current literature to provide context and a rationale for the dissertation chapters. It explores the advantages and drawbacks of different approaches to modeling species' responses to environmental change and identifies the need for more mechanistic modeling for endotherms in particular. It introduces and explains in brief detail the biophysical model, Niche Mapper™, that was substantially modified to improve generality and range of applicability as part of this dissertation. Finally, there is a brief synopsis of the three chapters each focused on a different endothermic species—two mammals and a bird—that illustrate the accuracy, broad applicability, and value of using Niche Mapper.

## *Background and Rationale*

Recent human influence on the planet has been so pervasive and profound as to justify the demarcation of a new geological epoch, the Anthropocene (Waters et al. 2016). One characteristic of the Anthropocene is an accelerated rate of species extinctions well above background rates (Ceballos et al. 2015). Some of the most important threats currently facing wildlife (climate change, habitat conversion, pollution) can change an animal's thermal relationship with the environment. Climate change, poised to join habitat loss and

overexploitation as a leading cause of extinction in the next century (Pacifici et al. 2015), clearly alters the environmental temperatures an animal experiences. Even species with the ability to shift distributions will likely experience higher mean environmental temperatures because range-shifts lag behind climate change (Mason et al. 2017). Habitat conversion can result in the partial or complete loss of shade that might provide important thermal refugia for species (Kearney 2013). In marine environments, exposure to oil pollution reduces plumage or pelage insulation, causing increased heat loss and, in some circumstances, hypothermia (Jenssen 1994). To effectively manage species in this rapidly changing world, it is necessary to be able to predict how species will be affected by these changes (Cahill et al. 2011, Guisan et al. 2013, Urban et al. 2016, Engler et al. 2017, Bonebrake et al. 2018). In particular, it is important to understand the fitness consequences of environmental changes from a physiological perspective (Fuller et al. 2010, Cooke et al. 2013, Mitchell et al. 2018).

Ectotherm body temperature is closely related to environmental temperatures, creating a strong relationship between animal performance and ambient temperatures (Buckley et al. 2012). Due to their ability to generate heat, endotherms typically maintain body temperatures within an elevated, relatively narrow range regardless of environmental temperatures. This allows endotherms to decouple, to some extent, performance from environmental conditions (Boyles et al. 2013), allowing more flexibility in terms of inhabiting different environments. However, endotherms do not operate completely independently from environmental conditions, because there are costs to maintaining homeothermy (Angilletta et al. 2010, Fuller et al. 2016, Levesque et al. 2016). Endotherms facing heat stress may expend water to dissipate heat through sweating or panting, avoid heat by using thermal refugia that may be less desirable in terms of food availability or predation risk, or be forced to reduce activity (Speakman & Krol 2010, Huey et al.

2012, Mason et al. 2017). Conversely, endotherms facing cold stress may increase activity, shiver, or metabolize fat stores to produce body heat sufficient to maintain their temperature (Kearney & Porter 2009, Huey et al. 2012).

These thermoregulatory mechanisms require time and resources that could otherwise be used for growth and reproduction, thus imposing limits on environmental conditions that can sustain populations (Buckley et al., 2012; du Plessis et al., 2012; Oswald & Arnold, 2012, Fuller et al. 2016). For example, researchers have documented that high temperatures were associated with reduced hunting and reduced reproductive success in African wild dogs (*Lycaon pictus*), making the species vulnerable to climate change (Woodroffe et al. 2017). The researchers proposed that the reduced hunting limited food intake, leaving less energy available for producing offspring. Similarly, there are negative fitness consequences for not defending an optimal body temperature as cellular efficiency is reduced as body temperatures deviate from optimal (Seebacher & Little 2017). For examples, wild rabbits with higher 24-hour amplitude in body temperature were found to have lower reproductive success (Maloney et al. 2018). It is thought that distributions are determined by these sorts of sublethal impacts of thermal stress on performance rather than physiological thresholds for direct temperature-related mortality (Buckley et al. 2012, Evans et al. 2015), making it important to be able to predict consequences of thermal stress.

The most common way researchers currently model and predict the environmental conditions suitable for a species is by statistically relating species occurrence information with locations with environmental predictors, typically climate and land cover data (Elith & Leathwick 2009, Guisan et al. 2013, Pacifici et al. 2015, Cabral et al. 2017). The resulting *n*-dimensional space that represents the range of environmental conditions at known presence

locations is considered the animal's bioclimatic "envelope." These envelopes are then projected onto different climate scenarios (e.g., Thomas et al. 2004, Hijmans & Graham 2006) to predict changes in distribution that might occur with changing climatic factors. This so-called correlative approach is widely used due to its relative ease and speed of use, low input data needs, and availability of modeling packages (Kearney & Porter 2009, Dormann et al. 2012, Peterson et al. 2015, Smit et al. 2016). Gridded climate and landcover datasets are increasingly available, as are databases of species occurrences, allowing the creation of a correlative species distribution model in a matter of hours. Furthermore, correlations implicitly capture a wide range of biotic and abiotic processes that limit species distributions, providing good predictions of a species' realized niche in the climate conditions being modeled (Kearney and Porter 2009, Buckley et al. 2010).

However, correlative models have been criticized for not providing much information about how the predictor variables limit a species' distribution (Dormann et al. 2012, Peterson et al. 2013, Evans et al. 2015, Yuan et al. 2018). For example, the correlation between a range of temperatures and occurrences of a species could reflect one or more of the following: a direct influence on the species (thermal stress experienced by the animal itself), an indirect influence (tolerable range of a critical resource), or simply a statistical relationship with no biological basis (Kearney and Porter 2009). Without knowing the limiting process(es), conservation and climate-adaptation actions are relegated to trial and error (Evans et al. 2015).

Furthermore, because correlative models rely on observed occurrences, these models predict a distribution close to the species' realized niche (Jankowski et al. 2018), a subset of the species' fundamental niche that adds biotic and dispersal restrictions to the abiotic restrictions of the fundamental niche (Peterson et al. 2015). Consequently, correlative models may

underestimate the range of tolerable conditions because they assume that persistence is only possible in areas with conditions similar to those found in the species' currently-observed range (i.e., its realized niche; Fuller et al. 2010, Meineri et al. 2014). Finally, making predictions into novel conditions, such as those that will result from climate change, requires extrapolation from current relationships and assumes that the same relationships persist in the future (Buckley & Kingsolver 2012, Pacifici et al. 2015).

At the other end of the modeling spectrum are mechanistic models, which explicitly model the process(es) thought to limit a species' distribution. Mechanistic approaches model the consequences of interactions between a species' functional traits (morphology, physiology and behavior) and its environment on the species' energetics, development and reproduction (Kearney & Porter 2009, Dormann et al., 2012). For example, a biophysical model uses fundamental principles of heat and mass transfer to model how an animal's morphology, physiology, and behavior interact with its environment in terms of energy, mass, and water balances to affect fitness and performance (Porter & Gates 1969; Kearney & Porter 2009, Porter et al. 2010). Outputs from the energy, mass or water balances can be used to estimate the energy and water costs for an animal in any given environment and to delineate unsuitable habitat. Individuals cannot survive in areas where they would have a long-term negative balance, and reproduction is not possible in areas where the animal has an inadequate positive balance (Kearney & Porter 2009; Kronfeld-Schor & Dayan 2013, Jankowski et al. 2013).

By explicitly modeling the process by which the environment limits a species' distribution, mechanistic models are easier to interpret and provide more information to wildlife managers (Yuan et al. 2018, Zhang et al. 2018). Predicted distributions are also based entirely on where the model predicts the possibility of survival, independent of observed distributions (Natori & Porter

2007, Kearney & Porter 2009, Dormann et al. 2012, Meineri et al., 2015). Predictions for novel environmental conditions do not require extrapolation, so a mechanistic approach is theoretically more reliable when predicting the effects of climate change (Buckley et al. 2010, Evans et al. 2015, Feng & Papeş 2017). When the objective is to estimate future distributions under climate change, it is more appropriate to use a modeling approach that predicts the fundamental niche of the species—as biophysical models do—because that niche informs the species' potential for response (Mitchell et al. 2008, Mitchell et al. 2012, Peterson et al. 2016). Furthermore, by explicitly considering how an animal's functional traits interact with the environment, these models allow exploration of how intraspecific trait variation or behavioral flexibility may help to buffer the effects of environmental change (Buckley 2008, Kolbe et al. 2010, Boyles et al. 2011, Buckley et al. 2015, Beever et al. 2017, Medina et al. 2018).

However, mechanistic models can be data-intensive and may require difficult-to-obtain information, limiting wider use of these models in comparison to correlative models (Kearney & Porter 2009; Dormann *et al.*, 2012; Meineri *et al.*, 2015). For example, to calculate a full energetic budget one needs to know not only the animal's energetic requirements but also the energetic content of its diet in order to compute its requisite foraging and assimilation rates. Such detailed, species-specific parameters sometimes limit broader application of mechanistic models. The large number of data inputs also presents a risk because errors in parameters compound, leading to inaccurate predictions (Buckley et al. 2010). Additionally, accurately predicting distributions requires that the modeled process is actually an important limiting process (Buckley et al. 2010).

Considering their respective strengths and weaknesses, mechanistic and correlative models may best be viewed as complementary modelling approaches, rather than one being

superior to the other (Dormann et al. 2012, Peterson et al. 2015). Given this relationship, there are several ways that combining approaches can address shortcomings of either approach on its own and improve predictions of environmental constraints on species' distributions (e.g., Buckley et al., 2010; Kearney et al., 2010; Dormann et al., 2012; Meineri et al., 2015; Briscoe et al., 2016). First, there is increased confidence in predictions where models from both approaches agree, and comparing differences in model predictions provides a range of potential outcomes (Hijmans & Graham 2006; Kearney et al. 2010). Second, correlative models, with their ability to quickly make predictions for a variety of species and incorporate a wide range of potential limiting processes, can be used to generate hypotheses that can be tested with a mechanistic model. Another possibility is the hybridization of the two approaches by using mechanistic model outputs as inputs to a correlative model (Elith et al., 2010, Dormann et al, 2012). For example, mechanistic models can produce spatial layers representing how macroclimate variables (e.g., temperature) and habitat features (e.g., shade availability) affect a species' energy, food or water requirements or activity time across a heterogeneous landscape (Long et al. 2014, 2016). These mechanistic output layers, which may be more proximate drivers of species persistence than the climate variable itself, can then be used as inputs for a correlative approach, creating a more informative model (Kearney & Porter, 2009; Buckley et al., 2010; Cahill et al., 2013, Urban et al. 2016).

There has been increasing recognition of the need to incorporate more mechanism into modeling how environmental conditions limit a species' distribution (Fuller et al. 2010, Huey et al. 2012, Evans et al. 2015, Urban et al. 2016, Methorst et al. 2017, Hayes et al. 2018). However, mechanistic model modelling has lagged for endothermic species compared to ectotherms (Boyles *et al.*, 2011; Oswald & Arnold, 2012; La Sorte & Jetz, 2013; Methorst et al. 2017). This

is due to the more complex connection between endotherm performance and environmental conditions discussed above, making it more difficult to model endotherm performance as a function of environmental conditions (Buckley et al. 2012). This goal of this dissertation is to demonstrate how a biophysical model can help to fill this gap, providing valuable information to wildlife managers in a rapidly changing world.

*Niche Mapper Introduction*

My dissertation research has been working with Niche Mapper™ (Porter and Mitchell 2006), a mechanistic heat and mass-balance biophysical model developed by my advisor, Warren Porter and colleagues, and summarized below. Specifically, I have worked on the endotherm animal sub-model and have made substantial modifications and additions to enhance model performance. The application demonstrations presented are the visible part of my dissertation work made possible by the time spent "behind the scenes" working with the model code. This work has resulted in 10 publications and book chapters in addition to the chapters presented here. Those additional publications include: Deville et al. (2014), Long et al. (2014), Fitzpatrick et al. (2015), Moyer-Horner et al. (2015), Long et al. (2016), Amélineau et al. (2018), Fitzpatrick et al. (2018), Zhang et al. (2018), Wang et al. (2018), and Lovelace et al. (in review). Abstracts for the published works are provided in an addendum at the end of the dissertation.

Niche Mapper consists of two sub-models: 1) a microclimate model that calculates environmental conditions at animal height, and 2) a biophysical animal model. There are two versions of the animal model: an ectotherm model and an endotherm model. My work has been with the endotherm model and hereafter the "animal model" refers to the endotherm model.

The microclimate model calculates the hourly profiles of air temperature, wind speed, relative humidity, solar and long wavelength thermal radiation, and subsoil conditions that the animal experiences (Porter et al. 1973, Fuentes & Porter 2013). To get hourly values, the model

fits a sinusoidal curve to user-specified maximum and minimum daily air temperatures, wind speeds, cloud cover, and relative humidity to estimate hourly values. Hourly clear sky solar radiation is calculated based on date and geographic location, before being adjusted to account for any cloud cover and overhead vegetation (McCullough & Porter 1971).

Long-wavelength thermal radiation from clear sky and clouds are computed separately using empirical air temperature correlations (Swinbank 1963, Idso & Jackson 1969). Thermal radiation from the ground is computed from the above-ground climate, outlined above, and hourly substrate temperatures computed using a heat and mass balance equation for the substrate surface. Deep soil temperature is taken to be the mean annual temperature and is the lower boundary condition for the hourly soil temperature profile. The hourly soil temperature profile is then derived from numerical solutions of the transient heat balance equation for all the ground soil nodes. The hourly boundary conditions are the (constant) deep soil node temperature and the above ground profiles of air temperature, wind speed, relative humidity, solar and thermal radiation.

Using the local microclimate hourly information provided by the microclimate model, the animal model then calculates radiative ($Q_{rad}$), convective ($Q_{conv}$), conductive ($Q_{cond}$), solar ($Q_{sol}$), and evaporative (respiratory, $Q_{resp}$, and cutaneous, $Q_{evap}$) heat fluxes between the animal and its microenvironment to solve a heat balance equation (Eq. 1). This equation is used to estimate metabolic rate, $Q_{gen}$, that allows the animal with fur or feathers to maintain its core temperature.

$$Q_{gen} - Q_{resp} - Q_{evap} = Q_{fur} = Q_{rad} + Q_{conv} + Q_{cond} - Q_{sol} \quad (1)$$

For an animal to be in thermal steady state with its environment, metabolic heat production ($Q_{gen}$), less evaporative heat loss from the respiratory system ($Q_{resp}$) and the skin ($Q_{evap}$), must equal heat flow through the fur via conduction and radiation ($Q_{fur}$), and the net heat

flux with the outside environment ($Q_{rad}$ + $Q_{conv}$+ $Q_{cond}$ - $Q_{sol}$). A metabolic rate that does not balance the equation will result in net heat loss or heat gain, rendering the animal unable to maintain its body temperature if this imbalance persists.

The heat balance equation is solved to provide the metabolic rate for the animal that allows it to maintain its core temperature for every hour of each model day (Figure 1). If the metabolic rate falls outside the user-specified target metabolic rate (i.e., resting metabolic rate x an activity multiplier), behavioral and/or physiological thermoregulatory options are engaged to prevent overheating (in warm conditions) or to minimize metabolic expenditure on heat production (in cold conditions). The heat balance equation is re-solved after each thermoregulatory change until a balance is reached at the target metabolic rate or until thermoregulatory options are exhausted.

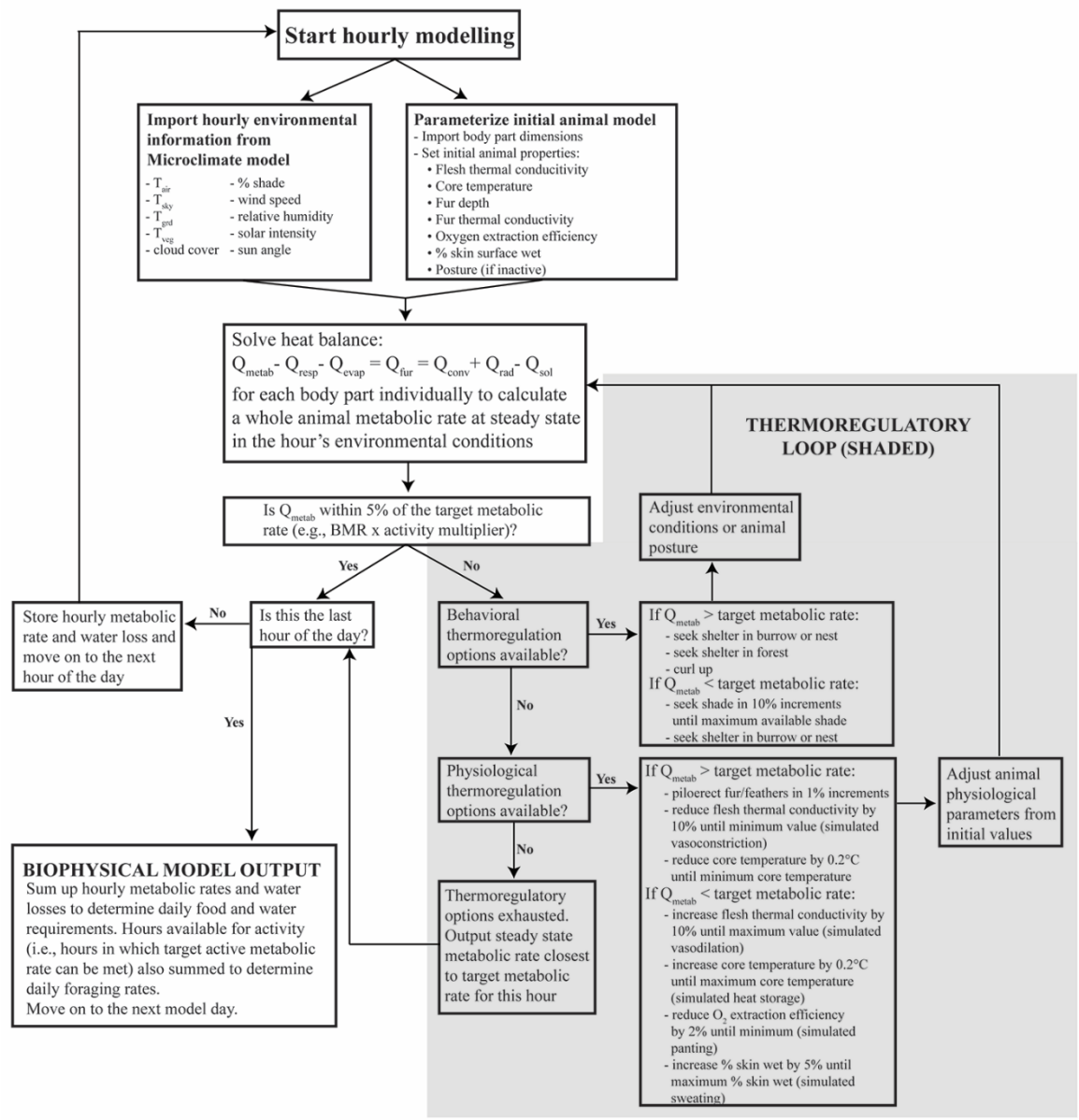


**Figure 1.** Schematic diagram of Niche Mapper's endotherm model operation.

There are several particularly relevant outputs in terms of quantifying thermal stresses experienced by the animal in a given environment that will be the focus of this dissertation. For animals that are heat stressed, the number of hours where they are predicted to be active without overheating is calculated and tracked by Niche Mapper by summing up the number of hours in a model day where the thermoregulatory options are sufficient to allow a heat balance at an active

metabolic rate. The cost of maintaining homeothermy in terms of water required for cutaneous (i.e., sweating) or respiratory (i.e., panting or gular fluttering) evaporative cooling is also calculated and tracked. For animals that are cold stressed, the portion of the predicted metabolic rate that satisfies the heat balance equation that is above the target metabolic rates can be used to quantify the cost of maintaining homeothermy (i.e., accounting for activity-thermoregulatory heat substitution; Humpheries & Careau 2011). These outputs allow Niche Mapper to predict how changes in climate, habitat alterations (e.g., loss of overhead shade), and changes in physical properties of the animal (e.g., body insulation) impose thermoregulatory costs on a model animal across space and time.

*Dissertation Overview*

There are three overarching goals for each of the chapters. First, each chapter is intended to provide a new test of Niche Mapper against empirical data, adding to the existing body of literature demonstrating the broad applicability of the model and the accuracy of its performance. Second, by focusing on different model animals across chapters, this dissertation aims to illustrate how the model can be adapted to any species with only basic information that can be gathered with relative ease. This can help address the common criticism that mechanistic models are too time-intensive to be practical conservation tools. Third, each chapter is intended to provide a novel use or represent an expansion of previous uses of Niche Mapper, rather than simply repeating prior uses.

Chapter 1: Using the American Pika (*Ochotona princeps*) as a model organism, I present a broadly-applicable use of Niche Mapper to add mechanism to species distribution modeling. Pikas are heat-sensitive mammals that lack the capacity to sweat and therefore buffer thermal stress by reducing activity during hot periods. I use Niche Mapper to calculate potential activity time across the western United States and use these outputs as inputs in a correlative model to

predict past, current, and future distributions. Predictions from this hybrid model are compared to predictions from a purely correlative model, illustrating the benefits and drawbacks of both approaches.

Chapters 2 and 3: Using the vervet monkey (*Chlorcebus pygerythrus*) as a model organism, I test Niche Mapper's ability to accurately predict body temperature and identify thermal stress by comparing model predictions to empirical data collected from a group of wild vervets. I also expand on the concepts presented in Chapter 1 by showing how other metrics of thermal stress produced by Niche Mapper (evaporative water loss requirements; increased heat production requirements) can be used to add mechanism to species distribution models.

Chapter 4: Using the double-crested cormorant (*Phalacrocorax auritus*) as a model organism, I present a novel use of Niche Mapper to model the sublethal thermoregulatory impacts of exposure to oil spills. Oil exposure reduces the insulative capacity of waterbird plumage. I demonstrate how Niche Mapper can be used to quantify the consequences, specifically increased metabolic heat production to compensate for the reduced insulation, using comparisons to empirical data collected from live cormorants.

*References*

Amélineau, F., J. Fort, P. Mathewson, D. Speirs, N. Courbin, S. Perret, W. Porter, R. Wilson, and D. Grémillet. 2018. Energyscapes and prey fields shape a North Atlantic seabird wintering hotspot under climate change. Royal Society Open Science 5:171883.

Angilletta MJ, Cooper BS, Schuler MS, Boyles JG. 2010. The evolution of thermal physiology in endotherms. Frontiers in Bioscience E2: 861-881.

Beever EA, Hall LE, Varner J, et al. 2017. Behavioral flexibility as a mechanism for coping with climate change. Frontiers in Ecology and the Environment 15: 299-308.

Bonebrake TC, Brown CJ, Bell J, et al. 2018. Managing consequences of climate-driven species redistribution requires integration of ecology, conservation and social science. Biological Reviews 93: 284-305.

Boyles JG, Seebacher F, Smit B, McKechnie AE. 2011. Adaptive thermoregulation in endotherms may alter responses to climate change. Integrative and Comparative Biology 51: 676-690.

Boyles JG, Thompson AB, McKechnie AE, Malan E, Humphries MM, Careau V. 2013. A global heterothermic continuum in mammals. Global Ecology and Biogeography 22: 1029-1039.

Briscoe NJ, Kearney MR, Taylor C, Brendan WA. 2016. Unpacking the mechanisms captured by a correlative SDM to improve predictions of a climate refugia. Global Change Biology 22: 2425-2439.

Buckley LB. 2008. Linking traits to energetics and population dynamics to predict lizard ranges in changing environments. American Naturalist 171: E1-E19.

Buckley LB, Urban MC, Angilletta MJ, Crozier LG, Rissler LJ, Sears MW. 2010. Can mechanism inform species' distributional models. Ecology Letters 13: 1041-1054.

Buckley LB, Kingsolver JG. 2012. Functional and phylogenetic approaches to forecasting species' responses to climate change. Annual Review of Ecology, Evolution, and Systematics 43: 205-226.

Buckley LB, Hurlbert H, Jetz W. 2012. Broad-scale ecological implications of ectothermy and endothermy in changing environments. Global Ecology and Biogeography 21: 873-885.

Buckley LB, Ehrenberger JC, Angilletta MJ. 2015. Thermoregulatory behavior limits local adaptation of thermal niches and confers sensitivity to climate change. Functional Ecology 29: 1038-1047.

Cabral JC, Valente L, Hartig F. 2017. Mechanistic simulation models in macroecology and biogeography: state-of-art and prospects. Ecography 40: 267-280.

Cahill AE, Aiello-Lammens ME, Fisher-Reid MC, et al. 2012 How does climate change cause extinction? Proceedings of the Royal Society B 280: 20121890.

Ceballos G, Ehrlich PR, Barnosky AD, García A, Pringle RM, Palmer TM. 2015. Accelerated modern human-induced species losses: Entering the sixth mass extinction. Science Advances 1: e1400253.

Cooke SJ, Sack L, Franklin CE, Farrell AP, Beardall J, Wikelski M, Chown SL. 2013. What is conservation physiology? Perspectives on an increasingly integrated and essential science. Conservation Physiology 1: doi: 10.1093/conphys/cot001.

Deville, A.-S., S. Labaude, J.-P. Robin, A. Béchet, M. Gauthier-Clerc, W. Porter, M. Fitzpatrick, P. Mathewson, and D. Grémillet. 2014. Impacts of extreme climatic events on the energetics of long-lived vertebrates: the case of the greater flamingo facing cold spells in the Camargue. Journal of Experimental Biology 217:3700-3707

Dormann, CF, Schymanski SJ, Cabral J, et al. 2012. Correlation and process in species distribution models: bridging a dichotomy. Journal of Biogeography 39: 2119-2131.

Du Plessis KL, Martin RO, Hockey PAR, Cunningham SJ, Ridley AR. 2012. The costs of keeping cool in a warming world: implications of high temperatures for foraging, thermoregulation and body condition of an arid-zone bird. Global Change Biology 18: 3063-3070.

Elith J, Leathwick JR. 2009. Species distribution models: ecological explanation and prediction across time and space. Annual Review of Ecology, Evolution, and Systematics 40: 677-697.

Elith J, Kearney M, Phillips. 2010. The art of modelling range-shifting species. Methods in Ecology and Evolution 1: 330-342.

Engler JO, Stiels D, Schidelko K, Strubbe D, Quillfeldt P, Bambilla M. 2017. Avian SDMs: current state, challenges and opportunities. Journal of Avian Biology 48: 1483-1504.

Evans MEK, Merow C, Record S, McMahon SM, Enquist BJ. 2016. Towards process-based range modeling of many species. Trends in Ecology and Evolution 31: 860-871.

Feng X, Papeş M. 2017. Can incomplete knowledge of a species' physiology facilitate ecological nice modelling? A case study with virtual species. Diversity and Distributions 23: 1157-1168.

Fitzpatrick, M., P. Mathewson, and W. Porter. 2018. Ecological Energetics of Whooping Cranes in the Eastern Migratory Population. Pages 239-257 *in* J. French, S. Converse, and J. Austin, editors. Whooping Cranes: Biology and Conservation. Academic Press, San Diego, CA.

Fitzpatrick, M. J., P. D. Mathewson, and W. P. Porter. 2015. Validation of a mechanistic model for non-Invasive study of ecological energetics in an endangered wading bird with counter-current heat exchange in its legs. PLoS ONE 10:e0136677.

Fuentes M, Porter WP. 2013. A new approach to model soil temperature: using microclimate models to predict the impacts of climate change on sea turtles. Ecological Modeling 251: 150–157.

Fuller A, Dawson T, Helmuth B, Hetem RS, Mitchell D. 2010. Physiological mechanisms in coping with climate change. Physiological and Biochemical Zoology 83: 713-720.

Fuller A, Mitchell D, Maloney SK, Hetem RS. 2016. Towards a mechanistic understandng of the responses of large terrestrial mammals to heat and aridity associated with climate change. Climate Change Responses 3: 10.

Guisan A, Tingley R, Baumgartner JB, et al. 2013. Predicting species distributions for conservation decisions. Ecology Letters 16: 1424-1435.

Hijmans RJ, Graham CH. 2006. The ability of climate envelope models to predict the effect of climate change on species distributions. Global Change Biology 12: 2272-2281.

Huey RB, Kearney MR, Krockenberger A, Holtum JAM, Jess M, Williams SE. 2012. Predicting organismal vulnerability to climate warming: roles of behaviour, physiology and adaptation. Philosophical Transactions of The Royal Society B. 36: 1665-1679.

Humpheries MM, Careau V. 2011. Heat for nothing or activity for free? Evidence and implications of activity-thermoregulatory heat substitution. Integrative and Comparative Biology 51: 419-431.

Idso SB, Jackson RD. 1969. Thermal radiation from the atmosphere. Journal of Geophysical Research 74: 5397-5403.

Jankowski JE, Londono GA, Robinson SK, Chappell MA. 2013. Exploring the role of physiology and biotic interactions in determining elevational ranges of tropical animals. Ecography 36: 1-12.

Jenssen BM. 1994. Effects of oil pollution, chemically treated oil, and cleaning on the thermal balance of birds. Environmental Pollution 86: 207-215.

Kearney M. 2013. Activity restriction and the mechanistic basis for extinctions under climate warming. Ecology Letters 16: 1470-1479.

Kearney M, Porter WP. 2009.Mechanistic niche modelling: combining physiological and spatial data to predict species' ranges. Ecology Letters 12: 334-350.

Kearney MR, Wintle BA, Porter WP. 2010. Correlative and mechanistic models of species distribution provide congruent forecasts under climate change Conservation Letters 3: 203-213.

Kolbe JJ, Kearney MR, Shine R. 2010. Modelling the consequences of thermal trait variation for the cane toad invasion of Australia. Ecological Applications 20: 2273-2285.

Kronfeld-Schor N, Dayan T. 2013. Thermal ecology, environments, communities, and global change: energy intake and expenditure in endotherms. Annual Review of Ecology, Evolution and Systematics 44: 11.1-11.20.

La Sorte FA, Jetz W. 2010. Avian distributions under climate change: towards improved projections. The Journal of Experimental Biology 213: 862-869.

Levesque DL, Nowack J, Stawski C. 2016. Modelling mammalian energetics: the heterothermy problem. Climate Change Responses 3: 7.

Long, R. A., R. Bowyer, W. P. Porter, P. Mathewson, K. L. Monteith, S. L. Findholt, B. L. Dick, and J. G. Kie. 2016. Linking habitat selection to fitness-related traits in herbivores: the role of the energy landscape. Oecologia 181:709-720.

Long, R. A., R. T. Bowyer, W. P. Porter, P. Mathewson, K. L. Monteith, and J. G. Kie. 2014. Behavior and nutritional condition buffer a large-bodied endotherm against direct and indirect effects of climate. Ecological monographs 84:513-532.

Lovelace, D., S. Hartman, P. Mathewson, B. Linzmeier, and W. P. Porter. In review. Modeling Dragons: an exploration of the impacts of environmental, physiological, and morphological constraints on the early evolution of dinosaurs. PLOS One

Mason THE, Brivio F, Stephens PA, Apollonio M, Grignolio S. 2017. The behavioral trade-off between thermoregulation and foraging in a heat-sensitive species. Behavioral Ecology 28: 908-918.

Mathewson PD, Porter, WP. 2013. Simulating polar bear energetics during a seasonal fast using a mechanistic model. PLoS One 8: e72863.

McClure, P. A., and W. P. Porter. 1983. Development of insulation in neonatal cotton rats (Sigmodon hispidus). Physiological Zoology 56:18-32.

McCullough EC, Porter WP. 1971. Computing clear day solar radiation spectra for the terrestrial ecological environment. Ecology 52: 1008-1015.

Medina, I., E. Newton, M. R. Kearney, R. A. Mulder, W. P. Porter, and D. Stuart-Fox. 2018. Reflection of near-infrared light confers thermal protection in birds. Nature Communications 9:3610.

Meineri E, Deville A-S, Grémillet D, Gauthier-Clerc, M, Béchet A. 2014. Combining correlative and mechanistic habitat suitability models to improve ecological compensation. Biological Reviews 90:314-329.

Methorst J, Bohning-Gaese K, Khaliq I, Hof C. 2017. A framework integrating physiology, dispersal and land-use to project species ranges under climate change. Journal of Avian Biology 48: 1532-1548.

Mitchell D, Snelling EP, Hetem RS, Maloney SK, Strauss WM, Fuller A. 2018. Revisiting concepts of thermal physiology: predicting responses of mammals to climate change. Journal of Animal Ecology 87: 956-973.

Mitchell, N., M. R. Hipsey, S. Arnall, G. McGrath, H. B. Tareque, G. Kuchling, R. Vogwill, M. Sivapalan, W. P. Porter, and M. R. Kearney. 2012. Linking eco-energetics and eco-hydrology to select sites for the assisted colonization of Australia's rarest reptile. Biology 2:1-25.

Mitchell, N. J., M. R. Kearney, N. J. Nelson, and W. P. Porter. 2008. Predicting the fate of a living fossil: how will global warming affect sex determination and hatching phenology in tuatara? Proceedings of the Royal Society of London B: Biological Sciences 275:2185-2193.

Moyer-Horner, L., P. D. Mathewson, G. M. Jones, M. R. Kearney, and W. P. Porter. 2015. Modeling behavioral thermoregulation in a climate change sentinel. Ecology and evolution 5:5810-5822.

Natori, Y., and W. P. Porter. 2007. Model of Japanese serow (Capricornis crispus) energetics predicts distribution on Honshu, Japan. Ecological Applications 17:1441-1459.

Oswald SA, Arnold JM. 2012. Direct impacts of climatic warming on heat stress in endothermic species: seabirds as bioindicators of changing thermoregulatory constraints. Integrative Zoology 7: 121-16.

Pacifici M, Foden WB, Visconti P, et al. 2015. Assessing species vulnerability to climate change. Nature Climate Change 5: 215-224.

Peterson AT, Papeş M, Soberón J. 2015. Mechanistic and correlative models of ecological niches. European Journal of Ecology 1: 28-38.

Porter WP, Gates DM. 1969. Thermodynamic equilibria of animals with environment. Ecological Monographs 39: 227-244.

Porter WP, Mitchell JW. 2006. Method and system for calculating the spatial-temporal effects of climate and other environmental conditions on animals. http://www.warf.org/technologies.jsp?ipnumber=P01251US

Porter, W. P., J. W. Mitchell, W. A. Beckman, and C. B. DeWitt. 1973. Behavioral implications of mechanistic ecology. Oecologia 13:1-54.

Porter WP, Ostrowski S, Williams JB. 2010. Modeling animal landscapes. Physiological and Biochemical Zoology 83: 705-712.

Seebacher F, Little AG. 2017. Plasticity of performance curves can buffer reaction rates from body temperature variation in active endotherms. Frontiers in Physiology 8: 575 doi: 10.3389/fphys.2017.00575

Smit B, Zietsman G, Martin RO, Cunningham SJ, McKechnie AE, Hockey PAR. 2016. Behavioural responses to heat in desert birds: implications for predicting vulnerability to climate warming. Climate Change Responses 3: 9.

Speakman JR, Krol E. Maximal heat dissipation capacity and hyperthermia risk: neglected key factors in the ecology of endotherms. Journal of Animal Ecology 79: 726-746.

Swinbank WC. 1963. Long-wave radiation from clear skies. Quarterly Journal of the Royal Meteorological Society 89: 339-348.

Thomas CD, Cameron A, Green RE, et al. 2004. Extinction risk from climate change. Nature 427: 145-148.

Urban MC, Bocedi G, Hendry AP, et al. 2016. Improving the forecast for biodiversity under climate change. Science 353: 6304

Waters CN, Zalasiewicz J, Summerhayes C, et al. 2016. The Anthropocene is functionally and stratigraphically distinct from the Holocene. Science 351: aad2622.

Wang Y, Porter W, Mathewson PD, Miller PA, Graham R, Williams JW. 2018. Mechanistic modeling of environmental drivers of woolly mammoth carrying capacity declines on St. Paul Island. Ecology 99: 2721-2730.

Woodroffe R, Groom R, McNutt JW. 2017. Hot dogs: high ambient temperatures impact reproductive success in a tropical carnivore. Journal of Animal Ecology 86: 1329-1338.

Yuan FL, Freedman AH, Chirio L, LeBreton M, Bonebrake TC. 2018. Ecophysiological variation across a forest-ecotone gradient produces divergent climate change vulnerability within species. Ecography 41: 1-11.

# CHAPTER 1: MECHANISTIC VARIABLES CAN ENHANCE PREDICTIVE MODELS OF ENDOTHERM DISTRIBUTIONS: THE AMERICAN PIKA UNDER CURRENT, PAST, AND FUTURE CLIMATES.

*Citation:* Mathewson PD, Moyer-Horner L, Beever EA, Briscoe NJ, Kearney M, Yahn JM, Porter WP. 2017. Mechanistic variables can enhance predictive models of endotherm distributions: the American pika under current, past, and future climates. Global Change Biology 23: 1048-1064.

## ABSTRACT

How climate constrains species' distributions through time and space is an important question in the context of conservation planning for climate change. Despite increasing awareness of the need to incorporate mechanism into species distribution models (SDMs), mechanistic modelling of endotherm distributions remains limited in the current literature. Using the American pika (*Ochotona princeps*) as an example, we present a framework whereby mechanism can be incorporated into endotherm SDMs. Pika distribution has repeatedly been found to be constrained by warm temperatures, so we used Niche Mapper, a mechanistic heat-balance model, to convert macroclimate data to pika-specific surface-activity time in summer across the western United States. We then explored the difference between using a macroclimate predictor (summer temperature) and using a mechanistic predictor (predicted surface-activity time) in SDMs. Both approaches accurately predicted pika presences in current and past climate regimes. However, the activity models predicted 8-19% less habitat loss in response to annual temperature increases of ~3-5°C predicted in the region by 2070, suggesting that pikas may be able to buffer some

climate-change effects through behavioral thermoregulation that can be captured by mechanistic modeling. Incorporating mechanism added value to the modeling by providing increased confidence in areas where different modeling approaches agreed and providing a range of outcomes in areas of disagreement. It also provided a more proximate variable relating animal distribution to climate, allowing investigations into how unique habitat characteristics and intraspecific phenotypic variation may allow pikas to exist in areas outside those predicted by generic SDMs. Only a small number of easily obtainable data are required to parameterize this mechanistic model for any endotherm, and its use can improve SDM predictions by explicitly modeling a widely applicable direct physiological effect: climate-imposed restrictions on activity. This more complete understanding is necessary to inform climate-adaptation actions, management strategies, and conservation plans.

## INTRODUCTION

The pervasive effects of global climate change on biodiversity are well documented (e.g., Parmesan & Yohe, 2003; Thomas, 2010; Bellard *et al.*, 2012), and threats due to climate change are playing a more prominent role in species assessments for conservation purposes (Staudinger et al, 2013). Predicting the impacts of climate change on species is therefore an important conservation challenge (e.g., McGuire & Davis, 2013). Species distribution models (SDMs), which combine spatial environmental data with information about a focal species to predict areas likely to support the species, are a primary tool used to address this challenge, as evidenced by the rapid increase in their use over the past decade (Franklin, 2010; Guisan *et al.*, 2013). SDMs can play valuable roles in informing conservation actions, including: 1) identifying potential future range contractions or shifts due to climate change to inform conservation status assessments; 2) prioritizing habitat reserves, corridors, and essential microrefugia for

conservation; and 3) informing decisions about when and to where species may need to be translocated (e.g., Schwartz, 2012; Guisan & Thuiller, 2005; Guisan *et al.*, 2013; Araújo *et al.*, 2011)

At one end of the modeling spectrum are correlative SDMs, which statistically relate species occurrence data to environmental variables (Elith & Leathwick, 2009). Variables thought to constrain a species' distribution are selected for use in the model, but the process(es) by which the variable(s) limit the species' distribution remain implicit. On the other end of the spectrum, mechanistic models explicitly model processes thought to limit a species' distribution (Kearney & Porter, 2009). Mechanistic approaches model the consequences of interactions between a species' functional traits (morphology, physiology and behavior) and its environment on the species' energetics, development and reproduction (Dormann *et al.*, 2012). Purely mechanistic models do not rely on known species distributions; rather, the predicted distributions are an emergent property of the process being modeled (Meineri *et al.*, 2015).

To date, most SDM efforts have used a correlative approach, due to their relative ease of use and wider availability, fewer and more easily met data requirements, and the range of biotic and abiotic interactions that they can (implicitly) capture (see reviews by, e.g., Elith & Leathwick, 2009; Kearney & Porter, 2009; Evans *et al.*, 2015). However, when it comes to predicting the impact of climate change on a species, purely correlative models provide little insight into *why* a decline is predicted, limiting their ability to inform conservation responses. Such omission has important implications for policy-makers, natural-resource managers, and other conservation practitioners, because without such insight, climate-adaptation actions in response to species declines are relegated to trial and error (Beever *et al.*, 2010; Evans *et al.*, 2015).

Furthermore, by relying on correlations rather than a process, transferring correlative models into novel environmental conditions risks erroneous extrapolation, a key issue for many studies of climate-change effects (Kearney & Porter, 2009; Veloz *et al.*, 2012). Mechanistic models, in contrast, do not require extrapolation when transferred into novel environmental conditions, and therefore may provide more accurate predictions regarding future shifts in suitable habitat due to climate change (Kearney & Porter, 2009; Rawson *et al.*, 2011; Tomlinson *et al.*, 2014). However, mechanistic models can be data-intensive and may require difficult-to-obtain or time-consuming information, limiting wider use of these models (Dormann *et al.*, 2012; Meineri *et al.*, 2015).

Using the two approaches in tandem may allow studies to take advantage of the respective strengths of each approach while counteracting the respective weaknesses, thereby increasing confidence in predictions (e.g., Buckley *et al.*, 2010; Kearney *et al.*, 2010; Dormann *et al.*, 2012; Meineri *et al.*, 2015; Briscoe *et al.,* 2016). One possibility is the integration of the two approaches by using mechanistic model outputs as inputs to a correlative model (Elith *et al.*, 2010). For example, mechanistic models can produce spatial layers representing how macroclimate variables (e.g., temperature) and habitat features (e.g., shade availability) affect a species' energy requirements or activity time across a heterogeneous landscape. These mechanistic output layers, which may be more proximate drivers of species persistence than the climate variable itself, can then be used as inputs for a correlative model (Kearney & Porter, 2009; Buckley *et al.*, 2010; Cahill *et al.*, 2013).

Mechanistic modelling of endotherms is particularly underrepresented in the existing literature as compared to ectotherms (Boyles *et al.*, 2011; Oswald & Arnold, 2012; La Sorte & Jetz, 2013). Although endotherms are better able to buffer themselves against changing thermal

conditions than ectotherms, such buffering has costs and limits. Endotherms facing heat stress may sweat or pant to increase evaporative heat loss, or avoid heat if local refugia exist. Conversely, endotherms facing cold stress may shiver or metabolize fat stores to produce body heat. These coping mechanisms require time and resources that could otherwise be used for growth and reproduction, thus imposing limits on the species' distribution (Buckley *et al.*, 2012; du Plessis *et al.*, 2012; Oswald & Arnold, 2012). Therefore, a model that predicts such thermoregulatory costs can provide valuable information about the processes by which climate limits distributions and how distributions may shift in a changing climate (Briscoe *et al.*, 2016).

Here, we show how a mechanistic model can be incorporated into distribution predictions of a heat-sensitive endotherm. Niche Mapper™ uses heat-transfer principles to calculate an animal's heat balance in its local microclimate (Porter & Mitchell, 2006). Informed by morphological, physiological, and behavioral information about an animal, the model calculates the necessary (in cold temperatures) or allowable (in warm temperatures) metabolic rate that will enable an animal to maintain its body temperature within a tolerable range. Niche Mapper can thus compare relative levels of heat stress (e.g., reduced activity) or cold stress (e.g., increased food requirements) across the landscape. This approach also allows us to better distinguish direct (e.g., energy deficits and activity reductions) from indirect (e.g., changes to species interactions and habitat structure; *sensu* Thomas 2010) effects of climate change.

The American pika (*Ochotona princeps* Richardson) is a small mammal typically found in relatively cool and moist, montane habitats (Hafner & Smith, 2010 but see, e.g., Shinderman, 2015; Ray *et al.*, 2016; and Varner & Dearing, 2014 for examples of populations occurring outside this general niche: all these examples are facilitated by fine-scale habitat complexity decoupling refugial conditions from coarse-scale climatic conditions). Pikas maintain a high

resting body temperature (40.1°C) that is close to their upper lethal temperature (43.1°C), have high metabolic requirements, and thick fur, which limits their ability to dissipate heat (Smith & Weston, 1990; Beever *et al.*, 2013). Consequently, individuals that are unable to behaviorally thermoregulate are prone to death from heat exposure in moderate temperatures (25.5-29.4°C) (MacArthur & Wang, 1973, 1974; Smith, 1974). Studies investigating pika distribution at ecoregional to continental scales have found warming temperatures to be the primary driver of distributional change over time (Grayson, 2005; Galbreath *et al.*, 2009) and chronic heat stress to be a leading predictor of pika persistence under recent climate conditions (Beever *et al.*, 2003, 2010, 2011, 2013; Wilkening *et al.*, 2011; Calkins *et al.*, 2012). At more local scales, the influence of warm temperatures on pika distributions is not as straightforward: while warm temperatures have been found to be a primary determinant of pika distributions in some locations (e.g., Moritz *et al.*, 2008; Stewart *et al.*, 2015), other aspects of climate and habitat characteristics have been identified as more important in other locations (e.g., Erb *et al.*, 2011; Yandow *et al.*, 2015; Schwalm *et al.*, 2016).

Despite the evidence of broad distributional changes being related to warm temperatures, it is unclear exactly *how* temperatures operate to limit pika distribution. Warm temperatures could influence pikas directly (e.g., through exceeding thermal limits or limiting time available to forage) or indirectly (e.g., through increased disease transmission, facilitation of competitors, changes in vegetation affecting food availability and quality, or reduced insulating snowpack layer in the winter). Pikas cope with heat stress by retreating to thermal refugia in the interstices of their rocky habitat (MacArthur & Wang, 1974; Smith, 1974; Moyer-Horner *et al.*, 2015). During the summer, pikas must be surface-active to feed, find mates, and defend territory. Furthermore, across most of their range, pikas must also build up food caches (“haying”) to

survive the winter months because they do not hibernate (Smith, 1974; Dearing, 1987). Collectively, these observations support a hypothesis that increased temperatures may limit pika distributions by restricting the amount of time available for foraging and haying activities.

Activity windows have been identified as a promising and widely applicable physiological process to incorporate into SDMs in order to better understand how warm temperatures affect distributions (Evans *et al.*, 2015), in contrast to other physiological processes like upper thermal tolerance, which has been found to poorly predict biogeography (e.g., Cahill *et al.*, 2013). Here, we use Niche Mapper to explicitly model this mechanism and test whether potential summer activity time is a robust predictor of pika distribution. We compare distributions of pikas in the United States predicted by 1) a correlative model using only macroclimate predictors vs. 2) a model that incorporates mechanism in the form of summer thermal environments converted to pika-specific allowable surface-activity time. We show how using the correlative and mechanistic approaches in tandem can help overcome the shortcomings of both approaches to provide more confident predictions of, and insights into, climate-change effects. Although we use the pika as a model organism to illustrate the framework, the general modeling approach can be used on any species whose distribution is constrained by thermoregulatory pressures. It therefore can help fill the existing knowledge gap regarding predicting the direct physiological effects of climate change on endotherms and thus facilitate better-informed conservation and management actions.

## MATERIALS AND METHODS

### *Niche Mapper Predictions of Surface-Activity Hours*

Niche Mapper is a coupled microclimate and animal heat- and mass-balance model that has been previously described in detail (e.g., Porter *et al.*, 2000; Porter & Mitchell, 2006). It has

been shown to accurately predict metabolic heat production, habitat use, or landscape distributions of a variety of animals, including mammals ranging in size from mice (*Mus* spp.) and gliding possum (*Petauroides volans)* to elk (*Cervus canadensis*) and polar bears (*Ursus maritimus*) (e.g., Porter *et al.*, 1994; Kearney *et al.*, 2010; Mathewson & Porter, 2013; Long *et al.*, 2014). Specific to pikas, Moyer-Horner *et al.* (2015) demonstrated that Niche Mapper can accurately predict both pika metabolic rate as a function of temperature and pika activity reductions in Glacier National Park, USA. We note that prior uses of Niche Mapper to predict habitat use and landscape distributions were purely mechanistic and thus required detailed information about the focal animal's physiology and diet properties. Here, we are exploring a methodology that only uses the heat balance aspect of Niche Mapper, minimizing the number of required inputs needed in order to make it easily adaptable to other species.

Briefly, Niche Mapper consists of two sub-models: 1) a microclimate model that calculates environmental conditions at animal height, and 2) a biophysical/behavioral/morphological animal model (Fig. 1). The microclimate model calculates hourly profiles of air temperature, wind speed, relative humidity, and solar and long-wavelength thermal radiation that an animal experiences (Fuentes & Porter, 2013; Kearney *et al.*, 2014). The animal model then solves a heat balance equation (Eq. 1) wherein the animal's metabolic heat generation ($Q_{gen}$) must equal heat transfer through its fur ($Q_{fur}$) and the net heat flux with its microenvironment [radiative ($Q_{rad}$), convective ($Q_{conv}$), solar ($Q_{sol}$), and evaporative (respiratory, $Q_{resp}$, and cutaneous, $Q_{evap}$)], in order for the animal to maintain its core temperature during each hour of the day:

$$Q_{gen} - Q_{resp} - Q_{evap} = Q_{fur} = Q_{rad} + Q_{conv} - Q_{sol} \quad (1)$$

Niche Mapper was used to predict the number of hours pikas could be active at 2x basal metabolic rate (a conservative field metabolic rate; Karasov, 1992) while still maintaining a heat balance during crepuscular and diurnal hours in the summer months (defined here as June-September) across the western United States. For each month, an "average" day was modeled, using the mean monthly maximum and minimum temperature, and the model day's allowable activity hours were multiplied by the number of days in that month (See Supporting Information for more details about Niche Mapper operation).

Activity-hour predictions were made for current, past, and future climate conditions. Current climate data came from 1981-2010 climate normals from the PRISM Climate Group at 800 m resolution (http://www.prism.oregonstate.edu/; Daly *et al.*, 2008). Climate data for the Last Glacial Maximum ("LGM"; ~22,000 years b.p; 4 km resolution) and the mid-Holocene ("MH" ~6,000 years b.p; 800 m resolution) were obtained from the WorldClim database (http://www.worldclim.org; Hijmans *et al.*, 2005). For future climate, we used predictions for 2070 climate conditions from global circulation models (GCMs) used in the IPCC Fifth Assessment (IPCC, 2013) that predicted conservative (MRI-CGCM3, RCP2.6), moderate (NorESM1-M, RCP4.5), and largest magnitude (MIROC-ESM-CHEM, RCP8.5) climate-change scenarios in the western United States. GCM data were obtained from the WorldClim database at 800 m resolution (See Supporting Information for additional information on spatial data acquisition). Activity predictions were also made assuming uniform maximum and minimum temperature increases of 3°C and 5°C in order to illustrate more simply how the two modeling approaches differ in their predictions of pika response to warming temperatures, without the confounding effect of spatially varying temperature changes.

Pika bodies were modeled as single ellipsoids with the properties listed in Table S1. Pikas are not known to pant or sweat, so the only thermoregulatory options allowed were for the core temperature to rise and for flesh thermal conductivity to increase (simulating vasodilation). For sensitivity analyses and other pika model-building details, see Moyer-Horner *et al.* (2015). Pikas inhabit talus and talus-like substrates (Tyser, 1980), but national land cover datasets have limited ability to identify such specific substrates at broad spatial scales (Moyer-Horner *et al*. in review; EAB, pers. obs.). Thus, we assumed that every pixel contained suitable rocky habitat and all substrate inputs for the microclimate submodel were for a rocky surface (Table S2). We assumed that no above-talus shade was available, because pikas are typically found in open, rocky areas. We assumed clear skies for all simulations in order to develop a model applicable to climate scenarios that lack cloud-cover data. A sensitivity analysis showed that incorporating cloud cover affected the absolute number of activity hours, but did not substantially affect relative amounts of activity across the pika's range in the United States, resulting in very similar predicted distributions with and without cloud cover (Fig. S1).

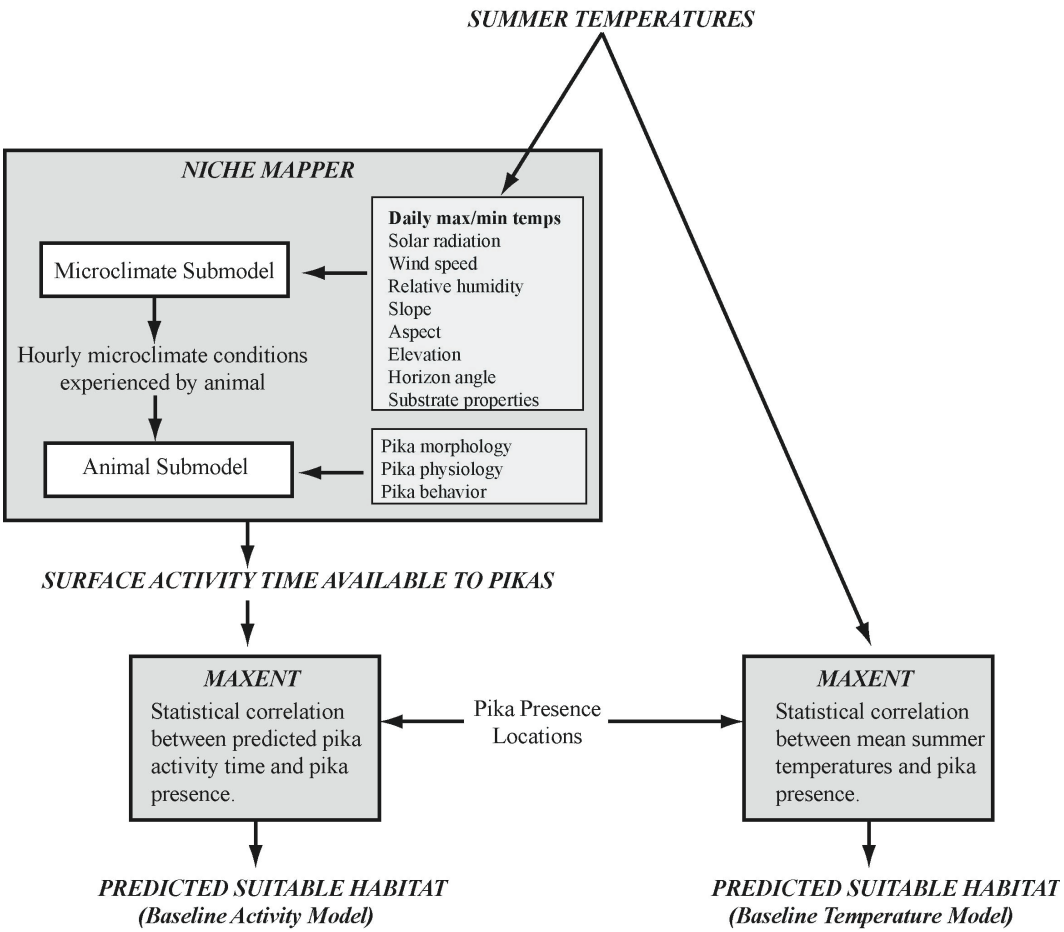


**Figure 1.** Flow diagram illustrating the how the two baseline models were developed and key input data. The baseline temperature model is a purely correlative model, relating macroclimate conditions to presence locations in order to predict distribution. The baseline activity model incorporates mechanism into distribution predictions by first translating the macroclimate data to a biologically-relevant mechanistic output (time available to be surface active). Additional climate predictors that potentially modify how summer temperatures or activity time limit distributions are added to these baseline models (see text) as an input to the Maxent model building process (i.e., entering the Maxent box along with summer temperatures or surface activity time.

*Species Distribution Models*

There is no known minimum amount of surface activity during summer needed for pika survival, so one option to build a distribution model based on activity time is to use the activity-hour threshold that separates extant from extirpated sites (e.g., Sinervo *et al.*, 2010). Such persistence/extirpation data are available for pikas in the United States from 39 sites in the hydrographic Great Basin. However, this approach assumes that the threshold identified at these sites is applicable throughout the species' range. Furthermore, similar presence/absence data are not available for many species, limiting wide use. Therefore, to provide a generally applicable methodology to convert activity hours into a predicted distribution, we used activity hours as a predictor within a correlative modelling framework (Fig. 1). We fit correlative models using Maxent, because this model is widely used, has been found to perform well compared to other models, and was developed for presence-only data (Elith *et al.*, 2006; Phillips *et al.*, 2006).

Presence data for the range-wide Maxent models were obtained from online zoological record databases and from prior pika studies to fill in known gaps in the database records. To minimize the effect of sampling bias on model predictions, we used the target-group background approach (Phillips *et al.*, 2009), using terrestrial mammal records to select background points (see Supporting Information for additional details on presence- and background point selection). Presence and background points were filtered to remove duplicate points in each 800-m pixel. Models were built using only hinge and product features in order to smooth the response curves and avoid overfitting (Elith *et al.*, 2010), while allowing for potential interactions. Models were evaluated using 10-fold cross-validation. Other model settings were set to default values, including the use of clamping when extrapolating, which treats variables outside the training range as if they were at the limit of the training range.

Baseline models to predict pika distributions were first built using only either mean temperature of the warmest quarter or summer activity predicted by Niche Mapper. This allowed for the most direct comparison between using the macroclimate predictor (summer temperature) and a mechanistic explanatory variable (summer activity). These models are referred to hereafter as the "temperature baseline model" and the "activity baseline model" (Fig. 1).

Precipitation and winter cold have been identified as important determinants of pika persistence in addition to summer temperatures, particularly at more localized scales (Beever *et al.*, 2010; Millar & Westfall, 2010; Erb *et al.*, 2011; Jeffress *et al.*, 2013; Schwalm *et al.*, 2016). The relative importance of summer activity time likely varies in response to these other variables across the pika's range. In areas with high plant productivity and/or shorter winters, fewer summer activity hours may be required because foraging is likely more efficient and/or smaller food caches are sufficient to survive the winter. To account for these potential interactions, we explored adding additional climate layers to the baseline models: minimum temperature of the coldest month (abbreviated here as "winter cold;" proxy for acute cold stress and winter duration; less correlated with the baseline inputs than mean temperature of the coldest quarter or growing-season duration), growing-season precipitation (calculated as the sum of the precipitation in months where the mean temperature is >5°C), and snowpack potential (calculated as the sum of the precipitation in months where the minimum temperature is < 0°C).

Models were built using current climate and pika distribution data, and then used to predict habitat suitability under past and future climate scenarios. We identified areas where the SDMs would require extrapolation under past and future climate scenarios using multivariate environmental similarity surfaces (MESS maps; Elith *et al.*, 2010). To facilitate easier

comparisons between predictions made by the different modeling approaches and evaluate the degree to which the approach influences estimates of percent range change, we converted Maxent's continuous output into a binary suitable/unsuitable output using the threshold that maximized training sensitivity plus specificity ("MSS"), as suggested for use with presence-only data by Liu *et al.* (2005, 2013).

*Model Evaluation*

To test whether summer activity hours predicted by Niche Mapper could distinguish between suitable and unsuitable habitat, we examined predicted activity at 39 long-term pika monitoring sites in the Great Basin (Beever *et al.,* 2003, 2008, *in review;* Wilkening *et al.*, 2011; EAB, *unpublished data*). We compared the average activity hours predicted by Niche Mapper for all pixels within a 3-km radius (matching the extent of field surveys around each historical record) at sites with persistent populations in 2015 (n=25) to the hours available within 3 km of sites that have been extirpated in the last century (n=14; hereafter, "recently-extirpated sites").

To evaluate model performance, we used area under the receiver-operator curve (AUC) and True Skill Statistic (TSS; Allouche *et al.*, 2006). TSS statistics were evaluated for both the 39 Great Basin pika sites (true presence/absence data) and for the 616 pika locations and 10,000 background (pseudoabsence) points used in the Maxent modeling (Additional details on these tests are found in Supporting Information). To account for the fact that pikas may be observed in an "unsuitable" pixel if that pixel is in close proximity to suitable habitat due to the metapopulation dynamics the species exhibits, we also calculated the number of known pika locations within 3 km of the nearest suitable habitat pixel. We used 3 km because it is an estimated limit of pika dispersal in most habitat types (Beever *et al.*, 2003; 2011) and is the

average (range: 1.1-4.5 km) genetic neighborhood distance found by Schwalm *et al.* (2016) at eight US National Park Service units in the western United States.

To evaluate the models' transferability to different climatic conditions, we used 48 fossil pika locations from the Quaternary period (Hafner, 1993; Grayson, 2005; Galbreath *et al.*, 2009) to test the models' ability to predict pika range retractions from the LGM (colder and drier than present) to the MH (drier and similar summertime temperatures in the Northern Hemisphere than present in some areas). In tests to quantify the models' abilities to track this observed range retraction, we assumed that in the mid-Holocene all MH and late Holocene (LH) fossil locations would be within 3 km from predicted thermally-suitable habitat and all LGM and early Holocene (EH) fossil locations will be more than 3 km from any predicted thermally-suitable habitat. Finally, we assumed that all recently-extirpated and current pika locations must be within 10-20 km (estimated maximum pika dispersal distance over millenia; Hafner, 1994; Hafner & Sullivan, 1995) of areas with predicted suitable habitat in the MH.

## RESULTS

### *Niche Mapper Activity Predictions*

Summer activity levels predicted by Niche Mapper corresponded well with the known distribution of *O. princeps* (Fig. S2). In the Great Basin, pika-extant sites averaged 19% more predicted surface activity time during summer than did pika-extirpated sites (1410 vs. 1159 hours) (Mann-Whitney $U = 32$, $p<0.001$; Fig. 2; Table S3). A threshold value of 1132 hours (53% of diurnal and crepuscular hours for the period) separated the extant site with the lowest predicted activity hours from all but four of the 14 extirpated sites (chi-square test of association $\chi^2= 24.01$, $p<0.001$).

*Species Distribution Model Results: 1981-2010 Climate Conditions*

Model response curves to the inputs were reasonable and expected: suitability declined with increasing summer temperature and decreasing available activity time (Figs. S3, S4). The two baseline models predicted similar raw (i.e., no threshold applied) habitat suitability scores for pixels within 3 km of the 616 pika presence locations (Table 1, paired t-test, t=-1.38, p=0.17).

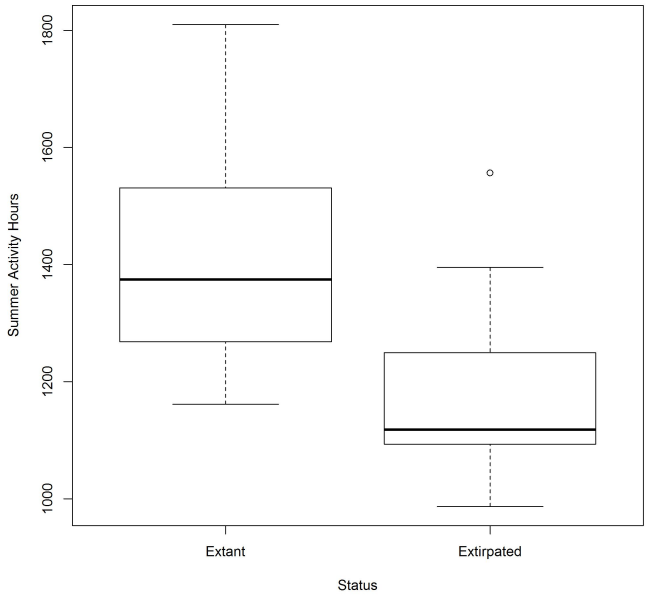


**Figure 2.** Comparison of predicted summer time activity hours at extant and extirpated historic monitoring sites in the Great Basin, USA. The outlying extirpated site is Duffer Peak, NV, which was recommended as a potential recipient site should pika translocations be considered (Beever et al. 2016).

When using the MSS threshold to delineate suitable and unsuitable habitat, baseline model predictions for suitable habitat using summer temperatures and summer activity agreed for 76% of all pixels in the western United States predicted as suitable by either model. The activity baseline model predicted 19% more suitable habitat across the western United States than did the

temperature baseline model, mostly in the northern and eastern portions of study area (Table 2; Fig. 3). The temperature baseline model predicted additional suitable habitat along the western coast and in the lower elevations of the Cascade Range.

For both baseline models, more than 95% of all pika records were within 3 km of suitable (defined using the MSS threshold) habitat (Table 1). When comparing predictions at the 39 Great Basin monitoring sites, both models accurately distinguish pika-extirpated sites from extant sites ($\chi^2$ test of association $p < 0.01$ for each; Table S4, Fig. S5). The activity baseline model identified all extant sites as suitable (the temperature model had two false negatives), but had three more false positives than did the temperature model (5 vs. 2).

When adding any combination of additional inputs, the mean-summer-temperature or summer-activity input consistently remained the most important factor, contributing >70% to every model. AUC values did not change appreciably (range: 0.889-0.920 in the Great Basin and 0.923-0.938 across the western United States), and all combinations of variables indicated good to excellent model fit (Swets, 1988). Thus, the TSS metric was primarily used to compare model performance.

**Table 1.** Average habitat suitability score for all pixels within 3 km of the known pika locations (n=616) used in the species distribution modeling for models built using summer temperature (ST), summer activity (SA), summer temperature plus winter cold (ST+WC), summer activity plus winter cold (SA+WC). The number of locations within 3 km of suitable habitat is noted in parentheses. Suitability was determined by using a threshold that maximizes specificity + sensitivity. All models predicted high mean suitability across known pika locations and predicted a strong decrease in suitability under climate change scenarios, however declines in habitat suitability were stronger for models that included summer temperature compared to models that included summer activity.

| Climate Scenario | | Model | | | |
|---|---|---|---|---|---|
| | | **ST** | **SA** | **ST+WC** | **SA+WC** |
| **1981-2010 Climate Conditions** | | 0.502 (586) | 0.501 (589) | 0.506 (597) | 0.509 (597) |
| **Global Circulation Model Predictions for 2070** | MRI-CGCM3 (Conservative change) | 0.512 (588) | 0.486 (596) | 0.501 (592) | 0.479 (589) |
| | NorESM1-M (Moderate change) | 0.358 (541) | 0.346 (565) | 0.332 (547) | 0.349 (563) |
| | MIROC-ESM-CHEM (Largest magnitude change) | 0.155 (300) | 0.188 (432) | 0.150 (319) | 0.216 (431) |
| **Uniform Temperature Increases** | +3°C | 0.277 (463) | 0.300 (508) | 0.285 (482) | 0.345 (528) |
| | +5°C | 0.147 (308) | 0.184 (440) | 0.157 (329) | 0.235 (457) |

**Table 2.** Area of suitable habitat ($km^2$) predicted by Maxent species distribution models using either mean summer temperature or predicted summer activity under different climate change scenarios. Percent change from current climate conditions is noted in parentheses. Model abbreviations: SA (summer activity); ST (summer temperatures); WC (winter cold).

| Climate Scenario | | Model | | | |
|---|---|---|---|---|---|
| | | **ST** | **SA** | **ST+WC** | **SA+WC** |
| **1981-2010 Climate Conditions** | | 414,355 | 494,540 | 366,000 | 344,193 |
| **Global Circulation Model Predictions for 2070** | MRI-CGCM3 (Conservative change) | 407,958 (-2%) | 479,405 (-3%) | 345,707 (-6%) | 303,128 (-12%) |
| | NorESM1-M (Moderate change) | 184,227 (-56%) | 283,609 (-43%) | 136,700 (-63%) | 156,502 (-55%) |
| | MIROC-ESM-CHEM (Largest magnitude change) | 52,911 (-87%) | 139,713 (-72%) | 44,462 (-88%) | 98,412 (-71%) |
| **Uniform Temperature Increases** | +3°C | 118,401 (-71%) | 224,232 (-55%) | 110,357 (-70%) | 170,239 (-51%) |
| | +5°C | 34,218 (-92%) | 139,713 (-78%) | 34,579 (-91%) | 87,368 (-75%) |

Adding growing-season precipitation to both baseline models improved model performance across the western United States by capturing additional presence locations in the Cascade Range, an area with a high density of presence points, but performed worse in the drier Great Basin where there are true presence/absence data (Table S4). Similarly, adding potential snow accumulation improved model performance across the western United States by capturing more presence sites in the Cascade Range at the expense of decreased performance in the Great Basin (Table S4).

Adding minimum temperature of the coldest month to both baseline models increased model performance both in the entire western United States and in the Great Basin (Table S4). Specifically, adding winter cold to the models expanded predicted suitable habitat in the lower elevations of the Cascade Range (moderate winter cold; encompassing pika presence sites not

identified as suitable by the baseline models) and decreased predicted suitability in lower-elevation areas in the Rocky Mountains (colder minimum winter temperatures; eliminating areas where no pikas have been documented) (Fig. S6).

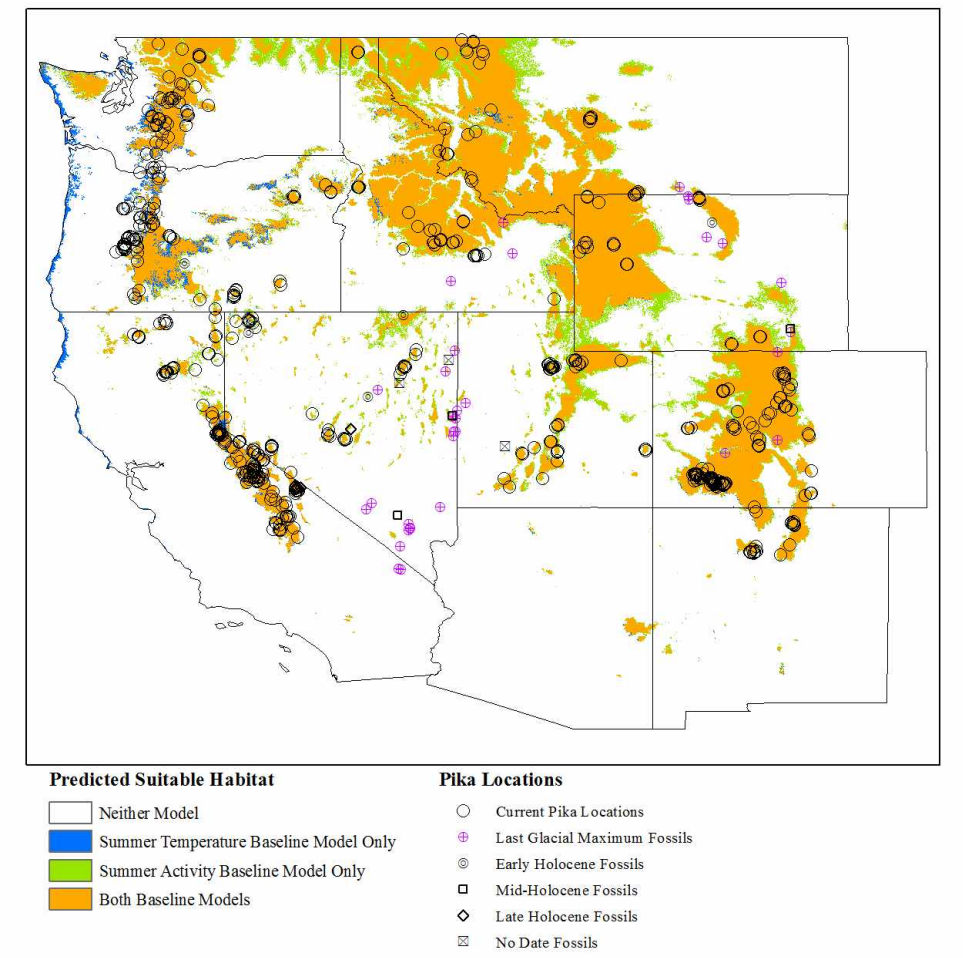


**Figure 3.** Baseline model predictions of climatically suitable habitat for pikas under 1981-2010 climate conditions. Summer activity time predicted by Niche Mapper was the only input to the activity baseline model, and mean summer temperature was the only input to the temperature baseline model. The current pika locations used to build the model are shown along with fossil pika locations reported by Mead (1987), Hafner (1993), Grayson (2005), Galbreath *et al.* (2009) in order to show sensitivity of the model to different climate conditions.

Adding either or both of the precipitation variables did not improve model performance above the baseline + winter-cold models, so additional analyses only considered the baseline (to most simply compare the effect of using summer-activity time or summer temperatures) and baseline + winter cold models (the best overall model).

*Species Distribution Model Results: Hindcasting*

MESS maps (Elith *et al.*, 2010) indicated that there was considerable extrapolation in the LGM, and to a lesser degree, the MH due to lower minimum temperatures (winter cold) than captured in the training data (Fig. S7). Both baseline models predicted extensive suitable habitat throughout the western United States during the LGM (Fig. S8). All recently-extirpated and current sites, and all but three fossil pika locations (Corn Creek [NV], Mescal/Antelope Creek [CA], and Kokoweef Cave [CA]) were within 4.5 km (the approximate resolution of the LGM climate data at these latitudes) of predicted suitable habitat (Table S5).

The baseline models predicted substantial reductions in suitable habitat in the mid-Holocene (Fig. S9). Both models predicted habitat loss at most of the LGM and EH fossil locations, yet still predicted habitat within 3 km of the MH and LH fossil locations, with the exception of Pintwater Cave, NV (Table 3). All recently-extirpated and current pika records were within 20 km of suitable habitat predicted in the MH by both models (Table 3).

Adding minimum winter temperatures contracted habitat suitability predicted by both models in the LGM in the southern latitudes, causing additional fossil pika sites to be missed (Fig. 4; Table S5). Suitable habitat contracted more in the summer activity model than it did the summer temperature model, due to a stronger interaction between activity hours and winter cold than between summer temperatures and winter cold.

Pintwater Cave was still the only MH or LH fossil site missed by >3km by both the baseline + winter cold models hindcasting to the MH (Table 3). The summer temperature + winter cold model also missed an additional Holocene fossil site (Horned Owl Cave, WY). Adding winter cold resulted in a small number of current or recently-extirpated locations to be missed in the MH predictions, exclusively lava-flow sites and low-elevation sites in the northwest Great Basin portions of Nevada, Oregon, and California (Table 3).

**Table 3**. Evaluation of model hindcasting to the mid-Holocene (MH) showing the number of sites misclassified by the models based on assumptions that 1) all Last Glacial Maximum (LGM) and early Holocene (EH) sites were unsuitable in the MH while all mid- and late Holocene (LH) sites were suitable in the MH and 2) that all recently-extirpated and current locations are within 10-20 km of suitable habitat in the MH. The former assumption was statistically evaluated with a chi square test of association. Model abbreviations: SA (summer activity); ST (summer temperatures); WC (winter cold).

| **Model** | No. of LGM and EH sites < 3 km from predicted suitable habitat (n=39) | No. of MH and LH sites > 3 km from predicted suitable habitat (n=9) | Recently-extirpated/Current Locations (n= 629) | |
|---|---|---|---|---|
| | | | No habitat <10 km | No habitat <20km |
| ST | 15 | 1[a] | 10 | 0 |
| SA | 16 | 1[a] | 3 | 0 |
| ST+WC | 7 | 2[b] | 16 | 9 |
| SA+WC | 9 | 1[b] | 17 | 9 |

[a]Chi square test of association $p<0.05$; [b] Chi square test of association $p<0.001$

*Species Distribution Model Results: Future Climate Warming*

There was some extrapolation beyond the range of environmental data captured in the training dataset when predicting to the more severe climate-change scenarios, with respect to mean summer temperatures and, to a lesser degree, winter cold (Fig. S7). Both baseline models predicted substantial reductions in thermally-suitable habitat throughout the western United States under the moderate- and warmest-magnitude climate change scenarios and <5% loss under the conservative scenario (Fig. 5, Table 2). The modeling approaches predicted differing magnitudes of declines in suitable habitat as temperatures increased, with the activity baseline model predicting >13-15% less habitat loss (absolute difference) under the moderate- and warmest-climate change scenarios (Table 2). When limiting the area of analysis to within 3 km of the pika presence locations used in the modeling rather than using the whole western United States, the activity model still predicted less future habitat loss (Table 1). Under the warmest scenario, the activity baseline model predicted >100 more pika presence sites to still be within 3 km of thermally-suitable habitat compared to the temperature model.

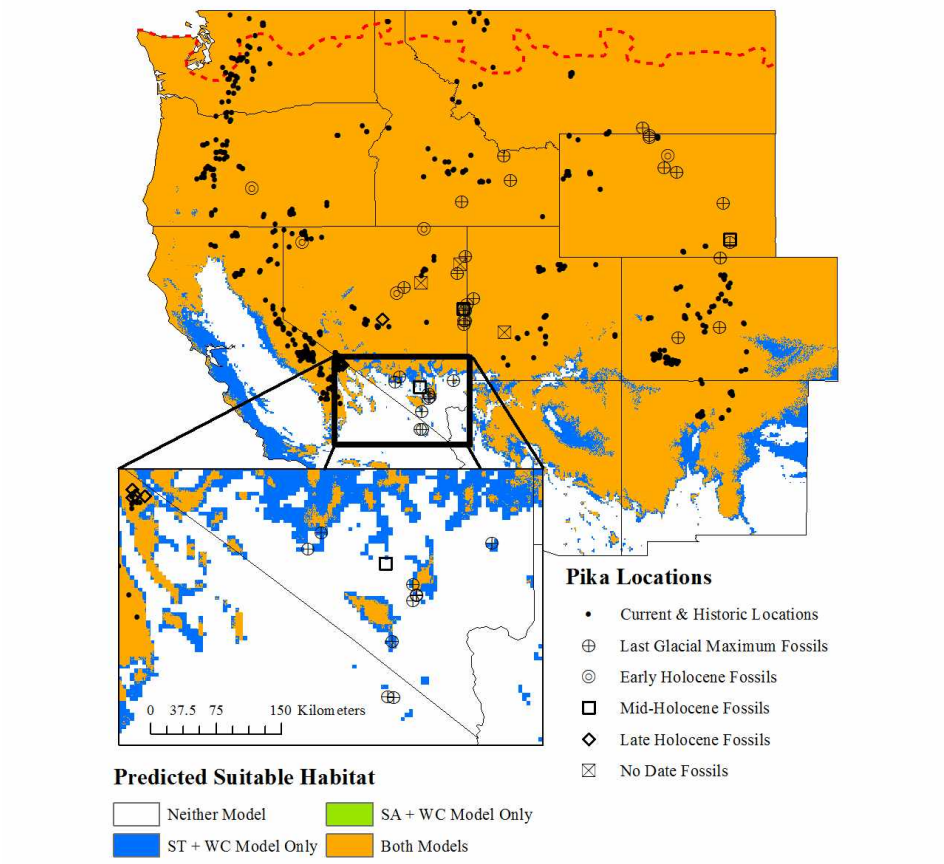


**Figure 4.** Hindcasting the summer temperature (ST) or summer activity (SA) baseline + winter cold models to the Last Glacial Maximum (~22,000 years before present), showing increased areas of predicted suitable habitat. A detailed view of the southern edge of predicted suitable habitat is shown in the inset. Average summer temperatures in the Western United States were ~13°C cooler than present. Three fossil locations (indicated as "No Date") were not assigned to a specific epoch. The approximate southern edge of glacial ice sheets is represented by the dashed red line.

Adding winter cold to the baseline models increased habitat loss predictions in the conservative and moderate scenarios. These scenarios predicted that there will be areas where minimum winter temperatures will get colder and summer temperatures are expected to increase

or remain the same (Table 2). As with the baseline models, the summer activity + winter cold model predicted less habitat loss with warming temperatures: 8% less in under the moderate scenario and 17% less under the warmest scenario (Table 2, Fig. 5). The difference in predicted habitat loss between summer temperature and summer activity models was even more pronounced when we assumed uniform temperature increases (Fig. 5).

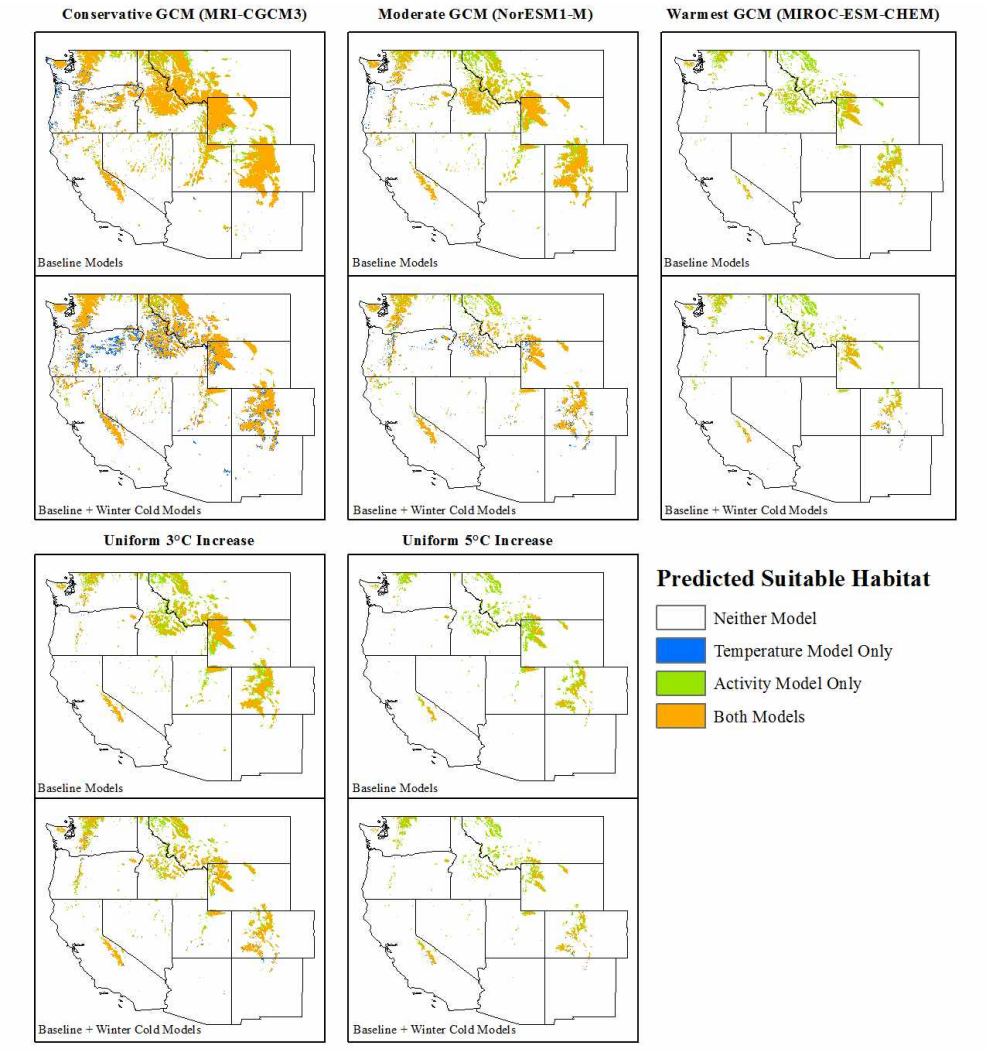


**Figure 5.** Habitat suitability predictions for various future climate scenarios using baseline models and with the baseline + winter cold models. The baseline models used either the mean temperature of the warmest quarter or summer activity predicted by Niche Mapper to predict habitat suitability. Minimum temperature of the coldest month was added to the two baseline models. Mean changes in mean summer/minimum winter temperatures in the western United States predicted by the global circulation models: conservative (+0.31/-0.08°C); moderate (+2.59/+0.83°C); warmest (+5.73/+4.05 °C). With the exception of the conservative GCM scenario, the summer activity models predicted less habitat loss than the summer temperature models.

# DISCUSSION

## *Comparing Model Predictions*

We aimed to explore how incorporating mechanism into a species distribution model affected model predictions. We found broad agreement between models using summer temperatures and models using summer surface-activity time with respect to both: 1) predicting suitable habitat at or near current pika locations, and 2) general patterns of habitat expansions and contractions under past- and future-climate scenarios. However, the models predicted different magnitudes of future range contraction, with the activity models predicting 8-19% less habitat loss than the temperature models, range-wide. Modeling a more proximate relationship between an animal and its environment enabled a better understanding of how climate limits pika distribution, how pikas persist in areas outside of their typical climate envelope, and how they might be able to buffer future climate-change effects.

The observed differences in predicted response to climate change are similar to prior comparisons of correlative and mechanistic modeling approaches (Morin & Thuiller, 2009; Buckley *et al.*, 2010, Buckley *et al.*, 2011). These results are also consistent with Araújo *et al.* (2011), who noted that SDMs can be good tools for identifying the direction of range shifts, but they are more uncertain when it comes to predicting the magnitude of the change. In contrast to the more opaque relationship between pika presence and temperatures, the more easily interpretable mechanistic input of activity time allows insight into the reason for differences in model predictions, both for the present and the future.

Under current climate conditions, the summer activity baseline model predicted more suitable habitat in the inland regions of the study area than did the summer temperature model (Fig. 3). In contrast, the summer temperature model predicted additional suitable habitat beyond

that predicted by the summer activity model along the Pacific coast and in the Cascade Range. A potential explanation for these differences is that the areas where summer activity predicts additional suitable habitat have a more continental climate with a wider range of daily temperatures. The mean summer temperature in these areas is relatively high, rendering them unsuitable by the temperature model. However, given the wide daily temperature range, there are enough hours in a day where Niche Mapper predicts activity is possible, resulting in these areas being considered suitable by the activity model. Conversely, the Pacific coastline and lower elevations of the Cascade Range have a more moderate climate, buffered by proximity to the ocean. The mean temperatures are not as high (allowing these areas to be considered suitable by the temperature model), but the reduced daily temperature range does not provide enough hours where Niche Mapper predicts surface activity is possible for these areas to be considered suitable by the activity model.

Similarly, for predictions under future climates, model divergences become more pronounced in the northern latitudes of the study area. For example, under the moderate-warming scenario, the activity + winter cold model predicted 2,150 $km^2$ less suitable habitat than the temperature + winter cold model below 40° latitude, but 19,376 $km^2$ more habitat above 40° latitude. Under the warmest future scenario, the activity + winter cold model predicted 2,446 $km^2$ more suitable habitat below 40° latitude but 43,195 $km^2$ more habitat above 40° latitude. At higher latitudes, longer day lengths in summer allow pikas to make up for activity time lost due to thermoregulatory retreats below the surface during the hottest part of the day; these longer day lengths thereby provide adequate time for foraging and haying. Thus, in terms of a pika's ability to be active, not all locations with the same mean summer temperature are functionally equivalent, and the effect of warmer maximum temperatures in the future may be buffered

through behavioral thermoregulation. This is a concept that becomes evident and is captured using mechanistic modeling but would be harder to detect using a purely correlative approach.

*Hindcasting suggests niche conservatism and instills confidence in future predictions*

In an important model-validation step not taken in many SDM studies, we show that the models built under current climatic conditions can be used to predict distributions under different climatic conditions through hindcasting. In contrast to Martínez-Meyer *et al.* (2004), who found that ecological niche models built using present-day pika locations poorly predicted LGM fossil locations, but similar to Galbreath *et al*. (2009), we found evidence of niche conservatism when hindcasting models to the LGM. The models missed only three to five of 49 fossil locations in the LGM. We note that across the entire study area, the models perhaps overpredict actual suitability. There was substantial extrapolation with respect to the winter cold input in the northern portion of the study area (Fig. S7), and we used Maxent's clamping option; thus, cold temperatures may have limited pika distributions in the LGM more than the coldest conditions in the current climate do. Indeed, Galbreath *et al*. (2009) used a full suite of bioclimatic variables in their hindcasting and did not predict the same extent of suitability in the LGM. However, Galbreath *et al*. (2009) appear to have missed a number of fossil locations that our models do predict as suitable. Furthermore, for the purposes of this work, which is focused on warm temperatures as the key driver of pika distributions, the most-informative regions of the LGM hindcasting are along the southern edges of predicted distributions. These are the areas where warm temperatures are limiting habitat suitability, and our models are in fact discriminating in these areas.

The models also accurately predicted range contraction from the LGM to the MH. Among the MH fossil locations, Pintwater Cave was the only MH/LH fossil location that no

model predicted suitable habitat within 3 km during the MH. We note that Grayson (2005) questioned pika persistence at this site in the Holocene, and these modeling results also suggest that these fossils might be erroneously dated. The ability of these models to be accurately applied to both current climate conditions and two past climate scenarios provides increased confidence in their ability to predict the effects of future climate warming, assuming that future climate change will not lead to no-analog niche dynamics (e.g., Veloz *et al*., 2012).

*Benefits of combining modeling approaches*

These results illustrate the value of using multiple modeling approaches when predicting species distributions. Mechanistically modeling a direct effect of warmer temperatures on organisms is theoretically more reliable than relying solely on climate correlations when extrapolating to novel conditions (Kearney & Porter, 2009; Elith *et al.*, 2010; Franklin, 2013). However, we were unable to test whether a mechanistic model is in fact more reliable when predicting pika distribution changes in response to climates markedly warmer than today. We do not have locations for pikas under such conditions and thus no way to evaluate whether one model performed better. Nonetheless, utilizing two modeling approaches can help to corroborate predicted trends and bracket the magnitude of potential habitat losses. Here, there is increased confidence in the large areas of habitat loss predicted by both models (Kearney *et al.*, 2010; Meineri *et al.*, 2015; Briscoe *et al.*, 2016). Meanwhile, the mechanistic model predictions identified additional areas that may remain suitable under warmer conditions, areas that should be considered in management planning (e.g., for identifying habitats to conserve in order to protect current populations or as translocation sites).

Integration with a correlative approach also improved interpretation of Niche Mapper's mechanistic predictions. Maxent's statistical framework allowed a mechanistic output with no

known threshold value (activity hours) to be converted into an index of habitat suitability without the need for a presence/absence data set. Furthermore, the importance of summer activity as a limiting process likely varies across the pika's range. Activity model predictions were improved by adding a winter-cold variable, which modified the importance of summer activity, expanding and contracting suitability predictions in logical ways. Areas where pikas currently exist with summer activity times slightly below the suitability threshold and milder winters were predicted as unsuitable by the activity baseline model, but suitable by the activity + winter cold model. This suggests that lower summer activity may be sufficient to facilitate pika persistence where winters are milder, potentially due to a longer growing season or reduced energetic costs in the winter (*sensu* Varner & Dearing, 2014, who found that haypile size correlated with winter duration). In contrast, areas with summer activity levels just above the threshold and with colder winters where pikas are not found were predicted as suitable by the activity baseline model, but unsuitable by the activity + winter cold model

We recognize that the baseline + winter cold models performed slightly worse in the hindcasting tests than the baseline models. However, that performance needs to be balanced against the uncertainty and reduced resolution of climate reconstructions for past epochs and the superior performance of these models under current climate conditions where there is less uncertainty regarding the climate data. Given these considerations, we do not believe the modest decline in performance in the hindcasting is reason to conclude that these models are worse than the baseline models.

Lastly, incorporating a mechanistic model also allows investigations of outlying areas that do not fit general distribution patterns found at the landscape level. For example, no model predicted suitable habitat in low-elevation lava-flow landscapes where pikas are known to exist

(e.g., Craters of the Moon and Lava Beds National Monuments, Newberry National Volcanic Monument; Jeffress *et al.*, 2013; Shinderman 2015; Ray *et al.*, 2016). One possible explanation is that surface connections to subsurface reservoirs of cool air and ice found in the lava tubes creates cooler surface microclimates around these connections than predicted using macroclimate data (Shinderman, 2015; Ray *et al.*, 2016). Another possible explanation is that these populations may have different morphological characteristics. Hall & Bowlus (1938) report that pikas in Craters of the Moon are smaller than neighboring mountain populations, and Moyer-Horner *et al.* (2015) illustrated the importance of body size and fur properties to a model pika's ability to maintain activity levels in warm temperatures. Indeed, if pikas are modeled with 10-20% reductions in body size and/or fur thickness, summer activity in areas of Craters of the Moon and Lava Beds National Monuments where pikas are found are predicted to be above the 1132-hour threshold identified for persistence at Great Basin sites (Fig. S10). Clearly, more detailed and comprehensive comparative measurements would be required to fully evaluate this idea. Nonetheless, this example illustrates how biophysical models like Niche Mapper can incorporate intraspecific phenotypic variation into species distribution models, an important contribution that mechanistic models can provide (Buckley, 2008; Kolbe *et al.*, 2010; Boyles *et al.*, 2011).

Another area where the models did not predict suitable habitat but where pikas are known to exist was at the very bottom of the Columbia River Gorge. This is a unique habitat with abundant shade on the talus and moss covering the talus, providing thermal buffering of surface microclimate temperatures (Varner & Dearing, 2014). For simplicity, the activity model assumed a bare rock surface and no shade, which is characteristic of the majority of pika habitat elsewhere in the species' range. However, when the substrate is changed in Niche Mapper's microclimate model to assume a shaded, moss-covered surface and region-specific cloud cover is considered,

predicted activity hours at Gorge locations of pika detection increased by up to 40% (Fig. S11) and results in more areas being classified as suitable habitat (Fig. S12). This ability to investigate the thermal buffering effects of specific microhabitats has important implications for incorporating the synergistic relationship of habitat alteration and climate change into predictions of species distribution changes (*sensu* Kearney, 2013).

*Broad applicability and relevance*

Whether, and how accurately, SDMs can be used to make accurate predictions of species responses under future climate conditions are topics of extensive debate and research. One way forward is to compare different modelling approaches to better understand the reliability of predictions under different conditions. We recognize that interspecific interactions and non-climatic, abiotic factors such as habitat quality and connectivity are also important to predicting current occupancy and future persistence (e.g., Schwalm *et al.*, 2016). However, climate remains a principal driver in many SDMs, and the primary goal of this work is to present a generally-applicable approach to endotherm SDM development through mechanistic modeling of a more proximal relationship between climate and species distribution.

For mechanistic models to be more widely used conservation tools, they must be able to be easily and quickly tailored for a range of species (Evans *et al.*, 2015). Heat-balance biophysical models like Niche Mapper are based on heat-transfer principles and thermodynamic laws that apply to any species. When being used to predict the impacts of chronic heat stress (e.g., activity restriction) or cold stress (e.g., increased food requirements), such models only require a few and easily obtainable inputs beyond those required for a purely correlative model to be tailored for specific species: animal size and body-part dimensions, fur properties, resting metabolic rate, and body temperature. This information can often be found in the existing

literature or estimated from well-established allometric equations. Thus, while we use pikas as an example, this modeling approach is broadly applicable to other species. In fact, its ability to investigate the effects of trait variation and habitat characteristics on animal performance may make the approach more valuable for focal species with greater intraspecific phenotypic variation or that are more habitat generalists than pikas. As illustrated by this work, incorporation of mechanism with other environmental variables and distribution data helps to provide a more complete understanding of how species may be limited by climate, an understanding that is necessary to inform climate-adaptation actions, management strategies, and conservation plans.

## ACKNOWLEDGEMENTS

We thank Chris Lowrey, Donelle Schwalm, and one anonymous reviewer for insightful reviews that improved this work. We thank Chris Ray, Tom Rodhouse, and Matt Shinderman for sharing data on pika presence locations in lava-dominated landscapes. PDM thanks the UW-Madison Zoology Department for one summer of graduate research funding in support of this work. NJB was supported by NERP Environmental Decisions Hub. Data collection on Great Basin pikas benefited from funding by the Great Basin LCC, Kosciuszko Foundation, Wilburforce Foundation, and World Wildlife Fund. Any use of trade, firm, or product names is for descriptive purposes only and does not imply endorsement by the U.S. Government.

## LITERATURE CITED

1. Allouche O, Tsoar A, Kadmon R (2006) Assessing the accuracy of species distribution models: prevalence, kappa and the true skill statistic (TSS). Journal of Applied Ecology, **43**, 1223-1232.
2. Araújo MB, Alagador D, Cabeza M, Nogués-Bravo D, Thuiller W (2011) Climate change threatens European conservation areas. Ecology Letters, **14**, 484-492.

3. Beever EA, Brussard PF, Berger J (2003) Patterns of apparent extirpation among isolated populations of pikas (*Ochotona princeps*) in the Great Basin. Journal of Mammalogy, **84**, 37-54.
4. Beever EA, Wilkening JL, McIvor DE, Weber SS, Brussard PF (2008) American pikas (*Ochotona princeps*) in Northwestern Nevada: A newly discovered population at a low-elevation site. Western North American Naturalist, **68**, 8-14.
5. Beever EA, Ray C, Mote PW, Wilkening JL (2010) Testing alternative models of climate-mediated extirpations. Ecological Applications, **20**, 164-178.
6. Beever RA, Ray C, Wilkening JL, Brussard PF, Mote PW (2011) Contemporary climate change alters the pace and drivers of extinction. Global Change Biology, **17**, 2054-2070.
7. Beever EA, Dobrowski SZ, Long J, Mynsberge AR, Piekielek NB (2013) Understanding relationships among abundance, extirpation, and climate at ecoregional scales. Ecology, **94**, 1563-1571.
8. Beever EA, O'Leary J, Mengelt C *et al.* (2016) Improving conservation outcomes with a new paradigm for understanding species' fundamental and realized adaptive capacity. Conservation Letters, **9**, 131-137.
9. Bellard C, Bertlesmeier C, Leadley P, Thuiller W, Courchamp F (2012) Impacts of climate change on the future of biodiversity. Ecology Letters, **15**, 365-377.
10. Boyles JG, Seebacher F, Smit B, McKechnie AE (2011) Adaptive thermoregulation in endotherms may alter responses to climate change. Integrative and Comparative Biology, **51**, 676-690.

11. Briscoe NJ, Kearney MR, Taylor C, Brendan WA (2016) Unpacking the mechanisms captured by a correlative SDM to improve predictions of a climate refugia. Global Change Biology, **22**, 2425-2439.
12. Buckley LB (2008) Linking traits to energetics and population dynamics to predict lizard ranges in changing environments. American Naturalist, **171**, E1-E19.
13. Buckley LB, Urban MC, Angilletta MJ, Crozier LG, Rissler LJ, Sears MW (2010) Can mechanism inform species' distribution models? Ecology Letters, **13**, 1041-1054.
14. Buckley LB, Waaser SA, MacLean HJ, Fox R (2011) Does including physiology improve species distribution model predictions of responses to recent climate change? Ecology, **92**, 2214-2221.
15. Buckley LB, Hurlbert AH, Jetz W (2012) Broad-scale ecological implications of ectothermy and endothermy in changing environments. Global Ecology and Biogeography, **21**, 873-885.
16. Cahill AE, Aiello-Lammens ME, Fisher-Reid MC *et al.* (2013) How does climate change cause extinction? Proceedings of the Royal Society B, **280**, 1-9.
17. Calkins MT, Beever EA, Boykin KG, Frey JK, Andersen MC (2012) Not-so-splendid isolation: modeling climate-mediated range collapse of a montane mammal *Ochotona princeps* across numerous ecoregions. Ecography, **35**, 780-791.
18. Ceia-Hasse A, Sinervo B, Vicente L, Pereira HM (2014) Integrating ecophysiological models into species distribution projections of European reptile range shifts in response to climate change. Ecography, **37**, 679-688.

19. Collins GH, Bauman BT (2012). Distribution of low-elevation American pika populations in the Northern Great Basin. Journal of Fish and Wildlife Management, **3**, 311-318.

20. Daly C, Halbleib M, Smith JI *et al.* (2008) Physiographically sensitive mapping of climatological temperature and precipitation across the conterminous United States. International Journal of Climatology, **28**, 2031-2064.

21. Dearing MD (1997). The function of haypiles of pikas (*Ochotona princeps*). Journal of Mammalogy, **78**, 1156-1163.

22. Du Plessis KL, Martin RO, Hockey PAR, Cunningham SJ, Ridley AR (2012) The costs of keeping cool in a warming world: implications of high temperatures for foraging, thermoregulation and body condition of an arid-zone bird. Global Change Biology, **18**, 3063-3070.

23. Elith J, Graham CH, Anderson RP, *et al.* (2006) Novel methods improve prediction of species' distributions from occurrence data. Ecography, **29**, 129-151.

24. Elith J, Leathwick JR (2009) Species distribution models: ecological explanation and prediction across time and space. Annual Review of Ecology, Evolution, and Systematics, **40**, 677-697.

25. Evans TG, Diamond SE, Kelley MW (2015) Mechanistic species distribution modelling as a link between physiology and conservation. Conservation Physiology, **3**, 1-16.

26. Franklin, J (2010) Moving beyond static species distribution models in support of conservation biogeography. Diversity and Distributions, **16**, 321-330.

27. Fuentes M, Porter WP (2013) A new approach to model soil temperature: using microclimate models to predict the impacts of climate change on sea turtles. Ecological Modeling, **251**,150–157.

28. Galbreath KE, Hafner DJ, Zamudio KR (2009) When cold is better: climate-driven elevation shifts yield complex patterns of diversification and demography in an alpine specialist (American pika, *Ochotona princeps*). Evolution, **63**, 2848-2863.

29. Grayson DK (2005) A brief history of Great Basin pikas. Journal of Biogeography, **32**, 2103-2111.

30. Guisan A, Thuiller W (2005) Predicting species distribution: offering more than simple habitat models. Ecology Letters, **8**, 993-1009.

31. Guisan A, Tingley R, Baumgartner JB *et al.* (2013) Predicting species distributions for conservation decisions. Ecology Letters, **16**, 1424-1435.

32. Hafner DJ (1994) Pikas and permafrost: post-Wisconsin historical zoogeography of *Ochotona* in the southern Rocky Mountains, U.S.A. Arctic and Alpine Research, **26**, 375-382.

33. Hafner DJ, Sullivan RM (1995) Historical and ecological biogeography of Neartic pikas (Lagomorpha: Ochotonidae). Journal of Mammalogy, **76**, 302-321.

34. Hafner DJ, Smith AT (2010) Revision of the subspecies of the American pika, *Ochotona princeps* (Lagomorpha: Ochotondae). Journal of Mammalogy, **91**, 401-417.

35. Hall ER, Bowlus HL (1938) A new pika (Mammalian genus *Ochotona*) from southeastern Idaho with notes on near-by subspecies. University of California Publications in Zoology, **42**, 335-340.

36. Hayes AR, Huntly NJ (2005) Effect of wind on the behavior and call transmission of pikas (*Ochotona princeps*). Journal of Mammalogy, **86**, 974-981.

37. Hijmans RJ, Cameron SE, Parra JL, Jones PG, Jarvis A (2005) Very high resolution interpolated climate surfaces for global land areas. International Journal of Climatology, **25**, 1965-1978.

38. IPCC (2013) Contribution of Working Group I to the Fifth Assessment Report of the Intergovernmental Panel on Climate Change. In: Climate Change 2013: The Physical Science Basis (eds Stocker TF, Qin D, Plattner GK, Tignor M, Allen SK, Boschung J, Nauels A, Xia Y, Bex V, Midgley PM), pp. 1-1535. Cambridge University Press, Cambridge, United Kingdom and New York, NY, USA.

39. Jeffress MR, Rodhouse TJ, Ray C, Wolff S, Epps CW (2013) The idiosyncrasies of place: geographic variation in the climate-distribution relationships of the American pika. Ecological Applications, **23**, 864-878.

40. Karasov WH (1992) Daily energy expenditure and the cost of activity in mammals. American Zoologist, **32**, 238-248.

41. Kearney M (2013) Activity restriction and the mechanistic basis for extinctions under climate warming. Ecology Letters, **16**, 1470-1479.

42. Kearney M, Porter W (2009) Mechanistic niche modeling: combining physiological and spatial data to predict species' ranges. Ecology Letters, **12**, 1-17.

43. Kearney MR, Wintle BA, Porter WP (2010) Correlative and mechanistic models of species distribution provide congruent forecasts under climate change Conservation Letters, **3**, 203-213.

44. Kearney MR, Isaac AP Porter WP (2014) microclim: Global estimates of hourly microclimate based on long-term monthly climate averages. Nature Scientific Data, **1**, 140006 doi: 10.1038/sdata.2014.6

45. Kolbe JJ, Kearney MR, Shine R (2010) Modelling the consequences of thermal trait variation for the cane toad invasion of Australia. Ecological Applications, **20**, 2273-2285.

46. La Sorte FA, Jetz W (2010) Avian distributions under climate change: towards improved projections. The Journal of Experimental Biology, **213**, 862-869.

47. Levy O, Dayan T, Porter WP, Kronfeld-Schor N. (*in press)* Foraging activity pattern is shaped by water loss rates in a diurnal desert rodent. American Naturalist.

48. Liu C, Berry PM, Dawson TP, Pearson RG (2005) Selecting thresholds of occurrence in the prediction of species distributions. Ecography, **28**, 385-393.

49. Liu C, White M, Newell G (2013) Selecting thresholds for the prediction of species occurrence with presence-only data. Journal of Biogeography, **40**, 778-789.

50. Long RA, Bowyer RT, Porter WP, Mathewson PD, Monteith KL, Kie JG (2015) Behaviour and nutritional condition buffer a large-bodied endotherm against direct and indirect effects of climate. Ecological Monographs, **84**, 513-532.

51. MacArthur RA, Wang LCH (1973) Physiology of thermoregulation in the pika, *Ochotona princeps*. Canadian Journal of Zoology, **51**, 11-16.

52. MacArthur RA, Wang LCH (1974) Behavioral thermoregulation in the pika *Ochotona princeps*: a field study using radiotelemetry. Canadian Journal of Zoology, **52**, 353-358.

53. Martínez-Meyer E, Peterson WT, Hargrove WW (2004) Ecological niches as stable distributional constraints on mammal species, with implications for Pleistocene

extinctions and climate change projections for biodiversity. Global Ecology and Biogeography, **13**, 305-314.

54. Mathewson PD, Porter, WP (2013) Simulating polar bear energetics during a seasonal fast using a mechanistic model. PLoS One, **8**, e72863.
55. Mead J (1987) Quaternary records of pika, *Ochotona*, in North America. Boreas, **16**, 165-171.
56. Millar CL, Westfall, RD (2010) Distribution and climatic relationships of the American Pika (*Ochotona princeps*) in the Sierra Nevada and Western Great Basin, U.S.A.; Periglacial landforms as refugia in warming climates. Arctic, Antarctic, and Alpine Research, **42**, 76-88.
57. Morelli TL, Smith AB, Kastely CR, Mastroserio I, Moritz C, Beissinger SR (2012) Anthropogenic refugia ameliorate the severe climate-related decline of a montane mammal along its trailing edge. Proceedings of the Royal Society B, **279,** 4279-4286.
58. Morin X, Thuiller W (2009) Comparing niche- and process-based models to reduce prediction uncertainty in species range shifts under climate change. Ecology, **90**, 1301-1313.
59. Moritz C, Patton JL, Conroy CJ, Parra JL, White GC, Beissinger SR (2008) Impact of a century of climate change on small-mammal communities in Yosemite National Park, USA. Science, **322**, 261-264.
60. Moyer-Horner L, Mathewson PD, Jones G, Kearney MR, Porter WP (2015) Modeling behavioral thermoregulation in a climate change sentinel. Ecology and Evolution, **5,** 5810-5822.

61. Oswald SA, Arnold JM (2012) Direct impacts of climatic warming on heat stress in endothermic species: seabirds as bioindicators of changing thermoregulatory constraints. Integrative Zoology, **7**, 121-16.

62. Parmesan C, Yohe G (2003) A globally coherent fingerprint of climate change impacts across natural systems. Nature, **421**, 37-42.

63. Phillips SJ, Anderson RP, Schapire RE (2006) Maximum entropy modeling of species geographic distributions. Ecological Modelling, **190**, 231-259.

64. Phillips SJ, Duki M, Elith J, Graham CH, Lehmann A, Leathwick J, Ferrier S (2009) Sample selection bias and presence-only distribution models: implications for background and pseudo-absence data. Ecological Applications, **19**,181-197.

65. Porter WP, Budaraju S, Stewart WE, Ramankutty N (2000) Calculating climate effects on birds and mammals: impact on biodiversity, conservation, population parameters, and global community structure. American Zoologist, **40**, 597-630.

66. Porter WP, Munger JC, Stewart WE, Budaraju S, Jaeger J (1994) Endotherm energetics: from a scalable individual-based model to ecological applications. Australian Journal Zoology, **42**, 125–162.

67. Porter WP, Mitchell JW (2006) Method and system for calculating the spatial-temporal effects of climate and other environmental conditions on animals. http://www.warf.org/technologies.jsp?ipnumber=P01251US

68. Porter WP, Kearney MK (2009) Size, shape, and the thermal niche of endotherms. Proceedings of the National Academy of Sciences USA, **106**, S19666-S19672.

69. Ray C, Beever EA, Rodhouse T (2016) Distribution of a climate-sensitive species at an interior range margin. Ecosphere. *In press.*

70. Rowland EL, Davison JE, Graumlich LJ (2011) Approaches to evaluating climate change impacts on species: a guide to initiating the adaptation planning process. Environmental Management, **47**, 322-337.

71. Schwalm D, Epps CW, Rodhouse TJ, Monahan WB, Castillo JA, Ray C and Jeffress MR (2016) Habitat availability and gene flow influence diverging local population trajectories under scenarios of climate change: a place-based approach. Global Change Biology, **22**, 1572-1584.

72. Schwartz MW (2012) Using niche models with climate projections to inform conservation management decisions. Biological Conservation, **155**, 149-156.

73. Sexton JP, McIntyre PJ, Angert AL, Rice KJ (2009) Evolution and ecology of species range limits. Annual Review of Ecology, Evolution, and Systematics, **40**, 415-436.

74. Shinderman M (2015) American pika in a low-elevation lava landscape: expanding the distribution of a temperature-sensitive species. Ecology and Evolution, **5**, 3666-3676.

75. Sinervo B, Méndez-de-la-Cruz F, Miles DB *et al.* (2010) Erosion of lizard diversity by climate change and altered thermal niches. Science, **328**, 894-899.

76. Smith AT (1974) The distribution and dispersal of pikas: influences of behavior and climate. Ecology, **55**, 1368-1376.

77. Staudinger MD, Carter SL, Cross MS *et al.* (2012) Biodiversity in a changing climate: a synthesis of current and projected trends in the US. Frontiers of Ecology and Environment, **11**, 465-473.

78. Stewart JAE, Perrine JD, Nichols LB, *et al.* (2015) Revisiting the past to foretell the future: summer temperature and habitat area predict pika extirpations in California. Journal of Biogeography, **42**, 880-890.

79. Swets JA (1988) Measuring the accuracy of diagnostic systems. Science, **240**, 1285-1293.

80. Thomas CD (2010) Climate, climate change and range boundaries. Diversity and Distributions, **16**, 488-495.

81. Tomlinson S, Arnall SG, Munn A, Bradshaw SD, Maloney SK, Dixon KW, Didham RK (2014) Applications and implications of ecological energetics. Trends in Ecology & Evolution, **29**, 280-290.

82. Tracy CR, Welch WR, Porter WP. 1980. Properties of Air, A Manual for Use in Biophysical Ecology. Technical Report No. 1. Laboratory for Biophysical Ecology. University of Wisconsin, Madison. 41 pp.

83. Tyser RW (1980) Use of substrate for surveillance behaviors in a community of talus slope mammals. The American Midland Naturalist, **104**, 32-38.

84. Varner J**,** Dearing MD (2014) Dietary plasticity in pikas (*Ochotona princeps*) as a strategy for novel resource landscapes. *Journal of Mammalogy*, **95**, 72–81.

85. Varner J**,** Dearing MD (2014) The importance of biologically relevant microclimates in species distribution models. *PLoS ONE,* **9**, e104648

86. Veloz S, Williams JW, Blois JL, He F, Otto-Bliesner B, Liu Z (2012) No-analog climate and shifting realized niches during the late Quaternary: implications for 21$^{st}$-century predictions by species distribution models. Global Change Biology, **18**, 1698-1713.

87. Welbergen JA, Klose SM, Markus N, Eby P (2008) Climate change and the effects of temperature extremes on Australian flying-foxes. Proceedings of the Royal Society B, **275**, 419-425.

88. Wilkening JL, Ray C, Beever EA, Brussard PF (2011) Modeling contemporary range retraction in Great Basin pikas (*Ochotona princeps*) using data on microclimate and microhabitat. Quaternary International, **235**, 77-88.
89. Yandow LH, Chalfoun AD, Doak DF (2015) Climate tolerances and habitat requirements jointly determine elevational distribution of the American pika (*Ochotona princeps*) with implications for climate change effects. PLoS One, **10**, e0131082.

## SUPPORTING INFORMATION

### *Additional Details on Niche Mapper Operations*

Niche Mapper consists of two sub-models: 1) a microclimate model that calculates environmental conditions at animal height, and 2) a biophysical/behavioral animal model (Figure 1). The microclimate model calculates the hourly profiles of air, temperature, wind speed, relative humidity, and solar and long wavelength thermal radiation that the animal experiences (Fuentes & Porter 2013). To get hourly values, the model fits a sinusoidal curve to user-specified maximum and minimum daily air temperatures, wind speeds, cloud cover, and relative humidity to estimate hourly values. Hourly clear sky solar radiation is calculated based on date and geographic location, before being adjusted to account for any cloud cover and overhead vegetation.

Long-wavelength thermal radiation from clear sky and clouds are computed separately using empirical air temperature correlations (McCullough & Porter 1971). Thermal radiation from the ground is computed from the above-ground climate, described above, and hourly substrate temperatures. Deep soil temperature is taken to be the mean annual temperature and is the lower boundary condition for the hourly soil temperature profile. The soil temperature is then

derived from numerical solutions of the one dimensional finite difference transient heat balance equation for the ground.

Using the information provided by the microclimate model, the animal model then calculates radiative ($Q_{rad}$), convective ($Q_{conv}$), solar ($Q_{sol}$), and evaporative (respiratory, $Q_{resp,}$ and cutaneous, $Q_{evap}$) heat fluxes between the animal and its microenvironment to solve a heat balance equation (Eq. 1). This equation is used to estimate metabolic rate, $Q_{gen,}$ that allows the animal to maintain its core temperature.

$$Q_{gen} - Q_{resp} - Q_{evap} = Q_{fur} = Q_{rad} + Q_{conv} - Q_{sol} \quad (1)$$

For an animal to be in thermal steady state with its environment, metabolic heat production ($Q_{gen}$), less evaporative heat loss from the respiratory system ($Q_{resp}$) and the skin ($Q_{evap}$), must equal heat flow through the fur via conduction and radiation ($Q_{fur}$), and the net heat flux with the outside environment ($Q_{rad} + Q_{conv} - Q_{sol}$). A metabolic rate that does not balance the equation will result in net heat loss or heat gain, rendering the animal unable to maintain its body temperature if this imbalance persists. No transient component, $Q_{st}$, in the heat balance is used here, because the pika has such a short time constant, it is effectively in steady state at all times.

The heat balance equation is solved to provide the metabolic rate for the animal that allows it to maintain its core temperature for every hour of each model day. If the metabolic rate falls outside the user-specified target metabolic rate (i.e., basal metabolic rate x activity multiplier), behavioral and/or physiological thermoregulatory options are engaged to prevent overheating in warm conditions or to minimize metabolic expenditure on heat production in cold conditions. The heat balance equation is re-solved after each thermoregulatory change until a balance is reached at the target metabolic rate or until thermoregulatory options are exhausted. If

thermoregulatory options are insufficient to allow a metabolic rate at or above the activity level, the animal is assumed to have its activity restricted for that hour. The number of hours for which activity can be maintained are then summed for each model day, and then multiplied by the number of days in the month the model day is representing. Total number of potential activity hours for June, July, August, and September were then summed to get the summer activity time used in the analyses.

*Additional Methods on Selection of Presence and Background Points for Maxent Models*

Current pika presence locations used to build the species distribution models were obtained from the online zoological record databases Global Biodiversity Information Facility (GBIF, www.gbif.org) and VertNet (www.vertnet.org). We limited searches for locations in the United States from 1981 to present to align with the temporal extent of the climate data. Additional locations to fill in gaps of known occurrence locations were obtained from studies described in: Beever *et al.* (2003), Simpson (2009), Collins & Bauman (2012), Rodhouse *et al.* (2010), Moyer-Horner *et al.* (2015), Stewart *et al.* (2015), Shinderman (2015), Ray *et al.* (2016), and Beever *et al.* (*in review*), as well as Beever (*unpublished data*). After paring down this list to only include one presence per 800 m grid cell, we had 616 unique pika presence locations that were used to develop the distribution models in Maxent.

When defining background points for Maxent to use we used the target group background approach to minimize the effect of sampling bias on predictions (Phillips et al. 2009). This approach corrects for biased presence data by using occurrence points of other species observed using similar methods as background points, which are assumed to have the same bias as the target species occurrence records. Here, we used occurrence points for all terrestrial mammals in GBIF and VertNet from 1981 to present from the western United States.

We retained one location per 800m grid cell, then randomly selected 10,000 of these points, weighting selection to account for the fact that northern latitude cells are larger than lower latitude cells in this wide (>12°) latitude span.

*Additional Details on Spatial Data Acquisition*

Current climate data include monthly maximum and minimum temperatures and precipitation from 1981-2000. These data were downloaded from the PRISM Climate Group at 800 m resolution (http://www.prism.oregonstate.edu/; Daly *et al.*, 2008). Climate data for the Last Glacial Maximum ("LGM"; ~22,000 years b.p.; ~4-km resolution at the equator) and the mid-Holocene ("MH" ~6,000 years b.p.; ~800-m resolution at the equator) were obtained from the WorldClim database (www.worldclim.org; Hijmans *et al.*, 2005). We used the CCSM4 and MIROC-ESM global circulation model (GCM) datasets from both time periods individually and averaged. The results presented are from models using the averaged data.

GCM datasets for 2070 climate conditions used in the Fifth Assessment IPCC report were obtained from the WorldClim database at 800 m resolution. The U.S. Geological Survey's National Climate Change Viewer (www.usgs.gov/climate_landuse/clu_rd/nccv.asp) was used to identify models predicting conservative (MRI-CGCM3, representative concentration pathway 2.6), moderate (NorESM1-M, representative concentration pathway 4.5), and warmest (MIROC-ESM-CHEM, representative concentration pathway 8.5) climate-change scenarios in the western United States.

For each climate scenario, mean temperature of the warmest quarter ("mean summer temperature") and minimum temperature of the coldest month ("winter cold") were derived from the monthly temperature in R using the "biovars" function in the DISMO package.

Digital elevation models (DEM) were obtained from the Shuttle Radar Topographic Mission at 90-m resolution (http://www2.jpl.nasa.gov/srtm/index.html). From these DEMs slope and aspect were calculated using tools in ArcMap™ (ESRI, 2011). All data layers were then re-sampled as needed, to achieve a final resolution of 800-m to ensure consistency with the climate data's resolution. Slope and aspect were used in calculations of incoming solar radiation in Niche Mapper's microclimate submodel. Horizon angles were also used by the microclimate model to calculate the timing of when solar radiation begins and ends hitting the ground at a given location. Horizon angles in 15° directional increments for each pixel were calculated from the digital elevation map using GRASS GIS 7.0 (GRASS Development Team, 2015) using a 5-km maximum distance to find any obstructions.

*Additional Details on Model Evaluation Tests*

To evaluate model performance, we used area under the receiver-operator curve (AUC) and the True Skill Statistic (TSS). Receiver-operator curves are plots of sensitivity against proportion of false positives using all possible thresholds (Fielding & Bell 1997). When using presence-only data, AUC provides the probability of a higher suitability being assigned to an average presence site than to an average background site (Elith *et al*., 2006). AUC values range from 0-1 with 0.5 being no better than chance and values > 0.9 considered to be excellent models (Swets, 1988). TSS is dependent on a given threshold and is calculated as sensitivity (the proportion of correctly classified presences) plus specificity (the proportion of correctly classified absences) minus one (Allouche *et al.*, 2006). Similarly, TSS values range from 0-1, with 1 being a perfect fit.

*References*


1. Allouche O, Tsoar A, Kadmon R (2006) Assessing the accuracy of species distribution models: prevalence, kappa and the true skill statistic (TSS). Journal of Applied Ecology, **43**, 1223-1232.
2. Beever EA, Brussard PF, Berger J (2003) Patterns of apparent extirpation among isolated populations of pikas (*Ochotona princeps*) in the Great Basin. Journal of Mammalogy, **84**, 37-54.
3. Collins GH, Bauman BT (2012). Distribution of low-elevation American pika populations in the Northern Great Basin. Journal of Fish and Wildlife Management, **3**, 311-318.
4. Daly C, Halbleib M, Smith JI *et al.* (2008) Physiographically sensitive mapping of climatological temperature and precipitation across the conterminous United States. International Journal of Climatology, **28**, 2031-2064.
5. Elith J, Graham CH, Anderson RP, *et al.* (2006) Novel methods improve prediction of species' distributions from occurrence data. Ecography, **29**, 129-151.
6. Fielding AH, Bell JF (1997) A review of methods for the measurement of prediction errors in conservation presence/absence models. Environmental Conservation, **24**, 38-49.
7. Fuentes M, Porter WP (2013) A new approach to model soil temperature: using microclimate models to predict the impacts of climate change on sea turtles. Ecological Modeling, **251**,150–157.
8. ESRI (2011) ArcGIS Desktop: Release 10. Redlands, CA: Environmental Systems Research Institute.

9. GRASS Development Team (2015) Geographic Resources Analysis Support System (GRASS) Software, Version 7.0. Open Source Geospatial Foundation.
10. Hijmans RJ, Cameron SE, Parra JL, Jones PG, Jarvis A (2005) Very high resolution interpolated climate surfaces for global land areas. International Journal of Climatology, **25**, 1965-1978.
11. McCullough EM, Porter WP (1971) Computing clear day solar spectra for the terrestrial ecological environment. Ecology, **52**, 1008-1015.
12. Moyer-Horner L, Mathewson PD, Jones G, Kearney MR, Porter WP (2015) Modeling behavioral thermoregulation in a climate change sentinel. Ecology and Evolution, **5,** 5810-5822.
13. Ray C, Beever EA, Rodhouse T (2016) Distribution of a climate-sensitive species at an interior range margin. Ecosphere. *In press.*
14. Rodhouse TJ, Beever RA, Garrett LK, Irvine KM, Jeffress MR, Munts M, Ray C (2010) Distributions of American pikas in a low-elevation lava landscape: Conservation implications from the range periphery. Journal of Mammalogy, **91**, 1287-1299.
15. Shinderman M (2015) American pika in a low-elevation lava landscape: expanding the distribution of a temperature-sensitive species. Ecology and Evolution, **5**, 3666-3676.
16. Simpson WG (2009) American pikas inhabit low-elevation sites outside the species' previously described bioclimatic envelope. Western North American Naturalist, **69**, 243-250.
17. Stewart JAE, Perrine JD, Nichols LB, *et al.* (2015) Revisiting the past to foretell the future: summer temperature and habitat area predict pika extirpations in California. Journal of Biogeography, **42**, 880-890.

18. Swets JA (1988) Measuring the accuracy of diagnostic systems. Science, **240**, 1285-1293.

*Supplemental Figures and Tables*

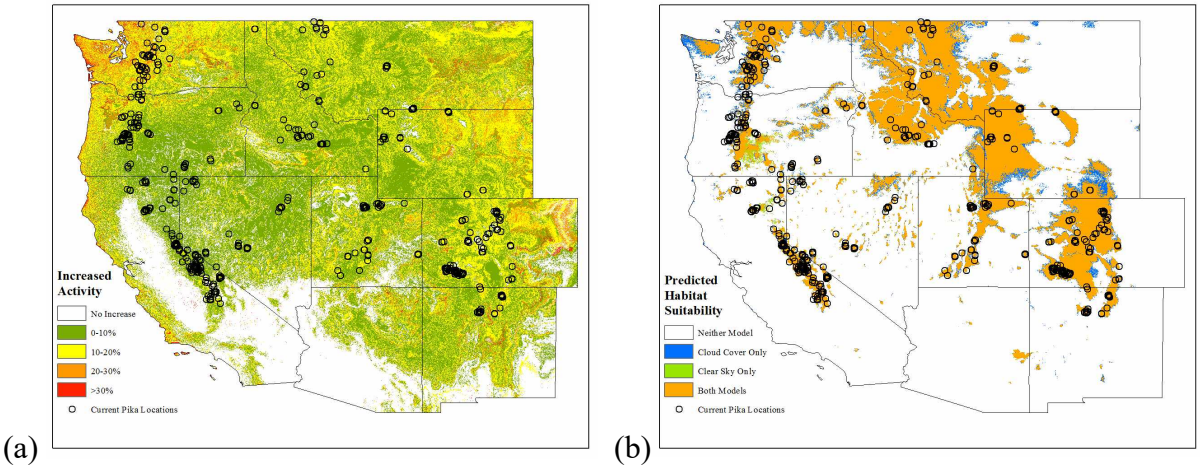


**Figure S1**. Sensitivity analysis on the effect of using cloud cover compared to assuming clear skies in Niche Mapper's activity time calculations for a) increase in activity hours (%) when cloud cover is included; and b) differences in predicted pika habitat suitability. 90% of pika locations had summer activity increases of <15% (range: 0-26%). When activity hours are converted to suitability across the landscape, including cloud cover makes little difference in areas of predicted suitability. There was 97% agreement overall in terms of suitable and unsuitable habitat predictions, and 86% agreement at locations predicted as suitable by at least one model. Cloud cover data are from New et al. (2002).

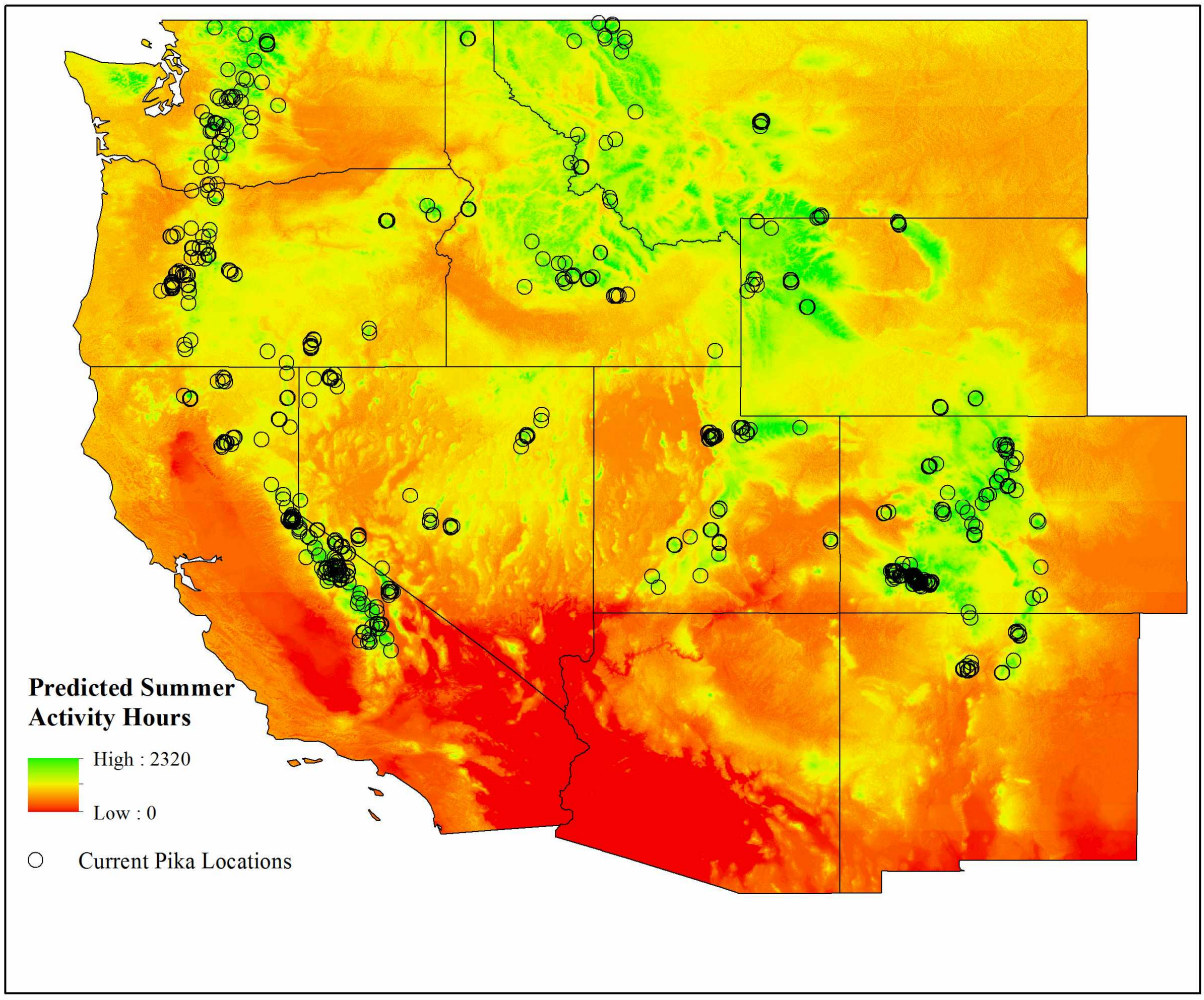


**Figure S2.** The number of activity hours predicted by Niche Mapper for pikas in the summer (June – September) across the western United States based on 1981-2010 average monthly maximum and minimum temperatures.

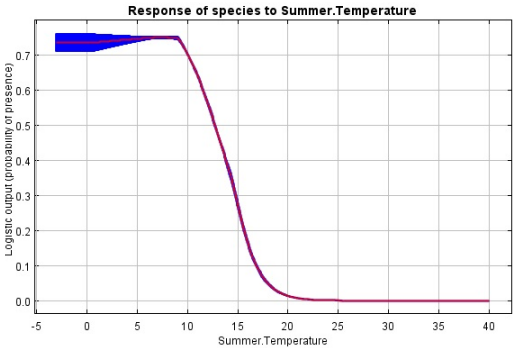


(a)

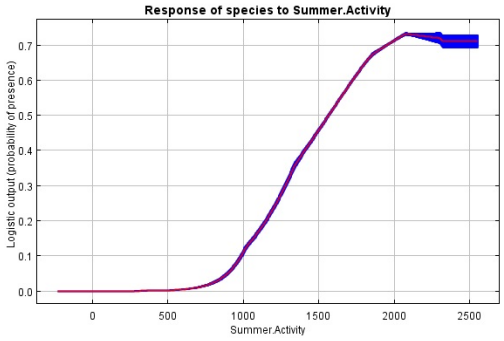


(b)

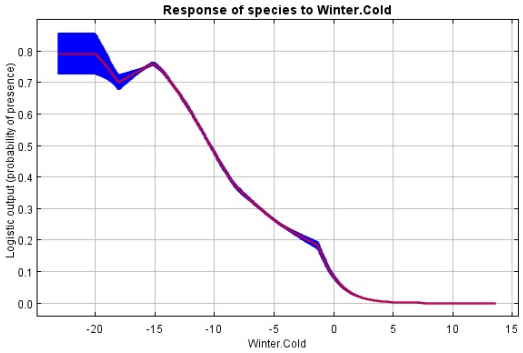


(c)

**Figure S3**. Maxent model response curves to individual variables used in the final distribution models: (a) mean summer temperatures; b) summer activity time predicted by Niche Mapper; c) minimum temperature of coldest month. This shows how predicted habitat suitability varies in response to each predictor individually. As expected, suitability decreases with increasing summer and winter temperatures, and increases with increasing activity.

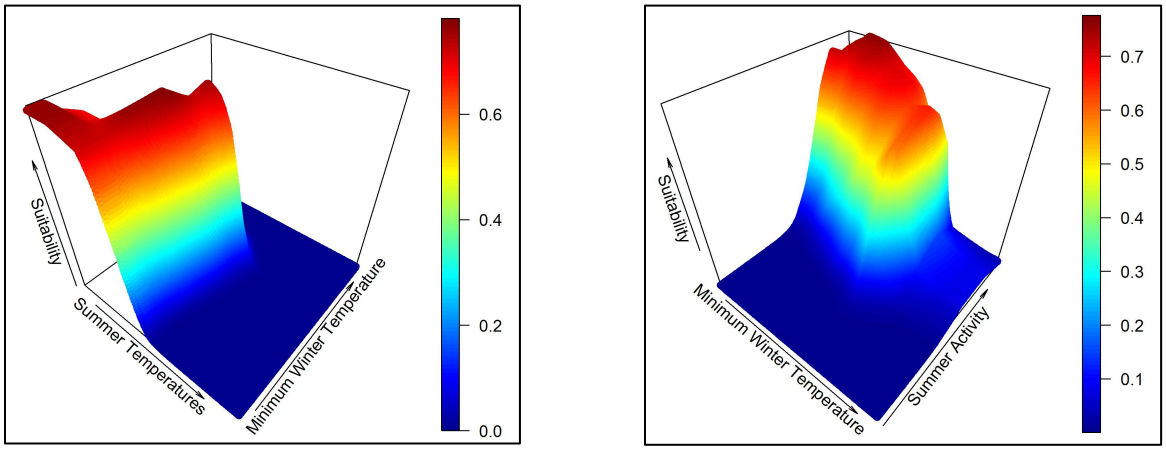


(a) (b)

**Figure S4**. Plots showing the combined effect of winter cold and summer temperature (a) or summer activity (b) on habitat suitability predicted by Maxent. Arrow directions indicate increasing temperatures or activity hours. Note the interaction between winter cold and summer activity: at moderate minimum winter temperatures, fewer summer activity hours are required for suitable habitat.

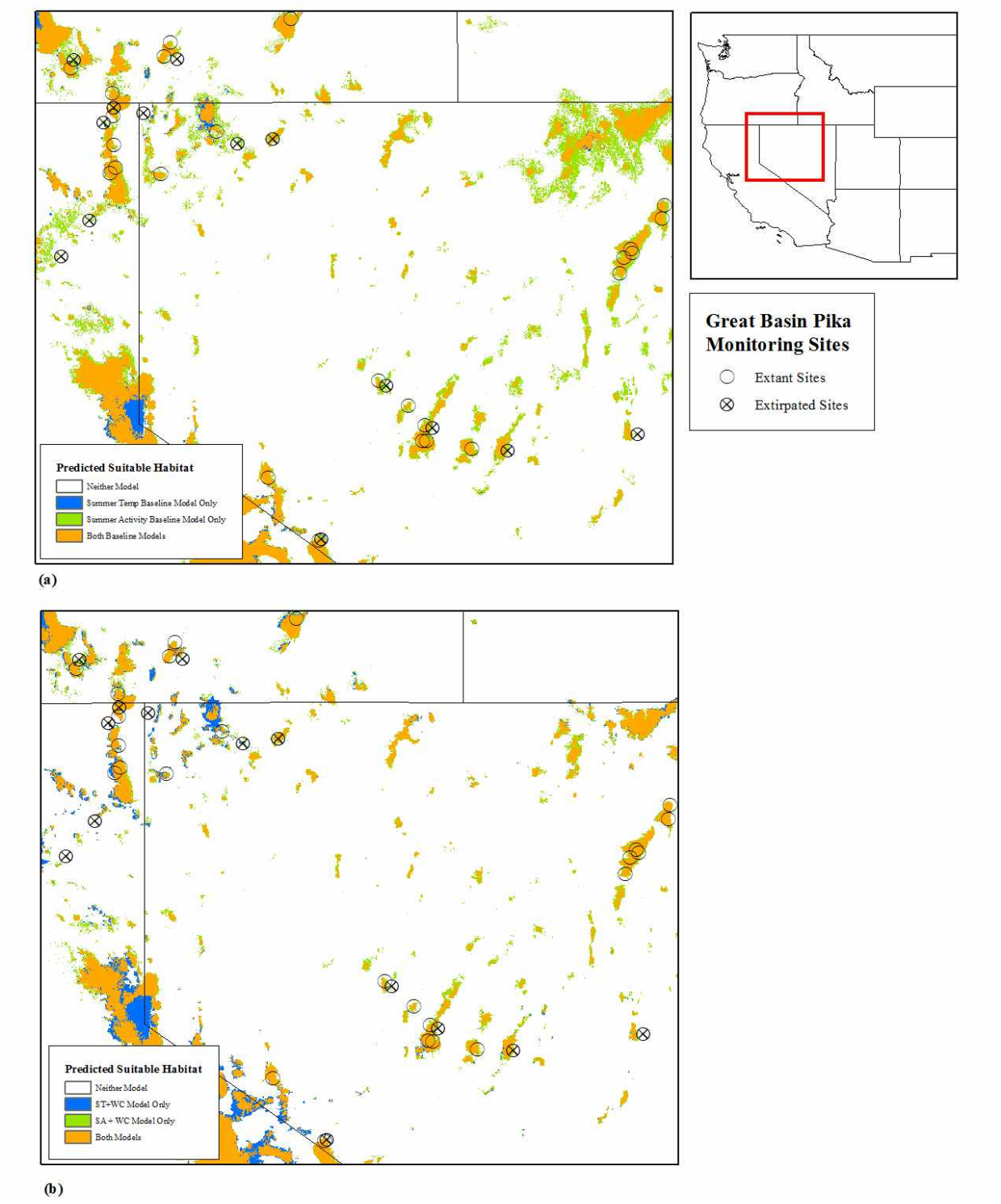


**Figure S5.** Detailed view of habitat predicted as suitable at the Great Basin pika monitoring sites by the baseline models (a) and by the models with winter cold added (b). Adding winter cold improved the models by making them more specific without reducing sensitivity to extant sites.

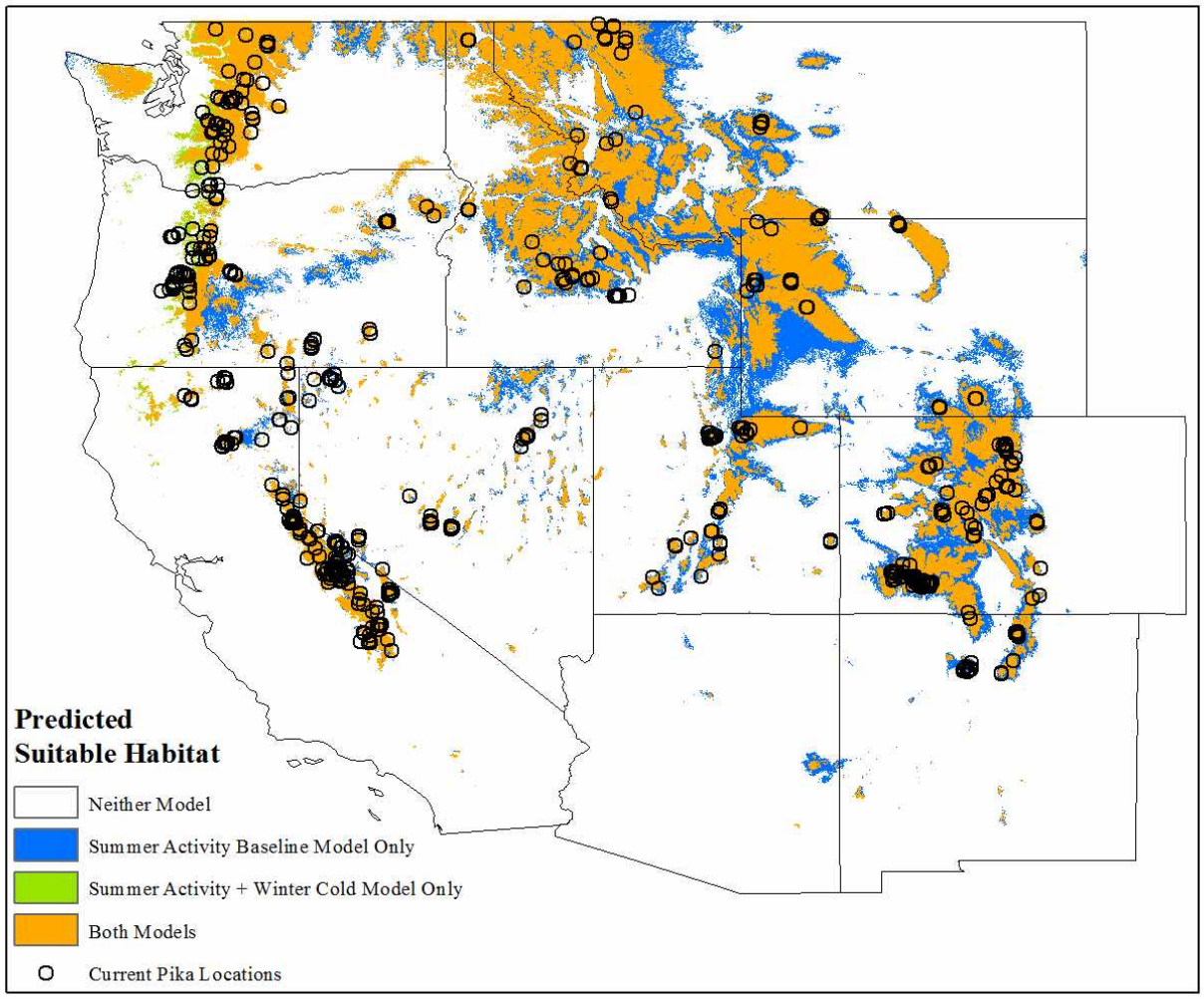


**Figure S6**. Comparing the activity-only model to the activity + winter cold model. The activity baseline model used only summer activity predicted by Niche Mapper to predict habitat suitability. The "activity + winter cold" model used both summer activity predictions and the minimum temperature of the coldest month derived from PRISM climate data, allowing for interactions between the input variables. Including winter cold in the model expanded habitat suitability in the western Cascades (in areas where pikas are known to exist) while contracting habitat suitability in other areas, with the biggest reductions in areas where pikas have not been documented.

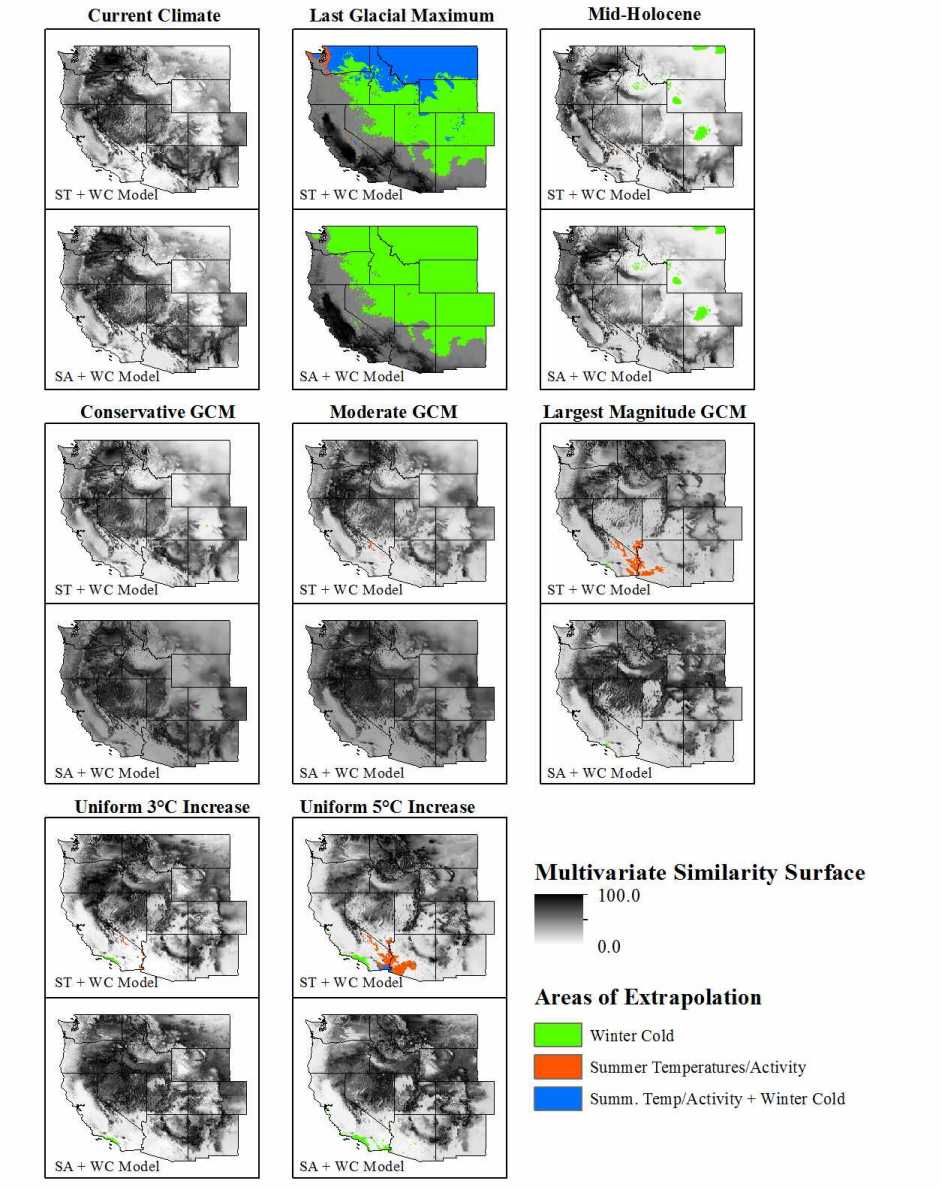


**Figure S7**. Multivariate Environment Similarity Surfaces (MESS), as described in Elith et al. (2010), showing how similar the climate conditions in each raster cell in the study area are to the values used in the model training (i.e., the values at the presence and background points). A score of 100 means that all environmental variables are at the median value from the training range; a score of 0 means that at least one variable is at the edge of the training range. Negative values (masked here in green, red, and blue), indicate locations where at least one variable is outside of the training range meaning that the model must extrapolate.

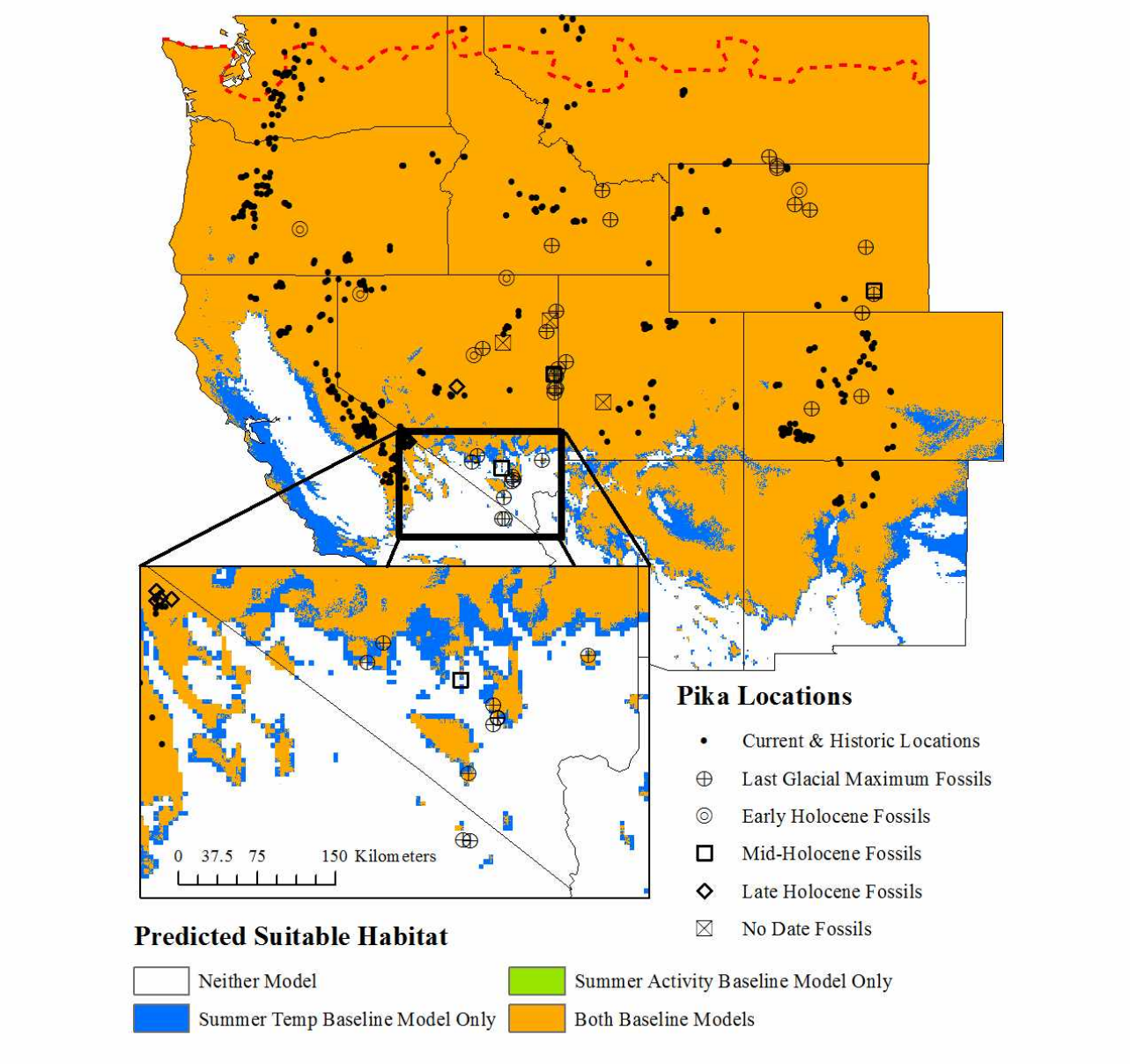


**Figure S8.** Hindcasting the baseline models to the Last Glacial Maximum (~22,000 years before present), showing increased areas of predicted thermally-suitable habitat. A detailed view of the southern edge of predicted suitable habitat is shown in the inset. Average summer temperatures in the Western United States were ~13°C cooler than present. Three fossil locations (indicated as "No Date") were not assigned to a specific epoch. The approximate southern edge of glacial ice sheets is shown by the dashed red line.

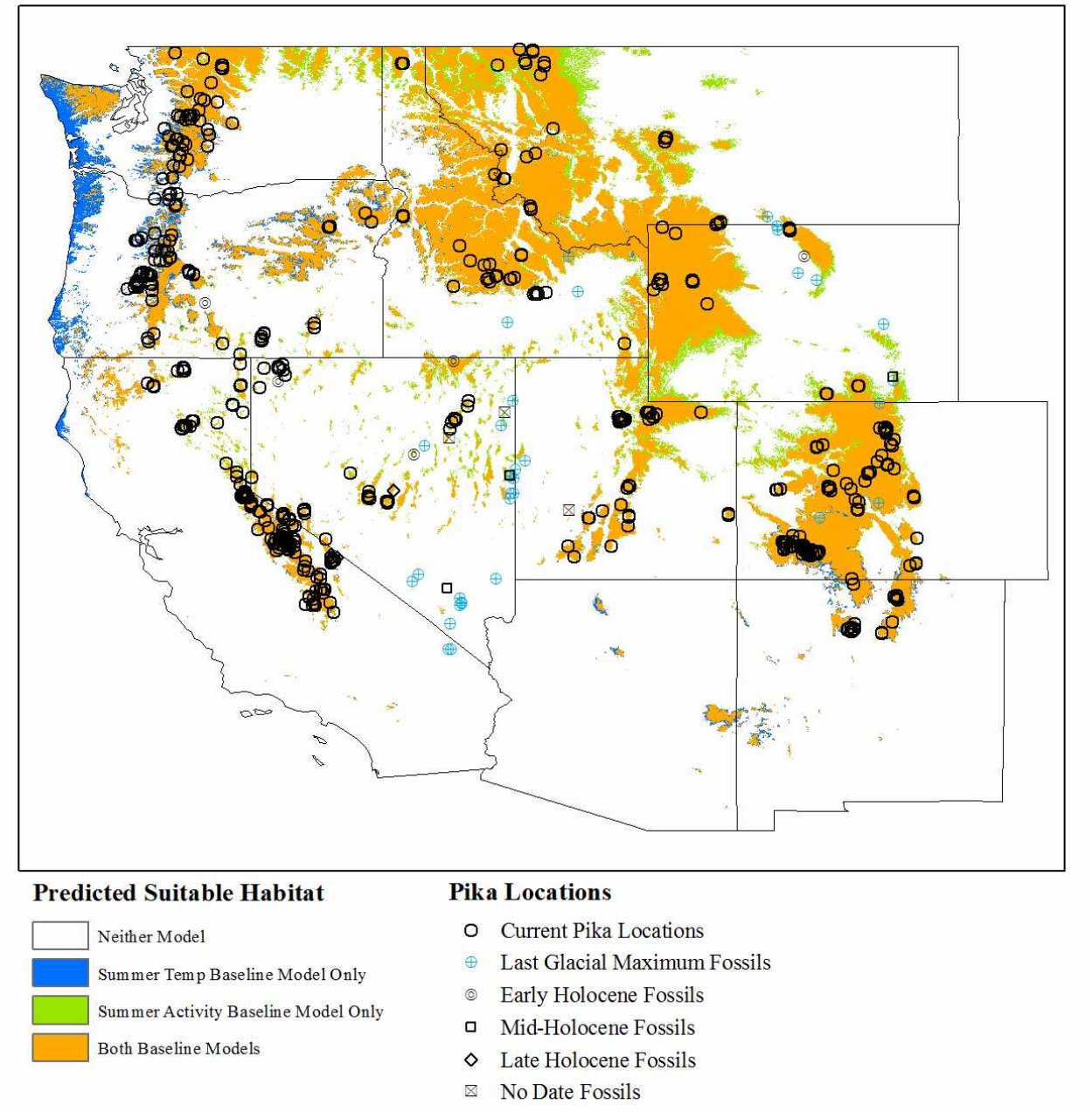


**Figure S9.** Hindcasting the baseline models to the Mid-Holocene (~6,000 years before present), showing substantial reductions of predicted thermally-suitable habitat from the Last Glacial Maximum. Average summer temperatures in the Western United States were 0.1°C warmer than present. Three fossil locations (indicated as "No Date") were not assigned to a specific time period.

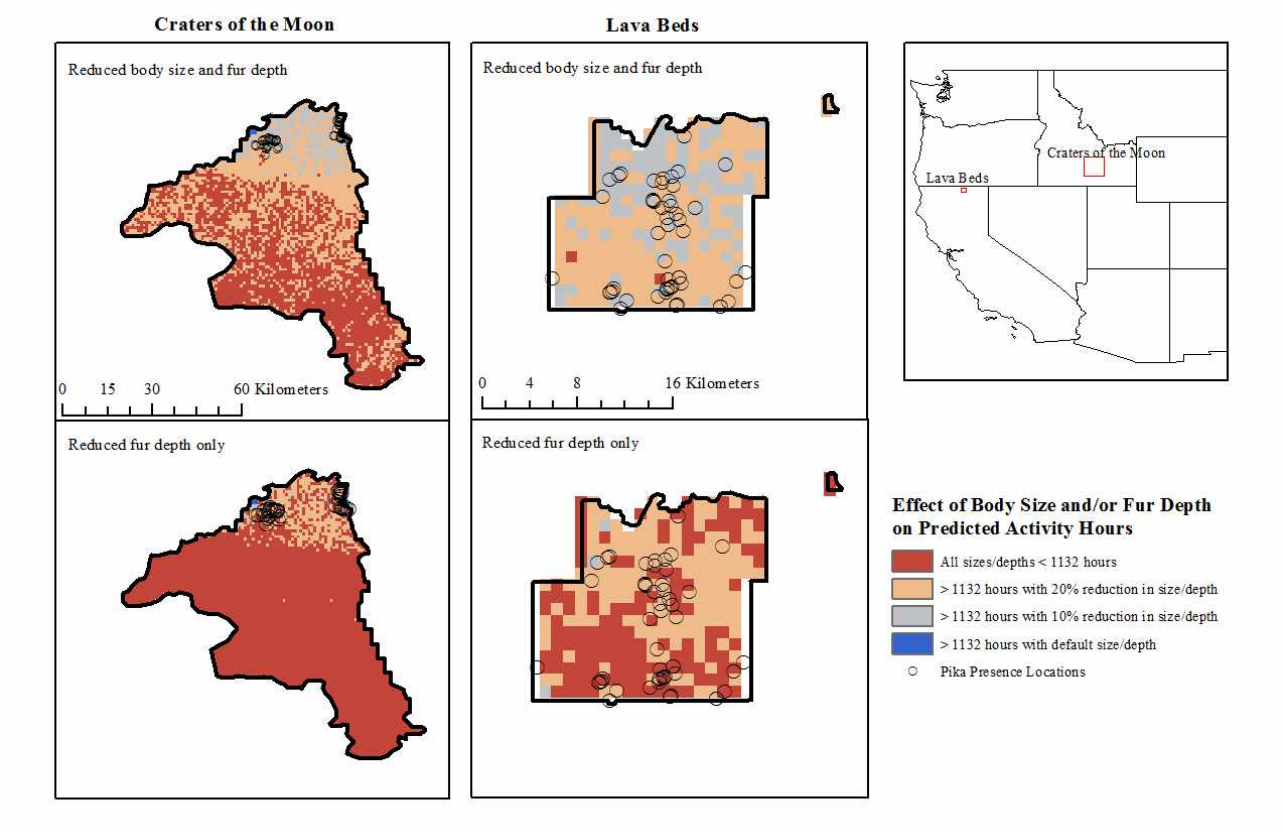


**Figure S10.** Areas of Craters of the Moon and Lava Beds National Monuments predicted to have summer activity above the 1132 hour threshold found to separate extant sites from most extirpated sites in the Great Basin using different assumptions of pika body size and/or fur depth. We compare predictions using the body size and fur depth used in the modeling ("default") to predictions assuming 10% reduction in size and/or fur depth, and 20% reduction in size and/or fur depth. These results illustrate how intraspecific phenotypic variation should be considered in species distribution modeling to examine presence locations outside of the species' normal climate envelope as well as ability to buffer climate change effects.

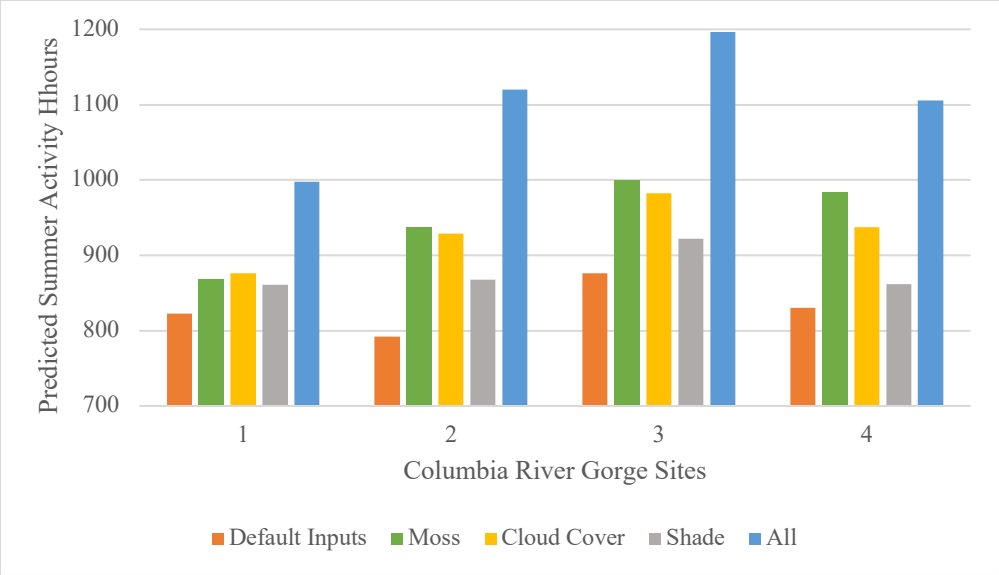


**Figure S11.** The effects of including site-specific habitat characteristics on Niche Mapper summer activity predictions at four pika locations in the Columbia River Gorge reported by Varner & Dearing (2014). Simulating a moss layer covering the talus (organic cap on the surface, 80% moisture on surface, and 55% reflectivity), average cloud cover (~30% June through September; data from New et al. 2002), and 50% shade from overhead vegetation increased the number of predicted activity hours individually and when considered together. Default landscape simulations in this study assumed characteristics typical of pika habitat throughout their range: a bare rock surface and no overhead shade.

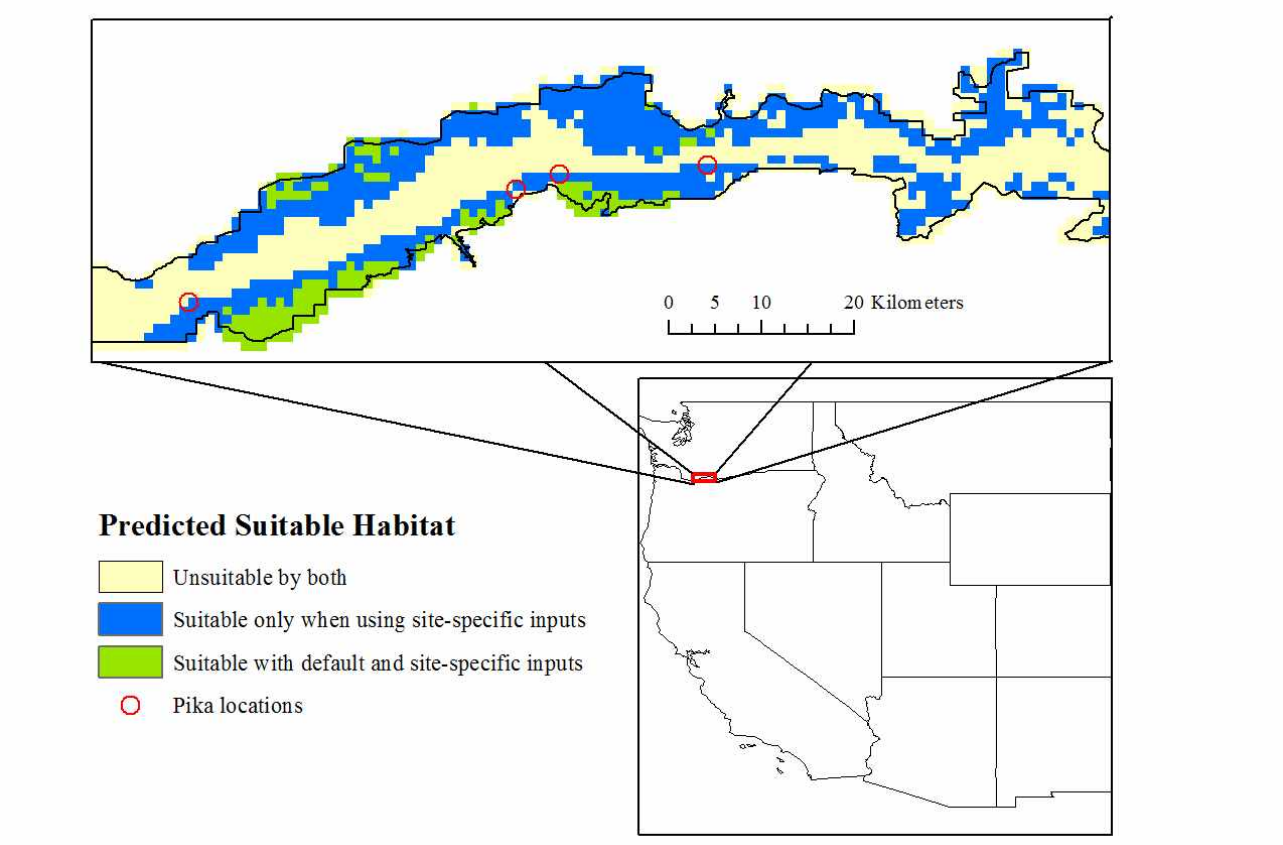


**Figure S12.** A comparison of habitat suitability predictions using the activity + winter cold model in the Columbia River Gorge National Scenic Area when activity time was calculated 1) assuming the default open, bare talus surface or 2) assuming site specific habitat characteristics described in Fig. S11. Locations where pikas have been documented (Varner & Dearing, 2014) are shown for reference.

**Table S1.** Properties used to parameterize Niche Mapper's animal model for an American pika (*Ochotona princeps*)

| Parameter (units) | Value | Source |
|---|---|---|
| Weight (g) | 150 | [1]: Mean body mass for this species 121-176 grams. |
| Basal metabolic rate (W) | 1.28 | [2]: Measured BMR on 16 pikas averaging 109 grams was 0.00855 W/g |
| Core temperature (ºC) Min/Reg/Max | 38/40.1/42.7 | [2]: Body temperatures measured by radio transmitters from 15 pikas in ambient temperatures -9.3 to 24°C ranged from 37.9-42.7°C (mean = 40.1)<br>[3]: Body temperatures of 12 pikas measured by rectal thermometer in ambient temperatures 2.0 to 24.4°C ranged from 39.3-41.0°C (mean = 40.1)<br>Body temperature of 1 pika measured by radio telemetry in ambient temperatures 10.0 to 27.6°C ranged from 39.1-41.0°C (mean = 40.4) |
| Flesh thermal conductivity (W/mC) | 0.4-2.8 | [4]: A collection of thermophysical property data on biological media, including a cold living hand (0.34 W/mC) and very warm living skin (2.8 W/mC). |
| $O_2$ extraction efficiency (%) | 20 | [5]: Mammal $O_2$ extraction efficiency is typically 20%. |
| Activity energy included in heat balance (%) | 80 | [6]: Based on measurements of mammalian muscle efficiency being around 20% as measured in rats and mice. |
| Hair solar reflectivity Dorsal/Ventral | 0.57/0.45 | Own measurements of average reflectivity across 350-2500nm wavelengths on mid-dorsal fur samples from one summer pelt from the UW Zoological Museum. |
| Hair length (mm) Dorsal/Ventral | Summer: 15/13 Winter: 22/19 | Own measurements on a summer pelt from Colorado from the UW Zoological museum: 14/12<br>[7]: Average hair lengths (n=3) from three pikas in summer pelage from Oregon: 15.3, 16.0, 16.9.<br>Winter pelage hair lengths assumed to be 50% longer based on [8]<br>July and August simulations used summer hair length; June and September simulations used an average of summer and winter hair length, on the assumption molt occurs during these months. |
| Fur depth (mm) | 50% of hair length | Own estimation (See [9] for a sensitivity analysis) |
| Hair diameter (μm) | 31 | Own estimation |
| Fur density (per $cm^2$) | 5000 | Own estimation based on measurements from other lagomorphs by [10] and [11] See [9] for a sensitivity analysis. |
| Ellipsoid length:width ratio | 3:1 | Own estimate of active body posture based on measurements from photographs of *O.princeps* found in internet searches |

[1] Smith AT, Weston ML (1990) *Ochotona princeps*. American Society of Mammalogists. Mammalian Species No. 352.
[2] MacArthur RA, Wang LCH (1973) Physiology of thermoregulation in the pika, *Ochotona princeps*. Canadian Journal of Zoology, **51**, 11-16.
[3] Smith AT (1974) The distribution and dispersal of pikas: influences of behavior and climate. Ecology, **55**, 1368-1376.
[4] Cho BT, editor (1969) Advanced Heat Transfer. Urbana, IL: U Illinois Press. 459 pp.
[5] Lacombe A (2002) Effects of temperature on metabolism, ventilation, and oxygen extraction in the Southern Brown Bandicoot *Isoodon obesulus* (Marsupialia: Peramelidae). Physiological and Biochemical Zoology, **4**, 405-411.
[6] Smith NP, Barclay CJ, Loiselle DS (2005) The efficiency of muscle contraction. Progress in Biophysics & Molecular Biology, **88**, 1-58.
[7] Johanna Varner unpublished data
[8] Howell, AH (1924) Revision of the American pikas. North American Fauna, **47**,1-57.
[9] Moyer-Horner L, Mathewson PD, Jones G, Kearney MR, Porter WP (2015) Modeling behavioral thermoregulation in a climate change sentinel. Ecology and Evolution, **5,** 5810-5822.
[10] Tregear RT (1965) Hair density, wind speed, and heat loss in mammals. Journal of Applied Physiology, **20**, 796–801
[11] Davis Jr. LB, Birkebak RC (1971) An analysis of energy transfer through fur, feathers, and other fibrous materials. Lexington, Ky.: Univ. Kentucky. Ph.D. diss., (as cited in Skuldt DJ, Beckman WA, Mitchell JW, Porter W (1975) Conduction and radiation in artificial fur. pp. 549-558 in Gates DM and RB Schmerl, eds., Perspectives of Biophysical Ecology. Ecological Studies Volume 12. Springer, Berlin.)

**Table S2.** Standard microclimate model inputs for Niche Mapper simulations of American pikas (*Ochotona princeps*) in the western United States

| Parameter (units) | Value | Source |
|---|---|---|
| Substrate thermal conductivity (W/mK) | 1.75 | [1]: Estimated based on values from various rocky substrates obtained online. |
| Substrate density (kg/m$^3$) | 2650 | [1]: Estimated based on values from various rocky substrates obtained online. |
| Substrate specific heat (J/kg-K) | 870 | [1]: Estimated based on values from various rocky substrates obtained online. |
| Substrate surface reflectivity (%) | 25 | [1]: Estimated based on values from various rocky substrates obtained online. |
| Timing of daily minimum and maximum air temperatures and wind speeds (min/max) | Sunrise/1 hour after solar noon | Own estimation |
| Timing of daily minimum and maximum relative humidity (min/max) | 1 hour after solar noon / Sunrise | Own estimation |
| Cloud cover (%) | 0 | Simplifying assumption of clear skies. |
| Shade (%) | 0 | Simplifying assumption of no trees in talus fields. |
| Daily wind speed range (m/s) | 0.1-4 | [2] Pikas not active in wind speeds > 4 m/s |
| Daily relative humidity (%) | Min = variable<br>Max = 100 | Maximum values set to 100% (simplifying assumption) and minimum values calculated based on the daily temperature range assuming constant water mass in the air over 24 hours [3] |
| Animal height (cm) | 9 | Own estimation based on personal observation |

[1] http://www.engineeringtoolbox.com
[2] Hayes AR, Huntly NJ (2005) Effect of wind on the behavior and call transmission of pikas (Ochotona princeps). Journal of Mammalogy, **86**, 974-981
[3] Tracy CR, Welch WR, Porter WP (1980) Properties of air: A manual for students in biophysical ecology. University of Wisconsin Laboratory of Biophysical Ecology, Technical Report #1 (3rd Edition)

**Table S3.** Total summer (June – September) activity hours predicted by Niche Mapper at pika research sites in the Great Basin, USA. Extirpated sites are noted in bold italics.

| SITE | SUMMER ACTIVITY HOURS | SITE | SUMMER ACTIVITY HOURS |
|---|---|---|---|
| ***Ft. Bidwell (NV)*** | ***987*** | Toby Canyon (NV) | 1318 |
| ***4 mi SW McDonald Peak (CA)*** | ***1077*** | Peterson Creek (NV) | 1319 |
| ***Red Mountain (NV)*** | ***1088*** | Mohawk Canyon (NV) | 1334 |
| ***2 mi E of SE end Eagle Lake (CA)*** | ***1093*** | Crane Mountain (OR) | 1348 |
| ***Wisconsin Creek (NV)*** | ***1095*** | Mustang Mountain (NV) | 1375 |
| ***Sugar Hill (CA)*** | ***1104*** | Long Creek (NV) | 1386 |
| ***20 mi NE Adel (OR)*** | ***1117*** | ***Highgrade Spr. A. (CA)*** | ***1395*** |
| ***Smiths Creek (NV)*** | ***1120*** | Kiger Gorge (OR) | 1407 |
| ***Summit Lake (NV)*** | ***1124*** | Big Indian Mountain (NV) | 1432 |
| ***Thomas Creek Ranger Station (OR)*** | ***1131*** | S. Twin R. (NV) | 1432 |
| Willow Creek (OR) | 1162 | Mt. Jefferson (NV) | 1469 |
| Blowout Mountain (NV) | 1165 | Green Mountain (NV) | 1531 |
| Warner Mountains. (CA) | 1185 | Smith Lake (NV) | 1538 |
| Hays Canyon (NV) | 1199 | Warren Peak (CA) | 1539 |
| ***Greenmonster Canyon (NV)*** | ***1250*** | ***Duffer Peak (NV)*** | ***1557*** |
| Fandango Peak (CA) | 1255 | Arc Dome (NV) | 1577 |
| Cougar Peak (OR) | 1261 | Steels Creek (NV) | 1665 |
| 5 mi NW of Eagle Peak (CA) | 1268 | Three Lks. (Lamoille Canyon; NV) | 1750 |
| ***Pinchot Creek (NV)*** | ***1305*** | Thomas Creek (NV) | 1810 |
| Stockade, Warner, Goat Creeks (OR) | 1305 | | |

**Table S4.** Evaluation metrics for performance of different models using current (1981-2010) climate conditions at 39 monitoring sites in the hydrographic Great Basin (25 extant sites; 14 extirpated sites) and across the western United States. Model abbreviations: SA (summer activity); ST (summer temperatures); WC (winter cold); PtSn (potential snow); GSP (growing season precipitation).

| | Great Basin Monitoring Sites | | | | Western United States | | | | |
|---|---|---|---|---|---|---|---|---|---|
| **Model** | **Test AUC** | **Sens.** | **Spec.** | **TSS** | **Test AUC** | **Sens.** | **Spec.** | **TSS** | **Records < 3 km from suitable habitat (n = 616)** |
| **SA** | 0.868 | 1.00 | 0.64 | 0.64 | 0.924 | 0.89 | 0.80 | 0.68 | 589 |
| **ST** | 0.851 | 0.92 | 0.79 | 0.71 | 0.923 | 0.89 | 0.81 | 0.71 | 586 |
| **SA+WC** | 0.866 | 0.96 | 0.71 | 0.67 | 0.935 | 0.91 | 0.85 | 0.76 | 597 |
| **ST+WC** | 0.860 | 0.96 | 0.79 | 0.75 | 0.932 | 0.91 | 0.83 | 0.74 | 597 |
| **SA+PtSn** | 0.851 | 0.84 | 0.79 | 0.63 | 0.936 | 0.90 | 0.83 | 0.73 | 585 |
| **ST+PtSn** | 0.857 | 0.84 | 0.86 | 0.70 | 0.931 | 0.90 | 0.82 | 0.72 | 583 |
| **SA + GSP** | 0.843 | 0.96 | 0.50 | 0.46 | 0.927 | 0.91 | 0.81 | 0.72 | 595 |
| **ST + GSP** | 0.840 | 0.92 | 0.71 | 0.63 | 0.928 | 0.90 | 0.82 | 0.72 | 587 |
| **SA+WC+ PtSn** | 0.857 | 0.88 | 0.71 | 0.59 | 0.938 | 0.92 | 0.83 | 0.75 | 591 |
| **ST+WC+ PtSn** | 0.853 | 0.84 | 0.86 | 0.70 | 0.936 | 0.91 | 0.84 | 0.75 | 593 |
| **SA+WC+ GSP** | 0.863 | 1.00 | 0.50 | 0.50 | 0.936 | 0.93 | 0.83 | 0.76 | 600 |
| **ST+WC+ GSP** | 0.866 | 1.00 | 0.50 | 0.70 | 0.935 | 0.94 | 0.81 | 0.75 | 602 |
| **SA+WC+ PtSn + GSP** | 0.866 | 0.92 | 0.64 | 0.56 | 0.939 | 0.94 | 0.82 | 0.76 | 594 |
| **ST+WC+ PtSn + GSP** | 0.863 | 0.96 | 0.57 | 0.53 | 0.938 | 0.95 | 0.81 | 0.75 | 602 |

**Table S5**. Distance (km) from nearest predicted suitable habitat for fossil pika locations not identified as suitable habitat in the Last Glacial Maximum. A site was considered to be not identified as suitable if it was more than 4.5 km from the nearest predicted suitable habitat to account for the resolution of the climate data (2.5 arc minutes; 4 km at the equator but ~4.5 km at the latitude of these sites). A total of 34 fossil pika locations dated to the Last Glacial Maximum were used in the analysis.

| | Summer Activity Baseline Model | Summer Temperature Baseline Model | Summer Activity + Winter Cold Model | Summer Temperature + Winter Cold Model |
|---|---|---|---|---|
| Corn Creek PR3, NV | 5.1 | 5.1 | 9.8 | 5.1 |
| Mescal & Antelope Caves, CA | 8.5 | 8.5 | 11.5 | 8.5 [a] |
| Kokoweef Cave, CA | 10.8 | 10.8 | 15.3 | 10.5[a] |
| Pintwater Cave, NV | - | - | 30.2 | 4.8[a] |
| Fortymile Canyon 11, Yucca Mountain, NV | - | - | 7.6 | - |
| [a]Predicted as suitable habitat using the MIROC climate data only. | | | | |

# CHAPTER 2: FIELD EXPERIMENTS CONFIRM BIOPHYSICAL MODEL'S ACCURACY TO COMPUTE PRIMATE ENERGETICS AND BEHAVIOR IN WILD VERVET MONKEYS.

*Intended Authors:* Paul D. Mathewson, Warren P. Porter, Louise Barrett, Peter Henzi, Richard McFarland

## ABSTRACT

Climate change has created an urgent need to understand how animal performance is affected by environmental conditions. To regulate body temperature within a narrow range, endotherms employ a variety of autonomic processes and behaviors. However, there are costs to this thermoregulation including evaporative water loss or reduced activity in response to environmental heat and increased energetic requirements from elevated metabolic heat production in the cold. Biophysical models that use principles of heat and mass transfer can be used to explore how an animal's morphology, physiology, and behavior interact with its environment in terms of energy, mass and water balances to affect fitness and performance. We used Niche Mapper™ (NM) to build a vervet monkey (*Chlorocebus pygerythrus*) biophysical model and test the model's ability to predict body temperature ($T_b$) variation and thermal stress using $T_b$ and behavioral data collected from a group of free-ranging vervets through observations and biologging. The mean observed $T_b$ in both males and females was within 0.5°C of the range of predicted $T_b$s for 91% of the time over the five-year study period. Vervets were observed to rest more during summer days when the model predicted higher evaporative water loss rates would be required to maintain activity. Vervets were also observed to reduce their overnight body temperature further on winter nights when NM predicted greater metabolic heat production

costs to maintaining body temperatures. This is the first time that NM's body temperature predictions have been validated against data from a wild endotherm. Overall, these results provide confidence that NM can accurately predict thermal stress and can be used to provide insight into the thermoregulatory consequences of morphological (e.g., body size, fur depth), physiological (e.g. $T_b$ plasticity) and behavioral (e.g., huddling, resting) adaptations. Such an approach allows users to test hypotheses about how animals adapt to thermoregulatory challenges and make predictions about potential responses to environmental change. Importantly, NM is a general model and can be adapted to other species with only basic information about the animal's morphology, physiology and behavior required.

## INTRODUCTION

Given the threat that global climate change poses to biodiversity (Cahill et al. 2012, Pacifici et al 2015, Scheffers et al. 2016, Urban et al. 2016) there is a pressing need to understand the relationship between animal performance and environmental conditions (Fuller 2010). Environmental temperature imposes an important ecological constraint on primate distributions (Korstjens et al. 2010, Lehmann et al. 2010, Campos et al. 2017), so knowledge of how primates respond to changes in the thermal environment is important to our understanding of how climate change will impact species survival in a taxon that is already facing substantial pressure. Approximately 60% of primate species are threatened with extinction even without the compounding effects of climate change (Estrada et al. 2017).

Primates, like all endotherms, employ a range of adaptations to cope with environmental challenges. Homeothermy – maintaining a body temperature within a relatively narrow range despite environmental temperature variation – is achieved through a combination of physiological (autonomic) and behavioral processes. Physiological processes can be costly in

terms of energy expenditure through increased metabolic heat production (Iwamoto & Dunbar 1983), and water loss through evaporation (Johnson & Elizondo 1979, Mitchell et al. 2009). In addition to increasing air temperatures, climate change is also expected to alter the availability and distribution of water and food resources (Humpheries et al. 2004, Diffenbaug & Field 2013, Fuller at al. 2016). Climatic effects have the potential to restrict the resources available to support physiological thermoregulatory processes (i.e., food energy for heat production and water for evaporative cooling), and subsequently the ability of endotherms to cope with changing environmental conditions. If unable to defend their optimal body temperature range, animals will experience reduced cellular efficiency and fitness (Seebacher & Little 2017, Maloney et al. 2017).

To alleviate the autonomic costs of thermoregulation, individuals can also engage in behaviors that influence heat exchange with the environment, including changing activity patterns (e.g., reducing activity in hot conditions: Campos & Fedigan 2009, Majolo et al. 2013, McFarland et al. 2014), adjusting postures (e.g., huddling, sun-basking: McFarland et al. 2015, Kelley et al. 2016, Eppley et al. 2017), or selecting thermally-advantageous microclimates (e.g., cave-use, shade-seeking: Barrett et al. 2004, Hill 2006, Pruetz 2007). Behavioral thermoregulation, however, also has associated costs. Most notably, behavioral thermoregulation may take place at the expense of other behaviors critical to survival (e.g., feeding, drinking and social activity; Hill et al. 2004; McFarland et al. 2014, Dunbar et al. 2009).

To succeed in an environment in which climatic factors vary across days and seasons, individuals must prioritize activities critical to survival and reproduction (e.g., Dunbar et al., 2009; McFarland et al. 2014). Therefore, fitness-related activities are essentially traded and prioritized according to social, ecological, and environmental factors. The fundamental challenge

for an endotherm is to balance these activities—and their associated costs—without operating in a long-term negative energy or water balance. The environmental space where this balance can be achieved represents a given species' potential distribution (Kearney & Porter 2009).

The most common approach to modeling species' distributions involves statistically relating a species' occurrence locations with environmental predictors, most often air temperature and precipitation (Elith & Leathwick 2009). The resulting *n*-dimensional space that represents the range of environmental conditions at known presence locations is considered the animal's bioclimatic "envelope". These envelopes are then projected onto future climate scenarios (e.g., Thomas et al. 2004, Hijmans & Graham 2006) to predict changes in distribution that might occur with changing climatic factors. However, this correlative approach to distribution modeling provides little insight into how environmental predictors limit distributions because the limiting processes (e.g., Dormann et al, 2012, Evans et al. 2015) remain implicit in the correlations. Without knowing the limiting processes, conservation and climate-adaptation actions are relegated to trial and error (Evans et al. 2015). Furthermore, correlative approaches require extrapolation into novel environments, such as those created by climate change, increasing the risk of erroneous predictions (Buckley & Kingsolver 2012, Pacifici et al. 2015).

In contrast, mechanistic models explicitly model the processes thought to limit a species' distribution. By explicitly modeling the process, predicted distributions are based entirely on the model's predictions of where survival is possible, independent of observed distributions. Mechanistic models are therefore more informative than correlative models and can be applied to novel conditions without extrapolation (for comprehensive comparisons of correlative and mechanistic approaches, see Kearney & Porter 2009, Buckley et al. 2010). For primates, one mechanistic approach that has been used involves time-budget models (Dunbar et al. 2009,

Willems & Hill 2009, Korstjens et al. 2010). These models are premised on the idea that high air temperatures force animals to spend more time resting at the expense of other critical activities (e.g., feeding, travelling, socializing, and mating). Empirically-derived relationships between air temperature and observed resting time, coupled with additional factors including indices of food availability, are then used to model a species' distribution. However, collecting the required behavioral and ecological data is time- and resource-intensive, restricting the scope of these models to well-studied species (Willems & Hill 2009). Furthermore, these models do not provide information about what traits or behaviors are important in determining when the species' activity becomes restricted because that information is hidden behind the observed regression.

An alternative mechanistic approach to understanding distributional limits is the use of biophysical models, which are based on fundamental principles of heat and mass transfer and model how an animal's morphology, physiology, and behavior interact with its environment in terms of energy, mass and water balances to affect fitness and performance (Porter & Gates 1969; Kearney & Porter 2009). Indeed, earlier studies have noted the need for biophysical models to help better understand primate ecology (Stelzner 1988, Hill et al. 2004, Barrett et al. 2004, Campos & Fedigan 2009). A biophysical model can thus be used to quantify thermal stresses incurred by an animal in any environment. These stresses include increased heat production requirements and increased food requirements in response to cold stress, or evaporative water loss or activity reduction in response to heat stress. This quantification provides important information that allows us to understand how a species' distribution is limited by environmental temperature (Kearney & Porter 2009). In the context of climate change, biophysical models can be used to investigate the direct impact of higher temperatures on the animal and how the resulting decreased cold stress and increased heat stress affect habitat

suitability across the landscape. By modeling these consequences mechanistically, taking account of the animal's specific characteristics, this approach also allows exploration of how intraspecific variation in morphological and physiological traits, as well as behavioral responses, might allow a species to buffer the impacts of climate change.

Here, we build and test a biophysical model for vervet monkeys (*Chlorocebus pygerythrus*; hereafter, "vervets") with Niche Mapper (Porter & Mitchell 2006; hereafter, 'NM'). NM (described in the methods) has previously been shown to accurately predict energetic requirements or thermal stress as a function of environmental conditions for a wide variety of animals, including the following mammals: American pika (*Ochotona princeps*; Moyer-Horner et al. 2015), Japanese serow (*Capricornus crispus*; Natori & Porter 2007), Giant Panda (*Ailuropoda melanoleuca*; Zhang et al. 2018), elk (*Cervus elaphus*; Long et al 2014), polar bear (*Ursus maritimus;* Mathewson & Porter 2013), and koala (*Phascolarctos cinereus*; Briscoe et al. 2016). The current study represents the first use of NM with a primate species.

We test NM's ability to predict body temperatures ($T_b$) – an important index of animal performance – by comparing model $T_b$ predictions to $T_b$ data collected from wild animals. The presence of a multiyear dataset of physiological ($T_b$), behavioral (activity budgets), and local climate data for a population of wild vervets that experiences both heat and cold stress (McFarland et al. 2014) provides a unique opportunity to test NM's ability to predict an animal's thermal response to the environment. We also illustrate how a biophysical model can be used to convert climate data into more proximate variables (i.e., water loss rates from sweating in the summer and additional heat production in the winter) that quantify thermal stress specific to the species' morphology, physiology and behavior.

METHODS

*1. Study site, subjects, and live animal data collection*

Data were collected between 2012 and 2016 from a population of wild vervet monkeys (*Chlorocebus pygerythrus*) living on the Samara Private Game Reserve in the Karoo, Eastern Cape, South Africa (32°22'S, 24°52'E). This semi-arid region has a seasonal climate, with hot, wet summers (November – March), and cold, dry winters (June – August). Annual rainfall is < 400 mm, while minimum and maximum air temperatures typically range between -5 and 40 ºC (McFarland et al. 2014). Vervets are small (females: 3-5 kg; males: 4-8 kg), diurnally-active, semi-terrestrial primates that live in multi-male – multi-female groups. Vervets are highly adaptable and can be found throughout sub-Saharan Africa, particularly in open-savannah and riverine habitats (Cawthon Lang 2006).

Behavioral data were collected from 78 adult male (> 6 years) and 67 adult female (> 4 years) vervets living in three groups across the five-year period. All animals lived on a completely natural diet and were individually recognizable (Pasternak et al. 2013; McFarland et al. 2014). Instantaneous scan data were used to collect data on the activity time budgets, postures, and shade-use of adult group members. Scan data were collected daily, every 30 minutes, from all individuals that could be located within a ten-minute period of the scan interval. The activity of each subject was recorded as one of the following mutually-exclusive behaviors: resting, feeding, moving, socializing, or other (see McFarland et al. 2014). During the five-year study period, 8,758 group scans were collected across the three study groups (Table S1).

Each year, a subset of the study animals was implanted with temperature-sensitive data loggers that recorded core $T_b$ at five-minute intervals (see Lubbe et al. 2014 and McFarland et al.

2015 for details of the capture, surgical procedures, and implanted devices). A minimum of three individuals per sex were concurrently implanted with temperature loggers at any given time (Table S1). Because NM generates estimates on an hourly basis, we calculated average hourly $T_b$ for each individual and then averaged those values to provide an hourly $T_b$ value for both males and females. The 24-hour $T_b$ pattern in vervets is closer to a square wave than a sinusoidal one with lower and upper modal temperatures (Lubbe et al. 2014). Between 2012 and 2016, the lower modal temperature for the current study animals (based on 479,530 individual vervet hour $T_b$ measurements) was 37.1°C and the upper modal temperature was 38.6°C (Fig. S1a). The modal temperatures were similar between sexes and across seasons (Fig. S1b).

All implanted animals were weighed prior to surgery (McFarland et al. 2015). Morphometric data needed for NM were collected from four males and two females during animal capture in June 2015. A tape measure was used to measure the length and width of each animal's head, torso, arms, legs and tails. Fur depth and hair lengths were measured at each of the above body sites using calipers. Hair length:fur depth ratios were also calculated from two males captured in June 2016; these ratios were applied to both sexes. The animal model used averages of the above measurements for each sex (Table 1). Pelt reflectance measurements were available from a previous study of vervet pelage heat-transfer characteristics (McFarland et al. 2016). Reflectance measurements were made on seven pelts every 5nm wavelength between 250-3500nm. Trapezoidal integration of each wavelength interval was scaled according to the solar energy in that interval to calculate overall solar reflectivity. Two pelt samples were used to measure hair diameter and density using an ocular calibration grid and micrometer with a light microscope.

Behavioral data collection was approved by the University of Lethbridge Animal Welfare (Protocol #1505, S.P. Henzi & L. Barrett). Body temperature data collection was approved by the University of the Witwatersrand's Animal Ethics Research Committee (Protocol # 2010/41/04, A Fuller and 2015/04/14B, R. McFarland).

*2. Modelling Methodology*

The vervet behavioral, ecological, morphometric, and pelage data collected as described above were used to build a vervet model in NM. The vervet model was then used to predict body temperatures and evaporative water loss for four seasons of wild vervet data collection. The model was validated through a comparison of predicted versus observed body temperatures. Lastly, we evaluated NM's ability to predict two metrics of thermal stress: higher evaporative water loss required to remain active in hot conditions and higher metabolic heat production requirements on cold nights.

*2.1 Niche Mapper Description*

This section provides a general description of NM operation; vervet-specific parameters are described later. NM consists of two submodels: a microclimate and an animal model. The microclimate model uses macroclimate data (viz., maximum and minimum daily air temperatures, relative humidity, cloud cover, and wind speed), substrate properties, vegetative cover, geographic location, topography, and time of year to calculate hourly environmental profiles from 2m height down to the ground, sky temperatures, and incoming solar radiation incident on the animal. Separate profiles are calculated for full sun and shaded microenvironments (see Fuentes & Porter 2013 for more details on the microclimate model calculations). The animal model then uses the hourly outputs from the microclimate model to iteratively solve a heat balance equation to find the metabolic rate needed for the animal to

maintain its $T_b$, accounting for convective, radiative, evaporative and solar heat fluxes with its microenvironment (see Mathewson & Porter 2013 for details on the heat balance calculations).

Animals are modelled as a series of simple shapes with well-understood heat transfer properties that enable surface temperatures to be calculated based on a given core temperature and dimensions of the body part. NM models heat flowing from the core to the skin surface, assuming distributed metabolic heat generation throughout the flesh of each body part. For bare body parts, heat fluxes with the environment are then computed using the calculated skin surface temperatures. For furred body parts, heat is modeled as traveling through a porous fur layer composed of a matrix of air and keratin via parallel conduction and radiative processes (see Kowalski & Mitchell 1979 for details) before heat exchange with the environment is calculated. NM solves the animal's heat balance for each hour of the day. Calculations begin by computing the metabolic heat production required for the animal to maintain a "normal", starting point body temperature specified by the user in that hour's environmental conditions assuming minimum shade cover. Thermoregulatory options are engaged if the required metabolic rate is above or below that hour's target metabolic rate. Target metabolic rates are specified by the user for diurnal, crepuscular, and nocturnal hours. Target metabolic rates are either resting metabolic rate (for times of the day when animals are assumed to be inactive) or a multiple of resting metabolic rate to simulate activity (for times of the day when animals are assumed to be active).

Behavioral thermoregulatory options of selecting a different microhabitat (e.g., shake seeking in the heat), if available, or changing posture (e.g., curling/huddling up in the cold) are engaged first, followed by physiological options. To minimize metabolic heat production above the target range in cold temperatures, animals are allowed to increase pelage/plumage depth until the depth is 50% of the hair length of that body part (to simulate piloerection), decrease flesh

thermal conductivity (to simulate vasoconstriction) and reduce $T_b$ to a user-specified minimum value. To maintain a metabolic rate in a hot environment, animals are allowed to increase thermal conductivity (to simulate vasodilation), increase $T_b$ to a user-specified maximum value, and increase surface area that is wet (simulating sweating). The model will always attempt to reach a heat balance with a metabolic rate within the target range, but if thermoregulatory options are exhausted before a metabolic rate within 2.5% of the target metabolic rate is reached, the model will return the closest value. Thus, the model prioritizes minimizing metabolic heat over defending a certain $T_b$ or reducing water loss.

Model outputs relevant to this work are predicted hourly $T_b$s, metabolic rates (increases above the target rate will indicate cold stress), and evaporative water loss rates (increase indicate heat stress). Because the model testing involves comparing predicted $T_b$ to observed $T_b$ (see below), we emphasize that any variation in predicted $T_b$ from the user-supplied default value is solely due to the model predicting that a $T_b$ change is needed to either maintain the target metabolic rate ($T_b$ increase) or avoid additional metabolic heat production ($T_b$ decrease) in that hour's environmental conditions. Daily $T_b$ cycling is not programmed into the model.

*2.2. Vervet Animal Model Parameterization and Simulated Metabolic Chamber Evaluation*

Based on the collected body morphometric data described above, vervets were modeled with ellipsoids for the head and cylinders for all other body parts (Fig. 1). Key biophysical inputs are summarized in Table 1.

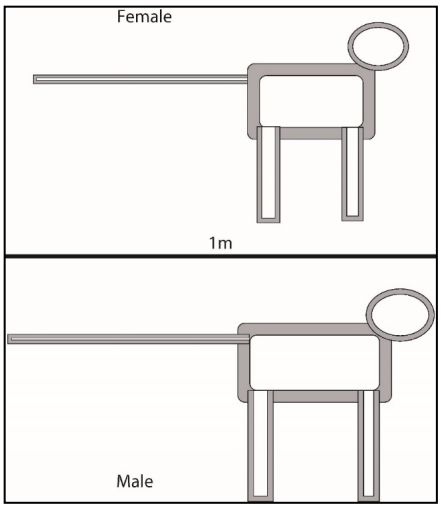


**Figure 1.** Vervet monkeys modeled as a series of simple shapes by Niche Mapper to approximate the measured body part dimensions. Gray shading represents fur thickness.

As an initial evaluation of model performance, we investigated whether the air temperatures at which the model predicts the animal will experience hot or cold stress (i.e., the upper and lower bound of its thermoneutral zone) are reasonable. In a real-world setting, air temperatures combine with ground and sky radiant temperatures, wind, and solar radiation to create the effective temperature that the animal experiences. To eliminate these confounding factors and identify more clearly predicted upper and lower critical temperatures, we placed the model animal into a simulated metabolic chamber. In the simulated metabolic chamber, all temperatures (air, ground, and sky) were manually set to the same temperature and then increased in 1°C increments. No solar radiation was allowed, relative humidity was set to 5%, and wind speeds were set to 0.1 m/s. The model vervet was not able to sweat in the metabolic chamber.

Model sensitivity to biophysical inputs was also assessed in the simulated metabolic chamber. Key model input values (body temperature, pelage properties, body part dimensions)

were increased and decreased to see how variation affected the model's predicted upper and lower critical temperatures and whole-body thermal conductivity. For this sensitivity analysis the upper critical temperature is the ambient temperature at which model vervets would not be able to maintain their resting metabolic rate without sweating or raising $T_b$ above the user-supplied maximum (sensu Mitchell et al. 2018). The lower critical temperature is the ambient temperature at which model vervets would need to raise their metabolic heat production above the resting rate in order to maintain the minimum $T_b$. Whole-body thermal conductivity was calculated as the slope of the predicted metabolic rate as a function of ambient temperature below the lower critical temperature (W/°C).

**Table 1.** Key properties used to parameterize Niche Mapper's animal model for vervet monkeys. Data sourced from the current study unless marked with superscript.

| Parameter | *Female* | *Male* |
|---|---|---|
| **Body mass** (kg) | 3.41 | 4.77 |
| **Head** | | |
| Vertical diameter (mm) | 88 | 95 |
| Horizontal diameter (mm) | 87 | 96 |
| Length (mm) | 126 | 133 |
| Fur depth/hair length (mm) | 19/40 | 21/45 |
| **Torso** | | |
| Vertical diameter (mm) | 143 | 173 |
| Horizontal diameter (mm) | 124 | 148 |
| Length (mm) | 350 | 390 |
| Dorsal fur depth/hair length (mm) | 15/49 | 15/49 |
| Ventral fur depth/hair length (mm) | 18/41 | 21/48 |
| **Arms** | | |
| Vertical diameter (mm) | 39 | 45 |
| Horizontal diameter (mm) | 42 | 54 |
| Length (mm) | 180 | 215 |
| Fur depth/hair length (mm) | 11/30 | 11/30 |

| | | |
|---|---|---|
| **Legs** | | |
| Vertical diameter (mm) | 49 | 55 |
| Horizontal diameter (mm) | 72 | 78 |
| Length (mm) | 220 | 265 |
| Fur depth/hair length (mm) | 13/47 | 13/47 |
| **Tail** | | |
| Vertical diameter (mm) | 24 | 25 |
| Horizontal diameter (mm) | 24 | 28 |
| Length (mm) | 505 | 575 |
| Fur depth/hair length (mm) | 7/26 | 7/26 |
| **Hair solar reflectivity (%)** [1] | 20 | |
| **Hair diameter** (μm) | 30 | |
| **Hair density** (per $cm^2$) | 1600 | |
| **Resting metabolic rate** (W) [2] | 3.39*mass (kg)$^{0.75}$ | |
| **Core body temperatures** (ºC)) | Min: 36<br>Default:38<br>Max:41 | |
| **Flesh thermal conductivity** (W/mC) [3] | 0.4 to 2.8 | |
| **$O_2$ extraction efficiency** (%) [4] | 20 | |
| **Activity energy included in heat balance** (%) [5] | 80 | |

[1] Vervet monkey pelage heat-transfer characteristics (McFarland et al. 2016)
[2] Standard regression for placental mammals used as a default in Niche Mapper. Provides a good fit with data from published studies of primate metabolic rates (Fig S4, Table S2) (Gordon et al. 1972).
[3] Thermophysical property data on biological media, including a cold living hand (0.34 W/mC), very warm living skin (2.8 W/mC) (Cho 1969).
[4] Mammal $O_2$ extraction efficiency is typically 20% (Lacombe 2002).
[5] Based on measurements of mammalian muscle efficiency being ~20% as measured in rats and mice (Smith et al. 2005).

With two exceptions, when one parameter was changed, all other inputs remained at their default level (as specified in Table 1). When analyzing the effect of body size, radial and linear dimensions of the body parts were scaled up or down proportionally to accommodate the increased body mass while still maintaining the same body part proportions and densities as the default model. When analyzing the effect of linear dimensions, radial dimensions were automatically adjusted in or out to maintain the same body part density and total body mass as

the default model. Thus, increasing linear dimensions would result in longer, thinner body parts while decreasing linear dimensions would result in shorter, thicker body parts.

*2.3 Testing Niche Mapper's Ability to Predict Body Temperature in Wild Vervets*

We then simulated vervets in the Samara Game Reserve for the five-year data collection period (2012-2016) and compared model predictions for $T_b$ to observed $T_b$ from the wild vervet study population. The primary purpose of these simulations was to test NM's ability to predict body temperature accurately in order to identify conditions under which vervets are thermally stressed. Such validation provides confidence that other outputs that are dependent on $T_b$, like metabolic rate and evaporative water loss, are also reliable.

For these simulations, hourly air temperatures were obtained from an on-site weather station. A constant monthly cloud cover based on 1960-1990 average values from New et al. (2002) was used for all hours of the day. Ground reflectivity was assumed to be 20% to simulate a mix of bare soil and grass, and we assumed that 100% shade was always available to the vervets. Daily wind speeds were assumed to vary from 0.1 m/s (at sunrise) to 4 m/s (one hour after solar noon), approximated from monthly long-term average (1970-2000) wind speeds ranging from 2.2 m/s to 3.5 m/s (mean = 2.8 m/s; Fick & Hijmans 2017). Relative humidity was assumed to vary from 100% (at sunrise) to a minimum at one hour after solar noon; the minimum was calculated based on the daily temperature range assuming constant water mass in the air over 24 hours (Tracy et al. 1980).

Within a given month we used the same activity multiplier for diurnal period, varying from a low of 2.25x resting metabolic rate (RMR) in the summer months to a maximum of 4.25x RMR in the winter months. These multipliers were derived through a calibration process to obtain the closest fit between predicted and observed $T_b$ for the 2012-2013 field season

simulations. This variation is reasonable based on observations of higher activity in the colder months, as well as daily activity needing to be condensed into fewer hours in the winter months when day lengths are shorter (McFarland et al. 2014). For nocturnal hours (defined here as all hours when the sun is below the horizon), the monkeys were modeled as being inactive up in a tree, where 2-meter climate conditions determine the relevant microclimate, with 85% canopy cover. Piloerection, vasodilation/vasoconstriction, sweating, and $T_b$ changes between the specified maximum and minimums (see Table 1) were all allowed for thermoregulation.

During nocturnal hours we modeled different postures. The least heat-conservative "stretched" posture was used to model all body parts exposed for heat exchange (e.g., a solitary individual draped across a branch). NM allows a vervet to assume a more heat-conserving "curled" position, simulated by combining the arms, legs, and torso into a single body part shape for the purposes of modeling (simulating a monkey wrapping its arms and legs around its torso). Finally, we allowed huddling (see details in Appendix 1) as the most heat-conservative nocturnal body posture because huddling is thought to be an important form of behavioral thermoregulation to minimize metabolic heat production overnight (McFarland et al. 2015). For the field simulations, we assumed a warm huddling scenario to provide an upper bound of predicted nighttime $T_b$: a vervet in between two other individuals with 75% of its dorsal and ventral halves in contact with neighbors.

Any single NM model will always thermoregulate to minimize thermal stress and, by extension, minimize variation in body temperatures changes from the default 38°C. For example, if we allowed vervets to seek shade and assume any nighttime posture, the model would immediately attempt to seek shade when the animal is first heat stressed during the day and start to huddle when it is first cold stressed at night before changing its body temperature.

Furthermore, during any diurnal hour, NM will always assume the vervet is active unless it is predicted to be unable to maintain active metabolic heat production when maximizing all thermoregulatory options. A real animal may not always follow the same set of priorities in every situation.

Therefore, a single set of model assumptions in terms of habitat choice, activity level, and posture is not universally applicable, and it would be inappropriate to evaluate NM's performance using a single model. To address this, we ran multiple simulations to bound the full range of possible $T_b$s that NM could predict. For diurnal hours vervets were either modeled as active with no access to shade (maximum predicted diurnal $T_b$) or inactive and uncurled with access to full shade (minimum predicted diurnal $T_b$). For nocturnal hours, vervets were either modeled as curled up and huddled (maximum predicted nocturnal $T_b$) or stretched out (minimum predicted nocturnal $T_b$). To complete the range of nocturnal postures, we also simulated vervets as curled up but not huddled.

We compared the mean observed $T_b$ for each hour to the maximum predicted $T_b$, minimum predicted $T_b$, and the average of the maximum and minimum predicted $T_b$. However, the most appropriate evaluation is how well NM's range of predicted temperatures capture the observed temperatures. To do this, we calculated the number of hours that the mean observed $T_b$ for each sex was between the minimum and maximum $T_b$ predicted by NM. We also calculated the number of hours during which the mean observed temperatures were within 0.25°, 0.5° and 1°C of NM's predicted range.

Finally, we calculated several daily metrics with both the observed and predicted $T_b$ data: minimum temperature, maximum temperature, mean temperature, and 24-hour amplitude of body temperature rhythm (difference between maximum and minimum body temperature). For

the observed data, these metrics were calculated based on hourly average temperatures for each sex, with the exception of 24-hour amplitude where individual amplitudes were calculated and an average for each sex was computed. For the predicted data, ranges for each metric were calculated using the maximum and minimum $T_b$ predictions.

*2.4 Evaluating Niche Mapper's Ability to Detect Thermal Stress in Wild Vervets*

We also used these simulations—in conjunction with the data collected on the wild vervet population—to test NM's ability to predict metrics of thermal stress that could be used to quantify the thermal "costs" to living in a particular environment. Quantifying these costs allows us to evaluate habitat suitability from a mechanistic perspective.

First, we evaluated NM's ability to detect heat stress by examining whether vervets were observed to rest more when NM predicted higher thermoregulatory costs (i.e., evaporative water loss) to maintaining activity. To do this we compared NM's predicted water loss rates (i.e., sweating) for an active individual to the proportion of the wild vervet study population observed to be resting between 10:00 and 16:00 in non-winter months; these are the hours we assume that resting is most likely to be the consequence of heat avoidance behavior. We used a generalized linear model (binomial error family; logit link) in R version 3.4.0 (R Core Team 2017), with the proportion of the group resting as the dependent variable and predicted sweating rate for a vervet active in the sun as the independent variable. Brain & Mitchell (1999) and Mitchell et al. (2009) found that baboons reduced evaporative water loss when they were water-restricted. Thus, we also looked at the influence of precipitation (as a proxy for free water availability and vegetation moisture content) as a predictor of resting on its own or as a modifier of NM's sweating rates as a predictor of resting (via interactions in the GLM). Cumulative precipitation as measured by the onsite weather station over the previous 7, 14, 30 and 60 days was added to the model as a

second independent variable to determine whether precipitation interacted with and modified the relationship between predicted sweating rates and observed resting rates. These precipitation-effect analyses were limited to December 2014 and onwards, when daily precipitation data collection began

To evaluate NM's ability to detect cold stress, a direct comparison of predicted $T_b$ to observed $T_b$ is likely not informative because vervets may choose to increase their metabolic rate in order to defend their lower modal $T_b$ in some situations while NM will always reduce $T_b$ down to the user-specified minimum in order to minimize metabolic heat expenditure above the target rate. Thus, we investigated whether NM predicted higher metabolic heat production requirements on nights when the wild vervets were observed have lower overnight $T_b$s, based on the assumption that observations of $T_b$ below the lower modal $T_b$ reflected vervets trying to minimize additional metabolic heat production in response to cold stress. We compared the night's minimum observed hourly $T_b$ (averaged across all individuals) to the maximum "average" hourly predicted metabolic rate for that night (i.e., the hour for which the average of the predicted metabolic rate for a stretched-out monkey and a huddled monkey was the highest). NM will predict a metabolic rate higher than the target resting metabolic rate if needed to maintain the lowest allowable $T_b$ in that hour's environmental conditions. If NM is able to predict cold stress, NM's predicted metabolic rate requirements should increase as observed minimum overnight $T_b$s decrease. The relationship between these two metrics of cold stress was evaluated using Spearman rank correlation test in R.

## RESULTS

### *Simulated Metabolic Chamber Analyses*

The predicted thermoneutral zone (TNZ) for the model vervets ranged from 15°C (males) and 16°C (females) to 32°C without any postural change (Fig. S3). Allowing a heat-conserving "curled" posture with arms and legs tucked into the torso reduced the lower critical temperature to 7°C (females) and 4°C (males) (Fig. S3). The model was most sensitive to changes in assumed resting metabolic rate, fur depth, the hair length:fur depth and body part length:width ratios (Table 2; Fig. S4,S5). The model was least sensitive to changes in hair diameter and density, although halving these values from the default value had a large effect (Fig. S4). Upper and lower critical temperatures increased and decreased, respectively, by one degree for each degree the Tb was able to vary from 38°C (Fig. S6).

*Testing Niche Mapper's Ability to Predict Body Temperature*

*a) Diurnal Hours*

Predicted Niche Mapper (NM) $T_b$s for animals assumed to be resting in the shade (minimum $T_b$ prediction) and active in the sun (maximum $T_b$ prediction) were compared to observed $T_b$s (Fig. 2). The average of predicted resting and active $T_b$s were also calculated to represent a mix of activity and inactivity for a given hour. As expected, during diurnal hours the minimum $T_b$ prediction was typically lower than the observed $T_b$, while the maximum $T_b$ prediction typically overestimated $T_b$ compared to observed $T_b$. On average, NM predicted $T_b$ to be at the observed upper modal temperature.

**Table 2.** Summary of vervet model sensitivity analysis results, showing the changes in whole body thermal conductivity (WBTC), upper critical temperature (UCT) and lower critical temperature (LCT) in response to 10% and 25% changes in key biophysical parameters. Values shown are for the female model; similar trends were observed for the male model.

| | | **10% Increase** | **10% Decrease** | **25% Increase** | **25% Decrease** |
|---|---|---|---|---|---|
| Fur depth | WBTC | -3% | 9% | -10% | +22% |
| | UCT | -1° | NC | -1° | +1° |
| | LCT | NC | +2° | -2 | +4 |
| Hair density | WBTC | -3% | 6% | -7% | +12% |
| | UCT | -1° | NC | -1° | +1° |
| | LCT | NC | 1° | -1° | +3° |
| Hair diameter | WBTC | NC | 3% | -6% | +9% |
| | UCT | -1° | NC | -1° | +1° |
| | LCT | NC | +1 | -1° | +3° |
| Hair length: fur depth ratio | WBTC | -7% | 13% | -17% | +34% |
| | UCT | -1° | NC | -1° | +1° |
| | LCT | -2° | +3° | -5° | +6° |
| Total body mass | WBTC | 2% | 11% | -8% | +19% |
| | UCT | NC | NC | -1° | +1° |
| | LCT | NC | +2° | -1° | +3° |
| Body part lengths | WBTC | +9% | -7% | +13% | -16% |
| | UCT | NC | -1° | 1° | -2° |
| | LCT | +2° | -1° | +3° | -4° |
| Resting Metabolic Rate | WBTC | -- | -- | -- | -- |
| | UCT | -1° | +1° | -3° | +2° |
| | LCT | -2° | +3° | -6° | +6° |

NM's average $T_b$ predictions were also compared with observed $T_b$ for each hour of the day across each season (Fig. 3). While there was close agreement for most hours (see Fig. S7 showing how most data points lie around the intersection of the upper modal temperature lines during these hours), there were times (5.4% of hours for females; 8.2% of hours for males) when the average NM temperature over- or under-predicted the observed $T_b$ by 1-3°C. During the first

diurnal hours, NM over-predict $T_b$ if any activity was assumed (e.g., average and maximum $T_b$ predictions for hours 04:00-05:00 in Fig. 3). For other hours, most of the over-predictions occur in the warmer months during the warmest hours of the day when the minimum NM prediction (representing a resting vervet) were closest to the observed $T_b$s (e.g., hours 12:00-15:00 in Fig. 3). Similarly, most of the under-predictions occur in the colder months, when the maximum NM prediction (representing an active vervet) were closest to the observed Tbs. (e.g., hours 14:00-16:00 in Fig. 3).

*b) Nocturnal hours*

Predicted NM $T_b$s for animals assumed to be sleeping in an uncurled posture (minimum Tb prediction) and huddled with other individuals (maximum Tb prediction) were compared to observed nocturnal Tbs (Fig. 4). The average of the maximum and minimum Tbs were also calculated to represent a mix of postures within the group. As expected, during nocturnal hours the minimum $T_b$ prediction was typically l lower than the observed $T_b$, while the maximum $T_b$ prediction typically over estimated $T_b$ compared to observed $T_b$. On average, NM predicted $T_b$ to be at the observed lower modal temperature.

During the first nocturnal hours, NM tended to under-predict $T_b$ (hours 17:00-19:00 in Fig. 5), as the vervets were shifting from active phase $T_b$ to inactive phase $T_b$. Once the lower modal temperature was reached (hours 21:00 to 06:00 in Fig. 5), the average NM predictions were similar to the observed $T_b$ for spring/fall and summer months. During winter months, the observed $T_b$ was closer to the maximum NM prediction (representing vervets huddling together) for much of the night.

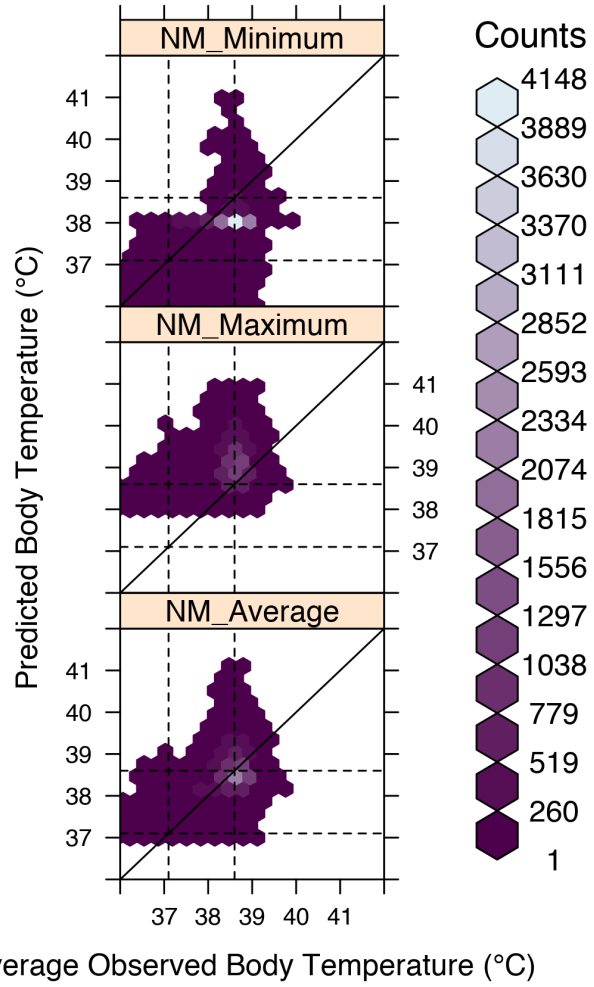


**Fig. 2.** Hexbin plots of predicted vs. observed body temperature ($T_b$) during diurnal hours. The minimum NM $T_b$ is for a vervet inactive in the shade; the maximum NM $T_b$ is for a vervet active in the sun. An average of the maximum and minimum $T_b$ predictions, representing a mix of activity and inactivity, is also shown. The lighter the color of the hexagon, the greater the number of data points in that location on the plot. The dashed lines indicate the two modal $T_b$s of the wild vervets and the solid line indicates a 1:1 relationship between observed and predicted $T_b$. Values shown are for the female model, but similar trends were observed for the male model.

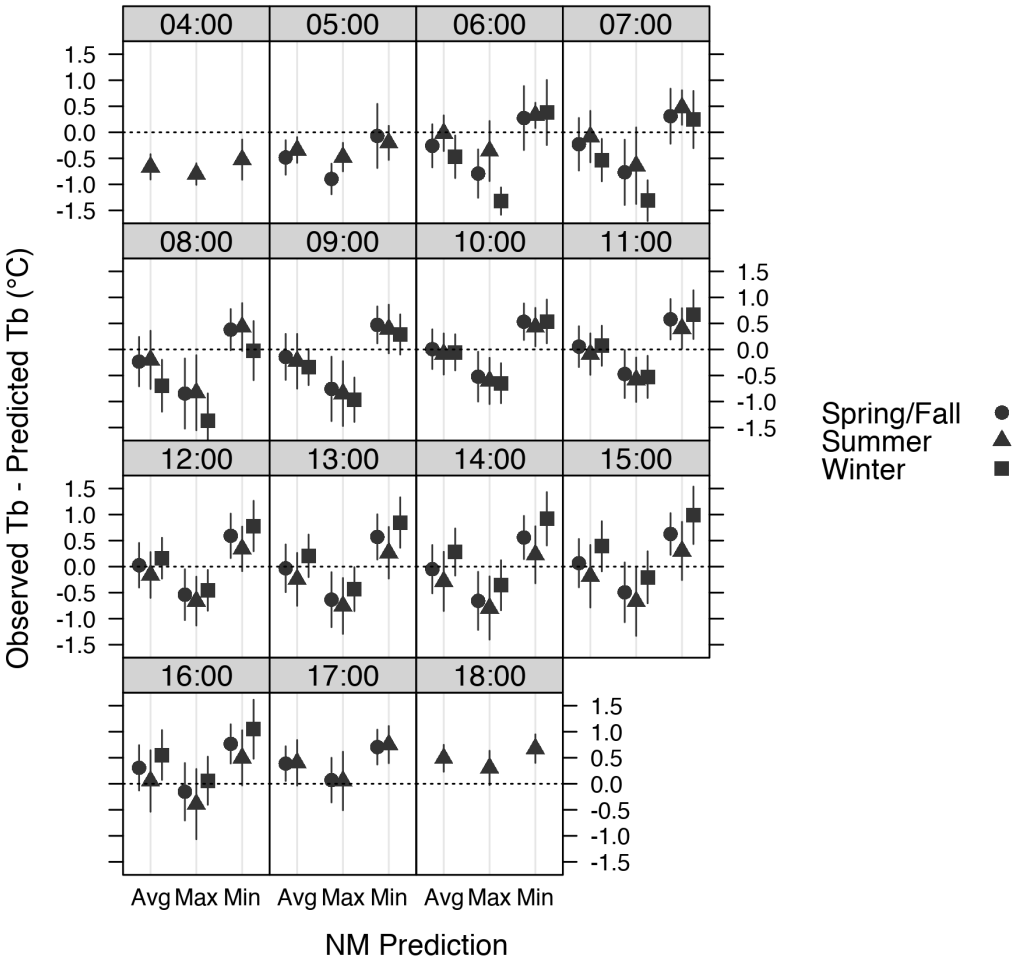


**Fig. 3.** The difference (± s.d.) between observed and predicted body temperatures ($T_b$) for diurnal hours between 2012 and 2016. The data are broken down by hour (04:00 to 18:00) and season (summer = December-February; winter = June-August; spring/fall=March-May; September-November). The minimum NM $T_b$ is for a vervet inactive in the shade; the maximum NM $T_b$ is for a vervet active in the sun. The average prediction is the average of the maximum and minimum $T_b$ predictions, representing a mix of activity and inactivity. Values shown are for the female model, but similar trends were observed for the male model.

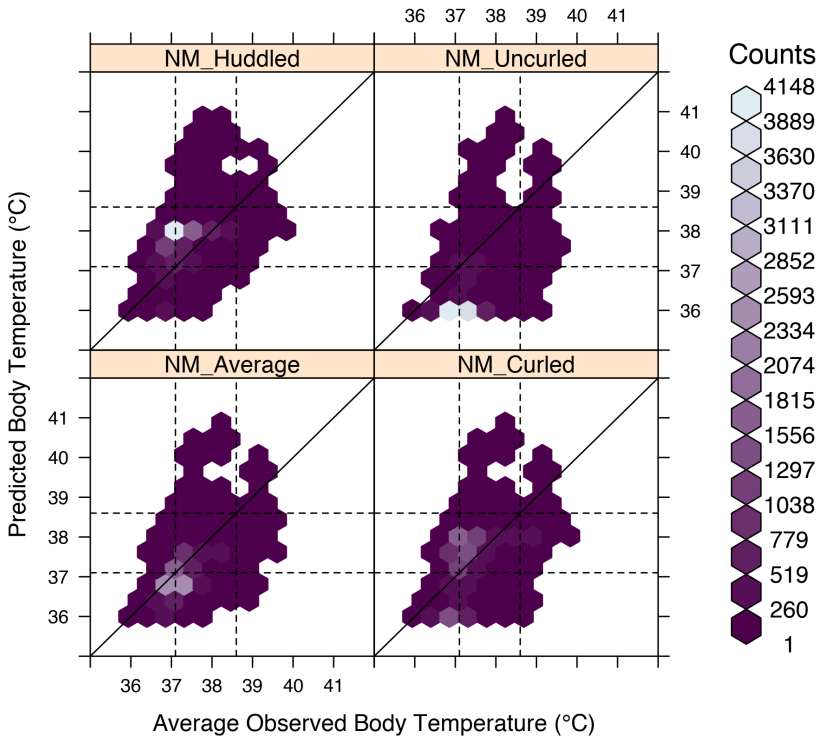


**Fig. 4.** Hexbin plots of predicted vs. observed body temperature ($T_b$) during nocturnal hours assuming different nighttime postures in the NM model. The huddled posture will produce the maximum $T_b$ prediction while the uncurled posture will produce the minimum $T_b$ prediction. The average $T_b$ is the average of the maximum and minimum $T_b$ predictions. The curled posture is shown to illustrate predictions assuming all potential postures separately. The lighter the color of the hexagon, the greater the number of data points are found in that location on the plot. The dashed lines indicate the two modal $T_b$ of the wild vervets and the solid line indicates a 1:1 relationship between observed and predicted temperature. Values shown are for the female model, but similar trends were observed for the male model.

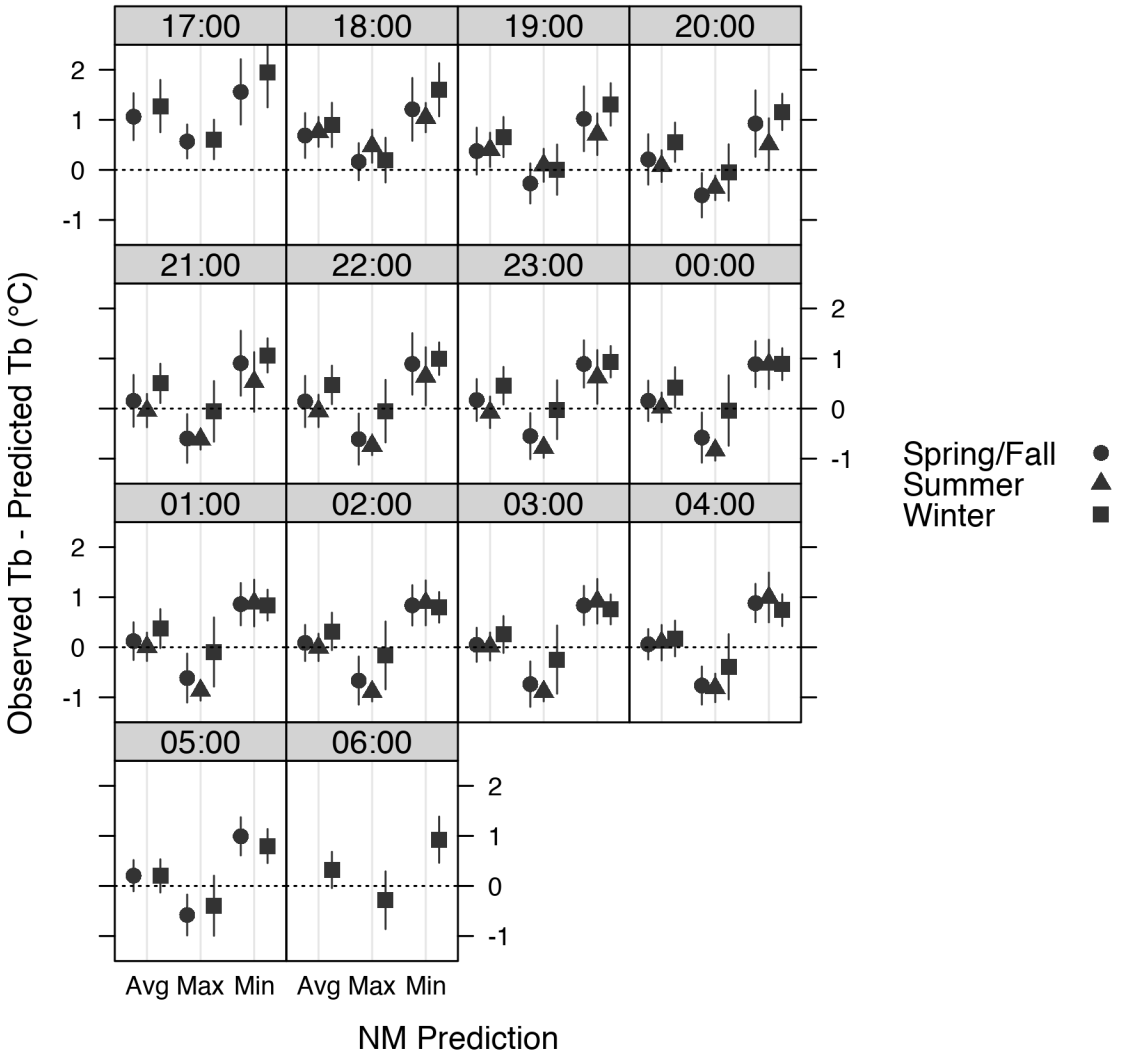


**Fig. 5.** The difference (± s.d.) between observed and predicted body temperatures ($T_b$) for nocturnal hours between 2012 and 2016. The data are broken down by hour (17:00 to 06:00) and season (summer = December through February; winter = June through August). The minimum NM $T_b$ is for a lone vervet stretched out; the maximum NM $T_b$ is for a curled up and huddled with others. The average prediction is the average of the maximum and minimum $T_b$ predictions, representing a mix of stretched out, curled, and huddled individuals. Values shown are for the female model, but similar trends were observed for the male model.

*c) Bracketing Possibilities*

As illustrated in the above results, a single model is not appropriate for every given hour. However, the range of potential $T_b$ predictions should encompass or nearly encompass the observed $T_b$ for any given hour. Observed $T_b$ were within the range of predicted $T_b$ for >68% of hours and within 0.5°C of the range for > 88% of the hours for both the male and female models (Table 3). During diurnal hours, when the models were more than 1°C away from the observed temperatures, it was mostly a consequence of the model overestimating $T_b$; during nocturnal hours, larger deviations were due mostly to the model underestimating $T_b$.

For diurnal hours, we also assessed the importance of shade availability. Removing access to shade (i.e., the minimum $T_b$ prediction is for a resting vervet in the sun) results in a >15% reduction in the percent of hours for which the predicted range encompasses the observed $T_b$, due entirely to an increased number of overestimates. For nocturnal hours, we investigated the effect of not allowing certain postures. Not allowing huddling (i.e., the maximum predicted $T_b$ is for a curled individual) reduced the percentage of hours for which the observed $T_b$ was within the predicted range by ~20% for both sexes. Not allowing curling or huddling resulted in the observed $T_b$ being within 0.5°C of NM's predicted $T_b$ for an uncurled vervet for <20% of the hours.

**Table 3.** Percentage of diurnal hours in the 2012-2016 field seasons (n=14,037) that the mean observed vervet body temperature ($T_b$) was within the boundaries of NM's predicted $T_b$ for an active individual in full sun and an inactive individual with and without access to shade. Also shown are the percentage of hours that the observed temperature was within 0.25°, 0.5°, or 1° C of the predicted range. The numbers in parentheses are the number of hours for which the mean observed $T_b$ was under/over the range predicted by NM. Removing access to shade increases the number of hours that NM's predicted range is higher than the observed temperatures.

| | | **Shade Available** | **No Shade Available** |
|---|---|---|---|
| Females | Within Range | 72.8% (1734/2083) | 55.8% (4126/2083) |
| | Within 0.25°C | 86.1% (892/1060) | 73.7% (2637/1060) |
| | Within 0.5°C | 93.7% (400/482) | 85.5% (1556/482) |
| | Within 1.0°C | 99.4% (59/27) | 96.7% (433/27) |
| Males | Within Range | 67.8% (2039/2481) | 50.0% (5436/2481) |
| | Within 0.25°C | 81.5% (1261/1332) | 68.4% (3099/1332) |
| | Within 0.5°C | 91.3% (662/562) | 82.8% (1850/562) |
| | Within 1.0°C | 98.7% (149/34) | 95.5% (598/34) |

**Table 4.** Percentage of nocturnal hours in the 2012-2016 field seasons (n=13,443) that the mean observed vervet body temperature ($T_b$) was within the boundaries of NM's predicted $T_b$ for a lone individual and a huddled individual. Also shown are the percentage of hours that the observed temperature was within 0.25°, 0.5°, or 1°C of the predicted range. The number in parentheses are the number of hours for which the mean observed $T_b$ was under/over the range predicted by NM. "Stretched only" refers to only modeling a lone individual splayed out (no range); "Stretched + curled" refers the range of $T_b$s predicted between an individual splayed out and a curled (arms and legs tucked into torso) individual; "Stretched + curled + huddled" refers to the range of $T_b$s predicted between an individual splayed out and an individual huddled between two others.

| | | **Stretched + curled + huddled** | **Stretched + curled** | **Stretched only** |
|---|---|---|---|---|
| Females | Within Range | 70.5% (864/3108) | 48.6% (864/6042) | NA |
| | Within 0.25°C | 80.5% (449/2175) | 59.7% (449/5417) | 8.2% (449/11898) |
| | Within 0.5°C | 88.5% (227/1314) | 69.8% (227/3828) | 16.5% (227/10992) |
| | Within 1.0°C | 98.2% (46/195) | 88.3% (46/1048) | 55.0% (46/5997) |
| Males | Within Range | 74.1% (1007/2479) | 56.3% (1007/4872) | NA |
| | Within 0.25°C | 82.8% (621/1693) | 67.3% (621/3772) | 8.8% (621/11639) |
| | Within 0.5°C | 90.6% (303/954) | 78.6% (303/2573) | 20.0% (303/10460) |
| | Within 1.0°C | 98.3% (46/180) | 93.8% (46/782) | 61.8% (46/5084) |

Finally, we compared NM's predictions to observed values for several daily $T_b$ metrics typically used to assess an animal's thermal performance (e.g., McFarland et al. 2015, Henzi et al. 2017). NM's predicted range was within 0.5°C of observed values for > 90% of the days for all of the daily metrics (Table 5). For days when the observed maximum temperature was outside of the predicted range, NM tended to over-predict maximum temperatures. For days when the observed minimum temperature was outside of the predicted range, NM tended to under-predict maximum temperatures. On days when the observed mean temperatures were outside the predicted range, the default models tended to under-estimate mean daily temperature, driven by under-estimating overnight $T_b$ in the winter months.

Figure 6 shows examples of NM's maximum and minimum predicted $T_b$ along with the range of observed $T_b$ for a hot and cold month.

**Table 5.** Percentage of days in the 2012-2016 field seasons (n=1,145) that the mean observed minimum, maximum, average, and 24 hour-amplitude vervet body temperature ($T_b$) was within the boundaries of NM's predicted $T_b$ between the coldest model (lone monkey stretched out at night; resting in shade during the day) and the warmest model (huddled at night; active in sun during the day). Also shown are the percentage of days that the observed metric was within 0.25°, 0.5°, or 1°C of the predicted range. The number in parentheses are the number of days for which the mean observed metric was under/over the range predicted by NM.

| | | **Female** | **Male** |
|---|---|---|---|
| Minimum Body Temperature | Within Range | 82.4% (26/175) | 89.2% (60/64) |
| | Within 0.25°C | 87.7% (8/133) | 94.6% (28/34) |
| | Within 0.5°C | 92.2% (5/84) | 97.9% (7/17) |
| | Within 1.0°C | 99.1% (1/9) | 99.9% (0/1) |
| Maximum Body Temperature | Within Range | 76.4% (137/133) | 72.2% (148/170) |
| | Within 0.25°C | 89.3% (58/64) | 86.7% (79/73) |
| | Within 0.5°C | 95.2% (30/25) | 94.8% (41/19) |
| | Within 1.0°C | 98.7% (12/3) | 99.0% (11/0) |
| Mean Body Temperature | Within Range | 89.2% (32/92) | 92.1% (40/51) |
| | Within 0.25°C | 96.3% (6/36) | 97.4% (14/16) |
| | Within 0.5°C | 99.3% (1/7) | 99.7% (2/2) |
| | Within 1.0°C | 100% (0/0) | 100% (0/0) |
| 24-hour Amplitude | Within Range | 96.6% (16/23) | 93.5% (3/71) |
| | Within 0.25°C | 99.0% (3/9) | 96.6% (2/37) |
| | Within 0.5°C | 99.8% (1/1) | 98.1% (1/21) |
| | Within 1.0° | 99.9% (0/1) | 99.7% (0/3) |

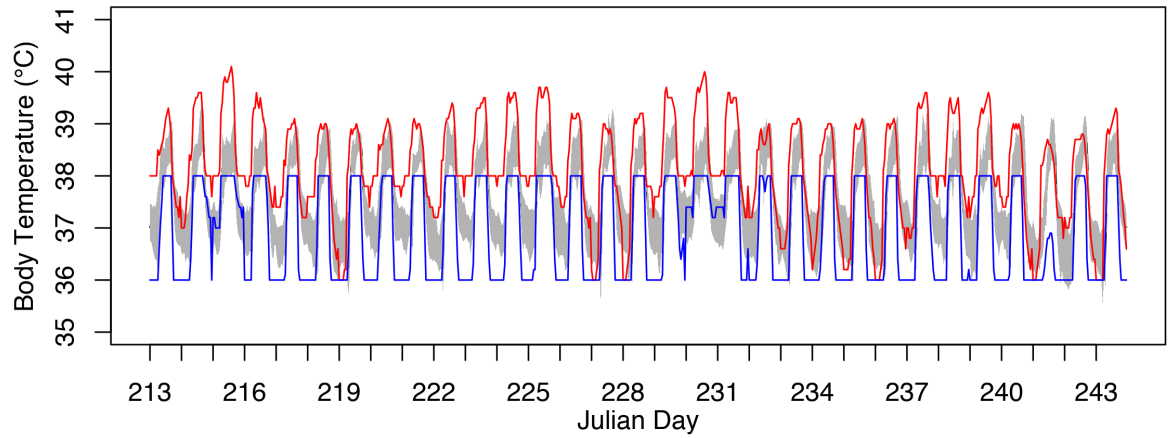


**(a)**

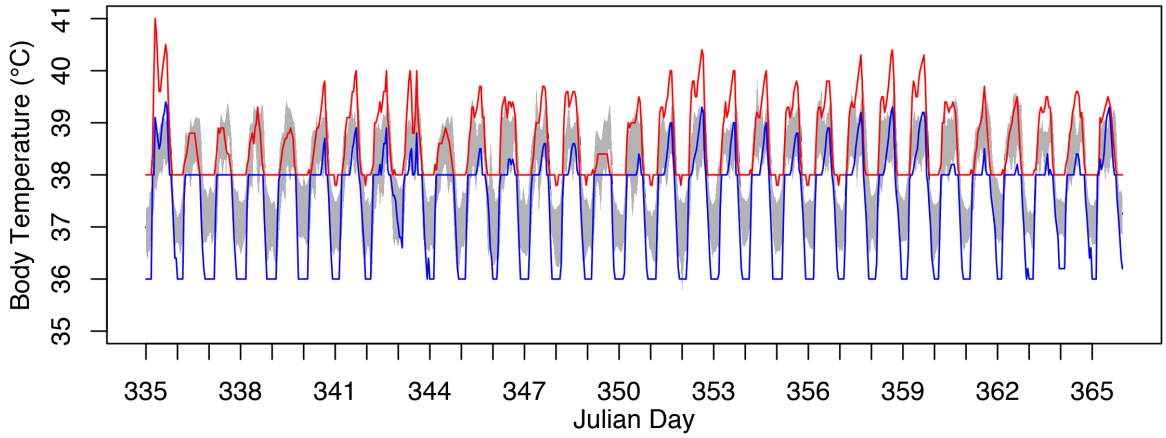


**(b)**

**Figure 6.** Example plots of NM's range of predicted body temperatures ($T_b$) and the range of observed $T_b$ for females for a winter month (a; August 2014) and a summer month (b; December 2014). During diurnal hours, the red line shows predicted $T_b$ for an active animal in full sun and the blue line shows predicted $T_b$ for an inactive animal in full shade. During nocturnal hours the red line shows the predicted $T_b$ for an individual huddled between two other individuals and the blue line shows predicted $T_b$ for a lone individual stretched out (i.e., all body parts available for heat exchange). The shaded gray area shows the range of observed $T_b$. for a given hour.

*Evaluating Niche Mapper's Ability to Detect Thermal Stress*

Across the non-winter months (September-May), there was a significant increase in the proportion of the group resting when NM predicted higher sweating rates in order to prevent hyperthermia when active. A higher proportion of the group was observed to be resting during hours when NM predicted a higher sweating rate to maintain activity ($z= 3.40$, $p<0.001$, $\beta \pm S.E. = 34.51 \pm 10.16$, $n= 8015$ hours). Using only those hours for which there were onsite precipitation data and activity observations, precipitation was not found to be significantly related to the proportion of the group resting or a significant modifier of sweating rate as a predictor of proportion of the group resting at any of the time-lag periods ($z<|0.3|$, $p>0.7$ for all).

In the winter months, NM predicted greater overnight metabolic heat production requirements on the nights when observed minimum $T_b$s were further below the lower modal temperature (Fig. 7; Spearman rho = -0.52 for females and -0.60 for males; $p<0.001$ for both).

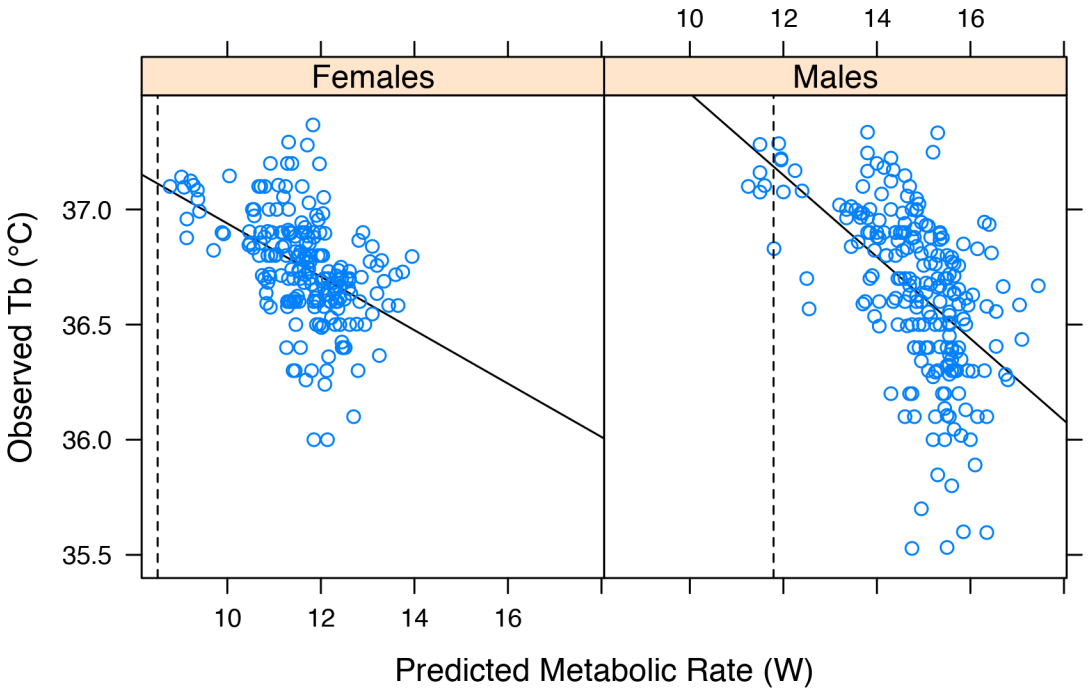


**Figure 7.** Observed minimum nighttime body temperature ($T_b$) plotted against that night's highest hourly metabolic rate predicted by NM in winter months (Jun-Aug; all years combined), showing that NM predicted higher metabolic heat production costs to maintain a minimum $T_b$ of 36°C on nights that vervets were observed to reduce their $T_b$ further below the lower modal $T_b$ of 37.1°C. The metabolic rate is the "average" maximum metabolic rate of a lone individual sleeping in an uncurled posture (maximum metabolic rate requirement) and a huddled vervet (minimum metabolic rate requirements). Also shown is the upper target resting metabolic rate NM is thermoregulating to meet (dashed black line) and the best fit regression line to indicate trends (solid line).

## DISCUSSION

### *Metabolic Chamber and Sensitivity Analyses*

As a first step in assessing Niche Mapper (NM) model performance, we placed the vervet model in a controlled environment (a simulated metabolic chamber) to ensure that the model

predicted a reasonable thermoneutral zone. We are unaware of any studies measuring the thermoneutral zone (TNZ) of vervets. There are studies reporting TNZs for night monkeys (Le Maho et al. 1981; 28°C to 30°C), rhesus monkeys (Johnson & Elizondo 1979: 24.7°C to 30.6°C), colobus monkeys and Sykes monkeys (Mueller et al. 1983; ~10°C to 28°C for both). Night monkeys are nocturnal and the monkeys in the Johnson & Elizondo study were acclimated to 26°C prior to the metabolic chamber experiments, leaving the Müller et al. study as the most appropriate point of comparison. Their study animals were acclimated to ambient daily temperature variation (~10-26°C), closer to the range of temperatures that vervets encounter in the wild (<0°C to >40°C). Compared to the data from the Müller et al. study and given the range of temperatures that vervets encounter in the wild, our predicted TNZ for the model vervets (15-32 degrees) seem reasonable.

The sensitivity analyses conducted in the simulated metabolic chamber identify biophysical properties that most influence the model's $T_b$ and metabolic rate predictions, informing data collection priorities for work with other species. The biophysical properties that were most influential were assumed resting metabolic rate, fur depth, the hair length:fur depth ratio and body part length:width ratios. All pelage inputs used here were from direct measurements, so we can be confident in their use. The fur thermal conductivities calculated by NM using these fur properties is 0.05-0.07 W/mC, depending on body part, which is within the 0.03 (flattened pelt) - 0.07 (backcombed pelt) W/mC range measured on a vervet pelt by McFarland et al. (2016). The backcombed pelt was considered by McFarland et al. (2016) to represent a pelt in its typical form.

The hair length:fur depth ratio is implicated in NM's piloerection approximations. If this option is allowed by users, the simulated fur thickness is allowed to increase to a specified

percentage of the hair length. Thus, increasing the ratio would allow greater thermal benefits from piloerection. This ratio would not be as important an input for species, such as lemurs, that lack the ability to piloerect (Chaplin et al. 2014).

With respect to body sizes, the sensitivity analyses show that the model predicts that larger vervets will be more cold-tolerant. The analyses also show that the model is sensitive to the length-to-width proportions of body parts, with more compact animals being more cold-tolerant. It is interesting that the male and female models are predicted to have a similar TNZ despite males being 45% larger than females. However, the females had smaller body part length-to-width ratios and relatively thicker fur, both of which appear to offset the thermal effect of smaller body size.

*Body Temperature Predictions*

In this first test of NM's ability to predict $T_b$ in wild animals, predicted maximum and minimum $T_b$s bracketed the observed $T_b$ for the majority of hours (Table 2). Importantly, although $T_b$s in NM were allowed to fluctuate above and below the observed upper and lower modal temperatures observed in the wild vervets, the "average" predicted $T_b$ typically clustered around the upper modal temperature during the day and the lower modal temperature during the night (Figs. 2 and 4). This indicates that NM is able to capture a vervet's typical response to fluctuating environmental conditions.

Larger (> 0.5°C) deviations between observed and the average predicted $T_b$ were sometimes observed. However, they follow logical patterns based on the time of day and time of year, allowing for reasonable explanations. For diurnal hours, most of the over-predictions occur in the warmer months when vervets have been shown to reduce activity as a possible means to avoid hyperthermia (McFarland et al. 2014). Thus, the "average" prediction would be expected

to over-predict $T_b$ because the "resting" prediction would be more appropriate for these hours. Similarly, most of the under-predictions occur in the colder months where two different mechanisms could be at play. First, on the colder days vervets have been shown to increase activity and foraging time as a possible means to maintain their upper modal temperature (McFarland et al. 2014), and there is unlikely to be much shade-seeking in the winter. Thus, the "average" prediction would be expected to under-predict $T_b$ because the "active" prediction would be more appropriate for these hours. Second, the $T_b$ cycling could be an entrained daily rhythm that happens every day regardless of the ambient temperatures (Levesque et al. 2012), even at the potential cost of additional heat loss on the coldest days of the year. NM model code does not have a built-in $T_b$ cycling. All predicted deviations from the specified default $T_b$ (38°C) are due to responses to environmental temperatures.

More activity than usual on a given day (e.g., changes in food availability requiring more travel) also could cause NM to under-predict daytime $T_b$ because our modeling assumed the same activity level for all days within a month for its "active" prediction. NM's $T_b$ predictions do not include the heat increment of feeding, so NM would be prone to under-predictions in post-feeding hours. Occasional swimming and drinking of cool water have also been observed in this group and was not considered in this modeling, which could account for some $T_b$ over-predictions in the warmer months.

Specific to nocturnal $T_b$, for the first hours after sunset, NM under-predicts $T_b$ (hours 17:00 and 18:00 in Fig. 5). This is likely due to NM assuming an immediate metabolic rate reduction from active to resting to occur at sundown. In reality, there may be some crepuscular activity of vervets in the trees as they settle down for the night and vervets may have a more gradual metabolic rate reduction from active to resting.

While the most common average nocturnal prediction was close to the observed $T_b$ (see Fig. S8) there are hours when the "average" prediction over- or under-predicts the observed $T_b$ by >2°C. These discrepancies could be due to the majority of individuals in the group choosing a more or less heat-conserving posture on certain nights, causing the "average" prediction to over-predict temperatures on hot nights (e.g., if most individuals choose to stretch out) or to under-predict temperatures on cold nights (e.g., if most individuals choose to huddle or curl up).

Some over-predictions could also be due to the observed $T_b$ cycling potentially being an entrained daily rhythm that happens every day, even if the nighttime $T_b$ reduction is not necessary to minimize heat loss on a particular day. As discussed for the diurnal hours, NM model code does not have a built-in $T_b$ cycling. All predicted deviations from the specified default $T_b$ (38°C) are due to responses to environmental temperatures to either minimize metabolic heat production (in the case of $T_b$ reductions in cold conditions) or to maintain minimum rates (in the case of $T_b$ increases in hot conditions).

Finally, some under-predictions could be due to the real vervets increasing metabolic rates to defend its lower modal $T_b$ rather further reducing $T_b$. For example, in some conditions it could be worth the extra metabolic expenditure to maintain a preferred $T_b$, provided that sufficient food resources are available to supply this additional energetic demand. In contrast, NM's thermoregulatory decision-making always chooses to minimize metabolic heat production and will reduce $T_b$ in such situations. NM will only predict an increased metabolic rate above the target range if it is needed to maintain the lowest allowable $T_b$ in that hour's environmental conditions after all other thermoregulatory options are exhausted.

*Predicting thermal stress*

We found that NM predicted greater overnight metabolic heat production required to maintain the model vervet's minimum $T_b$ on nights that vervets were observed to reduce $T_b$ to a greater degree than usual. We also found that as NM predicted higher sweating rates for vervets to remain active, a higher proportion of vervets were observed to be resting in the group scans. These results illustrate how NM can be used to mechanistically investigate thermal stress in vervets, using the same metrics identified by previous studies for this population: increased 24-h $T_b$ amplitude and huddling to cope with cold stress (Lubbe et al. 2014, McFarland et al. 2015) and increased resting to cope with heat stress (McFarland et al. 2014).

We did not find that the amount of recent rainfall influenced resting rates, contrary to our expectations based on Brain & Mitchell (1999) and Mitchell et al. (2009), who found that baboons took measures to reduce evaporative water loss only when they were water-restricted. This lack of a relationship between resting in hot conditions and precipitation, however, is likely due to precipitation not perfectly capturing water availability or animal hydration state. In this instance, there continuous standing water in a stream throughout the study period that may have allowed vervets to maintain activity via sweating even in periods of little precipitation. We note that a study investigating the influence of water availability and air temperature in the same vervets found that decreased water availability exacerbated stress hormone increases from high temperatures in the vervets, that vervets rested more in a hot-and-dry period compared to a hot-and-wet period, and that mortality was highest in the hot-and-dry period (C. Young, unpublished data). However, the hot-and-dry period in that study occurred after the conclusion of our study period.

*Study implications*

Vervets, like all endotherms, must balance maintaining its body temperature with the thermoregulatory costs incurred to do so, all while engaging in activities necessary for survival and reproduction. A biophysical model like NM can provide insight into the thermoregulatory consequences of morphological (e.g., body size, fur depth), physiological (e.g., heterothermy, sweating) and behavioral (e.g., huddling, shade-seeking, resting) adaptations and allow us to test hypotheses about how animals adapt to thermoregulatory challenges. We note that, as discussed above, these models cannot predict exactly what choice an animal will make during any given hour. The animal might not consistently prioritize reducing thermoregulatory costs or defending a particular $T_b$, but a model must be coded to follow a certain set of priorities. However, these models allow users to tailor models to investigate certain choices. For example, to investigate the evaporative water costs of staying active in a given environment, a model would be used that assumes that vervets never cease activity. Conversely, to investigate how much activity would be restricted if evaporative water costs are avoided, model would be used that assumes the animal will cease activity if sweating is required to maintain activity. Similarly, different allowable $T_b$ ranges could be modeled to explore the benefits of using increased heterothermy to reduce thermoregulatory costs (Hetem et al. 2016). NM is a generic model, so with basic information about body part dimensions, animal size, and fur properties listed in Table 1, it can easily be adapted to other species. Further investigation would be required, but basal metabolic rate—the key physiological input—appears to be estimated well by NM's default allometric equation, at least for haplorhines (Fig. S2).

Having a biophysical model that can accurately model an animal's fundamental energetic interactions with its environment allows researchers to explore questions about the fitness

implications of a species' morphology, physiology, and behavior in relation to its environment. For example, our results here provide support for the ideas of Lubbe et al. (2014), McFarland et al. (2015, 2016), and Henzi et al. (2017), that the observed heterothermy and huddling help improve fitness by reducing energetic costs during the cold winters experienced by this group of vervets. Such models can also provide insight into the importance of certain habitat characteristics such as shade availability to reduce heat-related costs or access to water to facilitate the use of sweating to thermoregulate.

Models like this might also be used to investigate whether spatial variation in morphology across a species' range could confer energetic advantages (e.g., Bergmann's and Allen's rule). Our sensitivity analyses show how different body sizes and fur properties affect thermal tolerance. For example, Turner et al. (2018) report spatial variation in body mass and limb length consistent with Bergmann's and Allen's rule in *Chlorocebus* spp., and NM could be used to explore this mechanistically. Similarly, biophysical models could be used to explore how disparate morphology, physiology and/or behavior between sympatric species could play a role in niche partitioning.

Finally, having an accurate biophysical model can provide insight into species responses to changing environments, either from climate change or land cover changes. In some places natural forest is being replaced by monocrop tree plantations, presumably resulting in hotter and drier environments that may impose thermoregulatory stress on some animals and affect the likelihood that such environments could serve as suitable habitat (Spehar & Rayadin 2017). In the context of exploring species' response to climate change, biophysical models enable a mechanistic approach to species distribution modeling. Such models allow researchers to investigate how direct effects of the climate on animals (e.g., enforced resting to avoid heat stress

or increased overnight metabolic heat production requirements) constrain distributions. Explicitly modeling the mechanism by which climate is thought to limit distributions may provide more accurate predictions of future distributions and is recognized as an important research area in need of development, particularly for endotherms (e.g., Buckley et al. 2012, Evans et al. 2015).

REFERENCES

Barrett L, Gaynor D, Rendall D, Mitchell D, Henzi SP (2004). Habitual cave use and thermoregulation in chacma baboons (*Papio hamadryas ursinus*). Journal of Human Evolution 46: 215-222.

Boyles JG, Seebacher F, Smit B, McKechnie AE (2011). Adaptive thermoregulation in endotherms may alter responses to climate change. Integrative and Comparative Biology 51: 676-690.

Brain C and Mitchell D (1999). Body temperature changes in free-ranging baboons (*Papio hamadryas ursinus*) in the Namib Desert, Namibia. International Journal of Primatology 20: 585-598.

Briscoe NJ, Kearney MR, Taylor C, Brendan WA (2016) Unpacking the mechanisms captured by a correlative SDM to improve predictions of a climate refugia. Global Change Biology 22: 2425-2439.

Buckley LB, Urban MC, Angilletta MJ, Crozier LG, Rissler LJ, Sears MW. 2010. Can mechanism inform species' distributional models. Ecology Letters 13: 1041-1054.

Buckley LB, Kingsolver JG. 2012. Functional and phylogenetic approaches to forecasting species' responses to climate change. Annual Review of Ecology, Evolution, and Systematics 43: 205-226.

Buckley LB, Hurlbert AH, Jetz W (2012). Broad-scale ecological implications of ectothermy and endothermy in changing environments. Global Ecology and Biogeography 21: 873-885.

Cahill AE, Aiello-Lammens ME, Fisher-Reid MC, et al. 2012 How does climate change cause extinction? Proceedings of the Royal Society B 280: 20121890.

Carne C, Semple S, Lehmann J (2015). Investigating constraints on the survival of orangutans across Borneo and Sumatra. Tropical Conservation Science 8: 940-954.

Campos FA and Fedigan LM (2009). Behavioral adaptations to heat stress and water scarcity in white-faced capuchins (*Cebus capucinus*) in Santa Rosa National Park, Costa Rica. American Journal of Physical Anthropology 138: 101-111.

Cawthon Lang KA. 2006 January 3. Primate Factsheets: Vervet (Chlorocebus) Taxonomy, Morphology, & Ecology. <http://pin.primate.wisc.edu/factsheets/entry/vervet>. Accessed 2017 April 29.

Chaplin G, Jablonski NG, Sussman RW, Kelley EA. 2014. The role of piloerection in primate thermoregulation. Folia Primatologica 85: 1-17.

Cho BT, editor (1969) Advanced Heat Transfer. Urbana, IL: U Illinois Press. 459 pp.

Danzy J, Grobler JP, Freimer N, Turner TR (2012). Sunbathing: a behavioral response to seasonal climatic change among South African vervet monkeys (*Chlorocebus aethiops*). African Primates 7: 230-237.

Dausmann KH (2014) Flexible patterns in energy savings: heterothermy in primates. Journal of Zoology 292: 101-111.

Diffenbaugh NS, Field CB, Dunbar RIM, Korstjens AH, Lehmann J (2009). Time as an ecological constraint. Biological Reviews 84: 413-429.

Dormann, CF, Schymanski SJ, Cabral J, et al. 2012. Correlation and process in species distribution models: bridging a dichotomy. Journal of Biogeography 39: 2119-2131.

Elith J, Leathwick JR. 2009. Species distribution models: ecological explanation and prediction across time and space. Annual Review of Ecology, Evolution, and Systematics 40: 677-697.

Eppley TM Watzek J, Dausmann KH, Ganzhorn JU, Donati G. 2017. Huddling is more important than rest site selection for thermoregulation in southern bamboo lemurs. Animal Behaviour 127: 153-161.

Estrada A, Garber PA, Rylands AB et al. (2017). Impending extinction crisis of the world's primates: why primates matter. Science Advances 3: e1600946

Evans TG, Diamond SE, Kelly MW (2015). Mechanistic species distribution modelling as a link between physiology and conservation. Conservation Physiology 3: doi:10.1093/conphys/cov056

Fick SE and Hijmans RJ. 2017. Worldclim 2: New 1-km spatial resolution climate surfaces for global land areas. International Journal of Climatology 37: 4302-4315.

Fuentes M and Porter WP (2013). A new approach to model soil temperature: using microclimate models to predict the impacts of climate change on sea turtles. Ecological Modeling 251: 150–157.

Fuller A, Dawson T, Helmuth B, Hetem RS, Mitchell D, Maloney SK (2010). Physiological mechanisms in coping with climate change. Physiological and Biochemical Zoology: Ecological and Evolutionary Approaches 83: 713-720.

Fuller A, Mitchell D, Maloney SK, Hetem RS. (2016) Towards a mechanistic understanding of the responses of large terrestrial mammals to heat and aridity associated with climate change. Climate Change Responses 3: 10.

Gordon MS, Bartholomew GA, Grinnell AD, Jorgensen CB, White FN. 1972. Animal Physiology: Principles & Adaptations (2nd ed). Macmillan Publ. Co., London. 592 pp.

Henzi SP, Hetem R, Fuller A, Maloney SK, Young C, Mitchell D, Barrett L, McFarland R (2017). Consequences of sex-specific sociability for thermoregulation in male vervet monkeys during winter. Journal of Zoology 302: 193-200.

Hetem RS, Maloney SK, Fuller A, Mitchell D. 2016. Heterothermy in large mammals: inevitable or implemented. Biological Reviews of the Cambridge Philosophical Society 91: 187-205.

Hill RA (2006). Thermal constraints on activity scheduling and habitat choice in baboons. American Journal of Physical Anthropology 129: 242-249.

Hill RA, Weingrill T, Barrett L, Henzi SP (2004). Indices of environmental temperatures for primates in open habitats. Primates 45: 7-13.

Hijmans RJ, Graham CH. 2006. The ability of climate envelope models to predict the effect of climate change on species distributions. Global Change Biology 12: 2272-2281.

Humpheries MM, Umbanhowar J, McCann KS. (2004). Bioenergetic prediction of climate change impacts on northern mammals. Integrative and Comparative Biology 44: 152-162.

Iwamoto T and Dunbar RIM (1983). Thermoregulation, habitat quality and behavioural ecology of Gelada Baboons. Journal of Animal Ecology 52: 357-366.

Johnson GS and Elizondo RS (1979). Thermoregulation in *Macaca mulatta*: a thermal balance study. Journal of Applied Physiology: Respiratory, Environmental and Exercise Physiology 46: 268-277.

Kearney M, Porter WP. 2009. Mechanistic niche modelling: combining physiological and spatial data to predict species' ranges. Ecology Letters 12: 334-350.

Kelley EA, Jablonski NG, Chaplin G, Sussman RW, Kamilar JM (2016). Behavioral thermoregulation in *Lemur catta*: the significance of sunning and huddling behaviors. American Journal of Primatology 78: 745-754.

Korstjens AH and Hillyer A (2016) Primates and climate change: a review of current knowledge. In: An Introduction to Primate Conservation. Wich SA and Marshall AJ, eds., Oxford University Press.

Korstjens AH, Lehmann J, Dunbar RIM (2010). Resting time as an ecological constraint on primate biogeography. Animal Behaviour 79: 361-374.

Kowalski GJ and Mitchell JW (1979). An Analytical and Experimental Investigation of the Heat Transfer Mechanisms within Fibrous Media. Trans. ASME Paper No. 79-WA/HT-40: 1-7.

Lacombe A (2002) Effects of temperature on metabolism, ventilation, and oxygen extraction in the Southern Brown Bandicoot *Isoodon obesulus* (Marsupialia: Peramelidae). Physiological and Biochemical Zoology 4: 405-411.

Le Maho Y, Goffart M, Rochas A, Felbabel H, Chatonnet J (1981). Thermoregulation in the only nocturnal simian: the night monkey: *Aotus trivirgatus*. American Journal of Physiology 240: R156-R165.

Lehmann J, Korstjens AH, Dunbar RIM (2008). Time and distribution: a model of ape biogeography. Ethology Ecology & Evolution 20: 337-359.

Lehmann J, Korstjens AH, Dunbar RIM (2010). Apes in a changing world—the effects of global warming on the behavior and distribution of African apes.

Levesque DL, Nowack J, Stawski C (2013). Modelling mammalian energetics: the heterothermy problem. Climate Change Responses 3: 7.

Long RA, Bowyer RT, Porter WP, Mathewson PD, Monteith KL, Kie JG (2014) Behaviour and nutritional condition buffer a large-bodied endotherm against direct and indirect effects of climate. Ecological Monographs 84: 513-532.

Lubbe A, Hetem RS, McFarland R, et al. 2014. Thermoregulatory plasticity in free-ranging vervet monkeys, *Chlorocebus pygerythrus*. Journal of Comparative Physiology B 184:799–809.

Majolo B, McFarland R, Young C, Qarro M (2013). The effect of climatic factors on the activity budgets of Barbary Macaques (*Macaca sylvanus*). International Journal of Primatology 34: 500-514.

Maloney SK, Marsh MK, McLeod SR, Fuller A. 2017. Heterothermy is associated with reduced fitness in wild rabbits. Biological Letters 13: 20170521.

Mathewson PD and Porter, WP (2013). Simulating polar bear energetics during a seasonal fast using a mechanistic model. PLoS One 8: e72863.

Mitchell D, Fuller A, Maloney SK (2009). Homeothermy and primate bipedalism: is water shortage or solar radiation the main threat to baboon (*Papio hamadryas*) homeothermy? Journal of Human Evolution 56: 439-446.

Mitchell D, Snelling EP, Hetem RS, Maloney SK, Strauss WM, Fuller A. 2018. Revisiting concepts of thermal physiology: predicting responses of mammals to climate change. Journal of Animal Ecology 87: 956-973.

McFarland R, Barrett L, Boner R, Freeman NJ, Henzi SP. 2014. Behavioral flexibility of vervet monkeys in response to climatic and social variability. American Journal of Physical Anthropology 154:357–364.

McFarland R, Fuller A, Hetem RS, Mitchell D, Maloney SK, Henzi SP, Barrett L (2015). Social integration confers thermal benefits in a gregarious primate. Journal of Animal Ecology 84:871–878.

McFarland R, Henzi SP, Barrett L, Wanigaratne A, Coetzee E, Fuller A, Hetem RS, Mitchell D, Maloney SK (2016). Thermal consequences of increased pelt loft infer an additional utilitarian function for grooming. American Journal of Primatology 78: 456-461.

Moyer-Horner L, Mathewson PD, Jones G, Kearney MR, Porter WP (2015) Modeling behavioral thermoregulation in a climate change sentinel. Ecology and Evolution 5**:** 5810-5822.

Müller EF, Kamau JMZ, Maloiy GMO (1983). A comparative study of basal metabolism and thermoregulation in a folivorous (*Colobus guereza*) and an omnivorous *(Cercopithecus mitis*) primate species. Comparative Biochemistry and Physiology 74A: 319-322.

Natori Y and Porter WP (2007). Model of Japanese Serow (*Capricornis crispus*) energetics predicts distribution on Honshu, Japan. Ecological Applications 17: 1441-1459.

New M, Lister D, Hulme M, Makin I (2002). A high-resolution data set of surface climate over global land areas. Climate Research 21: 1-25.

Pacifici M, Foden WB, Visconti P, et al. 2015. Assessing species vulnerability to climate change. Nature Climate Change 5: 215-224.

Pasternak G, Brown LR, Kienzle S, Fuller A, Barrett L, Henzi SP. 2013. Population ecology of vervet monkeys in a high latitude, semi-arid riparian woodland. Koedoe 55:1–9.

Porter WP, Gates DM. 1969. Thermodynamic equilibria of animals with environment. Ecological Monographs 39: 227-244.

Porter WP and Mitchell JW (2006). Method and system for calculating the spatial-temporal effects of climate and other environmental conditions on animals. http://www.warf.org/technologies.jsp?ipnumber=P01251US

Pruetz JD (2007). Evidence of cave use by savanna chimpanzees (*Pan troglodytes verus*) at Fongoli, Senegal: implications for thermoregulatory behavior. Primates 48: 316-319.

R Core Team (2017). R: A language and environment for statistical computing. R Foundation for Statistical Computing, Vienna, Austria. URL https://www.R-project.org/.

Sato H (2012). Diurnal resting in brown lemurs in a dry deciduous forest, northwestern Madagascar: implications for seasonal thermoregulation. Primates 53: 255-263.

Scheffers BR, De Meester L, Bridge TCL, et al. 2016. The broad footprint of climate change from genes to biomes to people. Science 354: 6313.

Seebacher F, Little AG. 2017. Plasticity of performance curves can buffer reaction rates from body temperature variation in active endotherms. Frontiers in Physiology 8: 575 doi: 10.3389/fphys.2017.00575

Smith NP, Barclay CJ, Loiselle DS (2005) The efficiency of muscle contraction. Progress in Biophysics & Molecular Biology 88: 1-58.

Spehar SN, Rayadin Y (2017). Habitat use of Bornean orangutans (Pongo pygmaeus morio) in an industrial forestry plantation in East Kalimantan, Indonesia. International Journal of Primatology 38: 358-384.

Stelzner JK (1988). Thermal effects on movement patterns of yellow baboons. Primates 29: 91-105.

Thomas CD, Cameron A, Green RE, et al. 2004. Extinction risk from climate change. Nature 427: 145-148.

Tracy CR, Welch WR, Porter WP (1980). Properties of air: A manual for students in biophysical ecology. University of Wisconsin Laboratory of Biophysical Ecology, Technical Report #1 (3rd Edition).

Turner TR, Schmitt CA, Cramer JD, Lorenz J, Grobler JP, Jolly CJ, Freimer NB (2018). Morphological variation in the genus *Cholorcebus*: ecographic and anthropogenically mediated variation in body mass, postcranial morphology, and growth. American Journal of Anthropology doi: 10.1002/ajpa.23459.

Urban MC, Bocedi G, Hendry AP, et al. 2016. Improving the forecast for biodiversity under climate change. Science 353: 6304

Willems EP and Hill RA (2009). A critical assessment of two species distribution models: a case study of the vervet monkey (*Cercopithecus aethiops*). Journal of Biogeography 36: 2300-2312.

Zhang Y, Mathewson PD, Zhang Q, Porter WP, Ran J (2018). An ecophysiological perspective on likely giant panda habitat responses to climate change. Global Change Biology 24: 1804-1816.

SUPPORTING INFORMATION

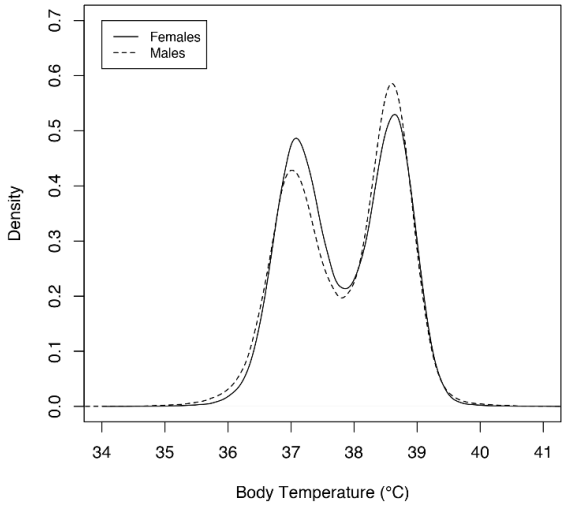


(a)

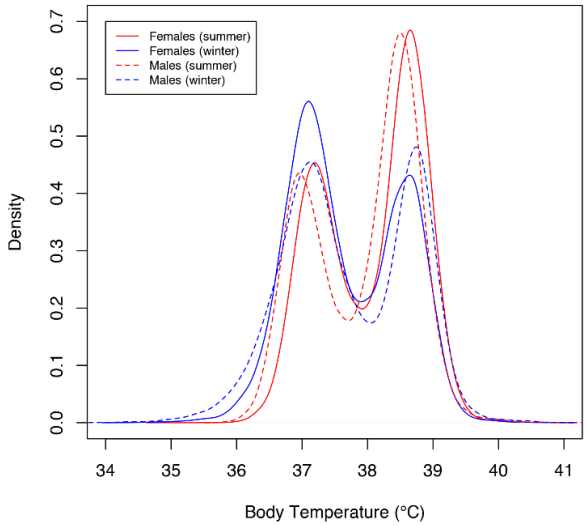


(b)

**Figure S1.** Kernel density distributions of observed wild vervet body temperatures for 235,176 male animal hours and 244,354 female animal hours between 2012 and 2016 (a) and seasonal kernel body temperature distributions (b). “Summer” refers to December, January, and February (n= 71,362 female hours and 72,384 male hours) and “Winter” refers to June, July, and August (n= 67,344 female hours and 61,608 male hours)

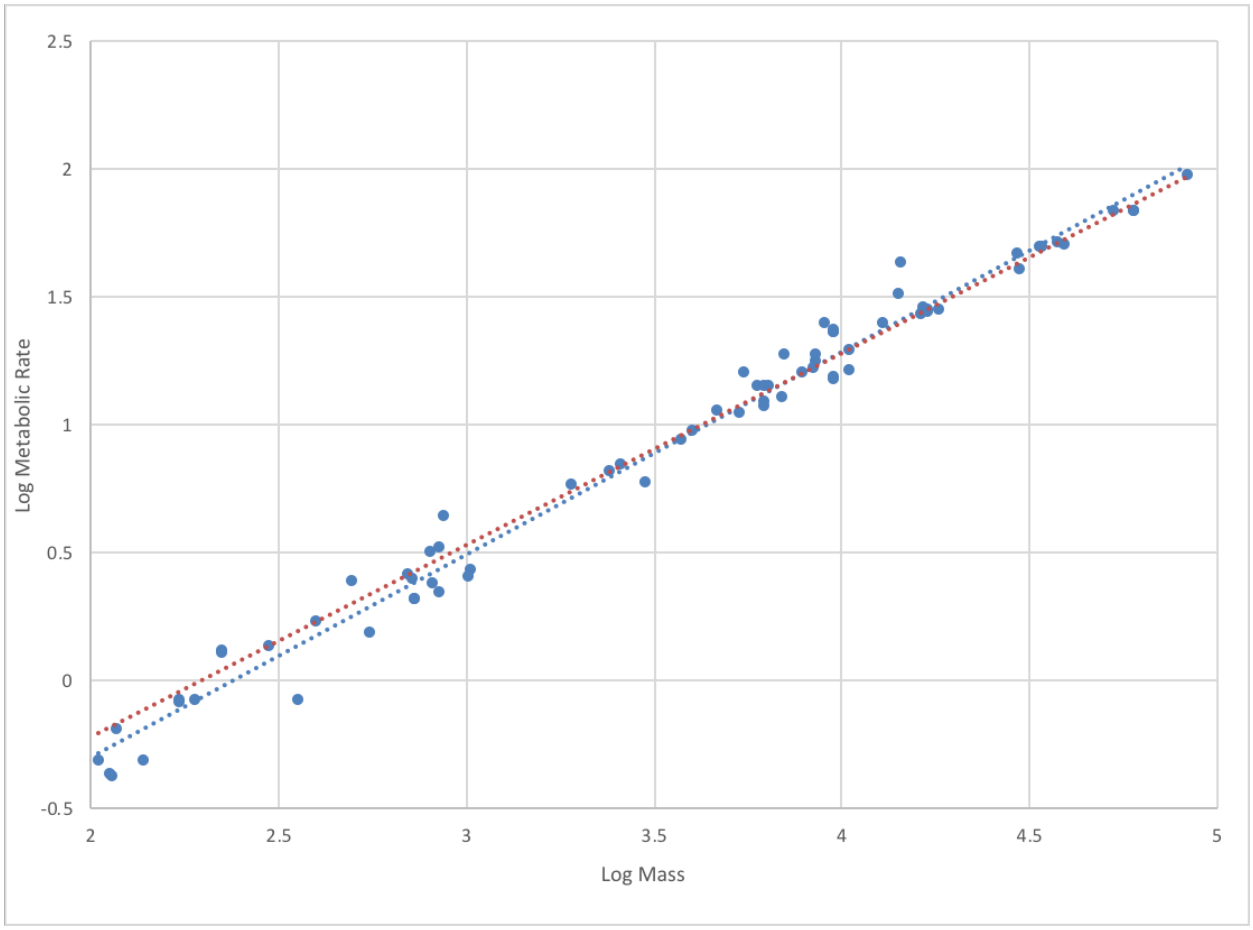


**Figure S2.** Plot of published haplorhine primate species resting metabolic rates (W) as a function of body mass (g). The best-fit line to the data is represented by the blue dashed line, and metabolic rates predicted using the regression used by Niche Mapper for placental mammals is shown by the red dashed line. See Table S2 for list of species with available resting metabolic rates.

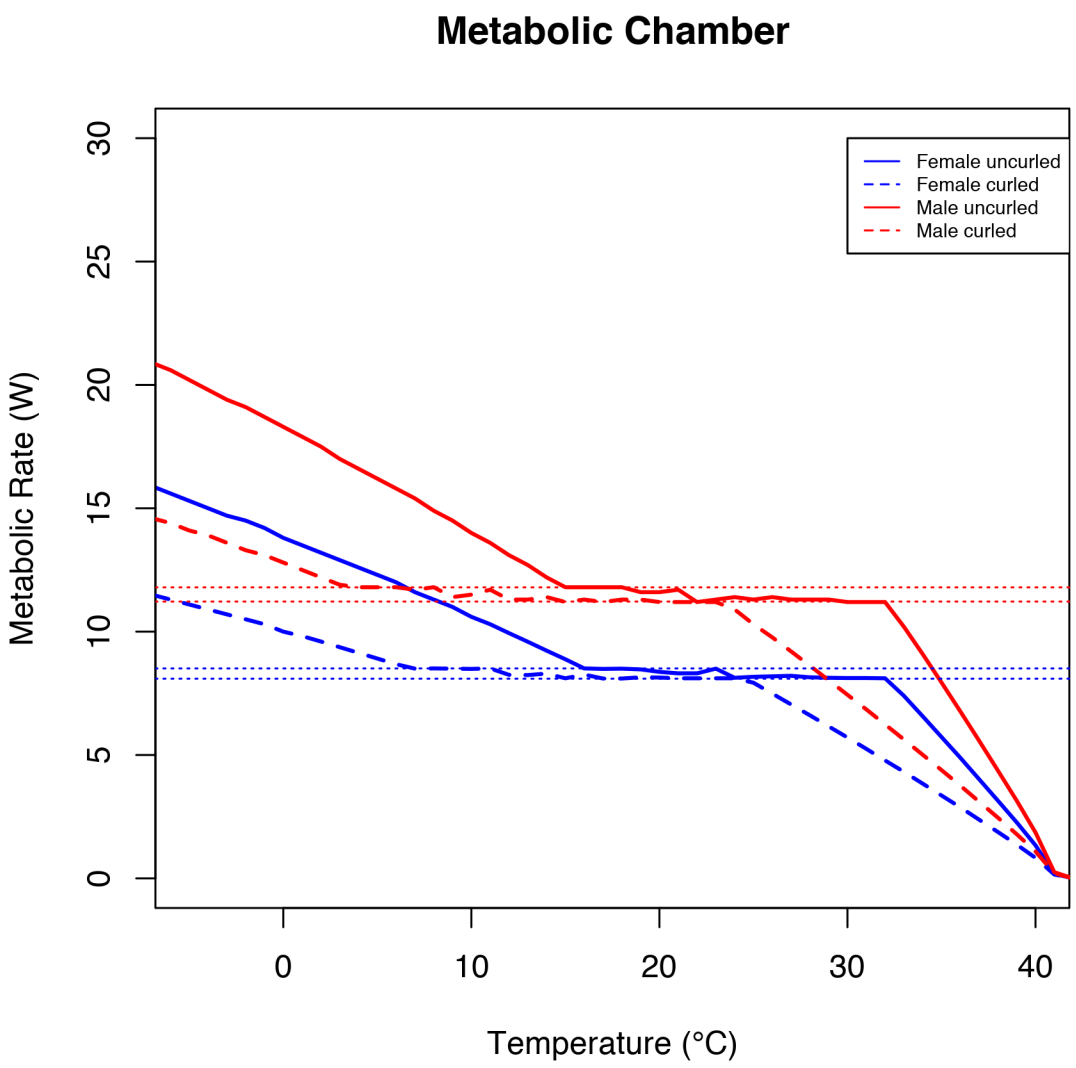


**Figure S3**. Metabolic chamber simulations for the vervet model using the default inputs (summarized in Table 1), assuming both an open posture (solid line; arms and legs exposed) and a heat-conserving, hunched posture (dashed line; arms and legs wrapped up against the torso). The horizontal dotted lines are placed ±2.5% of the estimated basal metabolic rate and indicate the target range that Niche Mapper was thermoregulating towards for males (red) and for females (blue). Predicted metabolic rates above the top dotted line for each sex indicate predicted cold stress; predicted metabolic rated below the lower dotted line for each sex indicate predicted heat stress. The predicted thermoneutral zone is the range of temperatures for which the predicted metabolic rate is between the horizontal dotted lines.

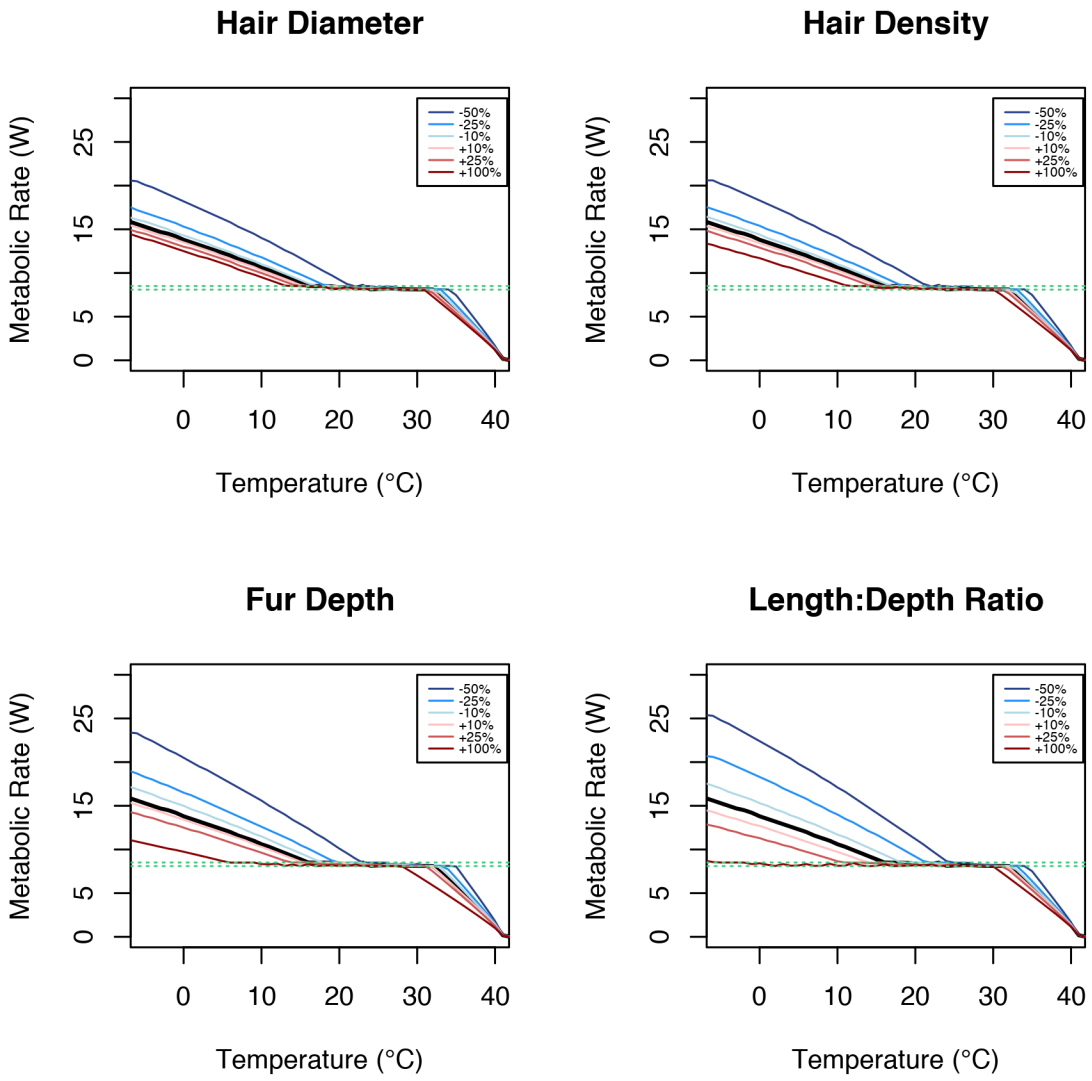


**Figure S4.** Fur property sensitivity analyses for the female vervet model. The thick black line represents the default inputs (summarized in Table S2), and the colored lines represent increased or decreased input values. The dashed green lines are placed ± 2.5% of the estimated basal metabolic rate. Predicted metabolic rates above the top line indicate predicted cold stress; predicted metabolic rated below the lower line indicate predicted heat stress. The predicted thermoneutral zone is the range of temperatures for which the predicted metabolic rates are between the dashed lines. The male model showed the same trends.

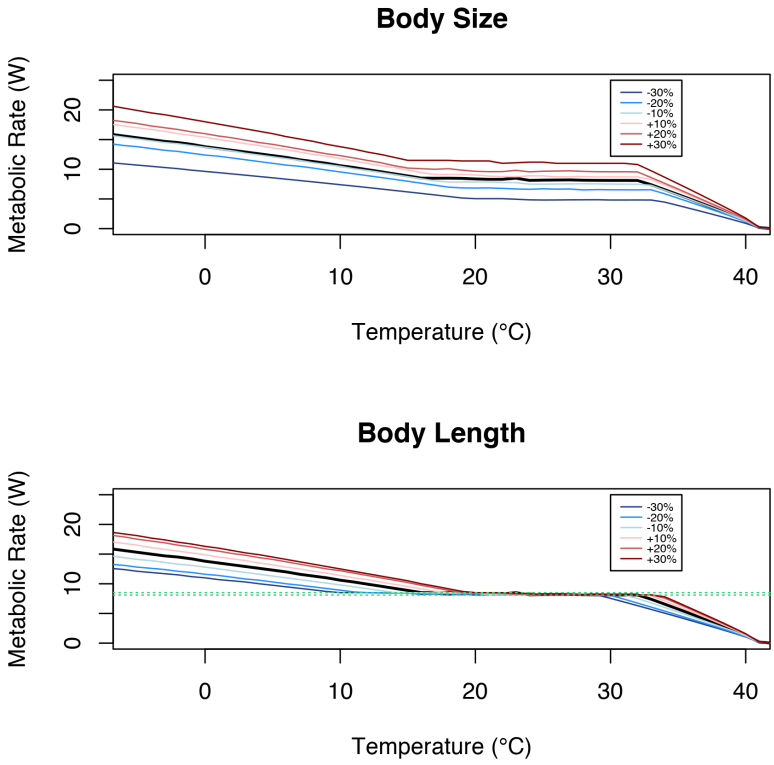


**Figure S5.** Sensitivity analyses of body size and body part lengths for the female vervet model. The thick black line represents the default inputs (summarized in Table S2), and the colored lines represent increased or decreased input values. For the body size, the total animal mass was altered and then the animal's linear and radial dimensions were both scaled up and down to maintain constant body part densities and relative proportions. For body length, the animal mass remained constant and the radial dimensions were increased or decreased in response to the changed linear dimensions to maintain constant body part densities. The dashed green lines are placed ±2.5% of the estimated basal metabolic rate (no lines are shown for the body size as each size has a different BMR). Predicted metabolic rates above the top line indicate predicted cold stress; predicted metabolic rated below the lower line indicate predicted heat stress. The predicted thermoneutral zone is the range of temperatures for which the predicted metabolic rate is between the dashed lines. The male model showed the same trends.

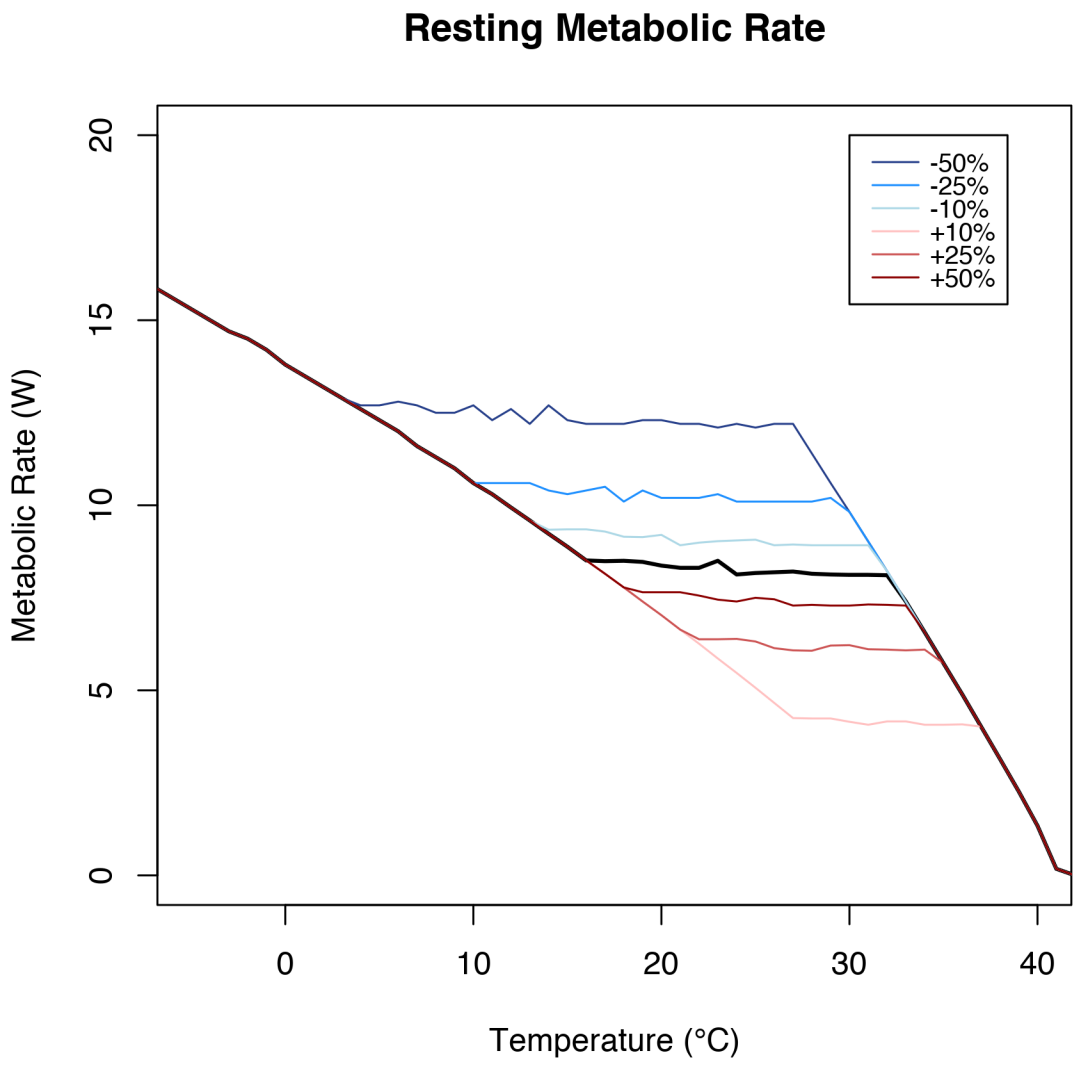


**Figure S6.** Sensitivity analyses of the assumed resting metabolic rate in the female vervet model. The thick black line represents the default inputs (summarized in Table S2), and the colored lines represent increased or decreased input values. The model attempts to thermoregulate to within ±2.5% of the resting metabolic rate. Predicted metabolic rates above this range indicate predicted cold stress; predicted metabolic rated below this range indicate predicted heat stress. The predicted thermoneutral zone is the range of temperatures for which the predicted metabolic rates are within this range. The male model showed the same trends.

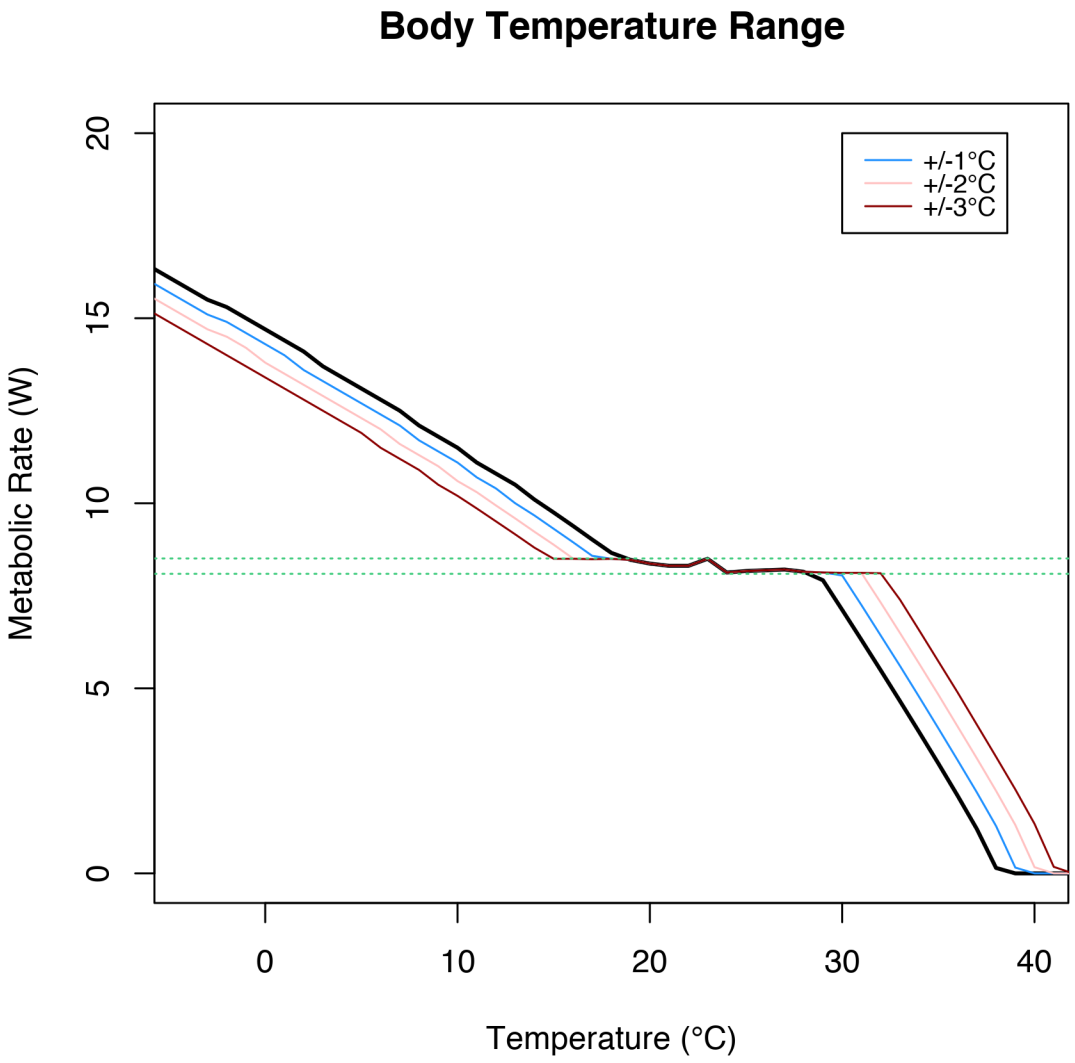


**Figure S7.** Sensitivity analyses of the increasing body temperature variability in the female vervet model. The thick black line represents maintaining a constant core temperature of 38°C, and the colored lines represent allowing 1°, 2°, and 3°C fluctuation around 38°C in response to cold or heat stress. The dashed green lines are placed ±2.5% of the estimated basal metabolic rate. Predicted metabolic rates above the top line indicate predicted cold stress; predicted metabolic rated below the lower line indicate predicted heat stress. The predicted thermoneutral zone is the range of temperatures for which the predicted metabolic rates are between the dashed lines. The male model showed the same trends.

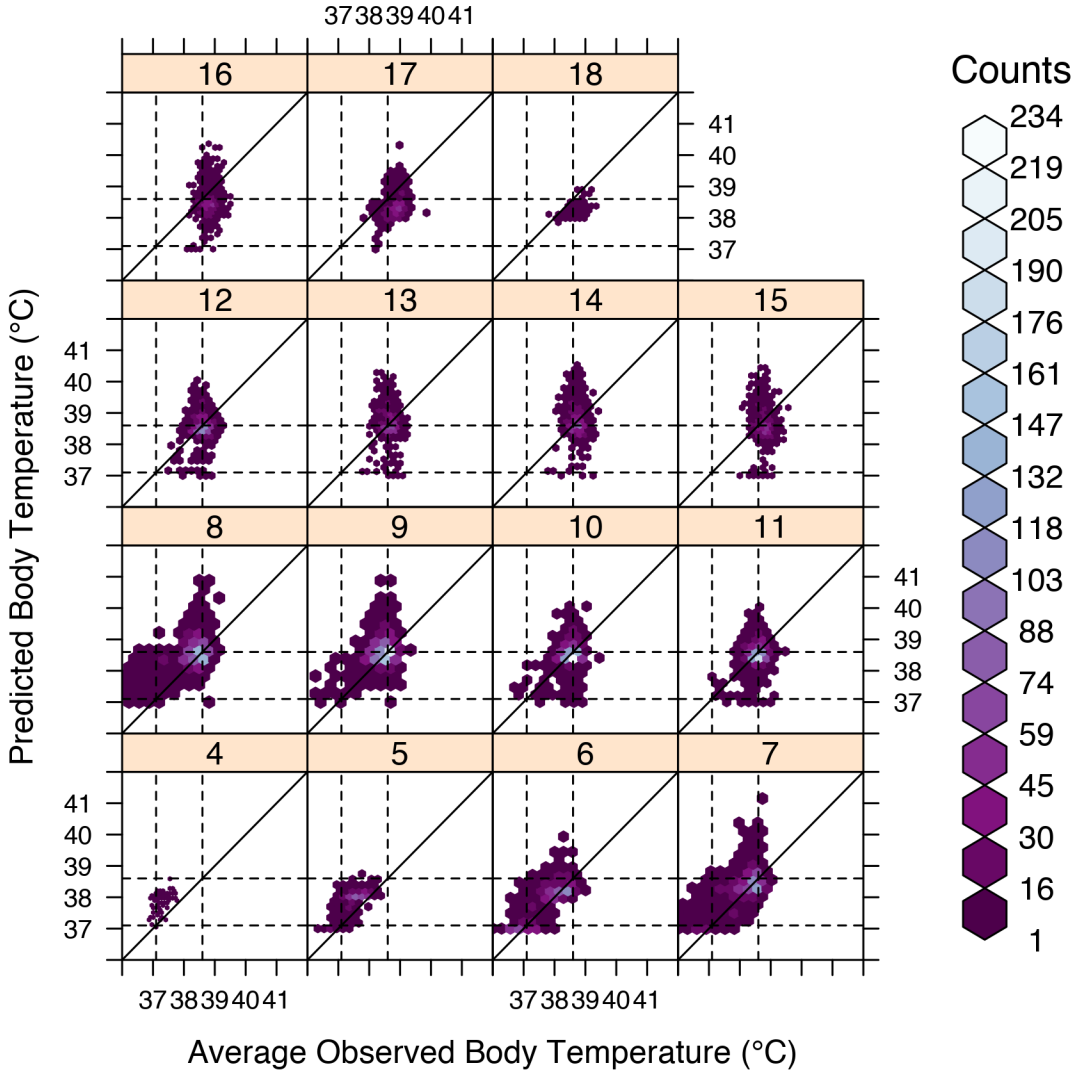


**Figure S8.** Hexbin plots of observed body temperatures vs. the average of body temperatures predicted by NM for a monkey at rest in the full shade and a monkey active in the full sun for each diurnal hour (04:00 through 18:00) between 2012 and 2016. The lighter the color of the hexagon, the greater the number of data points are found in that location on the plot. The dashed lines indicate the two modal body temperatures of the live vervets and the solid line indicates a 1:1 relationship between observed and predicted temperature.

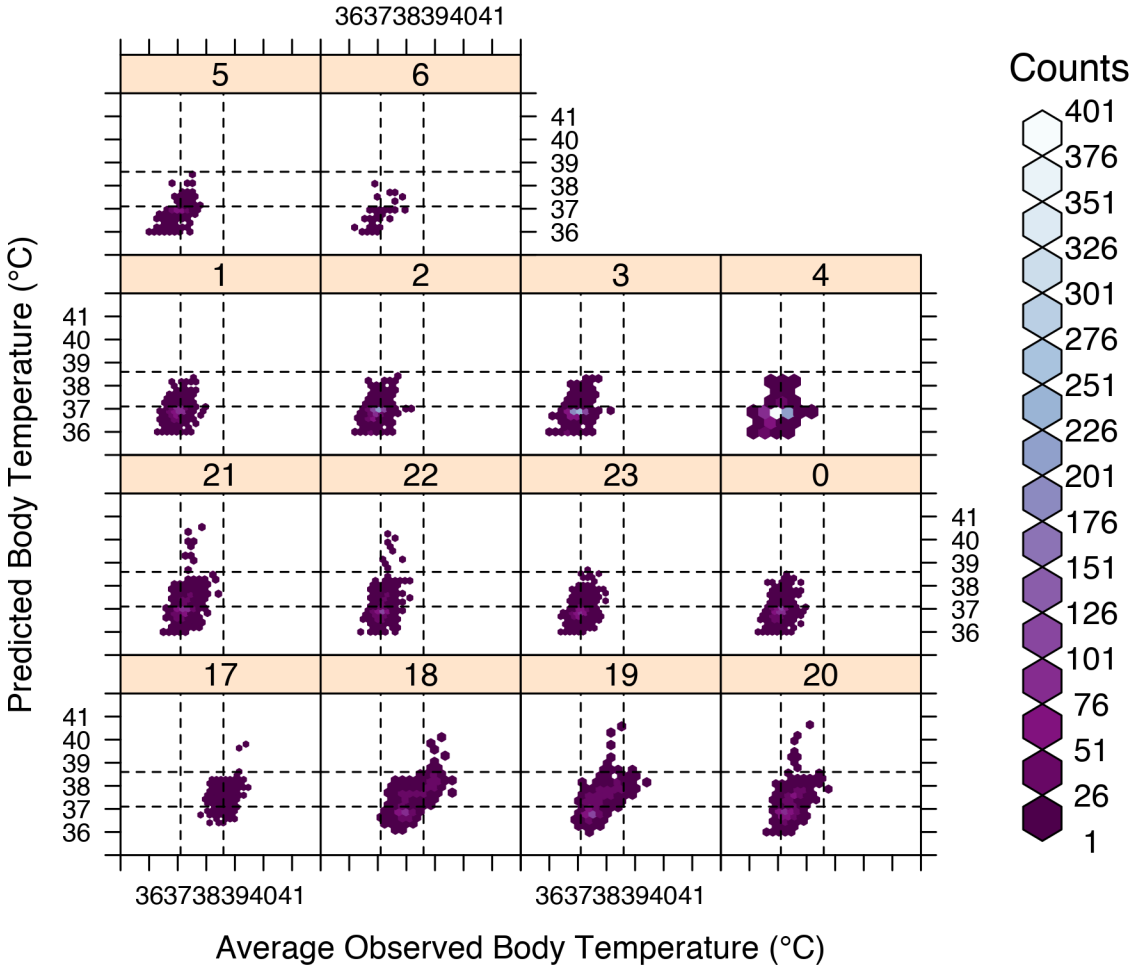


**Figure S9.** Average observed body temperatures plotted against the average nighttime body temperatures predicted by NM crepuscular and nocturnal hours (17:00 to 06:00). The lighter the color of the hexagon, the greater the number of data points are found in that location on the plot. The dashed lines indicate the two modal body temperatures of the live vervets.

**Table S1.** Summary of wild vervet body temperature and behavior observations at Samara Game Reserve, Eastern Cape, South Africa between 2012 and 2016.

| Season | Females with temperature implants | Males with temperature implants | Days of Body Temperature Data | Hours of Behavioral Observations |
|---|---|---|---|---|
| 2012-2013 | 11 | 11 | 277 | 1878 |
| 2013-2014 | 3 | 13 | 181 | 1943 |
| 2014-2015 | 13 | 10 | 355 | 2404 |
| 2015-2016 | 9 | 9 | 332 | 2533 |

**Table S2.** Haplorhine primate species with measured metabolic rate measurements found in a literature search.

| Species | Source | Species | Source |
|---|---|---|---|
| *Alouatta palliata* | [1], [2] | *Macaca fascicularis* | [1], [2] |
| *Aotus trivirgatus* | [1], [2], [3] | *Macaca fuscata* | [1], [3], [6] |
| *Ateles geoffroyi* | [2] | *Macaca mulatta* | [1], [4], [3] |
| *Callicebus moloch* | [2] | *Pan troglodytes* | [1], [2], [4], [3] |
| *Callimico goeldii* | [4] | *Papio anubis* | [2], [7] |
| *Callithrix geoffroyi* | [3] | *Papio cynocephalus* | [1], [3] |
| *Callithrix jacchus* | [1], [4] | *Papio hamadryas* | [5] |
| *Callithrix pygmea* | [1], [4], [5] | *Papio papio* | [1] |
| *Cebus albifrons* | [2] | *Papio ursinus* | [1], [3], [5] |
| *Cebus apella* | [2] | *Pongo pygmaeus* | [1], [2] |
| *Cercocebus albigena* | [2] | *Saguinus fuscicollis* | [2] |
| *Cercocebus torquatus* | [1], [3] | *Saguinus geoffroyi* | [1], [3], [7] |
| *Cercopithecus mitis* | [1] | *Saguinus imperator* | [2] |
| *Colobus guereza* | [1], [2] | *Saimiri sciureus* | [1], [7] |
| *Erythrocebus patas* | [1] | *Symphalangus syndactylus* | [2] |
| *Homo sapiens* | [1], [4], [3] | *Tarsius spectrum* | [1] |
| *Hylobates lar* | [1], [2] | *Tarsius syrichta* | [1], [4], [5] |
| *Leontopithecus rosalia* | [4], [3] | *Tarsius tarsier* | [5] |

[1] Ross C. 1992. Basal metabolic rate, body weight and diet in primates: an evaluation of the evidence. Folia Primatologica 58: 7-23.

[2] Leonard WR & Robinson ML. 1997. Comparative primate energetics and hominid evolution. American Journal of Physical Anthropology 102: 265-281.

[3] Snodgrass JJ. Leonard WR, Robertson ML. 2007. Primate bioenergetics: an evolutionary perspective. In: Ravosa M, Dagosto M (Eds.), Primate origins: adaptations and evolution. Springer, New York, pp. 703-722.

[4] Genoud M. 2002. Comparative studies of basal rate of metabolism in primates. Evolutionary Anthropology 11: 108-111.

[5] Clarke A, Rothery P, Isaac NJB. 2010. Scaling of basal metabolic rate with body mass and temperature in mammals. Journal of Animal Ecology 79: 610-619.

[6] Capellini I, Venditti C, Barton RA. 2010. Phylogeny and metabolic scaling in mammals. Ecology 91: 2783-2793.

[7] White CR and Seymour RS. 2003. Mammalian basal metabolic rate is proportional to body mass$^{2/3}$. Proceedings of the National Academy of Sciences of the United States of America 100: 4046-4049.

**Table S3.** Key properties used to parameterize Niche Mapper's microclimate model.

| Parameter (units) | Value | Source |
|---|---|---|
| Substrate thermal conductivity (W/mK) | 2.5 | General soil values from [1]. General values found to be sufficient when compared to site specific values [1]. |
| Substrate density ($kg/m^3$) | 2560 (mineral) 1200 (bulk) | General soil values from [1]. General values found to be sufficient when compared to site specific values [1]. |
| Substrate specific heat (J/kg-K) | 870 | General soil values from [1]. General values found to be sufficient when compared to site specific values [1]. |
| Substrate surface reflectivity (%) | 20 | [2]: Estimated based on values for sand and grass obtained online. |
| Timing of daily minimum and maximum air temperatures and wind speeds (min/max) | Sunrise/1 hour after solar noon | Own estimation |
| Timing of daily minimum and maximum relative humidity (min/max) | 1 hour after solar noon / Sunrise | Own estimation |
| Cloud cover (%) | Variable between months | Used 1960-1990 average monthly values from [3]. |
| Shade (%) | 0 or up to 100% available | Simplifying assumption of no trees on landscape. |
| Daily wind speed range (m/s) | 0.1-4.0 | Own estimation based on incomplete wind speed data from weather station on site |
| Daily relative humidity (%) | Min = variable Max = 100 | Maximum values set to 100% (simplifying assumption) and minimum values calculated based on the daily temperature range assuming constant water mass in the air over 24 hours [4] |
| Animal height (cm) | 50 | Own estimation based on personal observation |

[1] Kearney MR, et al. (2014) Microclimate modelling at macro scales: a test of a general microclimate model integrated with gridded continental-scale soil and weather data. Methods in Ecology and Evolution 5: 273-286.

[2] http://www.engineeringtoolbox.com

[3] New M, Lister D, Hulme M, Makin I (2002). A high-resolution data set of surface climate over global land areas. Climate Research 21: 1-25.

[4] Tracy CR, Welch WR, Porter WP (1980) Properties of air: A manual for students in biophysical ecology. University of Wisconsin Laboratory of Biophysical Ecology, Technical Report #1 (3rd Edition)

**Table S4.** Percentage of days in the 2012-2016 field seasons (n=1,145) that the mean observed minimum, maximum, average, and 24-amplitude female vervet body temperature was within the boundaries of Niche Mapper's predicted body temperature range. Also shown are the percentage of days that the observed metric was within 0.25°, 0.5°, or 1° of the predicted range. The numbers in parentheses are the number of days for which the mean observed metric was over/under the range predicted by Niche Mapper. During diurnal hours, the predicted range is between an active individual in full sun and a resting individual in full shade or full sun. At night, the range is between various body postures allowed. "Stretched only" refers to only modeling a lone individual stretched out (no range); "Curling only" refers to only modeling a lone individual with arms and legs tucked into the torso (no range); "Stretched+Curled" refers to the range of temperatures predicted between a lone stretched individual and a lone curled individual; "All postures" refers to the range of temperatures predicted between a long individual splayed out and an individual huddled between two others.

| | | Range of Nocturnal Body Postures Modeled | | | | |
|---|---|---|---|---|---|---|
| | | **All postures allowed** | **All postures allowed (no shade allowed*)** | **Stretched + Curled only** | **Curling only** | **Stretched Only** |
| Minimum $T_b$ | W/in Range | 82.4% (26/175) | 83.1% (27/161) | 42.3% (125/536) | NA | NA |
| | W/in 0.25°C | 87.7% (8/133) | 88.4% (9/124) | 50.2% (101/469) | 16.8% (491/461) | 3.8% (8/1093) |
| | W/in 0.5°C | 92.2% (5/84) | 93.0% (5/75) | 61.7% (66/372) | 39.7% (332/359) | 11.4% (5/1009) |
| | W/in 1.0°C | 99.1% (1/9) | 99.4% (1/6) | 93.6% (2/71) | 91.2% (40/61) | 69.4% (1/349) |
| Maximum $T_b$ | W/in Range | 76.4% (137/133) | 57.7% (374/114) | 78.7% (127/117) | 76.0% (140/135) | 75.9% (137/139) |
| | W/in 0.25°C | 89.3% (58/64) | 74.2% (253/42) | 90.3% (58/64) | 89.0% (60/65) | 88.8% (58/70) |
| | W/in 0.5°C | 95.2% (30/25) | 84.1% (172/10) | 95.3% (26/28) | 94.9% (31/27) | 94.9% (30/28) |
| | W/in 1.0°C | 98.7% (12/3) | 94.4% (64/0) | 99.0% (9/2) | 98.7% (12/3) | 98.7% (12/3) |
| Mean Tb | W/in Range | 89.2% (32/92) | 85.1% (100/71) | 70.3% (36/304) | 49.4% (282/297) | 28.8% (32/783) |
| | W/in 0.25°C | 96.3% (6/36) | 94.5% (45/18) | 89.8% (5/112) | 84.5% (77/100) | 55.9% (6/499) |
| | W/in 0.5°C | 99.3% (1/7) | 99.1% (8/2) | 95.8% (1/47) | 95.1% (13/43) | 84.9% (1/172) |
| | W/in 1.0°C | 100% (0/0) | 99.9% (1/0) | 99.6% (0/5) | 99.7% (0/3) | 98.2% (0/21) |
| 24-hour $T_b$ | W/in Range | 96.6% (16/23) | 93.9% (53/17) | 89.7% (85/33) | 64.0% (87/325) | 57.1% (468/23) |
| | W/in 0.25°C | 99.0% (3/9) | 97.0% (25/9) | 95.0% (37/20) | 79.7% (32/200) | 74.1% (287/9) |
| | W/in 0.5°C | 99.8% (1/1) | 98.6% (15/1) | 97.6% (16/11) | 91.4% (12/86) | 83.8% (1/185) |
| | W/in 1.0°C | 99.9% (0/1) | 99.9% (0/1) | 99.6% (0/5) | 98.3% (0/19) | 95.0% (55/1) |

* During diurnal hours, modeled no shade available so the diurnal temperature range is between an active individual in full sun and an inactive individual in full sun. This was done to evaluate the effect of having shade available to the vervets.

**Table S5.** Percentage of days in the 2012-2016 field seasons (n=1,145) that the mean observed minimum, maximum, average, and 24-amplitude male vervet body temperature was within the boundaries of Niche Mapper's predicted body temperature range. Also shown are the percentage of days that the observed metric was within 0.25°, 0.5°, or 1° of the predicted range. The numbers in parentheses are the number of days for which the mean observed metric was over/under the range predicted by Niche Mapper. During diurnal hours, the predicted range is between an active individual in full sun and a resting individual in full shade. At night, the range is between various body postures allowed. "Stretched only" refers to only modeling a lone individual stretched out (no range); "Curling only" refers to only modeling a lone individual with arms and legs tucked into the torso (no range); "Stretched+Curled" refers to the range of temperatures predicted between a lone stretched individual and a lone curled individual; "All postures" refers to the range of temperatures predicted between a long individual splayed out and an individual huddled between two others.

| | | Range of Nocturnal Body Postures Modeled | | | | |
|---|---|---|---|---|---|---|
| | | **All postures allowed** | **All postures allowed (no shade available*)** | **Stretched + Curled only** | **Curling only** | **Stretched Only** |
| Minimum $T_b$ | W/in Range | 89.2% (60/64) | 89.2% (60/64) | 64.7% (60/434) | NA | NA |
| | W/in 0.25°C | 94.6% (28/34) | 94.6% (28/34) | 75.0% (28/258) | 17.8% (685/256) | 8.6% (27/1020) |
| | W/in 0.5°C | 97.9% (7/17) | 97.9% (7/17) | 84.7% (7/168) | 35.7% (574/162) | 21.9% (7/887) |
| | W/in 1.0°C | 99.9% (0/1) | 99.9% (0/1) | 95.6% (0/50) | 76.4% (221/49) | 83.8% (0/186) |
| Maximum $T_b$ | W/in Range | 72.2% (148/170) | 52.1% (378/170) | 72.2% (148/170) | 71.8% (170/153) | 72.1% (171/149) |
| | W/in 0.25°C | 86.7% (79/73) | 69.2% (280/73) | 86.7% (79/73) | 86.5% (73/82) | 86.6% (74/79) |
| | W/in 0.5°C | 94.8% (41/19) | 83.0% (176/19) | 94.8% (41/19) | 94.2% (20/46) | 94.1% (24/43) |
| | W/in 1.0°C | 99.0% (11/0) | 93.8% (71/0) | 99.0% (11/0) | 99.0% (0/12) | 99.0% (0/12) |
| Mean $T_b$ | W/in Range | 92.1% (40/51) | 84.3% (129/51) | 77.7% (40/215) | 35.9% (524/210) | 31.6% (40/743) |
| | W/in 0.25°C | 97.4% (14/16) | 94.2% (51/16) | 90.9% (14/90) | 79.6% (147/87) | 58.3% (14/463) |
| | W/in 0.5°C | 99.7% (2/2) | 98.5% (15/2) | 98.1% (2/20) | 95.3% (34/20) | 82.4% (2/199) |
| | W/in 1.0°C | 100% (0/0) | 99.9% (1/0) | 100% (0/0) | 100% (0/0) | 99.3% (0/8) |
| 24-hour $T_b$ | W/in Range | 93.5% (3/71) | 91.7% (24/71) | 88.3% (68/66) | 45.8% (17/604) | 64.9% (331/71) |
| | W/in 0.25°C | 96.6% (2/37) | 95.5% (15/37) | 93.5% (37/37) | 59.7% (5/456) | 77.5% (221/37) |
| | W/in 0.5°C | 98.1% (1/21) | 97.7% (5/21) | 97.4% (21/9) | 74.1% (2/295) | 86.0% (139/21) |
| | W/in 1.0°C | 99.7% (0/3) | 99.7% (0/3) | 99.7% (4/0) | 93.6% (0/73) | 96.7% (35/3) |

* During diurnal hours, modelled no shade available so the diurnal temperature range is between an active individual in full sun and an inactive individual in full sun. This was done to evaluate the effect of having shade available to the vervets.

# APPENDIX 1: SIMULATING VERVET HUDDLING IN NICHE MAPPER

## METHODS

Niche Mapper allows a single inactive vervet to change its posture to a more heat-conserving "curled" position, simulated by lumping the arms, legs, and torso into a single lump. Thus, a "curled" single vervet is modeled as three shapes: head, torso/appendages lump, and tail. To simulate a vervet huddling with others in Niche Mapper, we assumed that the huddling monkeys would be arranged in a straight line to approximate a row of monkeys along a tree branch (Fig. A1).

To approximate turbulent wind flow in the environment, we used an average characteristic dimension when calculating the convective heat transfer coefficient on the assumption that wind direction will change over time; sometimes it will be parallel to the line of monkeys and sometimes it will be perpendicular to the line of monkeys. Thus, we calculated an average characteristic dimension using the characteristic dimension using the length of the monkey object (increases with increasing number of monkeys; Fig. A1a) and the "width" of the monkey object (same for one or for multiple monkeys; Fig. A1b). This results in a larger group of monkeys having a smaller convective heat transfer coefficient.

We assumed that direct contact between monkeys acts as perfect insulation and thus there is no heat loss or gain from the portions of monkeys in contact with another monkey. For a monkey at the end of the line, we assumed that it would turn its back to the environment and so we simulated different percentages of the ventral half of the torso/appendages lump being in contact with another monkey. For a monkey in the middle of a line, we simulated different

percentages of both the dorsal and ventral halves of the torso/appendages lump being in contact with a neighboring monkey.

Convective heat flux is calculated as: $Q_{conv} = h_c * \text{surface area} * (T_{surface}-T_{air})$. When we simulate huddling, there are several opposing things going on mathematically. Simulating huddling decreases the surface area of the monkey available for heat exchange with the environment, and, to a lesser extent, decreases the heat transfer coefficient ($h_c$) term, as described above. However, the decreased heat loss due to those terms going down results in an increased surface temperature, increasing the temperature gradient, and, in turn, the heat flux from each individual. The relative magnitude of the increases and decreases determines the net thermal advantage of huddling.

There is an analogous balancing of increasing and decreasing terms for radiant heat flux, which is calculated with a similar equation: $Q_{rad} = h_r * \text{surface area} * (T_{surface}-T_{sky/grd})$. However, the heat loss coefficient, $h_r$, does not directly consider the object shape like the convective heat transfer coefficient does.

To investigate the simulated effect of huddling on predicted metabolic rates and body temperatures, we simulated monkeys for the nights of June 13$^{th}$ and June 14$^{th}$, 2012. These nights were chosen because Niche Mapper predicted that a lone monkey (i.e., a monkey not huddling) would need to lower its body temperature to 36°C, the minimum we allow in the model, to minimize overnight metabolic heat production requirements. On the first night, the live monkeys were observed to reduce their body temperatures below 37°C, but on the second night they maintained body temperatures above 37°C. Thus, these two nights provide an opportunity to explore what effect huddling may have on body temperatures. Results are similar for males and females; only the results for females are shown here.

During these nights, body temperatures were being recorded with body temperature transmitters in nine females and 10 males in the group. The females ranged in weight from 2.7-3.89 kg, and the males ranged in weight from 2.26-5.86 kg. For the Niche Mapper modeling, an average-sized vervet was simulated (3.4 kg female; 4.8 kg male). The vervets were not observed overnight so there is no information on whether the monkeys actually huddled or what configuration any huddling took on either of these particular nights. This analysis is thus an exploration of whether huddling could explain the discrepancy between observed body temperatures and those predicted by Niche Mapper.

On-site weather stations recorded air temperature, which was used in the simulations. Identical wind speed profiles were used for each model day. During the nighttime hours, the modeling simulations assumed that the monkeys were inactive and attempting to maintain a basal metabolic rate.

## RESULTS

### *Night of June 13*

The mean observed hourly female body temperature declined to 36.6° overnight, while the minimum for any individual declined below 36° (Fig. 1). Niche Mapper predicted that a lone female would have to quickly drop its body temperature to the minimum body temperature allowed in the modeling, 36°, and keep it at 36° overnight to minimize thermoregulatory costs (Fig. 2). A lone female was predicted to require 90kJ of thermoregulatory costs overnight to maintain the minimum body temperature (Table A1). To put this into context, the expected daily basal metabolic rate for a 3.4 kg vervet is 738 kJ.

The ability to huddle slowed the body temperature decline down to 36° (Fig. A2). However, even with the maximum huddling simulated (75% contact) Niche Mapper predicted there would be some thermoregulatory costs associated with maintaining a body temperature of 36° (Table 1). However, huddling reduced these costs down to as low as 14-34 kJ (Table 1). The cost to maintain a body temperature of at least 37° is predicted to be 118 kJ for a lone individual and <50 kJ for a huddled monkey (Table A1).

*Night of June 14*

The mean observed temperature of the individuals with temperature transmitters declined to around 37.5° overnight, while the minimum observed individual body temperature hovered just below 37° (Fig. A3)

Niche Mapper predicted that a single female would have to drop its body temperature to 36° for most of the night to minimize thermoregulatory costs (Fig. A3). A lone female was predicted to incur 17 kJ of thermoregulatory costs overnight to maintain a minimum body temperature of 36° and 36 kJ to maintain a minimum body temperature of 37° (Table A1). In contrast to June 13th, huddling was predicted to allow a monkey to maintain a body temperature close to the mean observed temperature (Fig. A3), only incurring minor thermoregulatory costs when maintaining a minimum body temperature of 37° (Table A1).

## DISCUSSION

These results show that simulated huddling is sufficient for huddled monkeys to maintain a higher body temperature overnight than a lone monkey without incurring thermoregulatory costs in moderately cold conditions (e.g., June 14th, when temperatures when down to 6°C). The simulated huddling was not enough to allow them to maintain a temperature as high as observed

without thermoregulatory costs on colder nights (e.g., June 13th, where temperatures drop down to 0°C). However, huddling was predicted to confer energetic savings even if body temperatures were not as high as observed on these colder nights.

There are two different ways of interpreting the fact that even with huddling, Niche Mapper still predicted lower body temperatures than what was observed. First, it can simply be interpreted as Niche Mapper erroneously under-estimating body temperatures in these cold conditions. We would need a full suite of data to test this: body temperature, metabolic rates and surface temperatures. Given the lack of this data, we must rely on Niche Mapper's prior validations in a wide variety of other species and the fact that it tends to over-predict body temperatures at other times of the year as evidence that the model does not have a clear bias towards under-predicting body temperatures.

An alternate interpretation is that vervets do not always minimize thermoregulatory costs. Niche Mapper is always trying to minimize thermoregulatory costs and will always reduce body temperature to the minimum value before accepting additional metabolic heat production. However, live vervets may sometimes choose to expend some amount of energy to maintain a more optimal body temperature. This assumes that 37° is a preferred body temperature compared to 36°, which is supported by most observed body temperatures ranging between 37 and 40°. On the first night, the average female body temperature was just under 37°, while the minimum body temperature declined below 36°. The predicted cost for a lone female to maintain a body temperature of 37° that night is 118 kJ, equivalent to 16% of total daily basal metabolic expenditure (Table A1). However, costs for a huddled female to maintain 37° are predicted to be as low as 30 kJ, equivalent to only 4% of total daily resting metabolic rate. Thus, it may be worthwhile for a huddled individual to take on that minimal extra energetic cost in order to

maintain a preferred body temperature, but it might not be worth it for a lone female to take on the additional costs it would require.

On the second night, the observed average female body temperature was around 37.5° and the observed minimum temperature was around 37°. Niche Mapper predicted that huddling was sufficient for vervets to maintain a body temperature of 37° at negligible cost (Table A1). It also predicted that a lone female would only incur costs of 35 kJ (5% of daily RMR) to maintain 37°, which could be worth it for a lone individual similar to the huddled females on the first night, similar to a huddled female on the first night.

A final observation is that at the start of each night, Niche Mapper's predicted body temperature is about 1°C lower than observed. This is due to Niche Mapper assuming that the monkey's metabolic rate drops from the active level to basal immediately at sundown. In reality, there is a more gradual reduction in metabolic rate that would keep body temperatures higher.

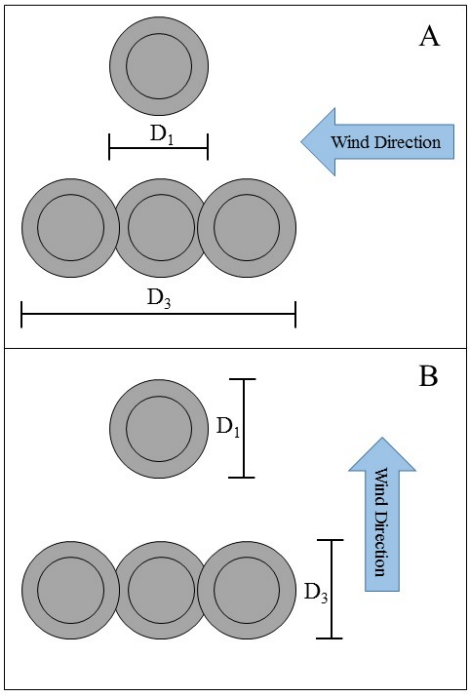


**Figure A1**. Schematic of a lone "curled" monkey and three huddled monkeys in a line along a branch as modeled by Niche Mapper. The perspective is that of looking straight down at the monkeys, with the inner circle representing the head and the outer circle representing the torso/appendage body part. Depending on the wind direction, the characteristic dimension (D), used in calculating a convective heat exchange coefficient, is larger for a huddled group of monkeys (A) or the same regardless of the number of monkeys huddled together along a branch (B).

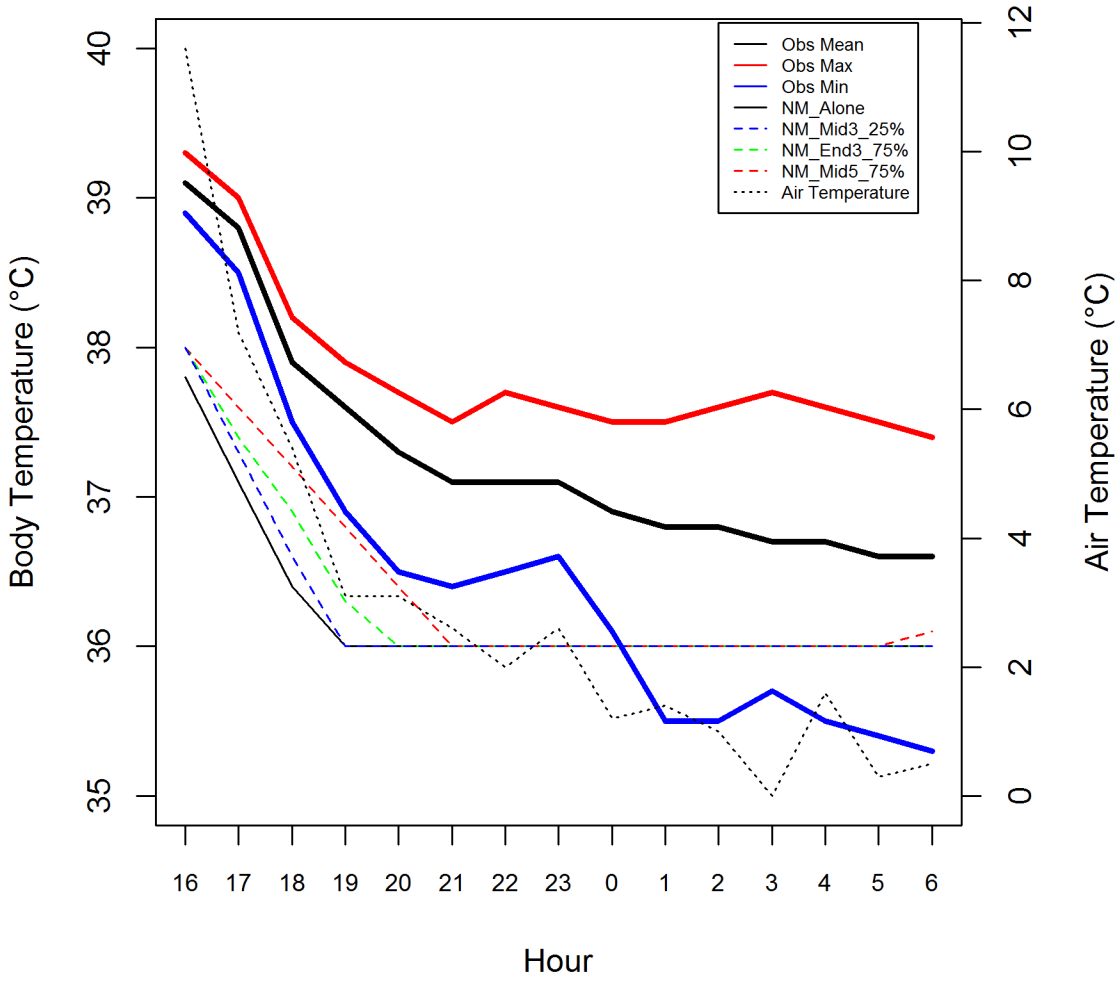


**Figure A2.** Observed ("Obs") and predicted ("NM") body temperatures for the night of June 13th. For the Niche Mapper predictions, predictions from four simulations are shown: single monkey not huddling ("Alone"), a monkey in the middle of a group of 3 monkeys with 25% contact (Mid3_25%), a monkey on the end of a group of 3 monkeys with 75% contact (End3_75%), and a monkey in the middle of a group of 5 monkeys with 75% contact between monkeys (Mid5_75%).

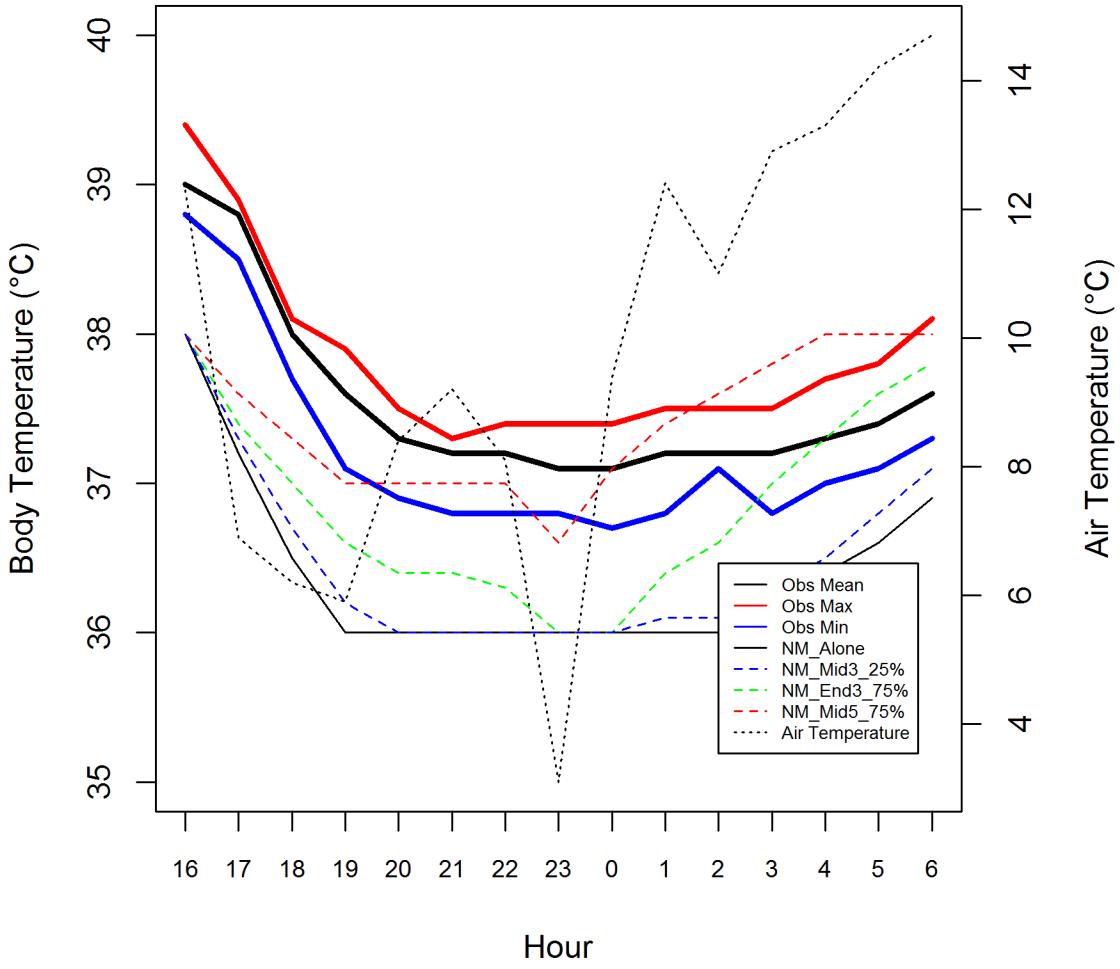


**Figure A3.** Observed ("Obs") and predicted ("NM") body temperatures for the night of June 14th. For the Niche Mapper predictions, predictions from four simulations are shown: single monkey not huddling ("Alone"), a monkey in the middle of a group of 3 monkeys with 25% contact (Mid3_25%), a monkey on the end of a group of 3 monkeys with 75% contact (End3_75%), and a monkey in the middle of a group of 5 monkeys with 75% contact between monkeys (Mid5_75%).

**Table A1.** Summary of predicted thermoregulatory costs (kJ) of maintaining minimum body temperatures of 36° and 37°C overnight on the nights of June 13th and 14th, 2012, assuming different huddling scenarios. Thermoregulatory costs are calculated as the difference between the metabolic rate predicted by Niche Mapper to maintain a given body temperature and the expected resting metabolic rate. End3= a monkey on the end of a group of 3 monkeys; End5= a monkey on the end of a group of 5 monkeys; Mid3= a monkey in the middle of a group of 3 monkeys; Mid5= a monkey in the middle of a group of 5 monkeys. The percentages indicate the percentage of torso in contact with neighboring monkeys while huddling.

| Overnight Huddling | | June 13th Min $T_b$ | | June 14th Min $T_b$ | |
|---|---|---|---|---|---|
| | | 36° | 37° | 36° | 37° |
| Alone | | 92.1 | 117.7 | 17.2 | 35.9 |
| End3 | 25% | 84.3 | 109 | 14.9 | 31.4 |
| | 50% | 71 | 95.3 | 9.7 | 25.2 |
| | 75% | 42.1 | 63.8 | 1.6 | 11.9 |
| End5 | 25% | 80.2 | 105.8 | 12 | 29.3 |
| | 50% | 62.4 | 87.1 | 7.1 | 21.3 |
| | 75% | 20 | 39.3 | 0 | 4.5 |
| Mid3 | 25% | 80.4 | 105 | 11.7 | 29.5 |
| | 50% | 66.5 | 90.1 | 8.4 | 22.6 |
| | 75% | 34.1 | 56.8 | 0.1 | 9.7 |
| Mid5 | 25% | 74.9 | 100.9 | 10.7 | 26.9 |
| | 50% | 57.2 | 81.1 | 5.6 | 18.3 |
| | 75% | 13.8 | 31.2 | 0 | 3.5 |

# CHAPTER 3: INCORPORATING MECHANISM TO PREDICTIONS OF PRIMATE DISTRIBUTIONS

*Authors (preliminary):* Paul D. Mathewson, Warren Porter, Richard McFarland

## INTRODUCTION

The potential advantages of using a biophysical model compared to correlative models to predict changes in suitable habitat in response to climate change have been previously reported (e.g., Kearney & Porter 2009, Buckley et al. 2010). Namely, predicted distributions are the result of modeling general principles of physics and heat transfer that require no extrapolation into novel climates. Moreover, explicitly modeling the range-limiting process(es) allows wildlife managers to better understand the potential impact of climate change and to make more informed management decisions. In contrast, correlative models require extrapolation into novel climates and provide managers with only limited insight into how climatic factors limit a species' distribution because the limiting processes are hidden behind the statistical correlations.

A significant challenge for using biophysical models to delineate suitable habitat is to identify thresholds at which survival is not possible in order to convert biophysical model outputs into distributional limits (Buckley et al. 2010; Buckley et al. 2018). This is particularly challenging for endotherms because the relationship between environmental temperature and animal performance is more complex than it is for ectotherms (Buckley et al. 2012). As such, development of mechanistic models for endotherms has lagged behind development for ectotherms (Boyles *et al.*, 2011; Oswald & Arnold, 2012; La Sorte & Jetz, 2013; Methorst et al. 2017). Furthermore, those mechanistic models that are developed often require detailed, species-specific information that is time consuming to develop, thus limiting more widespread adoption (Kearney & Porter 2009; Dormann *et al.*, 2012; Meineri *et al.*, 2015, Evans et al. 2015).

Niche Mapper's endotherm submodel is a general animal model, so it can calculate metrics such as energetic and evaporative water costs or allowable activity time for any animal provided basic information about morphology (animal mass and body part dimensions; pelage/plumage properties), physiology (resting metabolic rate), and behavior (e.g., times of day active, habitat types, etc.). This basic information can often be obtained relatively easily from live animals, museum specimens, existing literature, or estimated from established allometric relationships. However, to delineate suitable from unsuitable habitat from these outputs requires an understanding of where thermoregulatory costs will cause an animal to have a long-term negative energy or water balance or insufficient discretionary energy for reproduction. This additional analysis needs another set of inputs that are not as widely available or easy to obtain, including the water and energetic content of the species' diet, foraging rate, digestive efficiency, and fecal water content. Thus, the ability to purely mechanistically model a species' range is often limited to well-studied species with relatively simple diets (e.g., gliding possums or koalas subsisting entirely on eucalyptus leaves; Kearney et al. 2010, Briscoe et al. 2016), without making overly simplistic assumptions or accepting a high degree of uncertainty.

An intermediate approach that still incorporates mechanism into predictions is to create a hybrid model in which outputs from the biophysical model that are used as inputs into a correlative model to predict a species distribution (Elith *et al.*, 2010, Dormann et al. 2012). The biophysical model converts climate data into easier-to-interpret and biologically relevant layers such as energetic costs or activity restrictions specific to that account for focal animal's specific morphology, physiology and behavior and only require the basic information described above (Kearney & Porter 2009). The statistical framework of the correlative model allows these metrics to be converted into predicted distributions without the need for the additional data requirements.

This hybrid approach has been proposed as a pragmatic way of facilitating more widespread incorporation of mechanism in order to improve model predictions (Urban et al. 2016).

In chapter 1, I illustrated how this approach can be applied to a species susceptible to heat-related activity restrictions. However, unlike the pika, many species have the ability to dissipate heat through routes of evaporative water loss beyond simple respiratory loss (e.g., by specialized respiratory loss such as panting, or by sweating) and can thus maintain activity so long as sufficient water is available to them (either free or in their food) to replace the water lost (Fuller et al. 2016, Mitchell et al. 2018). This complicates the ability to calculate heat-related activity restriction, but the evaporative water loss rate required for the animal to stay active without overheating can itself be used to quantify the thermal cost of a given environment (e.g., Long et al. 2014).

Here, we use a biophysical primate model to translate weather data into more proximate variables that quantify thermal stress specific to the species' morphology, physiology and behavior: water loss rates from sweating in the summer and additional heat production needed to maintain body temperatures in the winter. We investigate whether modeling distributions using variables representing a more proximate relationship between an animal and its environment than simply relating distributions to climate data improves model performance or provides any additional insight for either current or future predictions.

## METHODS

### *Study Animal*

Vervet monkeys (hereafter "vervets"; *Chlorocebus pygerythrus*) are a small (females: 3-5 kg; males: 4-8 kg), diurnally-active, semi-terrestrial, semi-arborial African primate. Vervets are habitat generalists, found in a wide range of habitats throughout sub-Saharan Africa that contain

water sources and sleeping trees for predator avoidance (Cawthon Lang 2006). Consistent with their habitat generality, vervets are also among the most omnivorous primates (Cawthon Lang 2006). Being highly adaptable, vervets are among the primate species expected to best tolerate indirect effects of climate change such as habitat alteration in terms of structure and community composition (Korstjens & Hillyer 2016). However, they are still subject to the direct, physiological effects such as increased enforced resting time.

Vervets have been documented to engage in a variety of behavioral and physiological processes to address thermal stress, including increased heterothermy (Lubbe et al. 2014), increased feeding (McFarland et al. 2014), sunbathing (Danzy et al. 2012), and huddling (McFarland et al. 2015) in response to cold and increased resting in response to heat (McFarland et al. 2014). Vervets likely do not have autonomic selective brain cooling mechanisms and are therefore thought to rely on evaporative water loss and behavioral thermoregulation to prevent overheating (see Mitchell et al. 2009 positing this for baboons and other diurnally-active African primates occupying hot, dry environments).

*Niche Mapper Description*

Niche Mapper (Porter & Mitchell 2006) consists of two submodels: a microclimate model and a generic animal model. The microclimate model uses macroclimate data (e.g., maximum and minimum daily air temperatures, cloud cover, wind speed, and relative humidity), substrate thermal and reflective properties, geographic location, and time of year to calculate hourly environmental conditions at the animal's height. Separate profiles are calculated for full sun and shaded microenvironments (see Fuentes & Porter 2013 for more details on the microclimate model calculations). The animal model then uses the hourly outputs from the microclimate model in conjunction with information about the animal's morphology, physiology

and behavior to iteratively solve a heat balance equation to find the metabolic rate needed for the animal to maintain its body temperature, accounting for conductive, convective, radiative, evaporative and solar heat fluxes with its microenvironment (see Mathewson & Porter 2013 for details on the heat balance calculations).

Niche Mapper solves the animal's heat balance for each hour of the day, and if the calculated metabolic rate is outside of a user-specified error range around a target metabolic rate (i.e., resting metabolic rate or some multiple thereof to simulate activity), thermoregulatory options are engaged. If thermoregulatory options are exhausted before a metabolic rate within 2.5% of the target metabolic rate is reached, the model will return the closest value. Thus, cold stress can be quantified by the extent to which the calculated metabolic rate exceeds the target metabolic rate. For animals that can sweat and/or pant, heat stress can be quantified by the evaporative water loss rate required by the model to dissipate enough heat for the animal to maintain its target metabolic rate in hot conditions without overheating.

Niche Mapper has been previously shown to accurately predict heterothermy in vervets as a response to environmental conditions (See Chapter 2). It also accurately predicted energetic requirements and thermal stress as a function of environmental conditions for a wide variety of other species, including the following mammals: American pika (*Ochotona princeps*; Moyer-Horner et al. 2015), Japanese serow (*Capricornus crispus*; Natori & Porter 2007), Giant Panda (*Ailuropoda melanoleuca*; Zhang et al. 2018), elk (*Cervus elaphus*; Long et al 2014), polar bear (*Ursus maritimus*; Mathewson & Porter 2013), and koala (*Phascolarctos cinereus*; Briscoe et al. 2016).

Vervet model inputs came from direct measurements of wild vervets from a South African population or from the literature; see Chapter 2 for a detailed description and tests of the vervet model. For the simulations here, we used the female vervet model.

Vervets were modeled as thermoregulating to maintain an average metabolic rate of 2.5x BMR per hour during diurnal hours, and we calculated the evaporative water cost required for vervets to maintain their activity level throughout the day. We thus used Niche Mapper to calculate the average hourly water cost for maintaining diurnal activity in the warmest quarter of the year. This was done by using monthly temperature data as inputs to Niche Mapper to calculate the average hourly water cost for a typical day in each month in each landscape grid cell and then averaging these values across the warmest three months of the year. We assumed that vervets would seek shade, if available, to minimize evaporative water costs. Forests and closed shrublands were assumed to have 100% overhead shade available and grasslands, snow/ice, and barren/sparsely vegetated land cover types were assumed to have no overhead shade available. All other land cover types were modeled as having 50% overhead shade available.

As a metric of cold stress, we used Niche Mapper to calculate overnight thermoregulatory costs during the coldest quarter of the year. During crepuscular and nocturnal hours, vervets were modeled as inactive (thermoregulating to maintain basal metabolic rate). Although vervets do huddle together (see Chapter 2), the ability to huddle is driven by social standing in the group (McFarland et al. 2015). Thus, we calculated thermoregulatory costs of a lone model vervet allowed to curl up at night when cold, which provides an upper estimate applicable to all individuals in a group. Overnight thermoregulatory costs were calculated as the total predicted metabolic heat production needed above basal requirements to maintain a minimum body

temperature of 36°C during crepuscular and nocturnal hours. Overnight costs were calculated for an average day for each month and then the average overnight cost during the coldest quarter was calculated for each landscape grid cell.

Daily wind speeds were assumed to vary from 0.1 m/s (at sunrise) to 4 m/s (one hour after solar noon). Relative humidity was assumed to vary from 100% (at sunrise) to a minimum at one hour after solar noon, calculated based on the daily temperature range assuming constant water mass in the air over 24 hours (Tracy et al. 1980). A constant monthly cloud cover based on 1960-1990 average values from New et al. (2002; 30 min data resolution) was used for all hours of the day. Ground reflectivity was assumed to be 20% to simulate a mix of bare soil and grass for months when the average temperature was > 0°C; for months where the average temperature was ≤ 0°C a surface reflectivity of 78% was used to simulate snow-covered ground. A sensitivity analysis of these microclimate input assumptions was run for a sample location (Samara Game Reserve, South Africa; Figure S1).

*Spatial Data*

Climate data were obtained from WorldClim at 2.5-minute (~4 km) resolution. WorldClim version 2 data (average monthly data for 1970-2000) were used for the current climate modeling (Fick & Hijmans 2017). Future climate data are unavailable for Version 2 so we used two future climate scenarios from version 1.4 (Hijmans 2005) selected to represent the least and most stressful future climates from a thermal perspective: one representing the smallest predicted temperature increase and precipitation decrease from current (MG45) and one representing the largest predicted temperature increase and precipitation reduction from current (HG85) (Table S1; Figs. S2-4).

Land cover data (2001-2010) were obtained from the United States Geological Survey Landcover Institute at 0.5 km resolution (Broxton et al. 2014). Elevations came from the United States Geological Survey Global 30 Arc-Second Elevation digital elevation model (USGS 2015). Elevations were resampled to 2.5-minute resolution to match the climate data using the raster package in R version 3.4.2 (R Core Team 2017). Slope and aspect were calculated from the elevation layer using the raster package in R. Horizon angles in 15° directional increments for each pixel were calculated from the digital elevation map using GRASS GIS 7.0 (GRASS Development Team, 2015) using a 5-km maximum distance to find any obstructions. The horizon angles are used in Niche Mapper's microclimate model to estimate the timing of solar radiation hitting the ground at any given landscape location.

*Distribution Models*

We built species distribution models with Maxent (Phillips et al. 2006) because this modeling framework is widely used, has been found to perform well compared to other models, and was developed for presence-only data (Elith et al., 2006; Yates et al. 2018). Models were fit using either the bioclimate variables as proxies for the thermal stresses (e.g., mean temperature of the warmest quarter, mean temperature of the coldest quarter) or the variables created by Niche Mapper (i.e., evaporative water loss rates in the warmest quarter, additional nighttime heat production in the coldest quarter). The former model will be referred to hereafter as the "BioClim model" and the latter as the "NM model." We note here that we use a correlative approach with mechanistic inputs because we do not know the threshold for tolerable evaporative water loss or cold stress in order to simply use the NM outputs to delineate distributions. Furthermore, thresholds would likely vary spatially in relation to available

resources, the abundance of which would facilitate higher thresholds compared to areas with fewer resources.

Animals that rely on evaporative water loss to prevent overheating are likely to be most stressed when high temperatures coincide with little precipitation (Briscoe et al. 2016, Krockenberger et al. 2012, Kearney et al. 2010), and the availability of water reduces the "cost" to sweating as means of thermoregulating because the water lost can be replenished (Fuller et al. 2016, Mitchell et al. 2018). Thus, we included precipitation in the warmest quarter as an additional predictor variable in both models because we expect that higher precipitation would increase the suitability of hotter locations.

Vervets are one of seven species in the *Chlorocebus* genus, which until recently were all considered a single species, *Cercopithicus aethiops*. Due to this reclassification and ongoing taxonomic uncertainty, we collected location points for both *Cercopithecus aethiops* and *Chlorocebus* spp. from the Global Biodiversity Information Facility (GBIF, www.gbif.org) and from published studies presenting locations for "vervets" or "vervet monkeys" (Table S2). To identify the most probable *Chlorocebus pygerythrus* locations, we simplified the IUCN *Chlorocebus pygerythrus* distribution range (IUCN 2017) and used all location points within the simplified boundary (Fig. S5). After reducing locations to one point per 2.5-minute grid cell, there 388 presence locations used in the Maxent modeling. For background points, we used the target-group background approach to minimize presence point selection bias (Phillips et al. 2009) using all records of land mammals from mainland Africa from GBIF as background points. Limiting these points to one per 2.5-minute grid cell left 9,246 background points that were used in the Maxent modeling.

Predictor variables used in the distribution modeling are summarized in Table 1, and both the BioClim and NM models used the same set of presence locations and backgrounds points. The BioClim model was built allowing only hinge and product features to smooth the response curves and avoid overfitting (Elith et al., 2010), while allowing for interactions between predictor variables. We have an a priori expectation that response curves to sweating costs and cold stress predictor variables should be unidirectional, with suitability only declining as the stress metric increases. Thus, we built the NM model allowing only quadratic and product features because hinge features produced illogical response curves (Fig. S6). That said, we note that using either hinge or quadratic features in the NM model produced broadly similar distribution maps (Fig. S7).

The models were evaluated using 10-fold cross-validation. Other model settings were set to default values, including the use of clamping when extrapolating. To allow easier comparisons of predictions between model approaches, Maxent's continuous output was converted into a binary suitable/unsuitable output using the threshold that maximized training sensitivity plus specificity, as suggested for use with presence-only data by Liu et al. (2005, 2013). Recognizing the limitations of using a single threshold and the loss of information of thresholding in the first place we also present analyses using different threshold choices and using the continuous habitat suitability outputs.

**Table 1.** Predictor variables used in distribution models and reason for inclusion. We also show other bioclimate variables that are highly correlated (|Spearman rho| > 0.7) with the predictor variables used in the models.

| **Variables used in Maxent Modeling** | **Highly correlated bioclimate variables** | **Reason for Inclusion** |
|---|---|---|
| Mean temperature of the warmest quarter[1] | Mean annual temperature, maximum temperature of warmest month | Metric for direct heat stress; more informative than mean annual temperature; we assume that chronic heat stress is a greater limiting factor than acute heat stress. |
| Mean temperature coldest quarter[2] | Mean annual temperature, minimum temperature of coldest month. | Metric for direct cold stress; more informative than mean annual temperature; we assume that chronic cold stress is a greater limiting factor than acute cold stress. |
| Total precipitation in warmest quarter | Annual precipitation | Metric for water availability during period of greatest heat stress; more informative than annual precipitation; we assume that water availability is most limiting in driest and hottest periods. |

1 Replaced with sweating cost in the warmest quarter in the NM model

2 Replaced with nighttime thermoregulatory costs in the coldest quarter in the NM model.

## RESULTS

### *Species Distribution Model Results: Current Climate*

Within the vervet range and under current climate conditions, the models agreed on 76% of the area that either model predicted as suitable and both performed well, identifying suitable climate space at >88% of vervet locations (Fig. 1; Table 2). The only substantial areas that neither model predicted suitable climate space within this range is in the Kalahari Desert in southern Africa and the lowlands of northern Kenya and southern Ethiopia and Somalia. Overall,

the NM model predicted 10% more suitable climate space (Table 3), most distinctly along the eastern coast and southern South Africa.

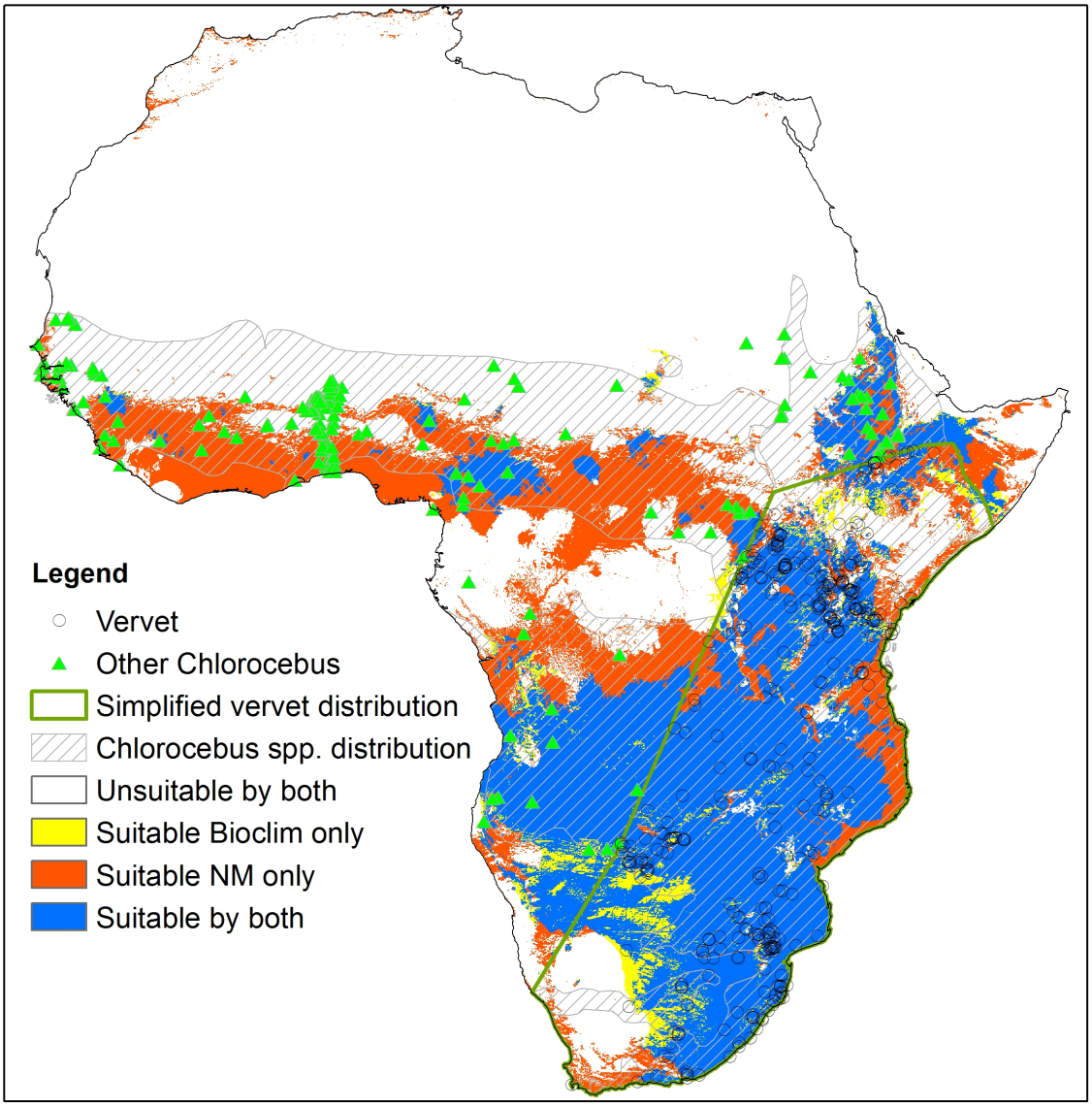


**Figure 1.** Suitable climate space under current climate conditions predicted by the bioclimate and Niche Mapper-hybrid Maxent distribution models. Vervet and other *Chlorocebus* spp. locations are also shown, as is the combined *Chlorocebus* species distribution range (IUCN 2017).

**Table 2**. Total area ($km^2$) within either the current IUCN vervet distribution or all of mainland Africa predicted as suitable by the BioClim and NM models under current (1980-2010) climate, moderate future climate (MG45) and a hot and dry future climate (HG85).

| | Models predicting suitable climate space | Climate Scenario | | |
|---|---|---|---|---|
| | | Current | 2070: MG45 | 2070: HG85 |
| IUCN Vervet Distribution | Neither | 1,153,674 | 1,255,817 | 2,626,424 |
| | BioClim Only | 465,546 | 493,993 | 273,806 |
| | NM Only | 946,687 | 1,871,088 | 2,419,785 |
| | Both | 4,401,897 | 3,346,907 | 1,647,790 |
| Mainland Africa | Neither | 17,895,720 | 18,359,547 | 19,877,832 |
| | BioClim Only | 715,306 | 818,369 | 429,937 |
| | NM Only | 4,309,557 | 5,474,467 | 6,584,468 |
| | Both | 6,619,996 | 4,881,196 | 2,641,343 |

**Table 3**. Evaluation statistics for the BioClim and NM models. Presence location omissions indicate the proportion of vervet locations within the current *C. pygerythrus* distribution (see text) or any *Chlorocebus* spp. location with habitat suitability predictions below the MSS threshold. Also presented are the proportions of presence locations for which no suitable climate space was predicted within 10 or 25 km.

| | BioClim Model | NM Model |
|---|---|---|
| AUC | 0.74 | 0.68 |
| TSS | 0.41 | 0.32 |
| Cross-validation test locations | 0.16±0.06 | 0.15±0.12 |
| Presence Location Omissions | | |
| *C. pygerythrus* locations (n=403) | 0.12 | 0.08 |
| Within 10 km | 0.07 | 0.01 |
| Within 25 km | 0.04 | 0.01 |
| *Chlorocebus* spp. locations (n=622) | 0.37 | 0.24 |
| Within 10 km | 0.33 | 0.16 |
| Within 25 km | 0.31 | 0.14 |

The BioClim model had higher AUC and TSS scores, due to the greater specificity (i.e., higher proportion of background pseudoabsence locations identified as unsuitable for vervets). The NM model had a lower omission rate (8% vs. 12%) for vervet locations within the vervet range (Table 2).

Outside of the vervet distribution, the predictions begin to diverge, particularly in West Africa where the NM model predicts substantially more suitable climate space. Across mainland Africa, the models only agreed on 57% of the area that either model predicted as suitable, with the NM model predicting 49% more suitable climate space (Fig. 1, Table 3). Notably, the areas

outside of the vervet distribution where the NM model predicts additional suitable climate space are primarily within the distributional ranges of other *Chlorocebus* species (Fig. 1). The NM model did predict some suitable climate space in the Congo rainforest basin and some higher elevation areas of northern Morocco, neither of which are areas where vervets are found. Neither model predicted any suitable climate space around vervet locations in the northernmost parts of the *C. tantalus* range or in the northwestern finger of *C. aethiops* range running along the Nile river.

Overall the NM model predicted suitable climate space within 25 km of 86% of all *Chlorocebus* spp. locations compared to the Bioclim model predicting suitable climate space within 25 km of 69% of all *Chlorocebus* spp. locations (Table 2).

These trends in differences between model predictions of habitat suitability hold even if other thresholds are used (Fig. S8). Examination of the continuous outputs also indicates the same trends (Fig. S9). Within the vervet range, the BioClim model predicted habitat suitability values 0.017±0.002 greater than the NM model for landscape pixels within 10 km of vervet occurrences. Outside the vervet range, the NM model predicted habitat suitability values 0.043±0.003 greater than the BioClim model for landscape pixels within 10 km of *Chlorocebus* spp. occurrences.

As expected, we found an interaction between the precipitation and mean temperature of the warmest quarter or evaporative water loss in the warmest quarter (Fig. S10). The interaction was stronger between precipitation and evaporative water loss, as greater precipitation was needed to maintain habitat suitability across the range of evaporative water losses. The interaction was only evident for moderate values in the BioClim model.

*Species Distribution Model Results: Future Climates*

The NM model predicted substantially more remaining suitable climate space in the future (Fig. 2, Table 3). Under the moderate future climate, the BioClim model predicted losses of 21% of suitable climate space within the current vervet range and 22% of suitable climate space throughout mainland Africa. The NM model predicted losses of 2% within the current vervet range and 5% throughout mainland Africa. Under the hot and dry future climate, the BioClim model predicted losses of 61% of suitable climate space within the current vervet range and 58% of suitable climate space throughout mainland Africa. The NM model predicted losses of 24% within the current vervet range and 15% throughout mainland Africa.

The NM model predicted that 22% of current vervet locations would be unsuitable under the hot/dry future climate scenario, while the BioClim model predicted that 60% of current vervet locations would be unsuitable under the hot/dry future climate scenario (Table 4). Both models agree on large areas of remaining suitable climate space where vervets are currently found in eastern South Africa and in Kenya/Tanzania (Fig. 2). A large area where vervets are currently known to exist but where both models predict habitat loss under the hot and dry future climate is south-central Africa (northern Botswana, southern Zambia, western Zimbabwe).

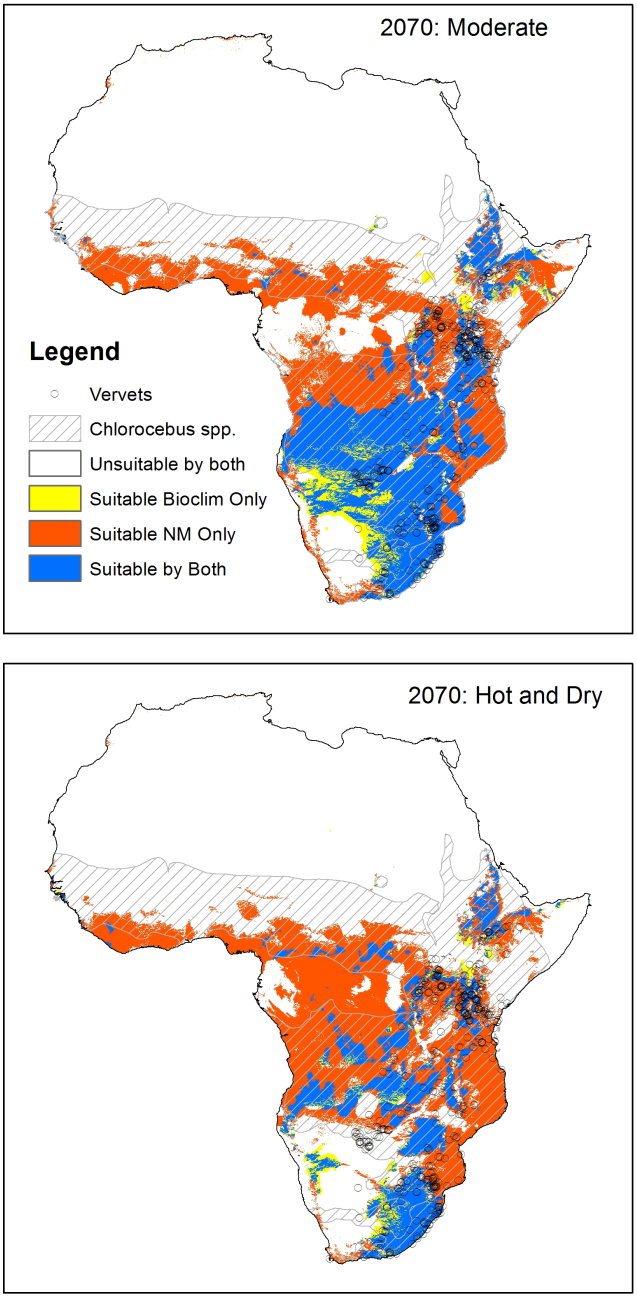


**Figure 2.** Suitable climate space under two 2070 climate scenarios predicted by the bioclimate and Niche Mapper-hybrid Maxent distribution models. Current vervet locations are also shown, as is the combined *Chlorocebus* species distribution range (IUCN 2017).

**Table 4.** Proportion of current presence locations of *C. pygerythrus* (see text; n=403) or any *Chlorocebus* spp. (n=622) considered unsuitable under moderate (MG45) and hot and dry (HG85) future climate conditions. Also presented are the proportion of current presence locations for which no suitable climate space was predicted within 10 or 25 km in the future.

| | MG45 | | HG85 | |
|---|---|---|---|---|
| | BioClim Model | NM Model | BioClim Model | NM Model |
| *C. pygerythrus* locations | 0.36 | 0.16 | 0.60 | 0.22 |
| Within 10km | 0.26 | 0.03 | 0.50 | 0.09 |
| Within 25km | 0.17 | 0.01 | 0.35 | 0.07 |
| *Chlorocebus* spp. locations | 0.55 | 0.34 | 0.72 | 0.41 |
| Within 10km | 0.47 | 0.21 | 0.64 | 0.30 |
| Within 25km | 0.40 | 0.17 | 0.52 | 0.25 |

The trend of the NM model predicting more remaining habitat in the future holds even if other thresholds are used (Fig. S11). Examination of the continuous outputs also indicates the same trend (Fig. S12). Within the vervet range, the NM model predicted habitat suitability values 0.06±0.003 (MG45 scenario) to 0.19±0.003 (HG85 scenario) greater than the BioClim model for landscape pixels within 10 km of vervet occurrences in the hot/dry future scenario. Outside the vervet range, the NM model predicted habitat suitability values 0.09±0.004 (MG45 scenario) to 0.16±0.004 (HG85 scenario) greater than the BioClim model for landscape pixels within 10 km of *Chlorocebus* spp. occurrences. In general, the NM model predicted lower reductions in future suitable climate space (Fig. S13).

Examination of multivariate environmental similarity surfaces indicates that neither model is relying on extrapolation within the vervets distributional range (Fig S13).

## DISCUSSION

Our main finding is that the two modeling approaches provided similar predictions under the climate conditions and within the area of the presence areas they were trained on, but diverged when making predictions outside of the training area and into future climates. Under the current climate and within current vervet range, the models agreed for 76% of locations where at least one model predicted suitable climate space. Under the current climate but outside the current vervet range, the models agreed for only 38% of locations where either model predicted suitable climate space. Within the current vervet range but under the most divergent future climate (HG85), the models agreed for 38% of locations where either model predicted suitable climate space.

Past reviews of species distribution modelling approaches have noted how purely mechanistic models should, in theory, predict a distribution close to a species' fundamental niche, while purely correlative models predict distributions closer to a species' realized niche (e.g., Meineri et al. 2014, Pacifici et al. 2015). The results of our modeling appear to be consistent with this theory because additional areas outside of the vervet distribution that the NM model predicted suitable climate space are largely found within the distributions of closely related *Chlorocebus* species. These other species are broadly similar in morphology and ecology and would not be expected to have markedly different thermal tolerances than vervets.

While it is impossible to know which model is producing more accurate predictions for the future with certainty, model performance at *Chlorocebus* spp. locations under current conditions in areas outside of the model training area (i.e., the vervet distribution) could provide

some insight. The fact that the NM model predicted suitable throughout most of the areas in West Africa (some of the hottest places where other *Chlorocebus* species are currently found) while the BioClim model did not predict much suitable climate space there suggests that the NM model might be better capturing the functional physiological tolerance of vervets to heat. This would indicate greater confidence in NM model predictions into the warmer future climates.

Even the NM model failed to identify suitable climate space in the vicinity of some known *Chlorocebus* spp. locations. Most of these omissions are in or along the edge of desert areas, particularly along the boundaries of the Saharan desert. One explanation for this could be the larger scale of the climate data we used. There may be smaller patches of suitable microhabitat within these larger 4.5 $km^2$ grid cells that facilitate presences in these locations. For example, a number of these omissions are in close proximity to the Nile River, which may create a narrow strip of suitable climate space (e.g., presence of shade or additional moisture in the soil) masked by conditions in the rest of the larger grid cell.

We also note that the BioClim model has higher AUC and TSS statistics. This is due to the NM model's lower specificity (i.e., predicting suitable climate space at more background point locations). However, because these background points are pseudoabsences rather than true absences, it is reasonable to place more weight on selectivity (i.e., correctly predicting suitable climate space at presence locations). Furthermore, a subjective analysis based on personal expert knowledge of vervets and other *Chlorocebus* spp. of the NM model's predicted range looks reasonable. The only general areas that the NM model predicts suitable climate space but where no vervets or other closely related species are found are in rainforests and areas of northern Morocco, Algeria and Tunisia. Both areas may be thermally suitable, but the former may not be

inhabited by *Chlorocebus* due to biotic interactions (e.g., guenons already filling available niches) while the latter may not be inhabited due to a dispersal barrier (the Sahara Desert).

Even if it is unclear which model is more accurate with its future predictions, employing different modeling approaches provides a range of potential future habitat suitability, which provides a benefit for conservation planning. There is greater confidence in areas where both models agree: more warranted concern for the populations in areas where both models predict the loss of habitat in the future and more confidence in conservation management planning for the future in areas where both models predict remaining suitable climate space. Furthermore, the NM model predicts substantially more remaining suitable climate space in the future that may encompass areas of good conservation opportunities that may have been written off if only relying on the purely correlative approach.

More generally, this work illustrates how incorporating a mechanistic approach helps to provide more insight into how species' distribution is limited by environmental factors. A primary way that it does this is by converting climate data into an easier-to-interpret water loss/nighttime heat production requirements on the landscape. In the context of model-building this allows more informed evaluation of response curves generated by Maxent, as discussed above in the methods. It also allows for more informed interactions with other predictors like land cover in order to capture how use of microhabitats (i.e., shade availability) affects how the focal animal actually experiences the landscape. For example, evaporative water loss patterns don't exactly follow the same patterns as the macroclimate temperature data does (see top row of Figure S1) because the presence of shade reduces the water-requirement cost to living in those areas. Note that even if we add a land cover layer to the BioClim model to try to implicitly capture this, the overall results change very little (Fig S14).

Without this insight and focus on a mechanism, a purely correlative model may end up being overfit to the particular combinations of temperature and precipitation found at the presence locations used to train the model simply because it provides the best statistical fit rather than for an underlying biologically-relevant reason. This is arguably the case here as just under half of the total suitable area across mainland Africa predicted by the NM model was within the vervet distribution area where the presence locations used to train the model were found. In contrast, 66% of the total suitable area across mainland Africa predicted by the BioClim model was within the vervet distribution area, and it did not predict suitable climate space around many of the other *Chlorocebus* spp. locations that the NM model did as discussed above.

Finally, we note that we used the same animal model with morphology derived from measurements on individuals from a South African population for simulations across mainland Africa. However, studies like Turner et al. (2018) and Cardini et al. (2013) report spatial variation in morphology. Using a single animal model was a simplifying assumption for the purposes of this study. However, NM is a general model and the morphology inputs could be varied spatially to explore whether incorporating observed morphological differences affect predicted model outputs (see, e.g., the model's sensitivity to vervet total mass, body part dimensions and proportions and fur properties), and, in turn, allow for more accurate distribution predictions. This is an important avenue of future research as phenotypic variability and plasticity may help buffer the effects of climate change (Buckley 2008, Boyles et al. 2011, Riddell et al. 2018).

In summary this work, along with the previous work with the American Pika (Chapter 1) illustrate how this hybrid approach can help address the need to incorporate more mechanism into species distribution models, particularly for endotherms (La Sorte & Jetz, 2013, Evans et al.

2015, Urban et al. 2016, Methorst et al. 2018). Using Niche Mapper to estimate cold stress, evaporative water loss, or activity restriction only requires basic information about the animal's morphology (body parts dimensions, pelage properties), physiology (resting metabolic rate, body temperature), and behavior (habitat use, activity pattern). These basic inputs are relatively easy to obtain from direct measurements (on live or museum specimens) or from the literature (e.g., allometric equations relating metabolic rate to body mass), allowing the approach to be more widely adopted. As illustrated here (and in Chapter 1), this complementary modeling can provide additional insight into the effects of climate change on species.

ACKNOWLEDGEMENTS

We thank Tegan Gaetano, Andrea Cardini, and Sarah Elton for sharing vervet locations from their respective published studies.

REFERENCES

Boyles JG, Seebacher F, Smit B, McKechnie AE. 2011. Adaptive thermoregulation in endotherms may alter responses to climate change. Integrative and Comparative Biology 51: 676-690.

Briscoe NJ, Kearney MR, Taylor C, Brendan WA. 2016. Unpacking the mechanisms captured by a correlative SDM to improve predictions of a climate refugia. Global Change Biology 22: 2425-2439.

Broxton PD, Zeng Z, Sulla-Menashe D, Troch PA. 2014. A global land cover climatology using MODIS data. Journal of Applied Meteorology and Climatology 53: 1593-1605.

Buckley LB, Urban MC, Angilletta MJ, Crozier LG, Rissler LJ, Sears MW. 2010. Can mechanism inform species' distributional models. Ecology Letters 13: 1041-1054.

Buckley LB, Cannistra AF, John Aji. 2018. Leveraging organismal biology to forecast the effects of climate change. Integrative and Comparative Biology 58: 38-51.

Cardini A, Dunn J, O'Higgins P, Elton S. 2012. Clines in Africa: does size vary in the same way among widespread sub-Saharan mankeys? Journal of Biogeography 40: 370-381.

Cawthon Lang KA. 2006 January 3. Primate Factsheets: Vervet (Chlorocebus) Taxonomy, Morphology, & Ecology. <http://pin.primate.wisc.edu/factsheets/entry/vervet>. Accessed 2017 April 29.

Danzy J, Grobler JP, Freimer N, Turner TR (2012). Sunbathing: a behavioral response to seasonal climatic change among South African vervet monkeys (*Chlorocebus aethiops*). African Primates 7: 230-237.

Dormann, CF, Schymanski SJ, Cabral J, et al. 2012. Correlation and process in species distribution models: bridging a dichotomy. Journal of Biogeography 39: 2119-2131.

Elith J et al. 2006. Novel methods improve prediction of species' distributions from occurrence data. Ecography 29: 129-151.

Elith J, Kearney M, Phillips. 2010. The art of modelling range-shifting species. Methods in Ecology and Evolution 1: 330-342.

Evans MEK, Merow C, Record S, McMahon SM, Enquist BJ. 2016. Towards process-based range modeling of many species. Trends in Ecology and Evolution 31: 860-871.

Fick SE and Hijmans RJ. 2017. Worldclim 2: New 1-km spatial resolution climate surfaces for global land areas. International Journal of Climatology 37: 4302-4315.

Fuentes M and Porter WP. 2013. A new approach to model soil temperature: using microclimate models to predict the impacts of climate change on sea turtles. Ecological Modeling 251: 150–157.

Fuller A, Dawson T, Helmuth B, Hetem RS, Mitchell D. 2010. Physiological mechanisms in coping with climate change. Physiological and Biochemical Zoology 83: 713-720.

GRASS Development Team. 2015. Geographic Resources Analysis Support System (GRASS) Software, Version 7.0. Open Source Geospatial Foundation.

Hijmans RJ, Cameron SE, Parra JL, Jones PG, Jarvis A. 2005. Very high resolution interpolated climate surfaces for global land areas. International Journal of Climatology 25: 1965-1978.

IUCN Red List of Threatened Species. Version 2017-3. <www.iucnlist.org>, Downloaded on July 14, 2017.

Kearney M, Porter WP. 2009. Mechanistic niche modelling: combining physiological and spatial data to predict species' ranges. Ecology Letters 12: 334-350.

Kearney MR, Wintly BA, Porter WP. 2010. Correlative and mechanistic models of species distribution provide congruent forecasts under climate change. Conservation Letters 3: 203-213.

Krockenberger AK, Edwards W, Kanowski J. 2012. The limits to the distribution of a rainforest marsupial folivore is consistent with the thermal intolerance hypothesis. Oecologia 168: 889-899.

Korstjens AH and Hillyer A. 2016. Primates and climate change: a review of current knowledge. In: An Introduction to Primate Conservation. Wich SA and Marshall AJ, eds., Oxford University Press.

La Sorte FA, Jetz W. 2010. Avian distributions under climate change: towards improved projections. The Journal of Experimental Biology 213: 862-869.

Liu C, Berry PM, Dawson TP, Pearson RG. 2005. Selecting thresholds of occurrence in the prediction of species distributions. Ecography 28: 385-393.

Liu C, White M, Newell G. 2013. Selecting thresholds for the prediction of species occurrence with presence-only data. Journal of Biogeography 40: 778-789.

Long RA, Bowyer RT, Porter WP, Mathewson PD, Monteith KL, Kie JG. 2014. Behavior and nutritional condition buffer a large-bodied endotherm against direct and indirect effects of climate. Ecological Monographs 84: 513-532.

Lubbe A, Hetem RS, McFarland R, et al. 2014. Thermoregulatory plasticity in free-ranging vervet monkeys, *Chlorocebus pygerythrus*. Journal of Comparative Physiology B 184:799–809.

Mathewson PD and Porter, WP. 2013. Simulating polar bear energetics during a seasonal fast using a mechanistic model. PLoS One 8: e72863.

Mathewson PD**,** Moyer-Horner L, Beever EA, Briscoe NJ, Kearney M, Yahn JM, Porter WP. 2017. Mechanistic variables can enhance predictive models of endotherm distributions: the American pika under current, past, and future climates. Global Change Biology 23: 1048-1064.

McFarland R, Barrett L, Boner R, Freeman NJ, Henzi SP. 2014. Behavioral flexibility of vervet monkeys in response to climatic and social variability. American Journal of Physical Anthropology 154:357–364.

McFarland R, Fuller A, Hetem RS, Mitchell D, Maloney SK, Henzi SP, Barrett L. 2015. Social integration confers thermal benefits in a gregarious primate. Journal of Animal Ecology 84:871–878.

Meineri E, Deville A-S, Grémillet D, Gauthier-Clerc, M, Béchet A. 2014. Combining correlative and mechanistic habitat suitability models to improve ecological compensation. Biological Reviews 90:314-329.

Methorst J, Bohning-Gaese K, Khaliq I, Hof C. 2017. A framework integrating physiology, dispersal and land-use to project species ranges under climate change. Journal of Avian Biology 48: 1532-1548.

Mitchell D, Snelling EP, Hetem RS, Maloney SK, Strauss WM, Fuller A. 2018. Revisiting concepts of thermal physiology: predicting responses of mammals to climate change. Journal of Animal Ecology 87: 956-973.

Moyer-Horner L, Mathewson PD, Jones G, Kearney MR, Porter WP. 2015. Modeling behavioral thermoregulation in a climate change sentinel. Ecology and Evolution 5**:** 5810-5822.

Natori Y and Porter WP. 2007. Model of Japanese Serow (*Capricornis crispus*) energetics predicts distribution on Honshu, Japan. Ecological Applications 17: 1441-1459.

New M, Lister D, Hulme M, Makin I. 2002. A high-resolution data set of surface climate over global land areas. Climate Research 21: 1-25.

Oswald SA, Arnold JM. 2012. Direct impacts of climatic warming on heat stress in endothermic species: seabirds as bioindicators of changing thermoregulatory constraints. Integrative Zoology 7: 121-16.

Pacifici M, Foden WB, Visconti P, et al. 2015. Assessing species vulnerability to climate change. Nature Climate Change 5: 215-224.

Phillips SJ, Anderson RP, Schapire RE. 2006. Maximum entropy modeling of species geographic distributions. Ecological Modelling 190: 231-259.

Phillips SJ, Duki M, Elith J, Graham CH, Lehmann A, Leathwick J, Ferrier S. 2009. Sample selection bias and presence-only distribution models: implications for background and pseudo-absence data. Ecological Applications 19: 181-197.

Porter WP and Mitchell JW. 2006. Method and system for calculating the spatial-temporal effects of climate and other environmental conditions on animals. http://www.warf.org/technologies.jsp?ipnumber=P01251US

R Core Team. 2017. R: a language and environment for statistical computing. R Foundation for Statistical Computing, Vienna, Austria. Available at: <https://www.R-project.org/>. Last accessed June 10, 2017.

Riddell EA, Odom JP, Damm JD, Sears MW. 2018. Plasticity reveals hidden resistance to extinction under climate change in the global hotspot of salamander diversity. Science Advances 4: eaar5471.

Turner TR, Schmitt CA, Cramer JD, Lorenz J, Grobler JP, Jolly CJ, Freimer NB. 2018. Morphological variation in the genus *Chlorocebus*: ecographic and anthropogenically

mediated variation in body mass, postcranial morphology, and growth. American Journal of Physical Anthropology 166: 682-707.

Tracy CR, Welch WR, Porter WP. 1980. Properties of air: A manual for students in biophysical ecology. University of Wisconsin Laboratory of Biophysical Ecology, Technical Report #1 (3rd Edition).

United States Geological Survey. 2015. Global 30 Arc-Second Elevation (GTOPO30). Available at: <https://lta.cr.usgs.gov/GTOPO30>. Last accessed July 24, 2017.

Urban MC, Bocedi G, Hendry AP, et al. 2016. Improving the forecast for biodiversity under climate change. Science 353: 6304

Yates KL et al. 2018. Outstanding challenges in the transferability of ecological models. Trends in Ecology & Evolution 33: 790-802.

Zhang Y, Mathewson PD, Zhang Q, Porter WP, Ran J. 2018. An ecophysiological perspective on likely giant panda habitat responses to climate change. Global Change Biology 24: 1804-1816.

SUPPORTING INFORMATION

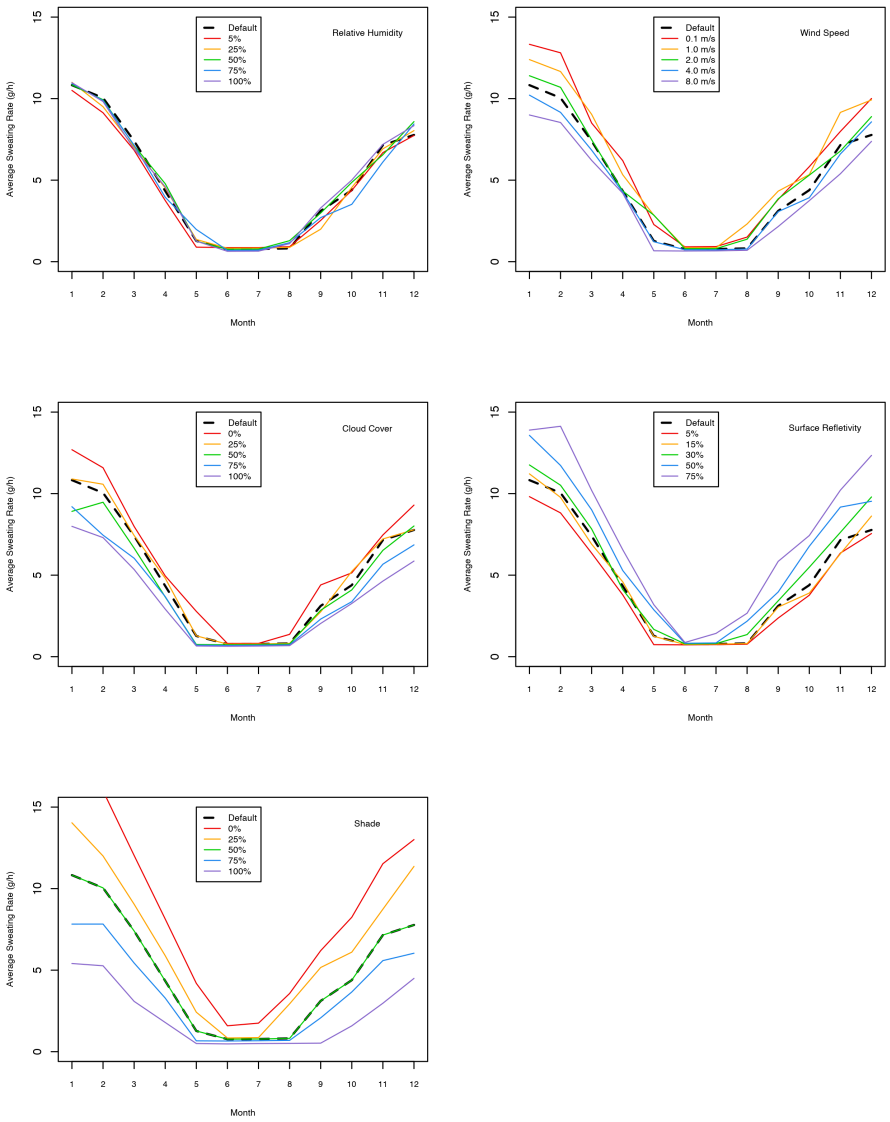


**Figure S1a.** Sensitivity analysis of microclimate model input assumptions on predicted average sweating rate. The sensitivity to a given parameter was evaluated by keeping all other inputs at their default levels and holding the parameter in question constant at various levels. The model is by far the most sensitive to assumption of shade availability and least sensitive to relative humidity assumptions. With the exception of shade availability, this analysis shows that predictions are unlikely to be substantially affected by realistic deviations from the assumed inputs. As noted in the text we ran three different simulations of shade availability: 0%, 50%, and 100%.

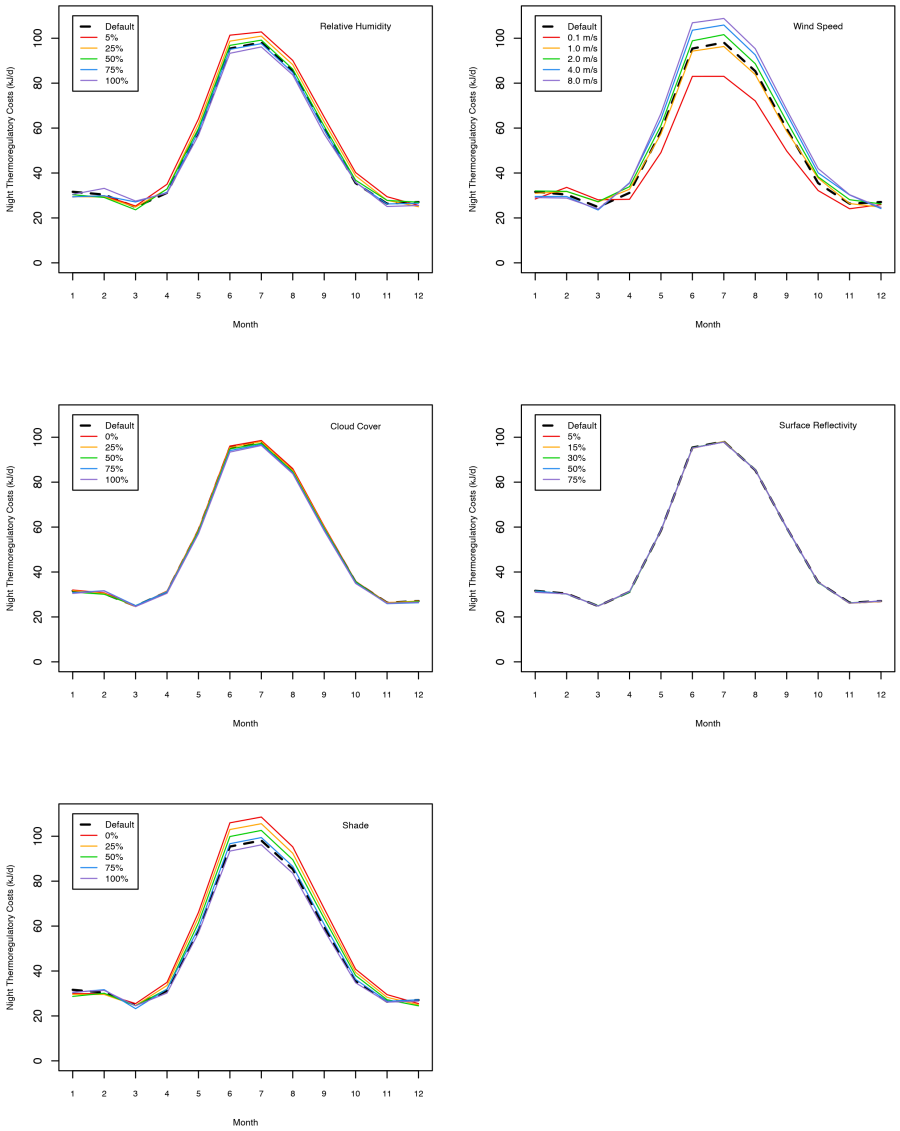


**Figure S1b.** Sensitivity analysis of microclimate model input assumptions on predicted overnight thermoregulatory costs. The sensitivity to a given parameter was evaluated by keeping all other inputs at their default levels and holding the parameter in question constant at various levels. The model is most sensitive to assumption of wind speed and overhead vegetative cover at night. However, so long as the actual windspeeds are between 1 and 4 m/s and the actual overhead vegetative cover is between 50% and 100%, deviations from the assumed inputs will not substantially affect results. Note that the model's insensitivity to cloud cover results from the default assumption of 85% overhead vegetative cover at night; thus most of the animal's radiant heat exchange is with vegetation rather than the night sky.

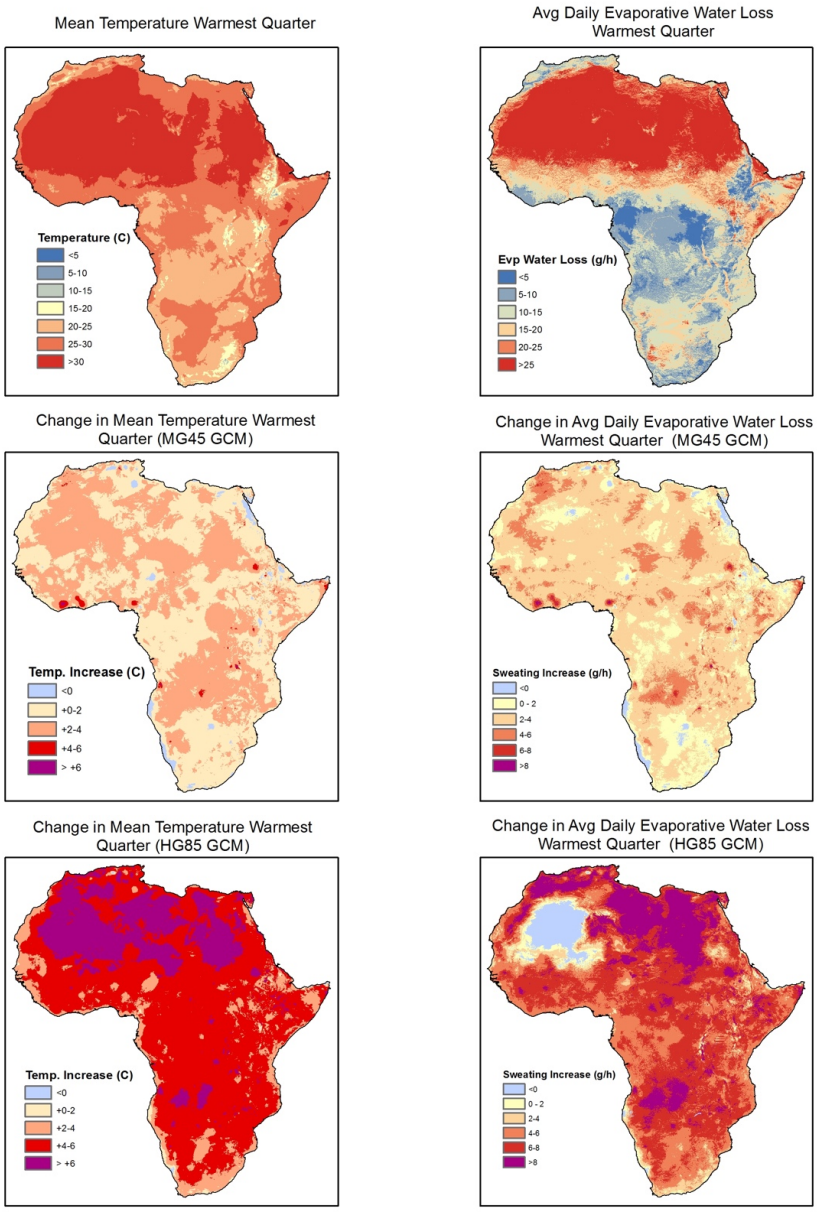


**Figure S2.** Maps showing mean temperature of the warmest quarter (top left) and predicted evaporative water loss in the warmest quarter (top right) under current climate conditions, as well as changes in these values under a moderate 2070 climate scenario (middle row) and hot/dry 2017 climate scenario. The reduced sweating costs in the hot 2070 scenario are due to reduced activity from overheating leading to less evaporative water loss. This is interpreted as this area being too hot to maintain activity even with sweating under these conditions while throughout the rest of continent, activity can still be maintained with sweating, albeit at a greater cost in terms of water loss.

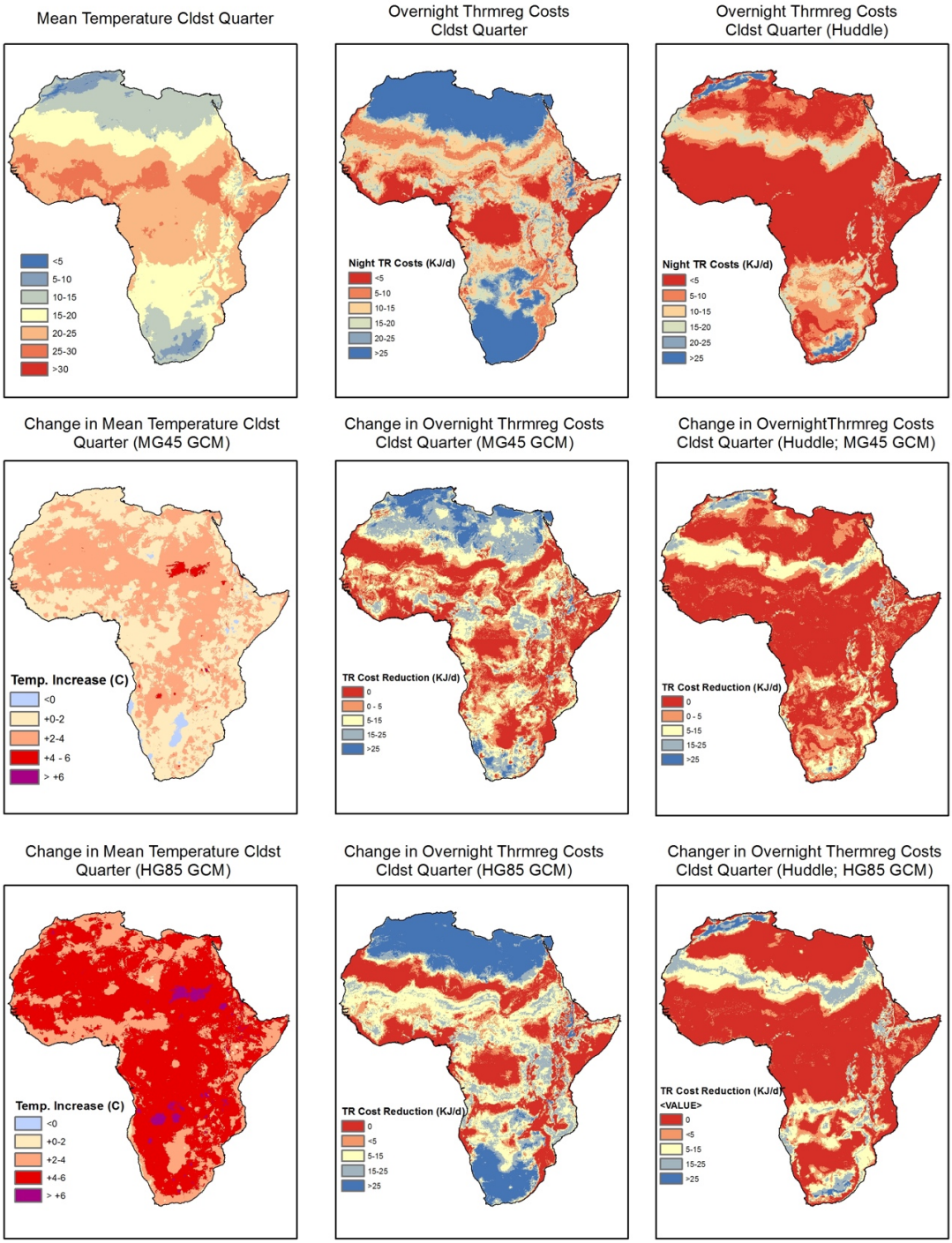


**Figure S3.** Maps showing mean temperature of the coldest quarter (top left) and overnight thermoregulatory metabolic costs in the coldest quarter with no huddling (top center) or with huddling allowed (top right) under current climate conditions, as well as changes in these values under a moderate 2070 climate scenario (middle row) and hot/dry 2017 climate scenario.

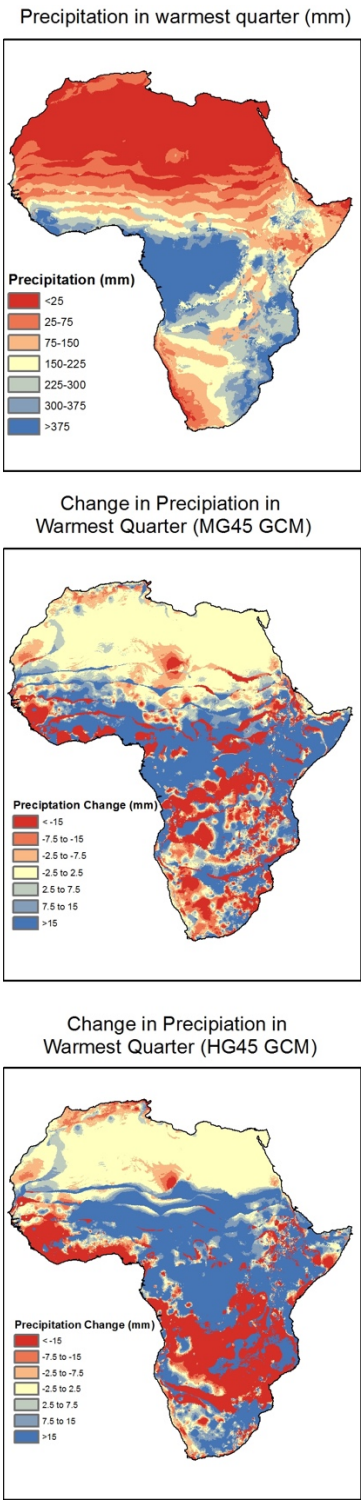


**Figure S4.** Maps showing total precipitation in the warmest quarter under current climate condition (top), as well as changes in these values under a moderate 2070 climate scenario (middle) and hot/dry 2017 climate scenario (bottom).

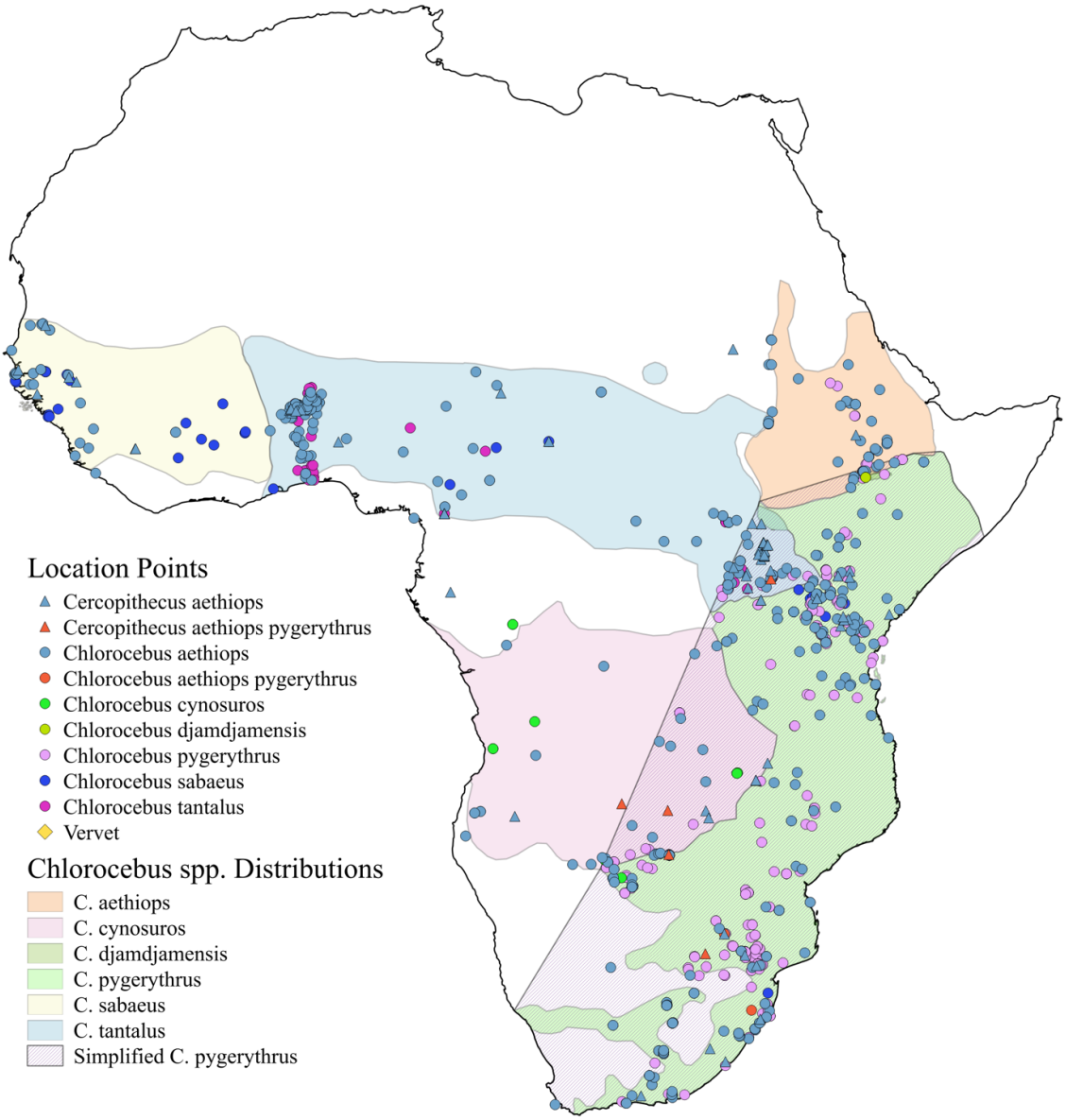


**Figure S5.** Map of potential *Cercopithecus aethiops* and *Chlorocebus* spp. locations obtained from GBIF or published studies. Locations are divided into the scientific name attributed to the monkey in the location record or study. Also shown are the IUCN distribution ranges for the seven currently-accepted *Chlorocebus* species. We simplified the distribution of *Chlorocebus pygerythrus* to capture the most potential locations of the vervet monkey (*Chlorocebus pygerythrus*). See text for additional information on this taxonomic uncertainty.

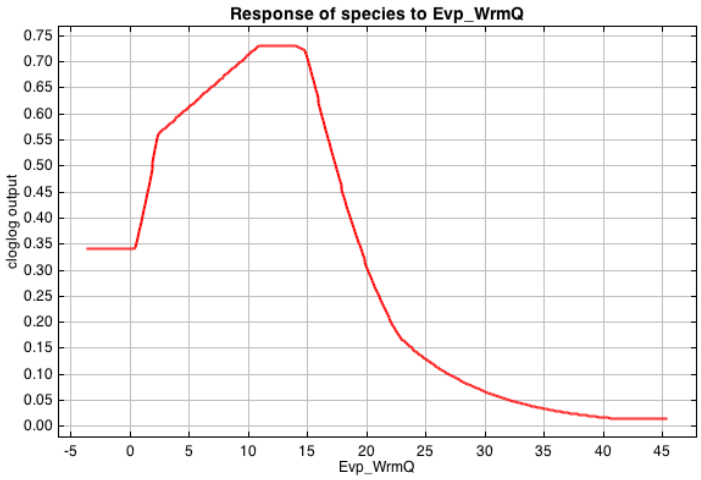


**(a)**

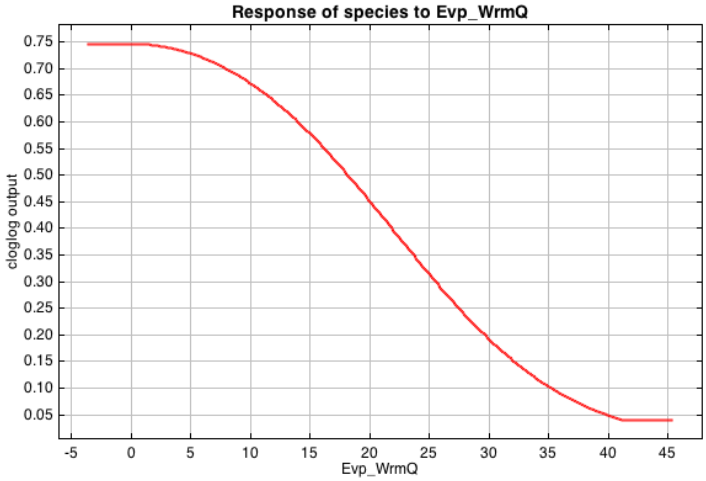


**(b)**

**Figure S6.** Maxent response curves for vervet habitat suitability as a function of sweating costs predicted by Niche Mapper in the warmest quarter using hinge features (a) or quadratic features (b). We have the expectation that habitat suitability should only decrease as sweating costs increase; thus the hinge features produce illogical results. Hinge features produce similarly illogical responses to nighttime thermoregulatory costs in response cold stress (curves not shown).

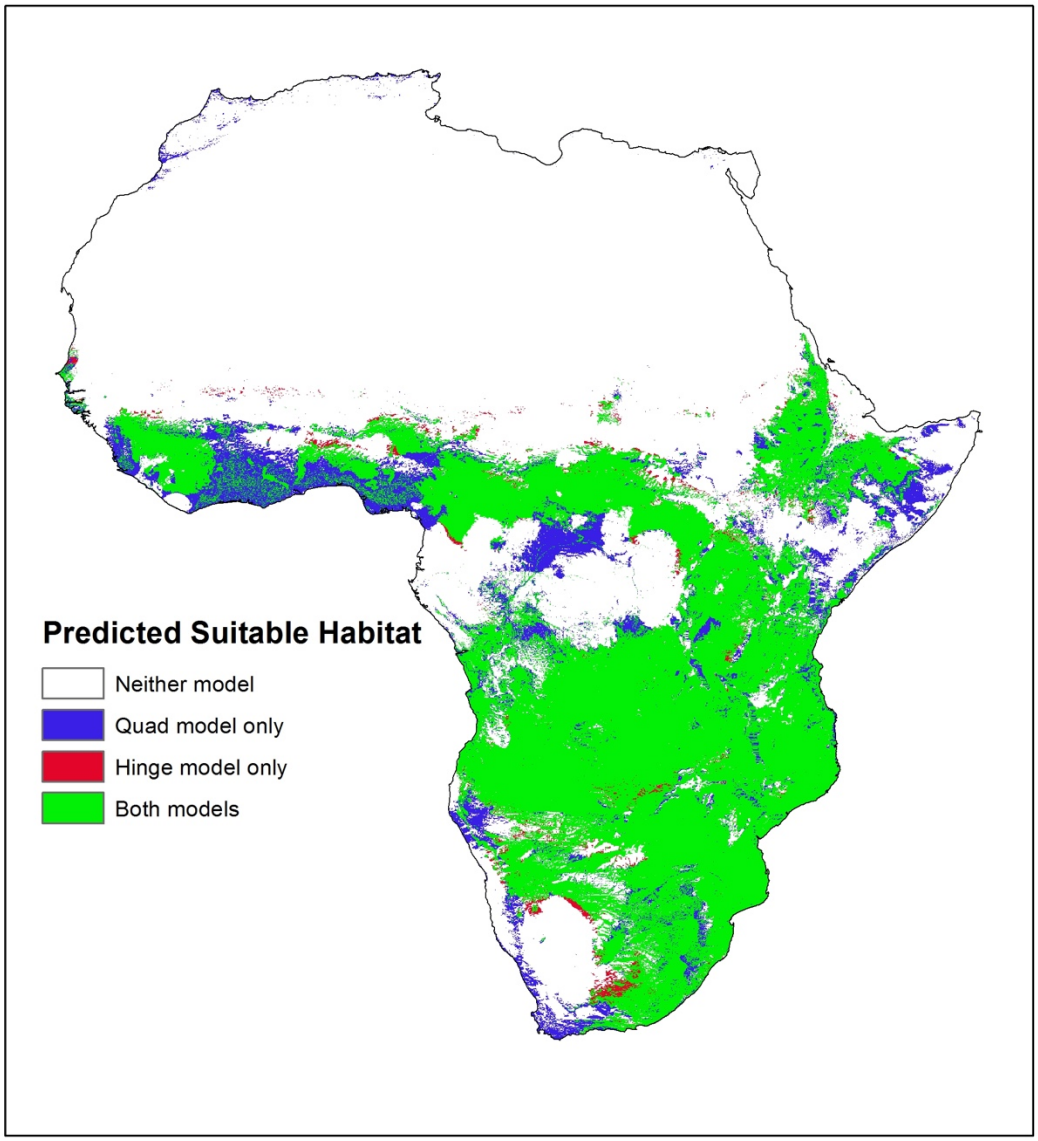


**Figure S7.** Comparison of predicted suitable climate space under current climate conditions by the hybrid model using either hinge features or quadratic features to create response curves. As shown, the predicted suitable climate space is largely similar, agreeing on suitability for over 92% of mainland Africa.

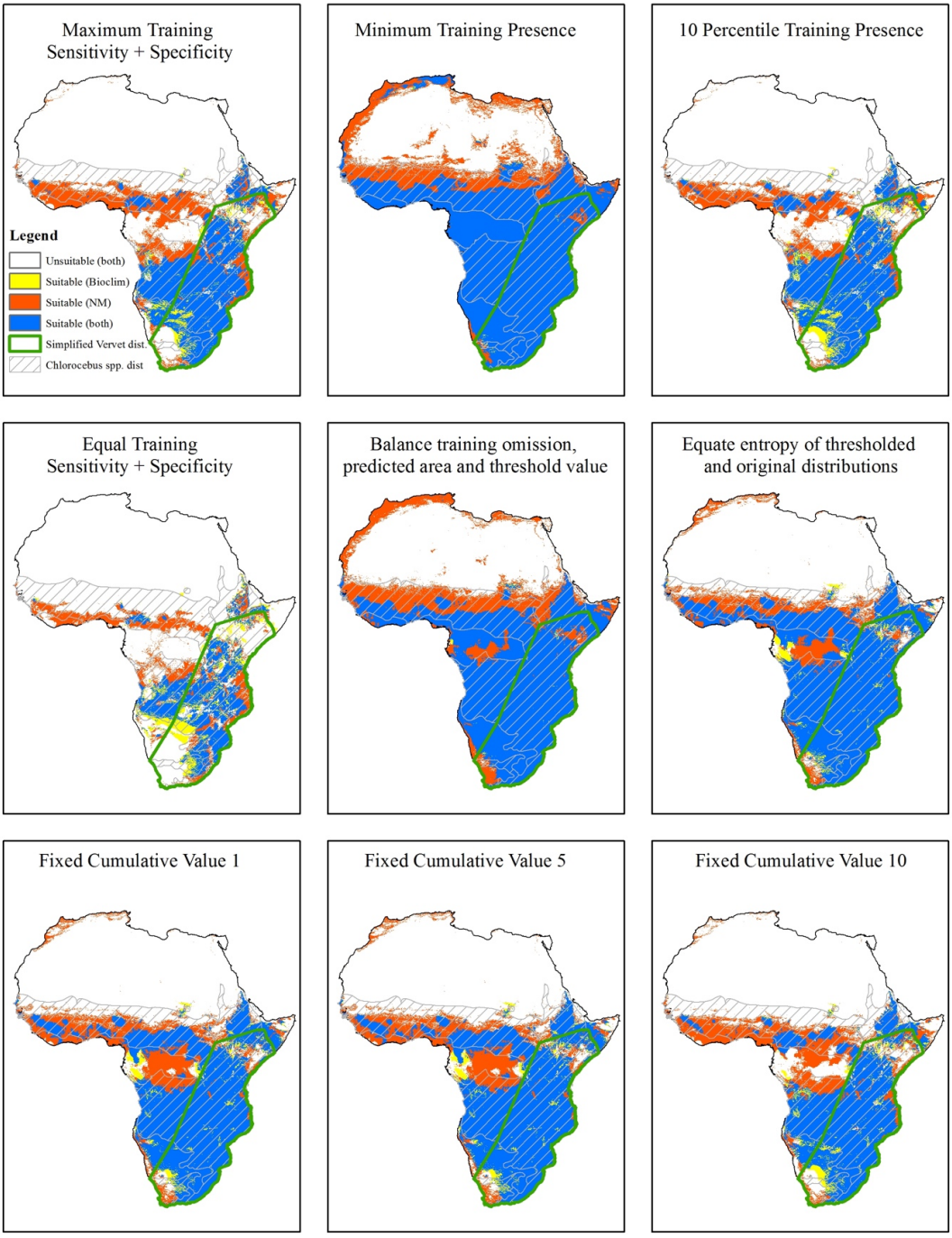


**Figure S8.** Comparison of predicted suitable climate space under current climate conditions using different thresholds from Maxent. The pattern of the NM model predicting more suitable climate space across sub-Saharan West Africa holds regardless of the threshold chosen.

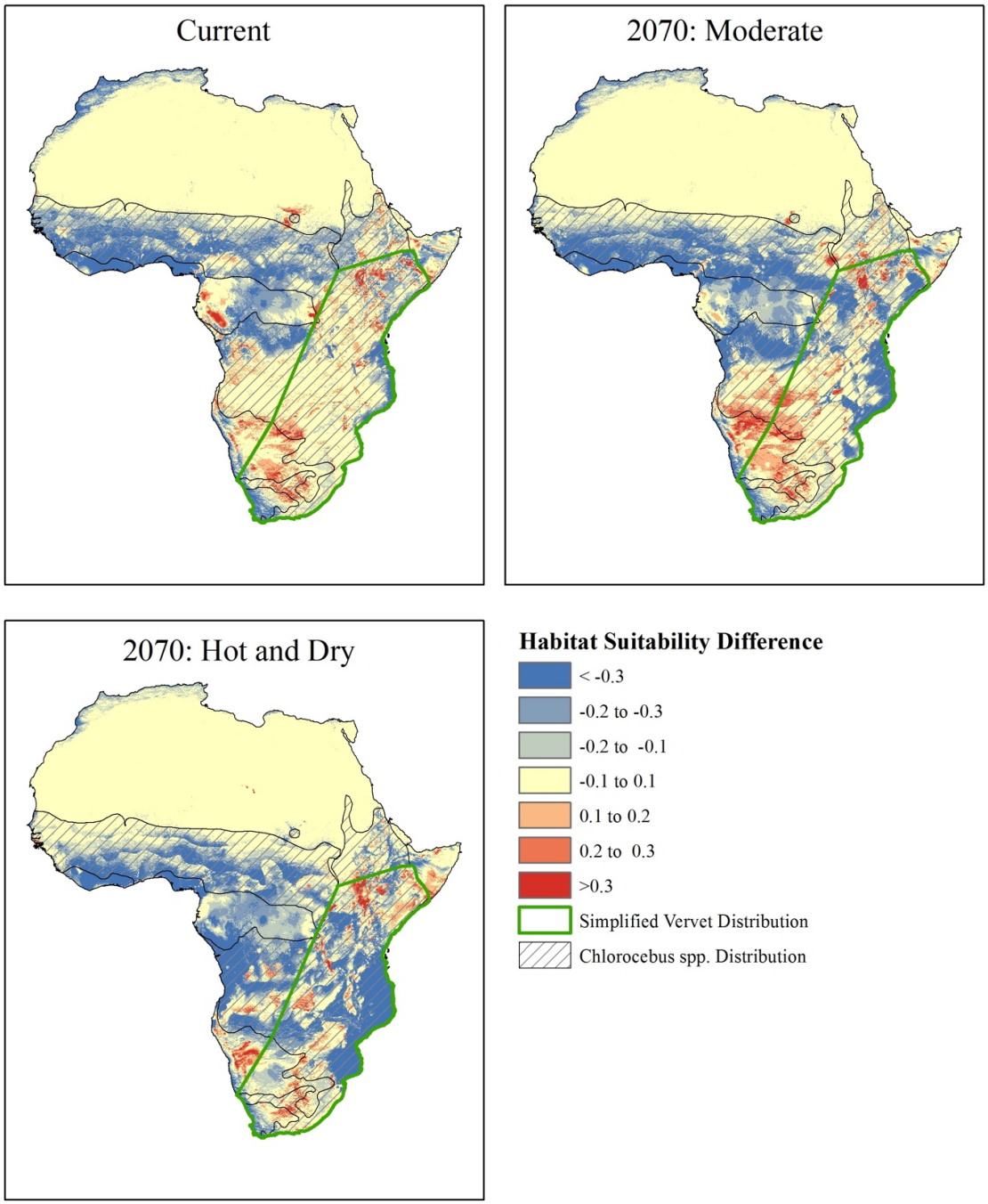


**Figure S9** Difference in habitat suitability between the BioClim and NM models. Negative values indicate the NM model predicts a higher habitat suitability; positive values indicate that the BioClim model predicts a higher habitat suitability. Under the current climate conditions, the predictions differed most notably in the West African portion of the *Chlorocebus* spp. distribution. Under the hot and dry future climate conditions, the NM model starts to predict notably greater habitat suitability within the current vervet distribution.

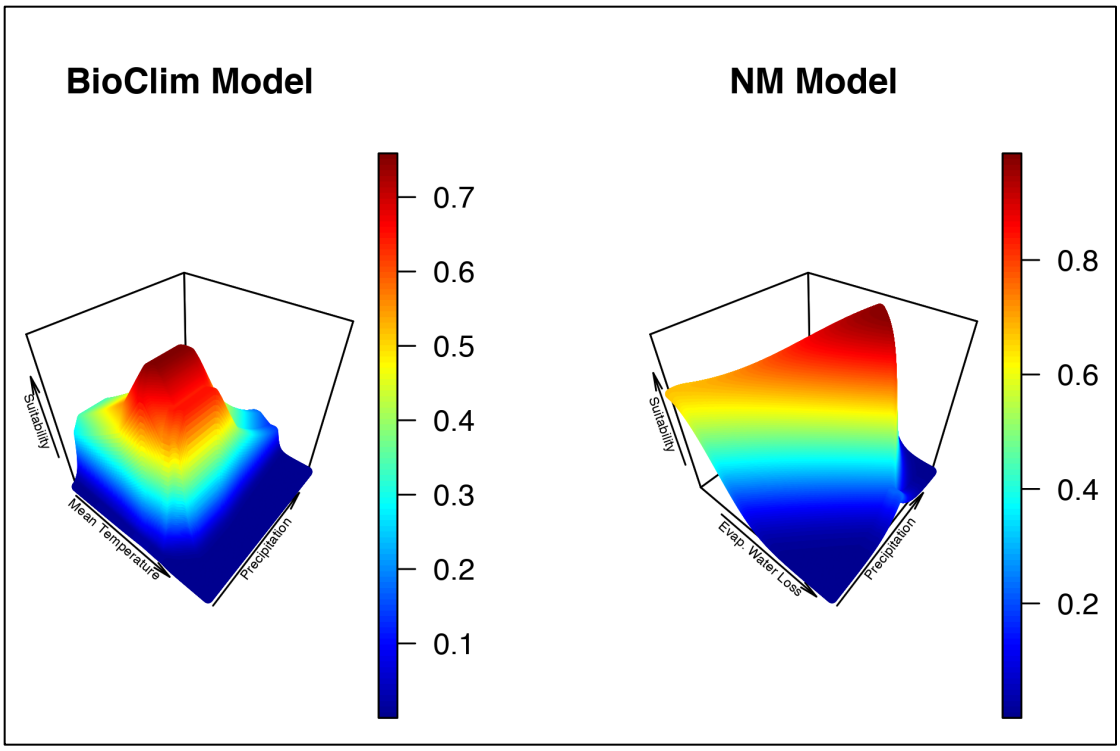


**Figure S10**. Plots showing the combined effect of precipitation and mean temperature of the warmest quarter (BioClim model) or precipitation and predicted evaporative water loss in the warmest quarter (NM model) on habitat suitability predicted by Maxent. Arrow directions indicate increasing values. Note the interaction between precipitation and predicted evaporative water loss: increased precipitation is required to maintain suitability as predicted evaporative water loss rates increase. The interaction is only present at moderate values in the BioClim model.

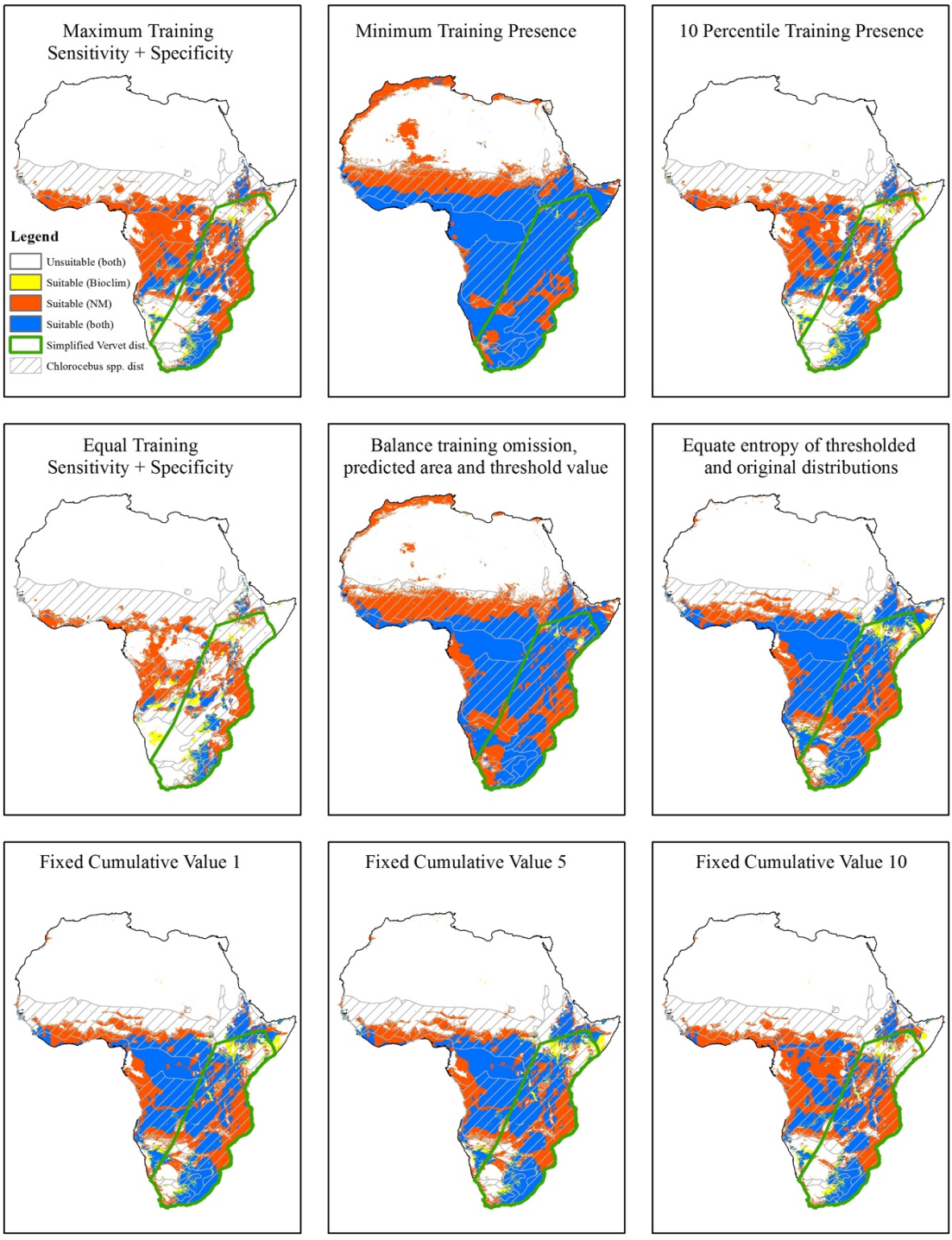


**Figure S11.** Comparison of predicted suitable climate space under 2070 HG85 conditions using different thresholds from Maxent. The pattern of the NM model predicting less suitable climate space loss both within the vervet distribution and within the *Chlorocebus* spp. distribution holds regardless of the threshold chosen.

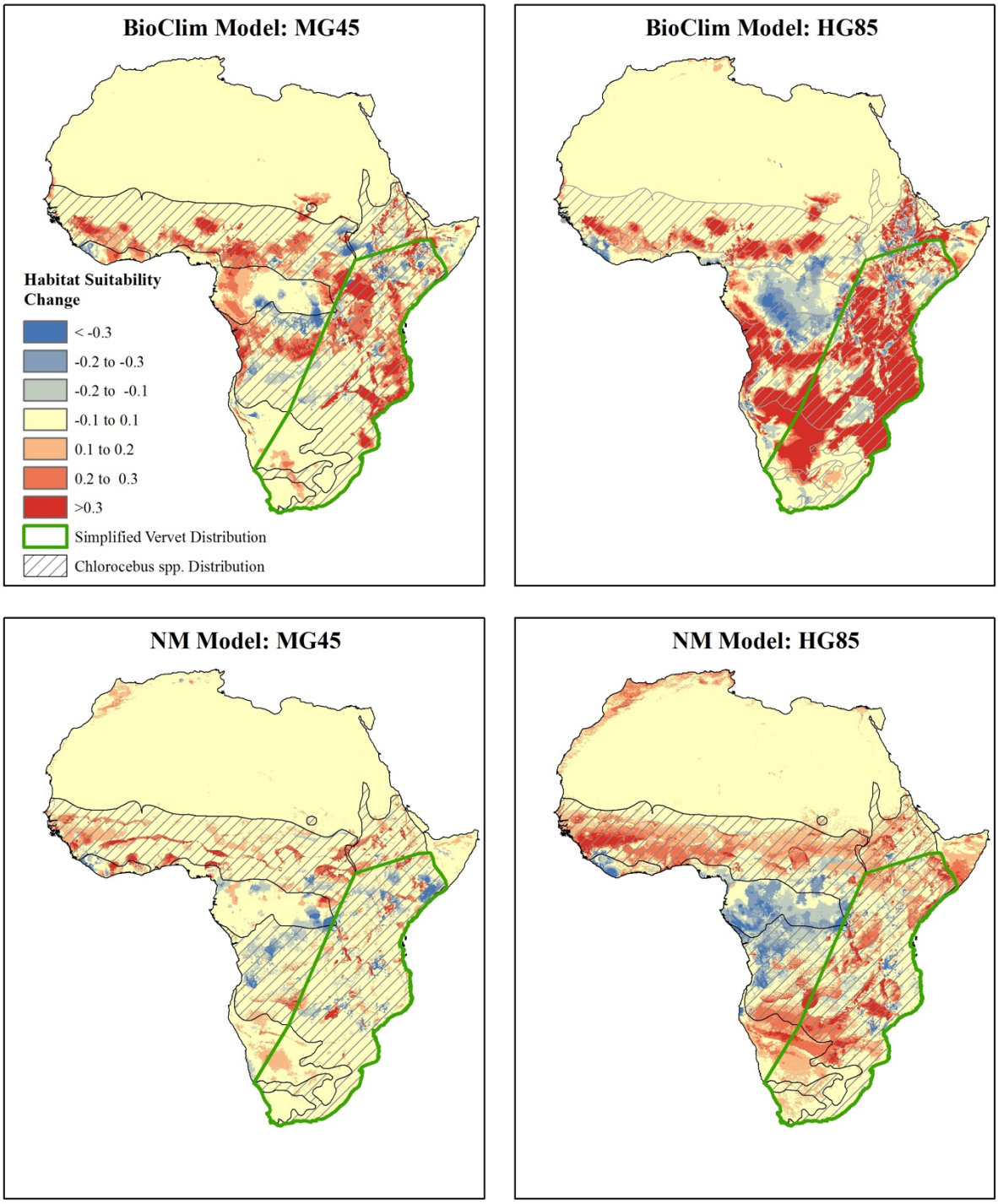


**Figure S12.** Predicted change in habitat suitability between current and moderate (MG45) and hot/dry (HG85) 2070 climate scenarios for the BioClim and NM models. The NM model predicts smaller reductions in habitat suitability both within the current vervet distribution

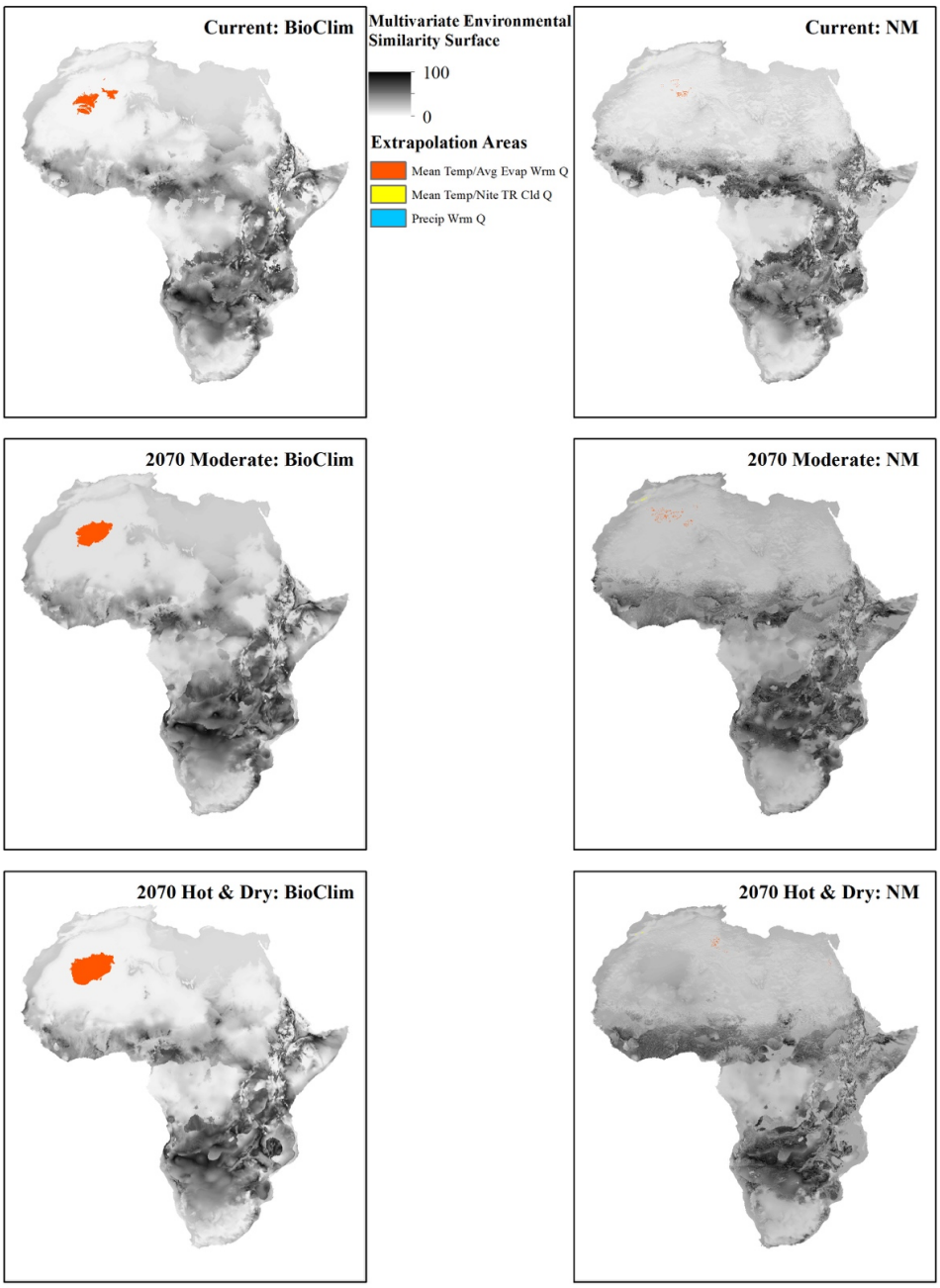


**Figure S13**. Multivariate Environment Similarity Surfaces (MESS), as described in Elith et al. (2010), showing how similar the climate conditions in each raster cell in the study area are to the values used in the model training (i.e., the values at the presence and background points). A score of 100 means that all environmental variables are at the median value from the training range; a score of 0 means that at least one variable is at the edge of the training range. Negative values (masked here in red, yellow, and blue), indicate locations where at least one variable is outside of the training range meaning that the model must extrapolate

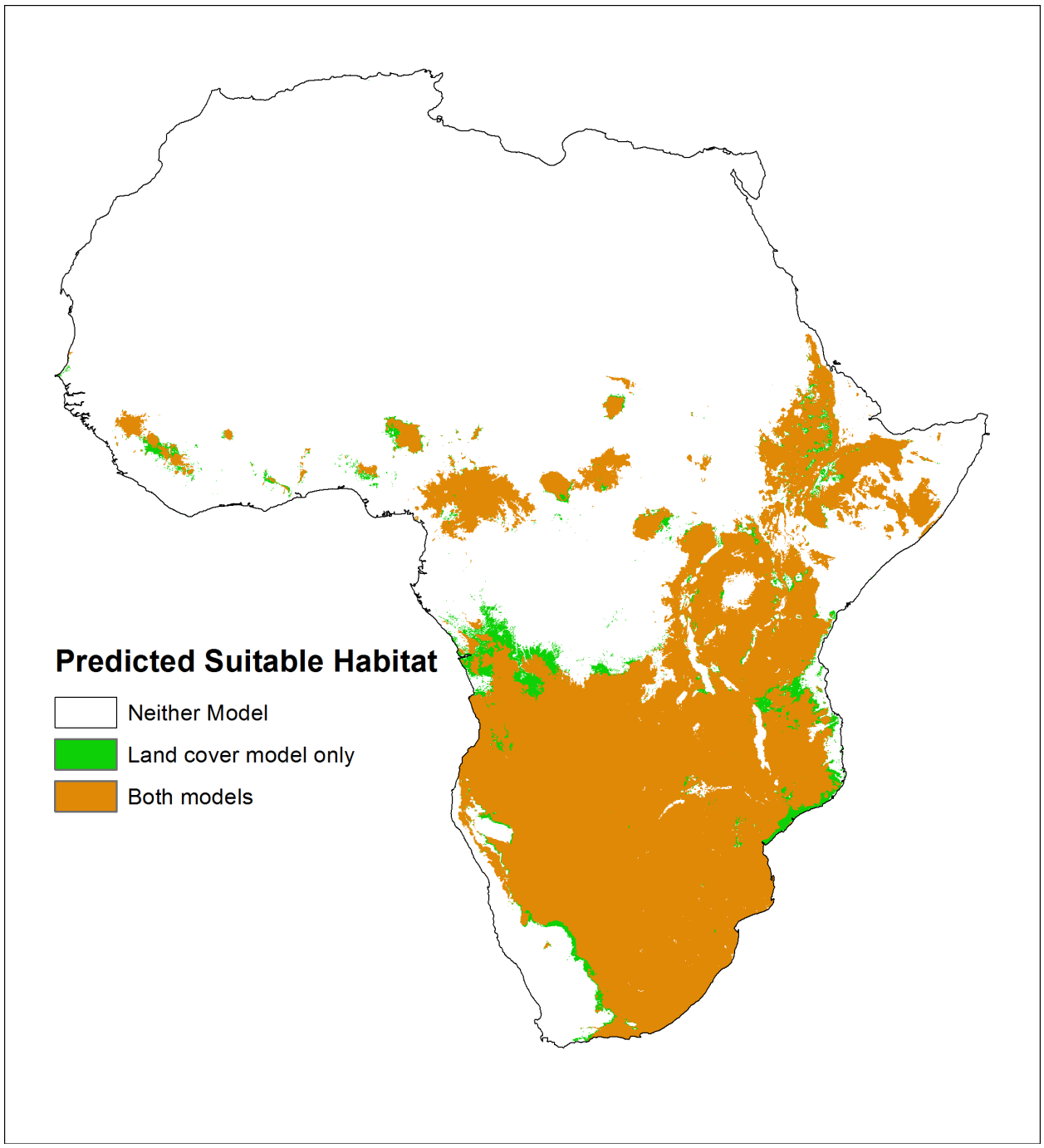


**Figure S14.** Comparison of predicted suitable climate space under current climate conditions by the BioClim model using land cover as an input and the BioClim model not using landcover as an input. As shown, the predicted suitable climate space is largely similar between the two models, with the models agreeing on over 98% of mainland Africa.

**Table S2.** Average temperature (°C; mean, minimum and maximum temperatures) and precipitation (%) change across mainland Africa between current climate conditions (1970-2000; WorldClim v2.0) and 2070 climate predictions from global circulation models available from WorldClim v1.4. For each temperature variable, the five GCMs predicting the smallest and largest increases from current temperatures are highlighted in blue and red, respectively. For the precipitation variables, the five GCMs predicting the greatest increase and largest decreases in precipitation from current precipitation are highlighted in blue and red, respectively. MIROC-ESM RCP 4.5) was identified as most consistently predicting the coolest and wettest future conditions, while HadGEM2-ES (RCP 8.5) was identified as most consistently predicting the warmest and driest future conditions

| GCM | RCP | $T_{mean}$, annual | $T_{max}$, warmest month | $T_{min}$, coldest month | $T_{mean}$, warmest quarter | $T_{mean}$ coldest quarter | Ppt, annual | Ppt, driest quarter | Ppt, warmest quarter |
|---|---|---|---|---|---|---|---|---|---|
| ACCESS1-0 | 4.5 | 2.6 | 3.1 | 2.2 | 2.6 | 2.5 | -1% | -7% | 15% |
| BCC-CSM1-1 | 4.5 | 1.9 | 2.4 | 1.7 | 1.9 | 2.0 | 4% | -14% | 17% |
| CCSM4 | 4.5 | 1.8 | 2.4 | 1.5 | 1.9 | 1.8 | 7% | 0% | 15% |
| CNRM-CM5 | 4.5 | 1.9 | 2.3 | 1.7 | 2.0 | 1.7 | 6% | 1% | 15% |
| GFDL-CM3 | 4.5 | 2.8 | 3.7 | 2.4 | 3.0 | 2.8 | 6% | -6% | 32% |
| GISS-E2-R | 4.5 | 2.0 | 2.5 | 1.5 | 2.1 | 1.9 | -9% | -10% | 10% |
| HadGEM2-AO | 4.5 | 2.7 | 3.0 | 2.2 | 2.7 | 2.6 | 1% | -18% | 11% |
| HadGEM2-CC | 4.5 | 2.8 | 3.4 | 2.5 | 2.9 | 2.7 | 1% | -16% | 12% |
| HadGEM2-ES | 4.5 | 2.7 | 3.4 | 2.4 | 2.8 | 2.6 | -4% | -18% | 4% |
| INMCM4 | 4.5 | 1.3 | 1.7 | 0.9 | 1.4 | 1.3 | -1% | -6% | 7% |
| IPSL-CM5A-LR | 4.5 | 2.8 | 3.1 | 2.7 | 3.0 | 2.5 | 27% | 4% | 52% |
| MIROC-ESM-CHEM | 4.5 | 2.0 | 2.8 | 1.5 | 2.1 | 1.9 | -2% | -9% | 5% |
| MIROC-ESM | 4.5 | 1.7 | 2.3 | 1.5 | 1.8 | 1.6 | 12% | -6% | 28% |
| MIROC5 | 4.5 | 2.5 | 3.6 | 2.0 | 2.9 | 2.4 | 8% | 3% | 15% |

| | | | | | | | | | |
|---|---|---|---|---|---|---|---|---|---|
| MPI-ESM-LR | 4.5 | 2.5 | 2.9 | 2.2 | 2.6 | 2.4 | 6% | -6% | 21% |
| MRI-CGCM3 | 4.5 | 2.5 | 3.3 | 2.0 | 2.8 | 2.4 | 6% | -4% | 13% |
| NorESM1-M | 4.5 | 1.7 | 2.3 | 1.3 | 1.8 | 1.6 | 1% | -5% | 7% |
| ACCESS1-0 | 8.5 | 3.9 | 4.4 | 3.6 | 3.9 | 3.8 | 1% | -12% | 12% |
| BCC-CSM1-1 | 8.5 | 3.2 | 3.6 | 3.1 | 3.1 | 3.3 | 7% | -12% | 20% |
| CCSM4 | 8.5 | 3.1 | 3.7 | 2.8 | 3.3 | 3.0 | 7% | 0% | 13% |
| CNRM-CM5 | 8.5 | 2.8 | 3.2 | 2.7 | 3.1 | 2.7 | 7% | -6% | 19% |
| GFDL-CM3 | 8.5 | 4.0 | 5.4 | 3.6 | 4.4 | 3.9 | 5% | -10% | 30% |
| GISS-E2-R | 8.5 | 3.0 | 3.5 | 2.3 | 3.0 | 2.9 | -14% | -16% | 5% |
| HadGEM2-AO | 8.5 | 3.8 | 4.2 | 3.2 | 3.8 | 3.6 | -8% | -18% | 4% |
| HadGEM2-CC | 8.5 | 4.3 | 5.1 | 4.0 | 4.4 | 4.2 | -1% | -23% | 13% |
| HadGEM2-ES | 8.5 | 4.3 | 5.1 | 3.8 | 4.4 | 4.1 | -3% | -24% | 15% |
| INMCM4 | 8.5 | 2.3 | 2.6 | 2.6 | 2.5 | 2.4 | 7% | -6% | 12% |
| IPSL-CM5A-LR | 8.5 | 4.3 | 4.6 | 4.0 | 4.7 | 3.9 | 39% | 10% | 52% |
| MIROC-ESM-CHEM | 8.5 | 3.0 | 3.8 | 2.6 | 3.2 | 3.0 | -1% | -18% | 4% |
| MIROC-ESM | 8.5 | 2.9 | 3.5 | 2.6 | 3.0 | 3.0 | 7% | -12% | 16% |
| MIROC5 | 8.5 | 3.6 | 4.6 | 3.0 | 4.1 | 3.3 | 6% | 1% | 8% |
| MPI-ESM-LR | 8.5 | 3.8 | 4.2 | 3.5 | 4.0 | 3.6 | 8% | -8% | 30% |
| MRI-CGCM3 | 8.5 | 3.4 | 4.1 | 3.0 | 3.6 | 3.4 | 9% | 3% | 23% |
| NorESM1-M | 8.5 | 2.8 | 3.6 | 2.4 | 3.0 | 2.7 | 1% | -9% | 9% |

**Table S2**. Published studies reporting locations for "vervet monkeys" or "vervets." Also shown is the scientific name the animals were referred to as in the papers and the country of the study location.

| **Study** | **Species name listed in study** | **Country** |
|---|---|---|
| Willems & Hill 2009 | *Cercopithecus aethiops* | Various |
| Danzy et al. 2012 | *Chlorocebus aethiops* | South Africa |
| Coleman & Hill 2014 | *Chlorocebus aethiops pygerythrus* | South Africa |
| Arsenau et al 2015 | *Chlorocebus aethiops pygerythrus* | South Africa |
| McDougall et al. 2010 | *Chlorocebus aethiops* | South Africa |
| Makin et al. 2012 | *Chlorocebus aethiops* | South Africa |
| Barrett et al. 2016 | *Chlorocebus pygerythrus* | South Africa |
| Barrett et al. 2006 | *Cercopithecus aethiops pygerythrus* | South Africa |
| Castelda et al. 2011 | *Cercopithecus aethiops* | Tanzania |
| Tweheyo et al 2012 | *Cercopithecus aethiops* | Uganda |
| Jaffe & Isbell 2010 | *Cercopithecus aethiops* | Kenya |
| Ogutu et al. 2017 | *Vervet monkey* | Kenya |
| Lee & Teichroeb 2016 | *Chlorocebus pygerythrus* | Uganda |
| Muoria et al. 2003 | *Cercopithecus aethiops* | Kenya |
| Isbell & Etting 2016 | *Chlorocebus pygerythrus* | Kenya |
| Saj et al. 2001 | *Cercopithecus aethiops pygerythrus* | Uganda |
| Tembo 1994 | *Cercopithecus aethiops pygerythrus* | Zambia |
| Hayward et al. 2005 | *Cercopithecus aethiops* | South Africa |
| Lee & Hauser 1998 | *Cercopithecus aethiops* | Kenya |
| Gaetano et al. 2014 | *Chlorocebus aethiops* | South Africa |
| Cardini et al. 2013 | *Chlorocebus aethiops* | Various |

*References*

Arseneau TJM, Taucher A, van Schaik CP, Willems EP. 2015. Males fight in between-group conflicts as protective parents or reluctant recruits. Animal Behaviour 110: 39-50

Barrett AS, Barrett L, Henzi P, Brown LR. Resource selection on woody plant species by vervet monkeys (*Chlorocebus pygerythrus*) in mixed-broad leaf savanna. African Journal of Wildlife Research 46: 14-21.

Cardini A, Dunn J, O'Higgins P, Elton S. 2012. Clines in Africa: does size vary in the same way among widespread sub-Saharan mankeys? Journal of Biogeography 40: 370-381.

Castelda SM, Napora ES, Nasseri NA, Vyas DK, Schulte BA. 2011. Diurnal co-occurrence of African elephants and other mammals at a Tanzanian waterhole. African Journal of Ecology 49: 250-252.

Coleman BT, Hill RA. 2014. Living in a landscape of fear: the impact of predation, resource availability and habitat structure on primate range use. Animal Behaviour 88: 165-173.

Danzy J, Grobler JP, Freimer N, Turner TR. 2012. Sunbathing: a behavioral response to seasonal climatic change among South African vervet monkeys (*Chlorocebus aethiops*). African Primates 7: 230-237.

Gaetano TJ, Danzy J, Mtshali MS, Theron N, Schmitt CA, Grobler JP, Freimer N, Turner TR. 2014. Mapping correlates of parasitism in wild South African vervet monkeys (*Chlorocebus aethiops*). South African Journal of Wildlife Research 44: 56-70.

Hayward MW, White RM, Mabandla KM, Bukeye P. 2005. Mammalian fauna of indigenous forest in the Transkei region of South Africa: an overdue survey. South African Journal of Wildlife Research 35: 117-124.

Isbell LA, Etting SF. 2017. Scales drive detection, attention, and memory of snakes in wild vervet monkeys (*Chlorocebus pygerythrus*). Primates 58: 121-129.

Jaffe KE, Isbell LA. 2010. Changes in ranging and agnostic behavior of vervet monkeys (*Cercopithecus aethiops*) after predator-induced group fusion. American Journal of Primatology 72: 634-*644.*

Lee PC, Hauser MD. 1998. Long-term consequences of changes in territory quality on feeding and reproductive strategies of vervet monkeys. Journal of Animal Ecology 67: 347-358.

Lee HC, Teichroeb JA. 2016. Partially shared consensus decision making and distributed leadership in vervet monkeys: older females lead the group to forage. American Journal of Anthropology 161: 580-590.

Makin D, Payne HFP, Kerley GIH, Shrader A. 2012. Foraging in a 3-D world: how does predation risk affect space use of vervet monkeys? Journal of Mammalogy 93: 422-428.

McDougall P, Forshaw N, Barrett L, Henzi SP. 2010. Leaving home: responses to water depletion by vervet monkeys. Journal of Arid Environments 74: 924-927.

Muoria PK, Karere GM, Moinde NN, Suleman MA. 2003. Primate census and habitat evaluation I the Tana delta region, Kenya. African Journal of Ecology 41: 157-163.

Ogutu JO, Kuloba B, Piepho H-P, Kanga E. 2017. Wildlife population dynamics in human-dominated landscapes under community-based conservation: the example of Nakuru Wildlife Conservancy, Kenya. PLoS ONE 12: e0169730.

Saj TL, Sicotte P, Paterson JD. 2001. The conflict between vervet monkeys and farmers at the forest edge in Entebbe, Uganda. African Journal of Ecology 39: 195-199.

Tembo A. 1994. Population characteristics of the vervet monkey in the Mosi-Oa-Tunya National Park, Zambia. African Journal of Ecology 32: 72-74.

Tweheyo M, Tumusiime DM, Turyahabwe N, Asiimwe A, Orikiriza L. 2012. Wildlife damage and control methods around Lake Mburo National Park, Uganda. International Journal of Pest Management 58: 25-31.

Willems WP, Hill RA. 2009. A critical assessment of two species distribution models a case study of the vervet monkey (*Cercopithecus aethiops*). Journal of Biography 36: 2300-2312.

# CHAPTER 4: EXPERIMENTAL AND MODELLED THERMOREGULATORY COSTS OF REPEATED SUBLETHAL OIL EXPOSURE IN THE DOUBLE-CRESTED CORMORANT, *PHALACROCORAX AURITUS*.

*Citation:* Mathewson PD, Hanson-Dorr KC, Porter WP, et al. 2018. Experimental and modeled thermoregulatory costs of repeated sublethal oil exposure in the Double-crested Cormorant, *Phalacrocorax auritus*. Marine Pollution Bulletin 135: 216-223.

## ABSTRACT

To fully understand the impact of oil exposure, it is important to understand sublethal effects like how increased thermoregulatory costs may affect survival and reproduction. However, it is difficult and time-consuming to measure these effects in wild animals**.** We present a novel use of a bioenergetics model, Niche Mapper™, to estimate thermoregulatory impacts of oiling, using data from captive Double-crested Cormorants (*Phalacrocorax auritus*) experimentally exposed to oil. Oiled cormorants had significant increases in surface body temperatures following exposure. Niche Mapper accurately predicted surface temperatures and metabolic rates for unoiled and oiled cormorants and predicted 13-18% increased daily energetic demands due to increased thermoregulatory costs of oiling, consistent with increased food consumption observed in experimentally oiled cormorants. We show that Niche Mapper can provide valuable insight into sublethal oiling effects by quantifying the extent to which thermoregulatory costs divert energy resources away from important life processes like maintenance, reproduction and migration.

## INTRODUCTION

The threat of oil pollution to marine birds is well-documented (e.g., Votier et al., 2005), and can affect marine birds indirectly (e.g., killing or contaminating food sources) or directly. The direct effects of oil exposure stem from the toxicity of ingested oil and adverse effects of plumage oiling, the latter being the focus of this work. Oil exposure compromises the integrity of a bird's feather microstructure by collapsing the interlocking structure of feather elements. This results in feathers matting together, causing the insulative air layer in the plumage to be displaced and a loss of waterproofing (O'Hara & Morandin, 2010). This, in turn, affects the thermal balance of oil-exposed birds that can require additional energetic expenditures to maintain homeothermy.

Experimental studies have documented increased metabolic heat production in response to oiling in several avian species (Table S1). The magnitude of increased heat production is dependent on dosage, environmental temperature, exposure to water, and differences in plumage types among species. At one extreme, heavily oiled birds in cold aquatic environments can die of hypothermia or starvation if unable to feed enough to offset increased energetic requirements (e.g., Oka & Okuyama, 2000). For birds in milder environments or that are less-heavily oiled, the increased energy expenditures following oiling may not be lethal but may still affect fitness by diverting resources away from maintenance, growth, and reproduction.

While large, catastrophic spills that cause immediate mass mortalities garner much of the media and scientific attention, there is growing recognition of the need to better understand the effect of exposure to chronic (low volume) oil discharges (Wiese & Robertson, 2004; Henkel et al., 2014; Fraser & Racine, 2016). A majority of anthropogenic oil pollution comes from chronic discharges from sources like the offshore oil and gas industry, shipping vessels and non-point

runoff from land-based activities (O'Hara & Morandin, 2010; Henkel et al., 2014). Chronic exposure can cause mortality in some locations (e.g., Wiese & Ryan, 2003), but there are also likely more widespread sublethal effects of such exposures.

To date we are unaware of attempts to model repeated sublethal oil exposure and predict the effects due to increased thermoregulatory costs. Here we present a novel use of a bioenergetics model, Niche Mapper™, to predict the thermoregulatory effect of oil exposure on the double-crested cormorant (*Phalacrocorax auritus*; hereafter cormorant), a large, diving waterbird often impacted by oil spills (Dorr et al., 2014). We develop an "oiled' cormorant model by modifying the inputs used by Niche Mapper to calculate body insulation to simulate oil introduced into the plumage. We then test Niche Mapper's ability to accurately model thermoregulation in oiled and unoiled cormorants by comparing predicted surface temperatures and energy expenditures to those measured in captive cormorants experimentally exposed to oil. Mechanistically modelling the thermoregulatory effects of oil exposure allows for simulations of wild animals' energetics to gain a more complete understanding of the effects of oil pollution on wildlife.

## METHODS

### *Summary of Live Cormorant Experiments*

As part of the Natural Resource Damage Assessment performed in response to the 2010 Deepwater Horizon (DWH) oil spill in the Gulf of Mexico, wild cormorants were captured from Mississippi and Alabama, USA, and transported to captive facilities at the National Wildlife Research Center, Mississippi Field Station (Bursian et al., 2017). The focus of the present work is developing modeling techniques and so we summarize the live bird experiments to provide context. For a detailed description of procedures see Cunningham et al. (2017).

All cormorants were individually housed in 1.5x1.5x1.8 m cages containing 190-liter plastic water tanks that were refilled daily. Cormorants were offered 600g of live channel catfish (*Ictalurus punctatus*) daily. All birds had an Advanced Telemetry Systems (ATS, Isanti, MN USA) F1815T very high frequency temperature transmitter surgically implanted in the coelom prior to study initiation to monitor internal body temperature daily (see Scherr 2009 for details). Cormorants were allowed to acclimate to captivity and recover from surgery for a minimum of 21 days prior to initiation of the oiling study.

Twenty-five cormorants were assigned to control (n=12) or oiled (n=13) treatment groups. Seven cormorants had evidence of preexisting illness based on monocyte counts and were assigned randomly between the control and oiled groups (4 and 3 birds, respectively). During the course of the trial, one bird from the control group (day 1) and two birds from the oiled group (day 15 and 19) died (Cunningham et al., 2017).

Cormorants in the oiled group were exposed to artificially weathered DWH oil by applying approximately 6.5 g of oil to both the breast and back by brush. The oil was applied across an area accounting for 20% of the total body surface area excluding wings and tail; subsequent preening by the birds further spread the oil. Cormorants in the control group received the same treatment except that oil was replaced with water. Oil or water was applied to the birds every three days through day 16 of the trial (Table S2). Body weight was measured every three days for the duration of the trial and at necropsy.

External body temperature of all cormorants was taken with a handheld scanning thermograph camera (FLIR®) three days prior to day 1 oiling, and every six days thereafter (Table S2). Birds were taken from their cage to an adjacent room where they were held at a standard distance and position for each photo to ensure reproducibility. Temperatures for

different body parts were extracted using FLIR® ThermaCAM 342 Researcher Pro 2.7 software. Food intake was calculated based on daily consumption of fish. Visual bird health checks were conducted twice daily (Cunningham et al., 2017).

*Niche Mapper Description*

Niche Mapper (Porter & Mitchell, 2006) is a bioenergetics model that has been previously shown to accurately predict energetic requirements as a function of environmental conditions and animal morphological and physiological properties for a wide variety of animals, including several waterbirds: cormorants (*Phalacrocorax* sp.), Brünnich's guillemots (*Ura lomvia*;), and little auks (*Alle alle*) (Fort et al., 2009, 2011; Göktepe et al., 2012). Niche Mapper consists of two submodels: a microclimate model and an animal model. The microclimate model uses macroclimate data (maximum and minimum daily air temperatures, cloud cover, wind speed, relative humidity), substrate properties, geographic location, and time of year to calculate hourly environmental conditions at the animal's height (see Fuentes & Porter, 2013 for details).

The animal model then uses the hourly outputs from the microclimate model and animal properties to iteratively solve a heat balance equation to find the metabolic rate needed for the animal to maintain its body temperature, accounting for convective, radiative, evaporative, conductive and solar heat fluxes with its microenvironment (see supplemental materials and Mathewson & Porter, 2013 for details). Most relevant to this work, Niche Mapper calculates animal surface temperatures based on core temperature, physical dimensions, and insulation of the body part in order to compute heat flux with the environment. Thus, the model allows us to explore how altered insulation (e.g., in response to oiling) affects surface temperatures and, ultimately, heat loss to the environment.

We updated the cormorant model used by Göktepe et al. (2012) to a multipart model with truncated cones for the beak and head, cylinders for the neck and legs, and an ellipsoid for the torso (Fig. S1). During diurnal and crepuscular hours, all body parts were exposed to the environment. During nocturnal hours, we assumed no heat loss for the head (tucked under wings) and 30% of the neck (in contact with torso) to simulate birds in a sleeping posture. Key animal model inputs are summarized in Table 1, and the following physiological thermoregulatory options were allowed: vasodilation and vasoconstriction, increasing body temperature, ptiloerection, and gular fluttering. Leg and beak body temperatures were allowed to drop below body temperatures for other body parts to simulate counter-current exchange mechanisms (Fitzpatrick et al., 2015). See supporting information for additional information on Niche Mapper operation.

*Niche Mapper Metabolic Chamber Simulations*

We first evaluated the unoiled cormorant model with a metabolic chamber simulation to compare predicted metabolic rates as a function of air temperature to those reported by Enstipp et al. (2006, 2008). In this simulation, all environmental temperatures (air, ground, and sky) were set to the same value and increased incrementally. We assumed no solar radiation, 5% relative humidity, and wind speeds of 0.1 or 1.0 m/s to account for uncertainty regarding the velocity of the airflow in the experimental metabolic chambers.

We also compared Niche Mapper heat production predictions for cormorants resting on the water surface to those measured by Enstipp et al. (2006) in a metabolic chamber. We simulated cormorants as having their legs fully submerged and 50-90% of their torso submerged. Double-crested cormorant plumage is partially wettable (Mahoney 1984). Based on studies by Enstipp et al. (2006) and Grémillet et al. (1998, 2005) on shallowly-submerged Double-crested Cormorant

and Great Cormorant (*Phalacrocorax carbo*) carcasses respectively, we assumed water penetration reduced the effective 'dry' insulation layer thickness in the model to 2 mm.

**Table 1.** Key cormorant model inputs for Niche Mapper.

| **Parameter** | **Value** | **Source** |
|---|---|---|
| Body temperature (°C) | 40-43 | Enstipp et al., 2006, 2008; this study. |
| Resting metabolic rate (W/kg) | 4.59 | Enstipp et al., 2006 |
| Plumage depth: head (dorsal/ventral; mm) | 2.8/2.8 | This study; measured on a male specimen from the UW Madison Zoology Museum |
| Plumage depth: neck (dorsal/ventral; mm) | 4.5/4.5 | This study; measured on a male specimen from the UW Madison Zoology Museum |
| Plumage depth: torso (dorsal/ventral; mm) | 4.5/14 | This study; measured on a male specimen from the UW Madison Zoology Museum |
| Plumage reflectivity (dorsal/ventral) | 0.134/0.155 | Göktepe et al., 2012 |
| Plumage element diameter (um) | 25 | Göktepe et al., 2012 |
| Plumage element density (# per $cm^2$) | 14,400 | Göktepe et al., 2012 |
| Flesh thermal conductivity (dorsal/ventral; W/mC) | 0.4-2.8 | Cho, 1969 |
| Oxygen extraction efficiency (%) | 34 | Göktepe et al., 2012 |
| Digestive efficiency (%) | 79 | Brugger, 1993 |
| Food % dry matter | 22 | USDA National Nutrient Database (report for raw, farmed, channel catfish) |
| Food dry matter % protein | 65 | USDA National Nutrient Database, correcting for bones accounting for 14% of weight (Martin et al., 2000) |
| Food dry matter % fat | 25 | USDA National Nutrient Database, correcting for bones accounting for 14% of weight (Martin et al., 2000) |
| Food dry matter % carbohydrates | 0.0 | USDA National Nutrient Database |

*Surface Temperature Comparisons*

For each day that FLIR images were taken of the live cormorants, we simulated model birds in a room with the same temperature and relative humidity as the photograph room, assuming negligible wind (0.1 m/s), no solar input, and that ceiling and floor temperatures were the same as air temperature (Table S2). We also simulated the model cormorants in the temperature of the animal room as the photographs were taken within minutes of the birds being taken into the photograph room, and the birds may not have reached a new thermal steady state assumed by Niche Mapper. Observed surface temperatures were expected to be between those predicted for birds simulated in the photograph and animal rooms. The mass and body temperature of the model bird was set to the average mass and body temperature of all unoiled birds at the time of the photograph, and we used a target resting metabolic rate of 4.59 W/kg (Enstipp et al. 2006). Surface temperatures predicted by Niche Mapper were then compared to temperatures extracted from the FLIR images of experimentally oiled birds.

Simulating Oil Exposure

To simulate oil exposure, we modified plumage layer inputs from the unoiled model. In the unoiled model, feather layer thermal conductivity is calculated using the thermal conductivities of air and keratin in relative proportion of the two materials in the layer. To simulate introduction of oil, we added the thermal conductivity of crude oil (0.135 W/mC; Elam et al., 1989) to the feather layer thermal conductivity calculation, partially or completely replacing the contribution of air. We also reduced feather layer depths, feather density, and ptiloerection abilities based on observations of feather matting and feather plucking in live oiled birds (Cunningham et al., 2017).

The first FLIR images of the oiled birds were taken before any oiling, and the surface temperature comparisons were made using the unoiled cormorant model as described above. Subsequent FLIR images were taken after one, three, five, and six oil applications. Surface temperature differences between oiled and control birds were similar between oil applications five and six. We thus developed models for three stages of oiling: one application (Stage 1), three applications (Stage 2), and five/six applications (Stage 3). For each oil-exposure model, the feather layer input changes were manipulated to reflect observed physical changes in the plumage (Cunningham et al., 2017) until the resulting surface temperature calculations were similar to the observed surface temperatures (Table 2).

Metabolic chamber simulations (as described earlier for the unoiled model), were performed for each of the model oiling stages to compare predicted effects to effects on live birds reported in the literature. For cormorants simulated in water we assumed a range of additional water penetration due to oil exposure, from no additional penetration (2mm insulating layer retained) to full penetration (skin in contact with water), to bound uncertainty in the true effect.

**Table 2**. Modifications to model cormorant plumage inputs used to simulate oil exposure.

| Body Part | Oil Stage 1 (one oil application) | Oil Stage 2 (three oil applications) | Oil Stage 3 (five/six oil applications) |
|---|---|---|---|
| **Head** | No effect | Plumage depth decreased 0.5 mm; Non-feathered portion of plumage matrix modeled as oil (25%) and air (75%); ability to ptiloerect reduced 13%. | Plumage depth decreased 0.5 mm; Non-feathered portion of plumage matrix modeled as oil (25%) and air (75%); ability to ptiloerect reduced 13%. |
| **Neck** | No effect | Plumage depth decreased 0.5 mm; Non-feathered portion of plumage matrix modeled as oil (25%) and air (75%); ability to ptiloerect reduced 13%. | Plumage depth decreased 0.5 mm; Non-feathered portion of plumage matrix modeled as oil (25%) and air (75%); ability to ptiloerect reduced 13%. |
| **Breast** | Non-feathered portion of plumage matrix modeled as oil (10%) and air (90%) | Plumage depth decreased 2 mm; non-feathered portion of plumage matrix modeled as oil (10%) and air (90%); ability to ptiloerect reduced 63%. | Plumage depth decreased 3 mm; non-feathered portion of plumage matrix modeled as oil (50%) and air (50%) ability to ptiloerect reduced 63% |
| **Back** | Non-feathered portion of plumage matrix modeled as oil | Plumage depth decreased 2 mm; non-feathered portion of plumage matrix modeled as oil; ability to ptiloerect reduced 63% | Plumage depth decreased 3 mm; non-feathered portion of plumage matrix modeled as oil; ability to ptiloerect reduced 63%; feather density reduced to 5,000 elements/$cm^2$. |

*Feeding Experiment Simulation*

To compare Niche Mapper predictions for daily energetic expenditure to observed energetic expenditure (using food consumption as a proxy) in the live cormorants, we simulated individual cormorants in their holding pens over the course of the experiment. The microclimate submodel used daily maximum and minimum air temperatures recorded in the animal room to calculate daily ambient temperature profiles, assuming minimum temperatures occurred one hour prior to sunrise and maximum temperatures occurred one hour after solar noon. We assumed no

solar input, negligible wind (0.1 m/s), and floor and ceiling temperatures being equal to air temperature.

Birds were observed to spend most of the day resting or preening, except for about two hours of swimming per day to forage for fish. Thus, we assumed an activity multiplier of 1.75x resting metabolic rate (RMR) for each hour to simulate resting and preening activities during diurnal and crepuscular hours (see Goldstein, 1988 reporting preening activity multipliers of 1.3-2.5 for a variety of species]. The water temperature was assumed to be the average of the daily maximum and minimum air temperature. Based on observations, the birds were simulated to spend 10% of their time in the tanks diving for fish using an activity multiplier of 5x RMR (Enstipp et al., 2006) and the rest of the time floating on the water surface with legs and 70% of the torso submerged. For nocturnal hours, we assumed no activity multipliers.

Body mass of the model birds was assumed to change linearly between the days when measurements were made. Oiled group individuals were modeled using the same model as the control birds for days prior to the first oiling. Transitions to oil stages 2 and 3 were assumed to occur following the oil application in between the days when FLIR images were taken (Table S2).

*Statistical Analyses*

To test the effect of treatment on observed surface temperatures we constructed linear models of surface temperature as a function of treatment group for each body part for each photograph day in R version 3.4.0 (R Core Team, 2017). Significance of treatment group was evaluated using an F-test. To test the effect of treatment on observed internal body temperature and food consumption we performed linear mixed effects analyses using the *lme4* package (Bates et al., 2015) in R. Fixed effects were experiment day and treatment class (oiled or

unoiled), with interaction allowed between the effects. Individual bird identifiers were included as a random effect, using both random intercepts and slopes (with experiment day as a covariate). Statistical significance of effects was evaluated using likelihood ratio tests comparing the full model to a model without the effect being tested.

## RESULTS

### *Experimental oiling*

Prior to oil application, there was no difference in observed surface temperatures between treatment groups for any body part (F-test; $p>0.05$). After one oil application, FLIR images demonstrated that the breast and back surface temperatures in the oiled birds were significantly higher than in the control birds (Table 3, Fig. S2). After subsequent oil exposure, FLIR images revealed that breast, back, neck and head temperatures were all significantly higher in the oiled birds than in the control birds (Table 3). There was no significant difference in mean daily internal body temperatures ($\chi^2$ (2) = 4.76, p = 0.09) or minimum daily body temperatures ($\chi^2$ (2) = 1.45, p = 0.48) over the study period between oiled and unoiled birds.

Prior to oil applications, there was no significant effect of treatment alone ($\chi^2$ (2) = 0.89, p = 0.64) or interaction between treatment and day ($\chi^2$ (1) = 0.36, p = 0.55) on observed food consumption (Fig. S4a). Birds in both groups were decreasing food consumption by 4-5 g $kg^{-1}$ $d^{-1}$ over the course of the quarantine period. Following the start of oil application, the treatment group became a significant determinant of food consumption (Fig. S4b). Control birds continued to decrease food consumption over time, although at a slower rate, while birds in the oiled group began to increase food consumption. In the post-oiling period, the interaction between

experiment day and treatment had a significant effect on food consumption ($\chi^2$ (1) = 10.426, p = 0.0012), with oiled birds eating more food as the experiment progressed.

**Table 3.** Average surface temperature (°C) for different body parts as measured in FLIR images of oiled and unoiled cormorants after different levels of oil exposure. Asterisks indicate that the surface temperature for that body part was significantly different than for the control group.

| | | **Body Part** | | | | | |
|---|---|---|---|---|---|---|---|
| Oil Applications | Group | Beak | Head | Neck | Breast | Back | Legs |
| **Prior to oiling*** | Oil | 29.4±0.3 | 29.4±0.4 | 25.1±0.4 | 20.1±0.3 | 26.9±0.3 | 24.7±0.8 |
| | Control | 29.6±0.4 | 29.0±0.3 | 25.0±0.3 | 20.2±0.2 | 26.3±0.3 | 25.0±1.2 |
| **One application†** | Oil | ***26.0±0.3**** | 26.9±1.1 | 22.4±0.5 | ***16.9±0.2**** | ***26.3±0.3**** | 22.0±0.8 |
| | Control | 28.0±0.3 | 27.8±0.3 | 22.8±0.3 | 15.8±0.4 | 23.1±0.2 | 21.5±1.1 |
| **Three Applications†** | Oil | 25.8±0.4 | ***30.3±0.2**** | ***24.6±0.3**** | ***17.2±0.4**** | ***27.9±0.3**** | 18.4±0.6 |
| | Control | 25.9±0.4 | 27.9±0.2 | 22.6±0.3 | 14.4±0.3 | 22.4±0.3 | 21.0±1.3 |
| **Five applications†** | Oil | 27.6±0.4 | ***30.6±0.4**** | ***25.2±0.4**** | ***19.0±0.2**** | ***29.2±0.4**** | 19.7±1.1 |
| | Control | 27.2±0.4 | 28.3±0.5 | 23.0±0.4 | 15.8±0.3 | 22.9±0.5 | 21.6±1.1 |
| **Six applications*** | Oil | 30.4±0.6 | ***31.1±0.4**** | ***27.0±0.3**** | ***22.8±0.3**** | ***30.2±0.5**** | **27.1±0.9*** |
| | Control | 29.3±0.4 | 29.6±0.2 | 24.4±0.3 | 19.0±0.3 | 24.8±0.4 | 23.7±0.4 |

*photograph room air temperature was 20°C; †photograph room air temperature was 17°C

During Stage 1 (excluding first day of oiling due to abnormally low consumption) oiled birds were observed to eat 10% less food than control birds. In Stage 2 and Stage 3 days, oiled birds were observed to eat 15% and 20%, more, respectively, than the control birds (Table S4). The oiled birds were able to maintain their body weight as well as the control birds, with the exception of two individuals that quickly lost weight immediately prior to death (Table S2, Fig S5).

*Unoiled Model*

Niche Mapper's metabolic rate predictions for unoiled cormorants resting in air were comparable to experimental data from live cormorants (Fig. 1). For cormorants in air, Niche Mapper predicted a lower critical temperature between 10 and 15°C and an upper critical temperature between 27 and 31°C. Below the thermoneutral zone, predicted whole body thermal conductance was between 0.33 and 0.44 W/°C in the simulated chamber (Table 4). For cormorants resting on the water surface, Niche Mapper metabolic rate predictions were within the range of metabolic rates observed in live cormorants (Fig. 1). Water exposure increased the predicted lower critical temperature to 24°C and whole body thermal conductance to 1.15 - 1.24 W/°C (Table 4).

Niche Mapper's predicted surface temperatures when modeling unoiled cormorants in the photograph room were within 1.2±0.3°C of the mean (± s.e.) observed temperatures for the beak, 0.3±0.2°C for the head, 2.5±0.3°C for the neck, 0.8±0.3°C for the back, and 1.0±0.3°C for the legs (Fig. 2a; Fig. S3a-f). Niche Mapper predicted higher breast temperatures by 4.2±0.5°C compared to average values from the FLIR images when assuming the photograph room air temperatures. With one exception (breast, day 10), the measured mean surface temperatures for

all body parts on all days fell between the surface temperatures predicted by Niche Mapper when using the photograph room air temperatures and those predicted when using the animal room air temperatures (Fig. 2a).

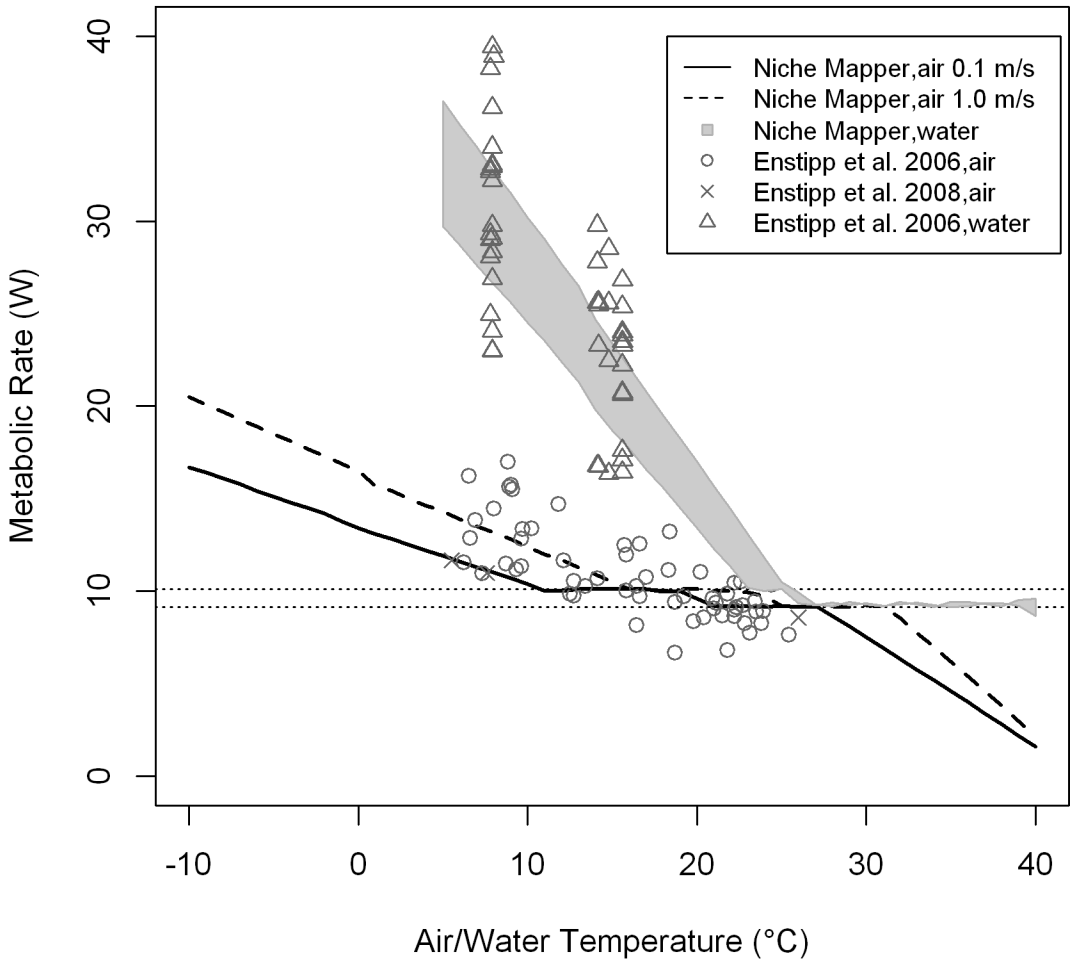


**Figure 1.** Niche Mapper (NM) metabolic rate predictions as a function of air and/or water temperature for a resting, average-sized (2.1 kg) cormorant using the input values from Table 1 compared to values reported for live cormorants. The shaded gray indicates the range of NM predictions assuming different percentages of the torso submerged in water (50% - 90%) and air/water velocities from 0.1 m/s to 1.0 m/s. NM thermoregulates until it reaches a metabolic heat production within 5% of the resting metabolic rate (horizontal dashed lines). Predicted metabolic

rates below the target range are unrealistic, but are included to show temperatures at which overheating is predicted to occur.

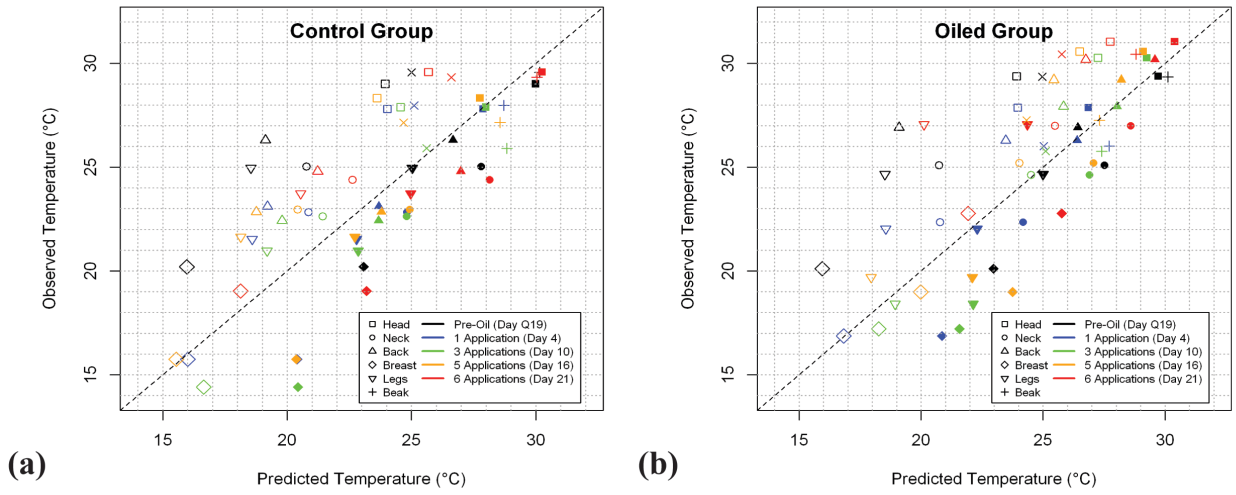


**Figure 2.** Surface temperatures predicted by Niche Mapper (NM) compared to mean surface temperatures measured by FLIR imagery on control (a) and oiled (b) live cormorants. Filled ("+" for the beak) symbols are temperature predictions assuming air temperatures of the photograph room. Open ("X" for the beak) symbols represent predictions assuming air temperatures of the animal room prior to the photographs being taken. Points above and below the dashed 1:1 line indicate NM under- and overpredicting surface temperatures, respectively. Note how the 1:1 line lies between the two sets of predictions. (Requires color printing).

*Oiled Model*

For the oiled birds, making the changes summarized in Table 2 resulted in surface temperatures predictions within 0.4±0.1°C of the mean observed temperatures for the beak, 1.0±0.1°C for the head, 1.9±0.1°C for the neck, 0.3±0.2°C for the back, and 0.9±1.2°C for the legs (Fig. 2b; Fig. S3g-j). As with the unoiled birds, Niche Mapper predicted higher breast

temperatures (4.0±0.3°C) when assuming the air temperature of the photograph room for the modelling. Predicted breast surface temperatures were closer to observed surface temperatures when using animal room air temperatures (mean difference = 0.29±0.4°C).

In the metabolic chamber simulations of oiled cormorants in air, the predicted lower critical temperature increased by 7-12°C and the predicted upper critical temperature increased by 3-5°C (Table 4, Fig. S6). Predicted whole body thermal conductance (W/°C) below the lower critical temperature of the unoiled model were increased by 32-73%, resulting in 31-76% increases in metabolic heat production required to maintain body temperatures (Table 4, Fig. S6). In the metabolic chamber simulations of oiled cormorants resting in water, metabolic rates and whole body thermal conductivities increased 13-46% and 10-35%, respectively, compared to the unoiled model resting in water (Table 4; Figs. S6,S7). As the degree of assumed water penetration increased, the difference between the oil stages decreased as the heat loss to water overwhelms other heat loss to the point where assuming full water penetration resulted in virtually identical predictions for all oiling stages.

*Predicted Food Intake*

Predicted daily food requirements were relatively constant throughout the experiment for unoiled birds, indicating little change in predicted thermoregulatory costs (Fig. 3a). For oiled group, Niche Mapper predicted virtually identical food requirements as the control birds up until oil applications began (Fig. 3b). Following oil application, Niche Mapper predicted food requirement increases of 10%, 13%, and 15% for oiled birds compared to the control birds for Stage 1, 2, and 3 oiling, respectively (Table S3). Compared to observed food consumption, predicted food requirements were generally lower than those observed, particularly in the quarantine period.

**Table 4.** Summary of predicted effects of oiling on lower critical temperature (LCT) and upper critical temperature (UCT), as well as metabolic rate (MR), and whole body thermal conductance (TC) below the thermoneutral zone (to -30°C in air and 5°C in water) for cormorants in air and resting on water. For cormorants resting on water, modeling assumed that 70% of the torso was submerged. Two air/water velocities were also assumed: 0.1 m/s and 1.0 m/s.

| | | 0.1 m/s velocities | | | 1.0 m/s velocities | | |
|---|---|---|---|---|---|---|---|
| | **Model** | **LCT/UCT (°C)** | **MR** | **TC** | **LCT/UCT (°C)** | **MR** | **TC** |
| Air | Unoiled | 10/27 | 10.4-23.8 | 0.33 | 15/31 | 10.5-30.4 | 0.44 |
| | Stage 1 | 17/30 | 13.3-31.3 | 0.44 | 22/33 | 13.8-40.5 | 0.58 |
| | Stage 2 | 20/32 | 15.6-36.8 | 0.52 | 25/36 | 16.6-49.6 | 0.69 |
| | Stage 3 | 22/32 | 17.0-40.2 | 0.57 | 26/36 | 18.2-54.3 | 0.76 |
| Water | Unoiled | 24/39 | 10.2-32.0 | 1.15 | 24/>40 | 10.8-34.4 | 1.24 |
| | Stage 1* | 25/>40 | 11.8-35.8 | 1.26 | 25/>40 | 12.7-38.9 | 1.38 |
| | Stage 2* | 25/>40 | 12.3-36.5 | 1.28 | 26/>40 | 13.6-40.4 | 1.41 |
| | Stage 3* | 26/>40 | 13.8-51.0 | 1.38 | 27/>40 | 15.1-44.1 | 1.53 |
| | Stage 1† | 26/>40 | 13.8-40.2 | 1.39 | 27/>40 | 14.7-43.3 | 1.51 |
| | Stage 2† | 26/>40 | 14.0-40.4 | 1.39 | 27/>40 | 15.4-44.5 | 1.53 |
| | Stage 3† | 27/>40 | 15.0-42.8 | 1.46 | 27/>40 | 16.4-47 | 1.61 |
| | All Stages‡ | 28/>40 | 16.6-47.0 | 1.57-1.58 | 28/>40 | 19.0-50.5 | 1.71-1.72 |

* Assuming oil exposure does not cause additional water penetration
† Assuming oil exposure reduces insulating layer to 1 mm
‡ Assuming oil exposure allows water to penetrate all the way to the skin.

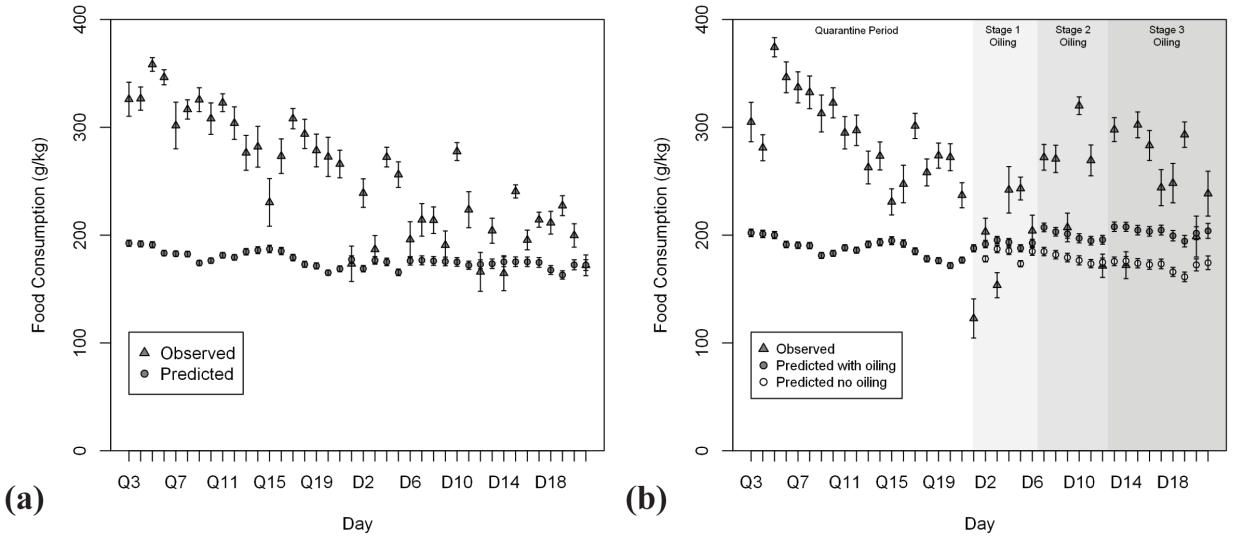


**Figure 3.** Niche Mapper predictions for mean daily food consumption per unit body mass (± s.e.) compared to observed consumption for the control (a) and oiled (b) cormorant groups. For the oiled group, also shown for comparison is the predicted food consumption of those individuals if no oiling was modeled. Intragroup variation predicted by Niche Mapper is solely due to differences in mass-specific energetic demands; body mass was the only model input that changed between individual simulations.

## DISCUSSION

### *Model Development and Testing*

Oiled cormorants had significant increases in surface body temperatures after a single exposure to 13g of oil and exhibited a cumulative effect over time, relative to unoiled birds due to repeated exposure to sublethal amounts of oil (Table 3). The effects of oil exposure predicted

by Niche Mapper are comparable to experimentally induced effects observed here in cormorants and from the literature for multiple species (Table S1). Using food consumption as a proxy for energetic expenditure, oiled cormorants consumed as much as 20% more food than unoiled cormorants and Niche Mapper predicted a similar trend and magnitude of increased food consumption due to increased thermoregulatory costs of repeated sublethal oil exposure. These findings provide support for both the cumulative thermoregulatory effects of repeated sublethal oil exposure on cormorants and for Niche Mapper's ability to predict the thermoregulatory consequences of oil exposure in birds.

The ability to accurately model thermoregulatory effects of repeated sublethal oil exposure is predicated on accurately modeling how oiling affects body surface temperatures because heat fluxes with the environment depend on animal surface temperatures. Overall, Niche Mapper's surface temperature predictions for unoiled cormorants agreed with observed surface temperatures in unoiled cormorants. Importantly, the observations were made in temperatures within the cormorant's expected thermoneutral range, and Niche Mapper calculated similar surface temperatures while assuming an experimentally-reported resting metabolic rate and the same body temperature as the live cormorants.

For the oiled bird models, the modifications to plumage inputs for the baseline (unoiled) model that allowed for the calculated surface temperatures to match the measured surface temperatures of oiled birds were logical and based on observed effects to the plumage (Cunningham et al. 2017), thus supporting the model's ability to accurately model heat flow processes in cormorants. For example, in the live bird experiment oil was applied only to the back and breast, and thus oil would need to be spread to the neck and head via preening over time. In the modifications for Stage 1 oiling, modeling the immediate introduction of oil to the

head and neck resulted in surface temperatures being too high. However, oil introduction to the head and neck was required for Stage 2 and 3 models in order to match observed surface temperatures on these body parts.

While Niche Mapper accurately predicted surface temperatures for most body areas overall, the breast area varied dependent on the underlying ambient temperatures modelled. Predicted breast surface temperatures were more accurate when the model assumed temperatures associated with the animal holding room than when assuming the temperature of the photograph room (Fig. 2). A likely explanation for this difference is the thicker plumage (12 mm) on the breast that prevents the surface from reaching a steady state as quickly as other body parts with thinner (<4 mm), or no, plumage. After only a few minutes in the photograph room, breast surface temperatures may still be more reflective of the birds in the animal room temperatures. Indeed, the observed breast surface temperatures were closer to the surface temperatures predicted by Niche Mapper when assuming the animal room air temperature.

Niche Mapper's metabolic heat production predictions for the unoiled cormorant model in a simulated metabolic chamber were similar to measurements made on live, unoiled cormorants in air and in water (Fig. 1). Metabolic chamber data do not exist for oiled cormorants for a similar comparison for our oiled cormorant models. However, changes in metabolic heat production and whole body thermal conductance in response to oiling reported for other species (Table S1) are useful points of comparison to evaluate Niche Mapper's predictions as we discuss below.

Lower levels of oil exposure (<20 g or "light" in Table S1) have been found to increase whole body thermal conductance in live birds in air by 0-84%. Niche Mapper predicted thermal conductance would increase 33% in cormorants in response to Stage 1 oiling, within the reported

range for other species. Prior studies of oiled birds exposed to air found that heat production increased by 8-20% following exposure to ~12 mL of crude oil (Table S1). Here, Stage 1 oiling represents exposure to a similar amount of crude oil (13 g), and the model predicted a 31-33% increase in metabolic heat production in cormorants.

Moderate oil exposure (20-50 g or "moderate" in Table S1) has been found to increase thermal conductance by 45-113% in live birds in air. In our study, Stage 2 oiling represents exposure to a total of 39 g of crude oil, and Niche Mapper predicted whole body thermal conductance would increase by 58%, within the reported range for other species. High levels of oil exposure (>50 g or "heavy" in Table S1) has been found to increase thermal conductance by 74-143% in live birds in air. Here, Stage 3 oiling represents exposure to a total of 65-91 g of crude oil, and Niche Mapper predicted whole body thermal conductance would increase by 73% in response to this exposure. McEwan & Koelink (1973) found that moderate and heavy oiling increased the lower critical temperature for mallards (*Anas platyrhynchos*) and scaups (*Aythya* sp.) by 13°C. At this oiling level, Niche Mapper provided a similar response, predicting that lower critical temperatures would increase 10-12°C in response to Stage 2 or 3 oiling.

We note that the studies in Table S1 applied oil in a single dose, while our oiled models were based on repeated applications to simulate chronic exposure. Thus, while Stage 3 oiling reflects cumulative application of 65-91 g of oil, some of the oil had likely been removed by preening or while swimming by the time the FLIR images used to calibrate the model were taken. This could contribute – along with intrinsic differences between plumage structure between species (*sensu* Jenssen, 1994)– to Niche Mapper's predictions for responses to moderate or heavy exposure being on the lower end of what has been reported in the literature. Given that we are modeling repeated sublethal exposure to oil, an observed scenario for many birds (see Bursian et al., 2017),

these results may reflect a more realistic situation with respect to thermoregulatory impacts of real-world oil exposure.

Predicted responses in metabolic heat production and whole body thermal conductance for oiled cormorants exposed to water are generally lower than what has been reported for other species (Tables 4, S1). However, cormorant plumage is partially wettable, and it is reasonable to expect a bird whose plumage naturally allows some water penetration prior to oil exposure to display less response after oiling than a bird whose plumage better resists water penetration. Indeed, unoiled cormorants increase metabolic rate 165-219% when resting in water compared to resting in air, while unoiled mallards and eiders only increase their metabolic rates 4-56% (Richman & Lovvorn, 2011). This indicates that unoiled cormorants experience much of the increased heat production documented in oiled mallards and eiders exposed to water simply as a result of its partially-wettable plumage, leaving less opportunity for oil exposure to cause additional heat loss. These findings indicate the importance and capability of Niche Mapper for modelling for plumage specific characteristics of avian species. Given this capability, empirical measurements of metabolic rates and buoyancy changes of oiled cormorants in water would be helpful to refine Niche Mapper predictions at various oil exposure levels.

Feeding Trial Experiment

Overall, oiled cormorants consumed as much as 20% more food than unoiled cormorants and Niche Mapper predicted up to 18% increased food consumption due to increased thermoregulatory costs of repeated sublethal oiling. While the overall direction and magnitude of change in predicted increases in food consumption were similar to observed changes, Niche Mapper did tend to underestimate absolute food consumption, particularly early in the study. Live birds lost weight (mean: 385 ± 23 g; no difference between control and oiled groups)

between capture and surgery, and then gained weight, mainly in the quarantine period (Fig S5). However, Niche Mapper's food requirements are calculated to exactly meet the energetic demands for maintaining body mass, activity, and thermoregulation and do not account for growth. As weight gains slowed toward the end of the experiment, the observed food consumption converged with the food requirements predicted by Niche Mapper (Fig. 3a).

During Stage 1 oiling days, Niche Mapper predicted that oiled birds would require 10% greater food consumption than control birds. However, the oiled birds were observed to eat less food than control birds, despite having higher body surface temperatures, and thus presumably requiring greater metabolic heat production. This overestimation could be explained by the first few days following oil application being a period of reduced food consumption while adjusting to the physical effects of being oiled.

During Stage 2 and 3 oiling days, oiled birds consumed more than the control birds, consistent with Niche Mapper's predicted increased thermoregulatory costs. Niche Mapper's underestimation (predicted 15-18% increase vs. observed 20% increase) of Stage 3 food consumption could be explained by factors other than increased thermoregulatory demands influencing food consumption at this exposure level. Anecdotal evidence suggests that oiled birds may have increased activity costs due to additional preening (Cunningham et al., 2017). Also, Harr et al. (2017a,b) observed increased edema, and loss of blood in gastrointestinal tracts and feces in some oiled birds, suggesting that oil ingestion could interfere with physiological factors such digestive efficiency or nutrient utilization.

The fact that observed food consumption did not solely reflect daily energy expenditure for maintenance, does not affect the main results of this study. The relevant comparison is how the predicted difference in food consumption between the oiled and unoiled birds compared to

the observed difference between the groups. Prior to oiling, the groups had similar food consumption; following oiling, the oiled group was observed to increase food consumption compared to the control group. This difference must be attributed to the oiling because the birds were otherwise treated identically, and the increases are consistent with Niche Mapper's predictions of increased thermoregulatory requirements due to reduced plumage insulation.

Niche Mapper accurately predicted heat production by unoiled cormorants over a wide temperature range as evidenced by the metabolic chamber simulations (Fig. 1). For the oiled models, Niche Mapper produced similar surface temperatures as observed in live birds (Fig. 2) when logical modifications based on qualitative observations were made to the plumage layer inputs. We are confident in these predictions because we are explicitly modeling the heat transfer processes determining surface temperatures rather than relying on correlations between air and surface temperatures. That being said, empirical measures of changes in some modelled parameters such physical changes to plumage, depth of water penetration, and surface temperature measures at a wider range of ambient temperatures may help inform the relationship of various physical and physiological changes and specific heat transfer processes.

The above suggestions would help in understanding the relative contributions of various physical and physiological processes to the overall impacts of sublethal exposure to oil on avian or any other insulated endotherm thermoregulation. That said, an advantage of Niche Mapper is this information is not necessarily required to measure overall thermoregulatory impacts. For example, when extending this work to other species, it ultimately does not matter whether the model captures the precise characteristics of changes (e.g., plumage structural changes) as long as the resulting change to plumage layer insulation is reasonable. One way to do this is to simply modify plumage inputs until a desired level (or range) of increased whole-body thermal

conductivity is achieved in the model, based on the range reported for other species (e.g., Table S1).

*Implications*

This work illustrates the cumulative thermoregulatory impacts of repeated sublethal exposure to oil in cormorants and how bioenergetics models can be used to provide important insight into thermoregulatory costs of oil exposure. As far as we are aware this is the first time that a bioenergetics model has been tested with live animal experiments for this purpose. The ability to model the effects of oil exposure are valuable because such information would be difficult and resource-intensive to obtain from direct measurements of wild animals. Exposure to wind and a wider range of temperatures experienced in natural habitats, including the generally cooler temperatures experienced at higher-latitude breeding grounds would be expected to increase thermoregulatory costs compared to what was reported here, and absence of ad libitum food may make compensation more difficult. Such information can provide valuable insight into how both large and chronic oil spills are affecting wildlife by quantifying the extent to which thermoregulatory costs are diverting resources away from other important life processes like reproduction and building energy stores for migration. We used cormorants as a model organism, but the approach can be generalized to any species for which the basic morphological and physiological information needed by Niche Mapper is known.

## ACKNOWLEDGMENTS

The captive animal study was funded by the U.S. Fish and Wildlife Service as part of the Deepwater Horizon Natural Resource Damage Assessment. Animal capture, care, and use were approved by IACUC and NWRC Attending Veterinarian under protocol QA-2326 and Federal

#MB019065-3, Mississippi and Alabama (#8017) scientific collection permits. The National Wildlife Research Center provided funding for the modeling. Special thanks to Alexander Crain, Lanna Durst, Paul Fioranelli, Raleigh Middleton, and Paul Burr for their technical assistance with animal care and sampling on this project. We thank Scott Willard for use of the FLIR camera. We thank Ben Zuckerberg for statistical advice and Bill Karasov for helpful comments on previous drafts of this manuscript. Constructive feedback from an anonymous reviewer also improved this work.

REFERENCES

Bates, D., Maechler, M., Bolker, B., Walker, S., 2015. Fitting linear mixed-effects models using lme4. J. Stat. Softw. 67, 1-48.

Brugger, K.E., 1993. Digestibility of three fish species by double-crested cormorants. The Condor 95, 25-32.

Bursian, S.J., et al., 2017. Overview of Avian Toxicity Studies for the Deepwater Horizon Natural Resource Damage Assessment. Ecotoxcol. Environ. Saf. 142, 1-7

Cho, BT, ed., 1969. Advanced Heat Transfer. Urbana, IL: U Illinois Press. 459 pp.

Cunningham, F., et al., 2017. Development of Methods for Avian Oil Toxicity Studies Using the Double Crested Cormorant (Phalacrocorax auritus). Ecotoxcol. Environ. Saf. 141, 199-208.

Dorr, B.S., et al., 2015. DWH Avian Toxicity Phase 2: Double-Crested Cormorant (Phalacrocorax auritus) External Oiling Scoping Study (M23). Final report to USFWS, Natural Resource Damage Assessment, 47 pp

Elam, S.K., Tokura, I., Saito, K., Altenkirch, R.A., 1989. Thermal conductivity of crude oils. Exp. Therm.Fluid Sci. 2, 1-6.

Enstipp, M.R., Grémillet, D., Jones, D.R., 2006. The effects of depth, temperature and food ingestion on the foraging energetics of a diving endotherm, the double-crested cormorant (Phalacrocorax auritis). J. Exp. Biol. 209, 845-859.

Enstipp, M.R., Grémillet, D., Jones, D.R., 2008. Heat increment of feeding in double-crested cormorants (Phalacrocorax auritus) and its potential for thermal substitution. J. Exp. Biol. 211, 49-57.

Fitzpatrick, M.J., Mathewson, P.D., Porter, W.P., 2015. Validation of a mechanistic model for non-Invasive study of ecological energetics in an endangered wading bird with counter-current heat exchange in its legs. PLoS ONE 10: e0136677

Fort, J., Porter, W.P., Grémillet, D., 2009. Thermodynamic modeling predicts energetic bottleneck for seabirds wintering in the northwest Atlantic. J. Exp. Biol. 212, 2483-2490.

Fort, J., Porter, W.P., Grémillet, D., 2011. Energetic modeling: a comparison of the different approaches uses in seabirds. Comp. Biochem. Phys. A 158, 358-365.

Fraser, G.S., Racine, V., 2016. An evaluation of oil spill responses for offshore oil production projects in Newfoundland and Labrado, Canada: Implications for seabird conservation. Mar. Pollut. Bull. 107, 36-46

Fuentes, M., Porter, W.P., 2013. A new approach to model soil temperature: using microclimate models to predict the impacts of climate change on sea turtles. Ecol. Model. 251, 150–157.

Göktepe, Ö., Hundt, P., Porter, W., Pereira, D., 2012. Comparing bioenergetics models of double-crested cormorant (Phalacrocorax auritus) fish consumption. Waterbirds 35, 91-102.

Goldstein, D.L. 1988. Estimates of daily energy expenditure in birds: The time-energy budget as an integrator of laboratory and field studies. Am. Zool. 28, 829–844.

Grémillet, D., Tuschy, I., Kierspel, M., 1998. Body temperature and insulation in diving Great Cormorants and European Shags. Funct. Ecol.12, 386-394.

Grémillet, D., Chauvin, C., Wilson, R.P., Le Maho, Y., Wanless, S., 2005. Unusual feather structure allows partial plumage wettability in diving great cormorants Phalacrocorax carbo. J. Avian Biol. 36, 57-63.

Harr, K.E., et al., 2017a. Weathered MC252 crude oil-induced anemia and abnormal erythroid morphology in double-crested cormorants (Phalacrocorax auritus) with light microscopic and ultrastructural description of Heinz bodies. Ecotoxicol. Environ. Saf. 146, 29-39.

Harr, K.E., et al., 2017b. Comparison of organ weights and histopathology between double-crested cormorants (Phalacrocorax auritus) dosed orally or externally with artificially weathered Mississippi Canyon 252 crude oil. Ecotoxicol. Environ. Saf. 146, 52-61.

Henkel, L.A., Nevins, H., Martin, M., Sugarman S., Harvey, J.T., Ziccardi, M.H., 2014. Chronic oiling of marine birds in California by natural petroleum seeps, shipwrecks, and other sources. Mar. Pollut. Bull. 79, 155-166.

Jenssen, B.M., 1994. Effects of oil pollution, chemically treated oil, and cleaning on the thermal balance of birds. Environ. Pollut.86, 207-215.

Mahoney, S.A. 1984. Plumage wettability of aquatic birds. Auk 101, 181-185.

Martin, R.W., Carter, E.P., Flick Jr., G.J., Davis, L.M., eds., 2000. Marine and freshwater products handbook. Technomic Publishing Company, Lancaster PA. 963 pp.

Mathewson, P.D., Porter, W.P., 2013. Simulating polar bear energetics during a seasonal fast using a mechanistic model. PLoS ONE, 8, e72863.

McEwan, E.H., Koelink, A.F.C., 1973. The heat production of oiled mallards and scaup. Can. J. Zool. 51, 27-31.

O'Hara, P.D., Morandin, L.A., 2010. Effects of sheens associated with offshore oil and gas development on the feather microstructure of pelagic seabirds. Mar. Pollut. Bull. 60, 672-678.

Oka, N., Okuyama, M., 2000. Nutritional status of dead oiled Rhinoceros Auklets (Ceronhinca monocerata) in the Southern Japan Sea. Mar. Pollut. Bull. 40, 340-347

Porter, W.P., Mitchell, J.W., 2006. Method and system for calculating the spatial-temporal effects of climate and other environmental conditions on animals. http://www.warf.org/technologies.jsp?ipnumber=P01251US

Porter, W.P., Munger, J.C., Stewart, W.E., Budaraju, S., Jaeger, J., 1994. Endotherm energetics: from a scalable individual-based model to ecological applications. Aust. J. Zool. 42, 125-162.

R Core Team, 2017. R: a language and environment for statistical computing. R Foundation for Statistical Computing, Vienna, Austria. https://www.R-project.org/.

Richman, S.E., Lovvorn, J.R., 2011. Effects of air and water temperatures on resting metabolism of auklets and other diving birds. Physiol. Biochem. Zool. 84, 316-332.

Scherr, H., 2009. Breeding dispersal, migration, and winter movements of the eastern interior population of double-crested cormorants. M.Sc. Thesis, Trent University, Peterborough, Ontario, Canada. 102 pp.

United States Department of Agriculture, 2016. USDA Food Composition Database for Standard Reference. Release 28. Available at: https://ndb.nal.usda.gov/. Accessed May 2016

Votier, S.C., et. al., 2005. Oil pollution and climate have wide-scale impacts on seabird demographics. Ecol. Lett. 8, 1157–1164

Wiese, F.K., Robertson, G.J., 2004. Assessing seabird mortality from chronic oil discharges at sea. J. Wildlife Manage. 68, 627-638

Wiese, F.K., Ryan, P., 2003. The extent of chronic marine oil pollution in southeastern Newfoundland waters assessed through beach bird surveys 1984-1999. Mar. Pollut. Bull. 46, 1090-1101.

SUPPORTING INFORMATION

*Additional details on Niche Mapper animal submodel operation*

Niche Mapper (Porter & Mitchell 2006) is a bioenergetics model that has been previously shown to accurately predict metabolic heat production as a function of environmental conditions for a wide variety of animals, including whooping cranes (*Grus Americana*) and the Australian night parrot (*Melopsittacus undulates)* (Fitzpatrick et al., 2015; Kearney et al. ,2016). It has also been used to estimate daily energetic requirements of the orange bellied parrot of Australia (*Neophema chrysogaster*), Hawaiian honeycreepers (*Melamprosops phaeosoma*), cormorants (*Phalacrocorax* sp.), greater flamingos (*Phoenicopterus roseus)*, Brünnich's guillemots (*Ura lomvia*), and little auks (*Alle alle*) (Porter et al., 2000; Porter et al., 2006; Fort et al., 2009; Fort et

al., 2011; Göktepe et al., 2012; Deville et al., 2014). Niche Mapper consists of two submodels: a microclimate model and an animal model. The microclimate model uses macroclimate data (maximum and minimum daily air temperatures, cloud cover, wind speed, relative humidity), substrate properties, geographic location, and time of year to calculate hourly environmental conditions at the animal's height (see Fuentes & Porter, 2013 for details).

The animal model then uses the hourly outputs from the microclimate model and animal information to iteratively solve a heat balance equation to find the metabolic rate needed for the animal to maintain its body temperature, accounting for convective, radiative, evaporative, conductive and solar heat fluxes with its microenvironment. Animals are modelled as a series of simple shapes that have known heat transfer properties, which enables surface temperatures to be calculated based on a given core temperature and dimensions of the body part (see Mathewson & Porter, 2013 for calculations).

Niche Mapper assumes distributed metabolic heat generation throughout the flesh of each body part. Heat then travels through a subcutaneous fat layer, if present on the body part, via conduction to reach the skin surface. From bare body parts, heat exchanges are then computed using the calculated skin surface temperatures. For furred or feathered surfaces, heat is modeled as traveling through a porous plumage layer composed of a matrix of air and keratin via parallel conduction and radiative processes (Kowalski & Mitchell, 1979; Porter et al., 1994) before heat exchange with the environment is computed.

Niche Mapper solves the animal's heat balance for each hour of the day, and if the calculated metabolic rate is outside of a user-specified error range around a target metabolic rate (i.e., resting metabolic rate or some multiple thereof to simulate activity), thermoregulatory options are engaged. Behavioral options of selecting a different microhabitat (e.g., shade) are

engaged first, if available. Physiological options are engaged next. To minimize metabolic costs in cold temperatures, animals are allowed to increase plumage depth (simulating ptiloerection), decrease flesh thermal conductivity (simulating vasoconstriction) and reduce body temperature to a user-specified minimum value. To maintain a metabolic rate without overheating in a hot environment, animals are allowed to increase thermal conductivity (simulating vasodilation), increase body temperature to a user-specified maximum value, increase respiratory rate (simulating panting or gular fluttering), and increase surface area that is wet (simulating sweating).

If thermoregulatory options are exhausted before a metabolic rate within 5% of the target metabolic rate is reached in the heat balance calculations, the model will return the closest value. A predicted metabolic rate >105% of the target rate is an indicator of cold stress for the animal and a predicted metabolic rate <95% of the target rate indicates overheating (i.e., the highest metabolic rate that satisfies the heat balance calculations is lower than the current target metabolic rate). Niche Mapper does not account for the physical work associated with increased respiratory rates or sweating; it simply calculates the evaporative water loss required to allow the model animal to maintain its target metabolic rate. Therefore, predicted energetic expenditures in temperatures higher than the thermoneutral zone are lower than expected in reality.

Niche Mapper uses diet properties and digestive efficiencies to compute food requirements needed to meet the computed daily energetic requirements for maintenance, activity, and thermoregulation. Thus, predicted food requirements are directly proportional to predicted energetic requirements, and the model assumes that animals will eat enough every day to exactly satisfy their energetic requirements. Relevant parameters used to convert energetic requirements to food requirements are found in Table 1.

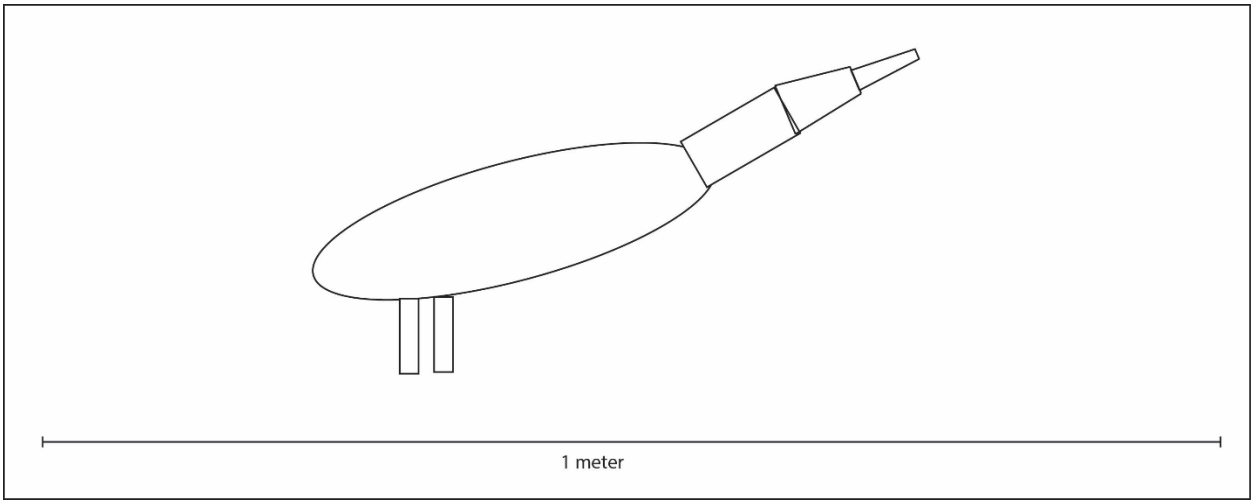


**Figure S1.** Cormorants as modeled by Niche Mapper. Each body part is modeled as a simple geometric shape maintaining a user-specified core temperature. Temperature profiles within each part are calculated assuming distributed metabolic heat generation throughout the flesh and accounting for heat exchange between the body part surface and the environment. The metabolic rate that allows the body temperature to be maintained is calculated for each body part and summed together to predict total energetic requirements for the animal in its microenvironment.

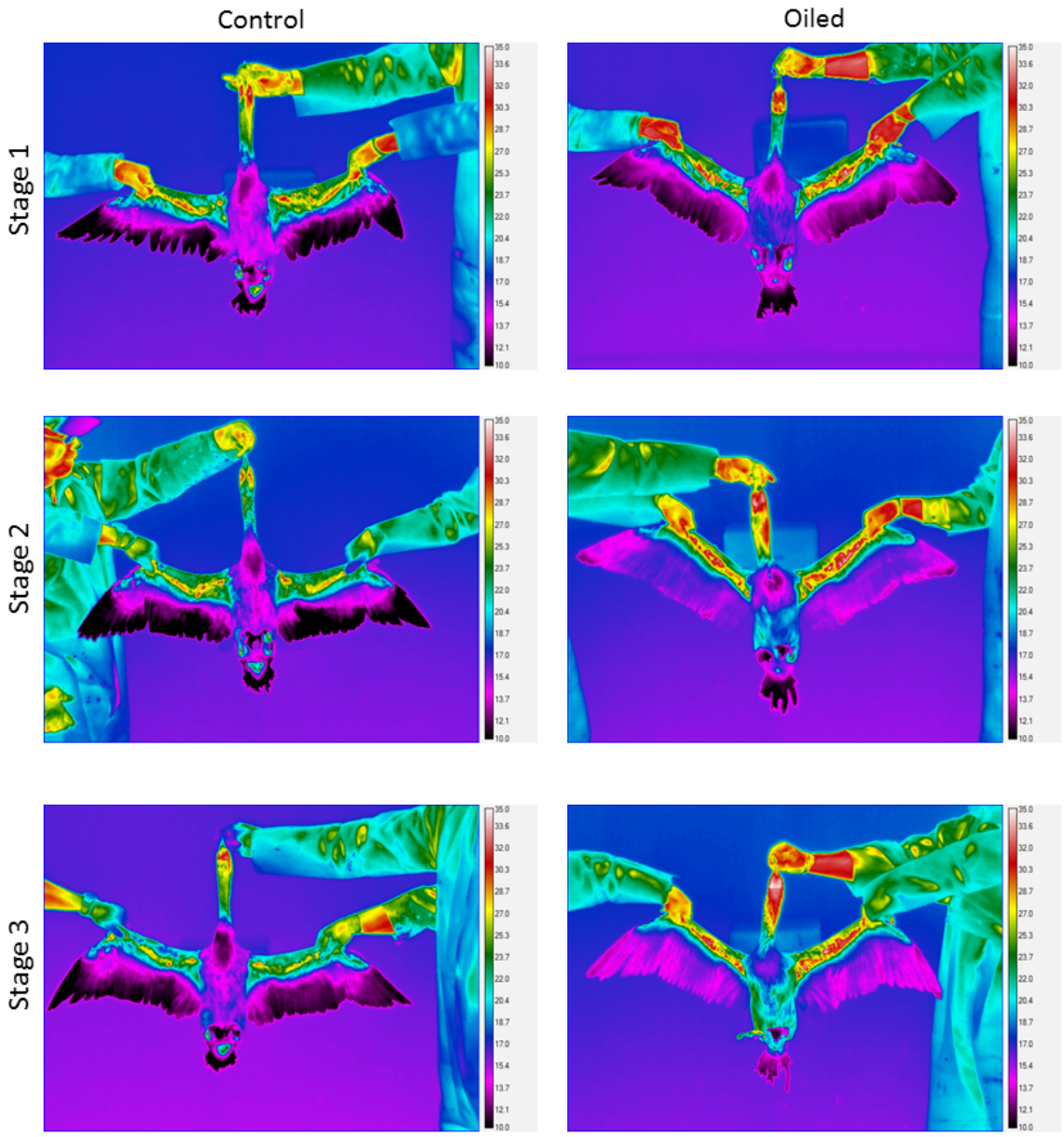


**Figure S2**. Thermograph (FLIR) images of Double-crested Cormorants experimentally exposed to repeated sublethal amounts of oil. Cormorants were exposed to 6.5 g of oil on the breast and back applied every 3 days. The three stages of oiling represent one application (Stage 1), three applications (Stage 2), and six applications (Stage 3). The figure highlights cumulative increase in body surface temperature over modelled oiling stages as well as the spread of oil through preening to other surface areas such as the head and neck relative to control birds.

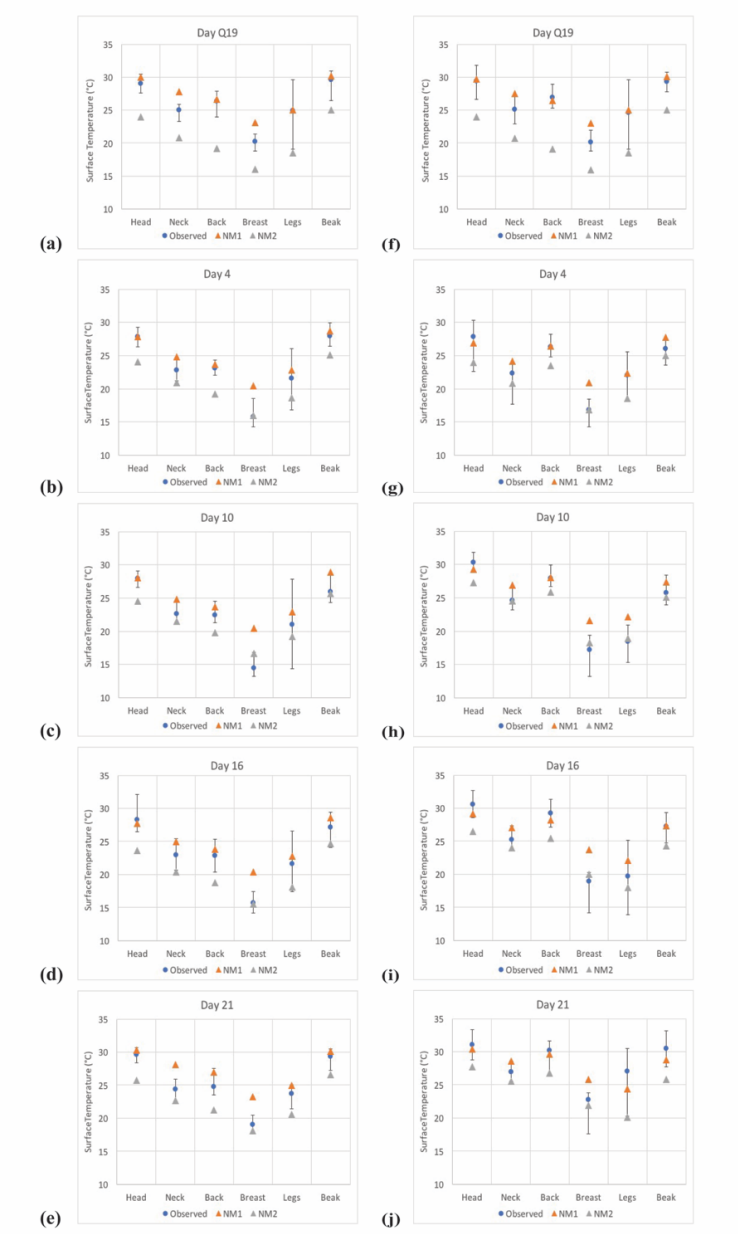


**Figure S3.** Comparison of surface temperatures of the control (unoiled) birds (a-e) and oiled birds (f-j) predicted by Niche Mapper to the average temperatures measured on live birds using FLIR imagery. The error bars for the observed data points extend from the maximum individual surface temperature to the minimum individual surface temperature. NM1 predictions used the air temperatures in the photograph room and NM2 predictions used the air temperatures from the holding room at the time the photographs were taken. Observed temperatures generally were between the two predictions and closer to NM1 predictions, as expected.

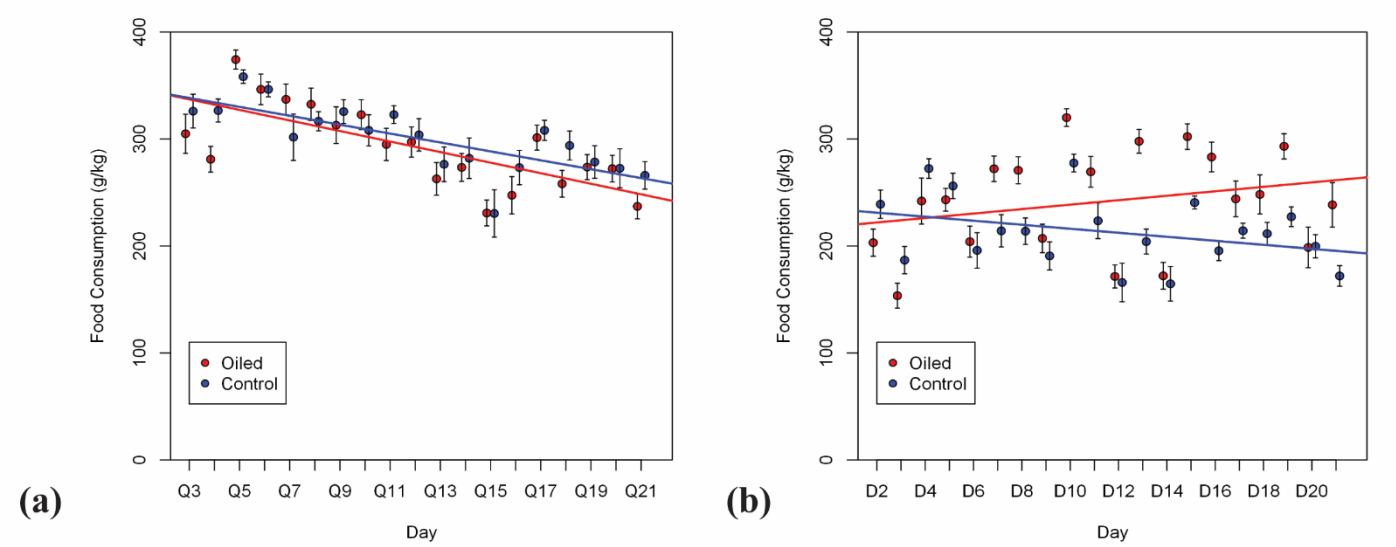


**Figure S4.** Average (± s.e.) food consumption per kg body weight observed in the cormorants prior to oiling (a) and after the start of oil applications (b). Regression lines from the generalized linear mixed model treating individual bird identity as a random factor are also shown to highlight the different comparative trends between the groups pre- and post-oiling Both groups showed a similar trend prior to oiling. After oiling the two groups showed opposite food consumption trends with the oiled group beginning to increase food consumption.

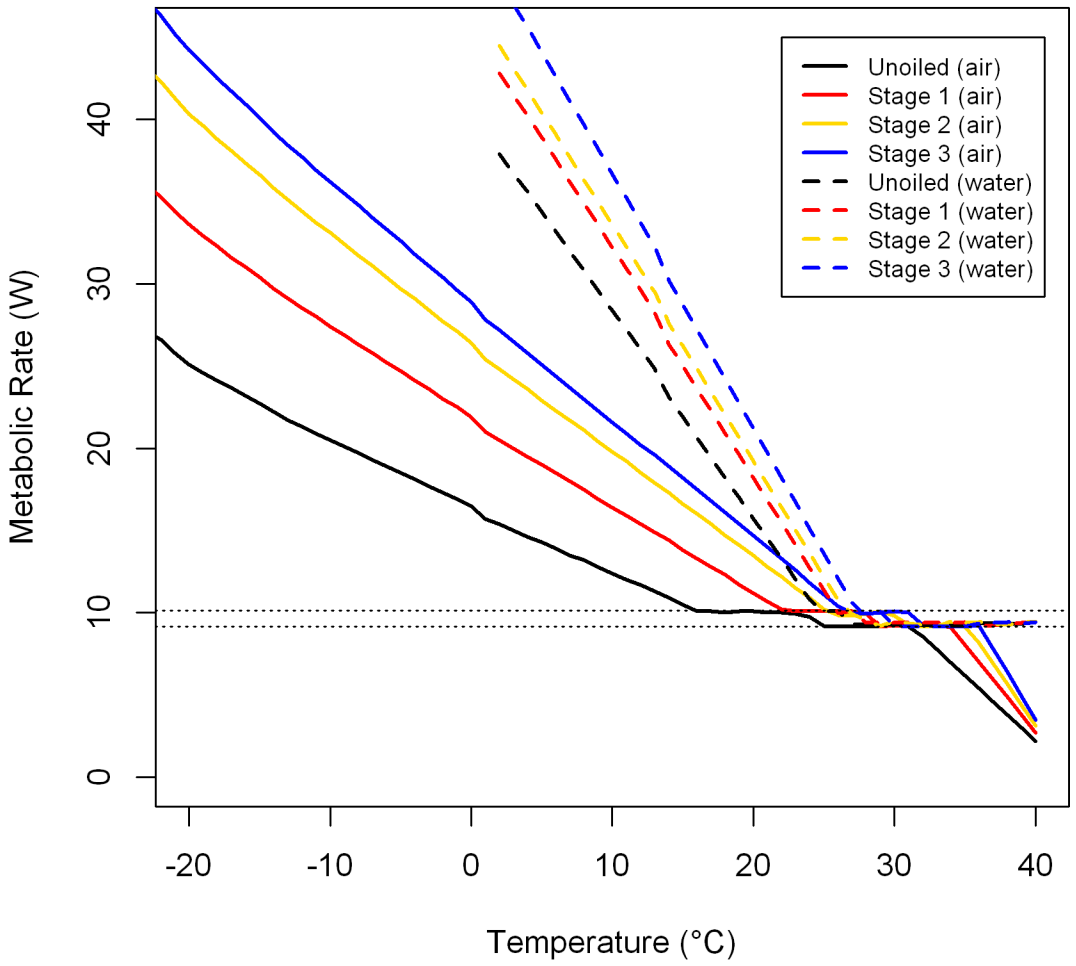


**Figure S5.** Predicted metabolic heat production requirements as a function of air and water temperatures for unoiled and oiled cormorant models in metabolic chamber simulations. The cormorant in the water was modeled with 70% of its torso submerged and assuming no additional water penetration into the plumage due to oil exposure.

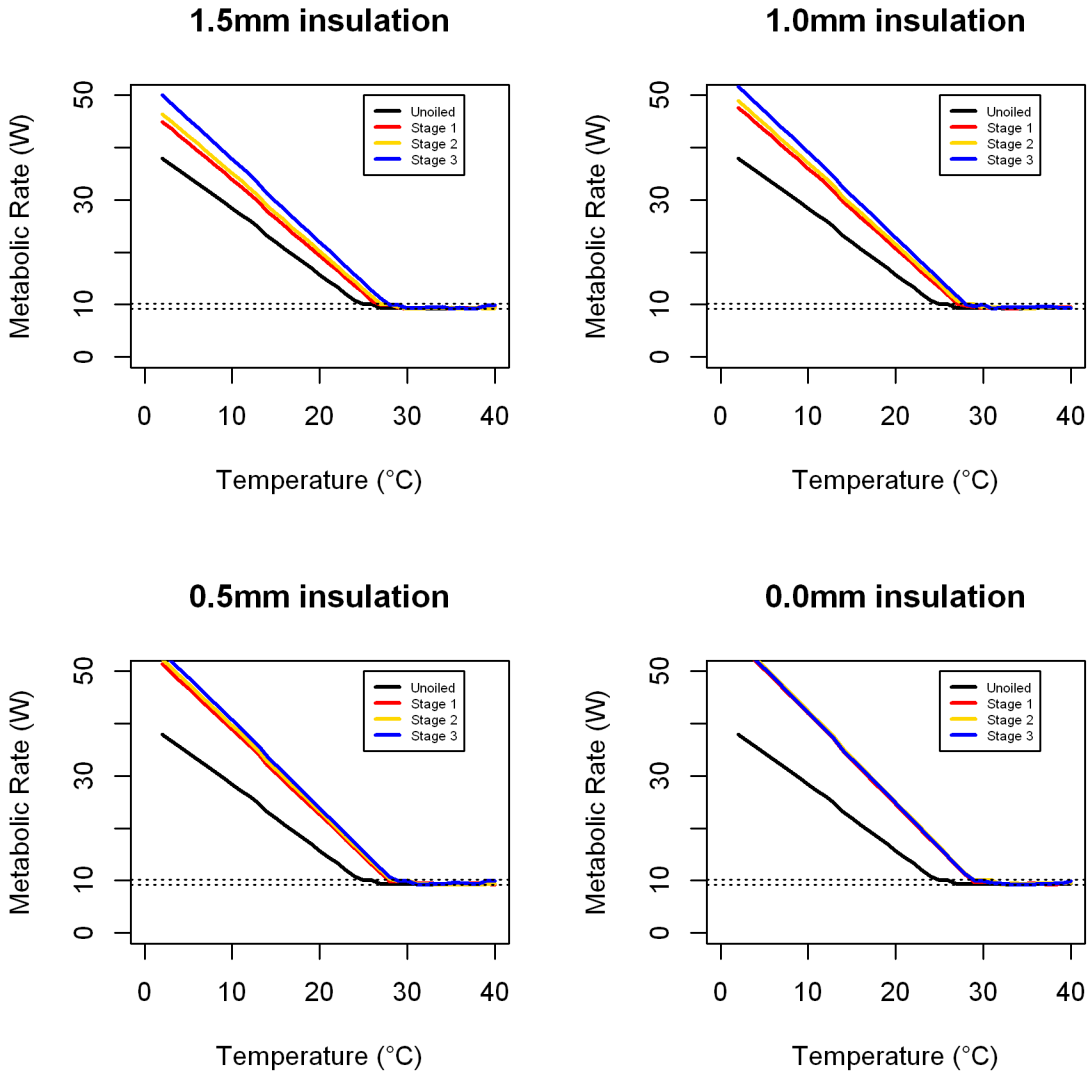


**Figure S6.** Predicted metabolic heat production of cormorants resting on the water surface with 70% of its torso submerged assuming different levels of water penetration due to oil exposure. Unoiled cormorants in water were modeled as having a 2mm insulation layer (see text). The horizontal dashed lines show ±5% of the resting metabolic rate.

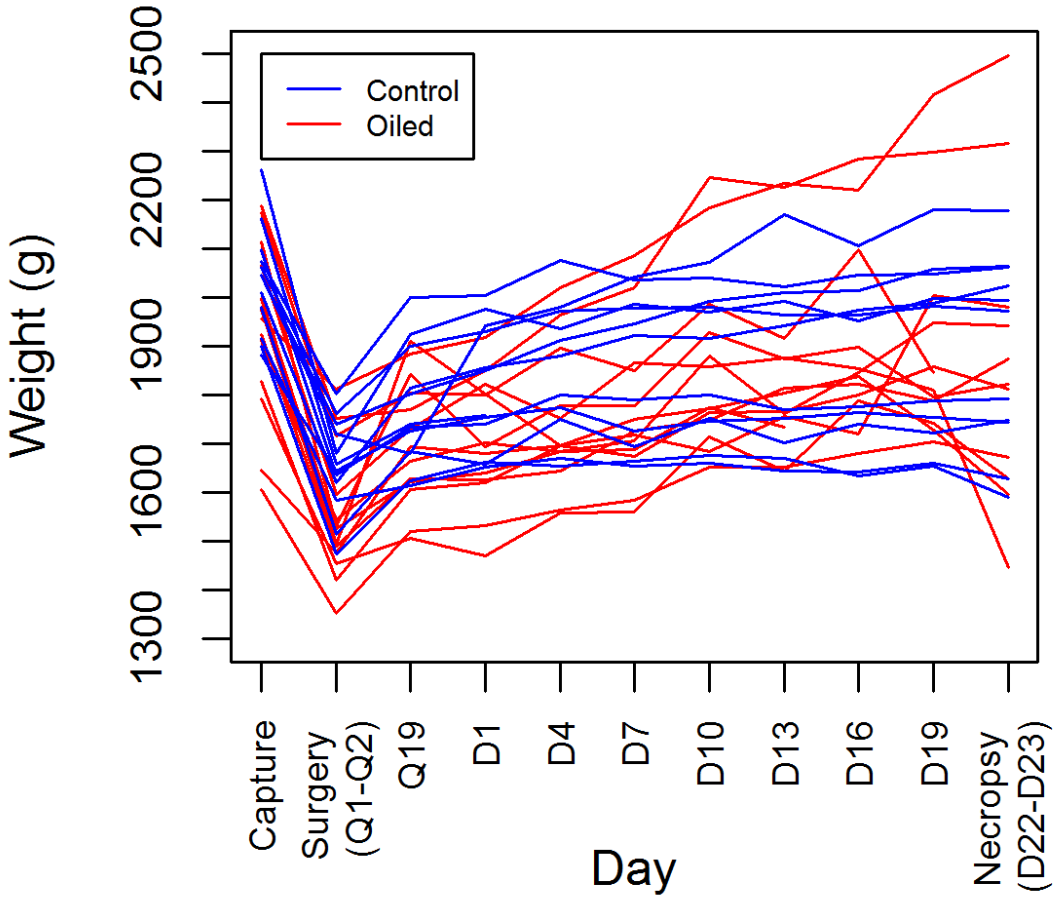


**Figure S7.** Changes in cormorant body mass over time. Median weight gain between surgery and day Q19 was 7.9 grams per day. Median weight gain after day Q19 was 3 grams per day. Note that the x-axis tick marks are not all equal time intervals.

**Table S1.** Summary of studies measuring the effect of oiling on metabolic heat production and thermal conductance in live birds exposed to air or water.

| | Species | Amount of oil | Type of Oil | Air or Water | Temperature (°C) | Time after oiling | Difference (%) | Source |
|---|---|---|---|---|---|---|---|---|
| **Metabolic Heat Production** | Mallard | 12 mL | Crude | Air | -12 | Day of to 14 days | 8-12 | 1 |
| | | 500 mL | Crude | Water | 21 | One day | 49 | 2 |
| | | 2000 mL | Crude | Water | 21 | One day | 161 | 2 |
| | Common Eider | 12.5 mL | Crude | Air | 5 | Day of | 20 | 3 |
| | | 2.5 mL | Crude | Water | 5-8 | Day of | -- | 4 |
| | | 10-15 mL | Crude | Water | 5-8 | Day of | 25-39 | 4,5 |
| | | 12.5 mL | Crude | Water | 5 | Day of | 343-361 | 3,6 |
| | | 30mL | Crude | Water | 5-8 | Day of | 86-110 | 4,5 |
| | | 50 mL | Crude | Water | 5-6 | Day of | 287 | 5 |
| | | 70 mL | Crude | Water | 5-6 | Day of | 390 | 5 |
| **Thermal Conductance** | Mallard | 15 g | Diesel | Air | -25 to 27 | Day of | 84 | 7 |
| | | 15 g | Diesel | Air | -25 to 27 | 3 days | 36 | 7 |
| | | 15 g | Diesel | Air | -25 to 27 | 4 days | 1 | 7 |
| | | 15 g | Diesel | Air | -25 to 27 | 7 days | 10 | 7 |
| | | 50 g | Diesel | Air | -25 to 27 | Day of | 113 | 7 |
| | | 50 g | Diesel | Air | -25 to 27 | 5 days | 45 | 7 |
| | | 200 g | Mineral | Air | -25 to 27 | Day of | 143 | 7 |
| | Black duck | 5 g | Lubricating | Air | -25 to 27 | Day of | 44 | 7 |
| | | 10 g | Lubricating | Air | -25 to 27 | Day of | 64 | 7 |
| | | 20 g | Lubricating | Air | -25 to 27 | Day of | 88 | 7 |
| | Common Eider | 12.5 mL | Crude | Air | 5 | Day of | -3 | 3 |
| | | 12.5mL | Crude | Water | 5 | Day of | 350-375 | 3,6 |
| | Mallard | "Light" | Crude | Air | -2 to 30 | Day of | 13 | 8 |
| | | "Moderate" | Crude | Air | -2 to 30 | Day of | 58 | 8 |
| | | "Heavy" | Crude | Air | -2 to 30 | Day of | 74 | 8 |
| | Scaup | "Light" | Crude | Air | -2 to 30 | Day of | 34 | 8 |
| | | "Moderate" | Crude | Air | -2 to 30 | Day of | 26 | 8 |
| | | "Heavy" | Crude | Air | -2 to 30 | Day of | 98 | 8 |

Sources: [1] Lambert et al., 1982; [2] Jenssen & Ekker, 1989; [3] Jenssen & Ekker, 1990; [4] Jenssen & Ekker, 1991a; [5] Jenssen & Ekker, 1991b; [6] Jenssen & Ekker, 1988; [7] Hartung & Hart, 1967; [8] McEwan & Koelink, 1973

**Table S2**. Schedule for the feeding experiment simulations along with the daily minimum and maximum temperatures in the holding room. Bird masses (± std. error) from each weighing are also shown for reference.

| Experiment Day | Julian Day | Holding Room Tmin (°C) | Holding Room Tmax (°C) | Average Mass Oiled (g) | Average Mass Control (g) | Photo or Oil? | Oil Simulation Stage in Niche Mapper Simulation |
|---|---|---|---|---|---|---|---|
| Capture | -- | -- | -- | 1937±49 | 2037±30 | -- | -- |
| Surgery (Q1/Q2) | 21/22 | -- | -- | 1551±36 | 1653±27 | -- | -- |
| Q19 | 39 | 11.1 | 22.2 | 1707±35 | 1771±34 | FLIR | No oil |
| Q20 | 40 | 11.9 | 23.9 | | | | No oil |
| Q21 | 41 | 11.2 | 22.0 | | | | No oil |
| 1 | 42 | 11.1 | 16.7 | 1705±36 | 1816±36 | OIL | No oil |
| 2 | 43 | 11.2 | 20.9 | | | | Stage 1 |
| 3 | 44 | 10.9 | 15.5 | | | | Stage 1 |
| 4 | 45 | 11.1 | 15.6 | 1742±38 | 1855±39 | FLIR[a]/OIL | Stage 1 |
| 5 | 46 | 10.9 | 22.0 | | | | Stage 1 |
| 6 | 47 | 11.3 | 14.2 | | | | Stage 1 |
| 7 | 48 | 10.4 | 14.2 | 1770±41 | 1858±44 | OIL | Stage 2 |
| 8 | 49 | 10.9 | 14.0 | | | | Stage 2 |
| 9 | 50 | 10.5 | 14.0 | | | | Stage 2 |
| 10 | 51 | 11.1 | 13.7 | 1861±49 | 1874±43 | FLIR[b]/OIL | Stage 2 |
| 11 | 52 | 11.1 | 17.1 | | | | Stage 2 |
| 12 | 53 | 11.3 | 16.3 | | | | Stage 2 |
| 13 | 54 | 10.8 | 16.3 | 1851±50 | 1877±50 | OIL | Stage 3 |
| 14 | 55 | 10.9 | 13.9 | | | | Stage 3 |
| 15 | 56 | 11.2 | 13.5 | | | | Stage 3 |
| 16 | 57 | 11.1 | 13.7 | 1905±53 | 1874±48 | FLIR[c]/OIL | Stage 3 |
| 17 | 58 | 10.8 | 13.9 | | | | Stage 3 |
| 18 | 59 | 10.8 | 19.6 | | | | Stage 3 |
| 19 | 60 | 11.6 | 21.4 | 1912±63 | 1894±52 | | Stage 3 |
| 20 | 61 | 11.6 | 15.1 | | | | Stage 3 |
| 21 | 62 | 11.7 | 14.6 | | | FLIR[c] | Stage 3 |
| Necropsy | 63/64 | -- | -- | 1872±89 | 1891±57 | | -- |

[a] images serve as the basis for Stage 1 oil effects; [b]images serve as the basis for Stage 2 oil effects; [c]images serve as the basis for Stage 3 oil effects.

**Table S3.** Observed and predicted food consumption (grams catfish per day per kg body mass ± std. error) for unoiled (control) and oiled cormorants during the different oiling stages of the experiment from the general linear model treating individual bird identification as a random factor. Two predictions from Niche Mapper are presented: one assuming no change in the insulating air layer from oil exposure when floating on water and one assuming oil exposure allows full penetration of water to the skin.

| | **Observed** | | **Niche Mapper Predictions** | | |
|---|---|---|---|---|---|
| | Control | Oiled | Control | Oiled (no change in insulation in water) | Oiled (water penetration to the skin) |
| Stage 1 | 230±11 | 209±10 | 172±4 | 192±3 | 202±4 |
| Stage 2 | 214±11 | 252±10 | 174±4 | 199±4 | 208±4 |
| Stage 3 | 203±10 | 253±10 | 172±5 | 203±4 | 208±5 |

**Table S4**. Sensitivity analysis of important inputs affecting food consumption calculations. The parameters were changed by ±10% for an example cormorant simulated in the same conditions as the cormorants in the holding room of the experiment. The resulting changes in food consumption requirements are reported.

| **Parameter** | **Change in Food Consumption Requirements** |
|---|---|
| Digestive Efficiency | ±9-11% |
| Food % Dry Matter | ±9-11% |
| Food % Protein | ±6-8% |
| Food % Fat | ±2-3% |
| Food %Ash | ±1% |
| Body Temperature* | ±4-8% |
| Plumage depth* | ±1% |
| Feather element length* | ±0-1% |
| Feather element diameter* | ±0-1% |
| Feather element density* | ±1% |
| *Affects food requirements by altering energetic requirements | |

REFERENCES

Deville, A-S., et al., 2014. Impacts of extreme climatic events on the energetics of long-lived vertebrates: the case of the greater flamingo facing cold spells in the Camargue. J. Exp. Biol. 217, 3700-3707.

Fitzpatrick, M.J., Mathewson, P.D., Porter, W.P.,2015. Validation of a mechanistic model for non-Invasive study of ecological energetics in an endangered wading bird with counter-current heat exchange in its legs. PLoS ONE 10: e0136677

Fort, J., Porter, W.P., Grémillet, D., 2009. Thermodynamic modeling predicts energetic bottleneck for seabirds wintering in the northwest Atlantic. J. Exp. Biol. 212, 2483-2490.

Fort, J., Porter, W.P., Grémillet, D., 2011. Energetic modeling: a comparison of the different approaches uses in seabirds. Comp. Biochem. Phys. A 158, 358-365.

Göktepe, Ö., Hundt, P., Porter, W., Pereira, D., 2012. Comparing bioenergetics models of double-crested cormorant (Phalacrocorax auritus) fish consumption. Waterbirds 35, 91-102.

Hartung, R., Hunt, G.S., 1967. Energy metabolism in oil covered ducks. J. Wildlife Manage. 31, 798.

Lambert, G., Peakall, D.B., Philogène, B.J.R., Engelhardt, F.R., 1982. Effect of oil and oil dispersant mixtures on the basal metabolic rate of ducks. B. Environ. Contam. Tox., 29, 520-524.

Jenssen, B.M., Ekker, M., 1988. A method for evaluating the cleaning of oiled seabirds. Wildlife Soc. B. 16, 213-215

Jenssen, B.M. & Ekker, M. 1990. Effects of plumage oiling on thermoregulation in common eiders residing in air and in water. Transactions of the 19th IUCB Congress, Trondheim, 1989: 281-287.

Jenssen, B.M., Ekker, M., 1989. Rehabilitation of oiled birds: a physiological evaluation of four cleaning agents. Mar. Pollut. Bull. 20, 509-512.

Jenssen, B.M., Ekker, M., 1991a. Effects of plumage contamination with crude oil dispersant mixtures on thermoregulation in Common Eiders and Mallards. Arch. Environ. Con. Tox. 20, 398-403

Jenssen, B.M., Ekker, M. 1991b. Dose dependent effects of plumage-oiling on thermoregulation of Common Eiders Somateria mollissima residing in water. Pp. 579-584 in Sakshaug E, Hopkins CCE, Øritsland NA, (eds): Proceedings of the Pro Mare Symposium on Polar Marine Ecology, Trondheim. 12-16 May 1990.

Kearney, M.R., Porter, W.P.P., Murphy, S.A., 2016. An estimate of the water budget for the endangered night parrot of Australia under recent and future climates. Clim. Change Resp. 3. 14.

Kowalski, G.J., Mitchell, J.W., 1979. An Analytical and Experimental Investigation of the Heat Transfer Mechanisms within Fibrous Media. Trans. ASME Paper No. 79-WA/HT-40: 1-7.

Mathewson, P.D., Porter, W.P., 2013. Simulating polar bear energetics during a seasonal fast using a mechanistic model. PLoS ONE 8, e72863.

McEwan, E.H., Koelink, A.F.C., 1973. The heat production of oiled mallards and scaup. Can. J. Zool. 51: 27-31.

Porter, W.P. & Mitchell, J.W. 2006. Method and system for calculating the spatial-temporal effects of climate and other environmental conditions on animals. http://www.warf.org/technologies.jsp?ipnumber=P01251US

Porter, W.P., Munger, J.C., Stewart, W.E., Budaraju, S., Jaeger, J., 1994. Endotherm energetics: from a scalable individual-based model to ecological applications. Aust. J. Zool. 42, 125-162.

Porter, W., Vakharia, N., Klousie, W., Duffy, D., 2006. Po'ouli landscape bioinformatics models predict energetics, behavior, diets, and distribution on Maui. Integr. Comp. Biol. 46, 1143-1158.

Porter, W.P., Budaraju, S., Stewart, W.E., Ramankutty, N., 2000. Calculating climate effects on birds and mammals: impacts on biodiversity, conservation, population parameters, and global community structure. Am. Zool. 40, 597-630.

# APPENDIX 2: PREDICTED THERMOREGULATORY IMPACTS OF OIL EXPOSURE AT A LANDSCAPE SCALE

## INTRODUCTION

Evaluating spatially and temporally explicit effects of sub-acute oil exposure to wildlife is a logical next step with the oiled cormorant model. Modeling the mechanism (i.e., reduced insulation leading to greater heat transfer to the environment) through which oil exposure imposes thermoregulatory costs provides the ability to confidently make predictions for birds in the wild. Exposure to wind and a wider range of temperatures experienced in natural habitats, including the generally cooler temperatures experienced at higher-latitude breeding grounds would be expected to increase thermoregulatory costs compared to what was observed and

predicted in the controlled feeding experiments described in Chapter 4. In this appendix, we use the oiled cormorant model described and tested in in Chapter 4 to predict the potential seasonal and latitudinal thermoregulatory costs of sub-lethal oil exposure on wintering and breeding cormorants. This is intended to be a demonstration of how Niche Mapper can be a tool to better understand the full impact of oil exposure on wildlife.

## METHODS

To investigate the effect of oil exposure on thermoregulatory costs in wild cormorants, we modeled monthly energy expenditures for perched cormorants weighing 2.1 kg across the eastern United States. During diurnal and crepuscular hours, all body parts were modeled as being exposed to the environment. Based on observations of sleeping cormorants, during nighttime hours, the head was assumed to be tucked under the wings and not exchanging heat with the environment. Similarly, 30 percent of the neck was assumed to be in contact with the torso and not exchanging heat with the environment. Birds were modeled as unoiled and in oil stages 1-3, as described in Chapter 4, for a total of four different oil-exposure scenarios.

We model a perched bird rather than trying to simulate a more realistic activity budget for several reasons. First, modeling the effect of oiling on heat loss while swimming is outside the scope of what we were able to validate against empirical data in terms of how oil exposure would affect water penetration into the plumage (Mathewson et al. 2018). Furthermore, it is reasonable to assume that while diving, the activity metabolism offsets most, if not all, of any increased thermoregulatory costs in the oiled birds. Niche Mapper also does not calculate a heat balance during flight; energetic costs of flight are simply supplied by the user. As with the time

spent diving, it is reasonable to assume that the activity metabolism from flight would offset most or all of any additional thermoregulatory costs from oiling while in flight.

Finally, according to published time-activity budgets, 40-80% of daylight hours are spent perched (King et al. 1995; Duerr et al. 2012) and 10-20% of daylight hours are spent on the water surface. This indicates that the amount of time we will be underestimating potential additional thermoregulatory expenses due to heat loss to water is fairly small. Therefore, this approach allows us to best isolate differences in potential thermoregulatory costs due to oil exposure across most of a cormorant's day when we would not expect activity offsets.

We used Niche Mapper to calculate the total resting metabolic heat production requirements and thermoregulatory costs of a perched cormorant for an average day for each month of the year at all landscape pixels. Thermoregulatory costs were calculated as the difference between the metabolic rate computed by Niche Mapper in its heat balance calculation to be required for the animal to maintain its body temperature and the expected resting metabolic rate for cormorants (Enstipp et al. 2006). Thermoregulatory costs were tracked on a daily basis, as well as separately for diurnal/crepuscular and nocturnal hours.

For the spatially-variable environmental inputs, elevations and 1981-2010 average monthly maximum and minimum temperatures were obtained from the PRISM Climate Group at 4 km resolution (http://www.prism.oregonstate.edu/; Daly *et al.*, 2008). Cloud cover (1960-1990 long-term monthly averages) were obtained from New et al. (2002) at 50 km resolution and resampled to 4 km to match the climate data resolution. We assumed daily wind speeds ranging from 0.1-4 m/s, and relative humidity profiles were calculated assuming a daily maximum of 100% and minimum values calculated based on the daily temperature range assuming constant water mass in the air over 24 hours (Tracy et al. 1980). For temperatures and windspeeds,

maximums were assumed to occur at one hour after solar noon and minimums at sunrise. For relative humidity, the maximum was assumed to occur at sunrise and the minimum one hour after solar noon. Substrate reflectivity was assumed to be 25% in landscape grid cells, a reasonable value for grass, rocks such as granite and sandstone, and bare ground. We used generic soil properties from Kearney et al. (2014a) and Kearney et al. (2014b), who found that these generic values were sufficient to allow predicted soil temperature profiles to match measured profiles.

RESULTS

Predicted daily resting energetic requirements are summarized in Table A1 and shown in Figs. A1 and A2. The increased thermoregulatory costs predicted for oiled birds compared to unoiled birds are summarized in Table A2 and shown in Figs. A3 and A4.

Across their northern breeding range in the Great Lakes and New England states, oiled birds are predicted to have 23% (Stage 1, May) to 83% (Stage 3, April) higher total daily resting energetic requirements than unoiled birds in April and May, as birds are returning to their breeding grounds. In June, July and August, Stage 1 oiling increases predicted daily resting requirements by <12%; Stage 3 oiling increases daily resting requirements by 27-37% in these warmer months. Between April and September, 72-100% of predicted thermoregulatory costs in oiled cormorants at these latitudes were incurred during nocturnal hours (Table S2).

For birds wintering along Gulf Coast states, oiled birds are predicted to have 29% (Stage 1; February) to 79% (Stage 3; December) greater total resting energetic requirements than unoiled birds in the coldest months (Dec-Feb; Table A1). The smallest thermoregulatory increases were predicted in October, when oiling increased daily resting requirements by 14% (Stage 1) to 41% (Stage 3). Between October and March, 86-100% of the thermoregulatory costs

in oiled cormorants wintering in the Gulf States were predicted to be incurred at night (Table A3).

## DISCUSSION

As expected, these simulations did predict greater relative impacts from oiling in these landscape simulations in the colder months of the year than was observed and predicted in the feeding experiments. In these experiments, where the birds were housed in indoor cages and heating laps were used to prevent temperatures from dropping below 50°F, oiling increased daily food consumption up to 20% at the highest oil exposure. These landscape simulations predict that in December through February, birds wintering in Gulf states exposed to oil would have to increase resting heat production by 29-79% in order to maintain their body temperature. Similarly, birds arriving at northern breeding ground states in April, oil exposure is predicted to require 34-83% greater heat production to maintain body temperatures.

The relative difference in actual daily energetic costs between unoiled and oiled birds will be somewhat lower than reported here because during daylight hours, activity will increase total costs similarly for both oiled and unoiled birds and could offset at least some of the predicted daytime thermoregulatory costs. Therefore, the proportion of the total daily energetic requirements that nighttime thermoregulatory costs comprise will be somewhat lower. However, the vast majority of the thermoregulatory costs were predicted to occur at night when the increased heat loss would not typically be offset by heat production from activity. The fact that most of the thermoregulatory costs are incurred at night means that the energetic effect of oiling is magnified because that additional cost will need to be made up for during the day by extra time foraging. Foraging is more energetically demanding than the other diurnal activities the birds would otherwise likely undertake (e.g., resting, preening, wing-spreading).

Although no reduction in body temperature relative to unoiled birds was observed for oiled birds in the feeding experiments, cormorants that are more thermally stressed may reduce body temperatures below the minimum of 40°C allowed in this modeling. This would reduce the thermoregulatory costs from the decreased insulation in oiled cormorants. Conversely, oil exposure also likely increases water penetration so there could be additional daytime thermoregulatory costs during the time spent loafing on the water surface. Furthermore, this modeling only calculates the energetic costs of oiling due to increased thermoregulatory costs; oiling could also make flying or diving more energetically expensive. Further investigation is needed to untangle these various dynamics to understand the true additional energetic costs of oil exposure.

These results also provide insight into the intuitively logical concept that the timing of oil exposure makes a difference regarding the exposure's impact on the bird. Predicted thermoregulatory costs were substantially lower in the warmer months (June, July, August in the breeding states; March, October in the Gulf states). Thus, when evaluating the impact of an oil spill on wildlife, it is important to have an evaluation tool that can take into account the ambient weather conditions.

Such information can provide valuable insight into how both large and chronic oil spills are affecting wildlife by quantifying the extent to which thermoregulatory costs are diverting resources away from other important life processes like reproduction and building energy stores for migration. For example, these results could be integrated into a time-budget model such as that from King et al. (1995) or Seefelt & Gillingham (2008) to translate increased thermoregulatory costs into increased foraging and travel time between roosting and foraging areas. This could potentially have an impact on hatching success if the adults need to be away

more frequently to accommodate the increased food requirements. Information on increased thermoregulatory costs could also be combined with empirical data on fat deposition and increases in pectoral muscle and gut mass in preparation for migration. If such physiological preparation is delayed, so too would arrival in the breeding grounds, potentially affecting fitness.

REFERENCES

Daly C, Halbleib M, Smith JI *et al.* 2008. Physiographically sensitive mapping of climatological temperature and precipitation across the conterminous United States. International Journal of Climatology 28:2031-2064.

Duerr AE, Capen DE, Donovan TM. 2012. Energetic considerations for managing double-crested cormorants on Lake Champlain. Journal of Great Lakes Research 38: 131-140.

Enstipp MR, Gremillet D, Jones DR. 2006. The effects of depth, temperature and food ingestion on the foraging energetics of a diving endotherm, the double-crested cormorant (*Phalacrocorax auritis*). The Journal of Experimental Biology 209: 845-859.

Grémillet D, Chauvin C, Wilson RP, Le Maho Y, Wanless S. 2005. Unusual feather structure allows partial plumage wettability in diving great cormorants *Phalacrocorax carbo*. Journal of Avian Biology 36: 57-63.

Kearney MR, Isaac AP, Porter WP. 2014a. microclim: Global estimates of hourly microclimate based on long-term monthly climate averages. Scientific Data*,* 1.

Kearney MR, Shamakhy A, Tingley R, Karoly DJ, Hoffmann AA, Briggs PR, Porter WP. 2014b. Microclimate modelling at macro scales: a test of a general microclimate model integrated with gridded continental-scale soil and weather data. Methods in Ecology and Evolution 5: 273-286.

King DT, Glahn JF, Anderws KJ. 1995. Daily activity budgets and movements of winter roosting double-crested cormorants determined by biotelemetry in the Delta region of Mississippi. Colonial Waterbirds 18: 152-157.

New M, Lister D, Hulme M, Makin I. 2002. A high-resolution data set of surface climate of global land areas. Climate Research 21: 1-25.

Seefelt NE, Gillingham JC. 2008. Bioenergetis and prey consumption of breeding double-crested cormorants in the Beaver Archipelago, Northern Lake Michigan. Journal of Great Lakes Research 34: 122-133.

Tracy CR, W.R. Welch WR, Porter WP. 1980. Properties of air: A manual for students in biophysical ecology. University of Wisconsin Laboratory of Biophysical Ecology, Technical Report #1 (3rd Edition).

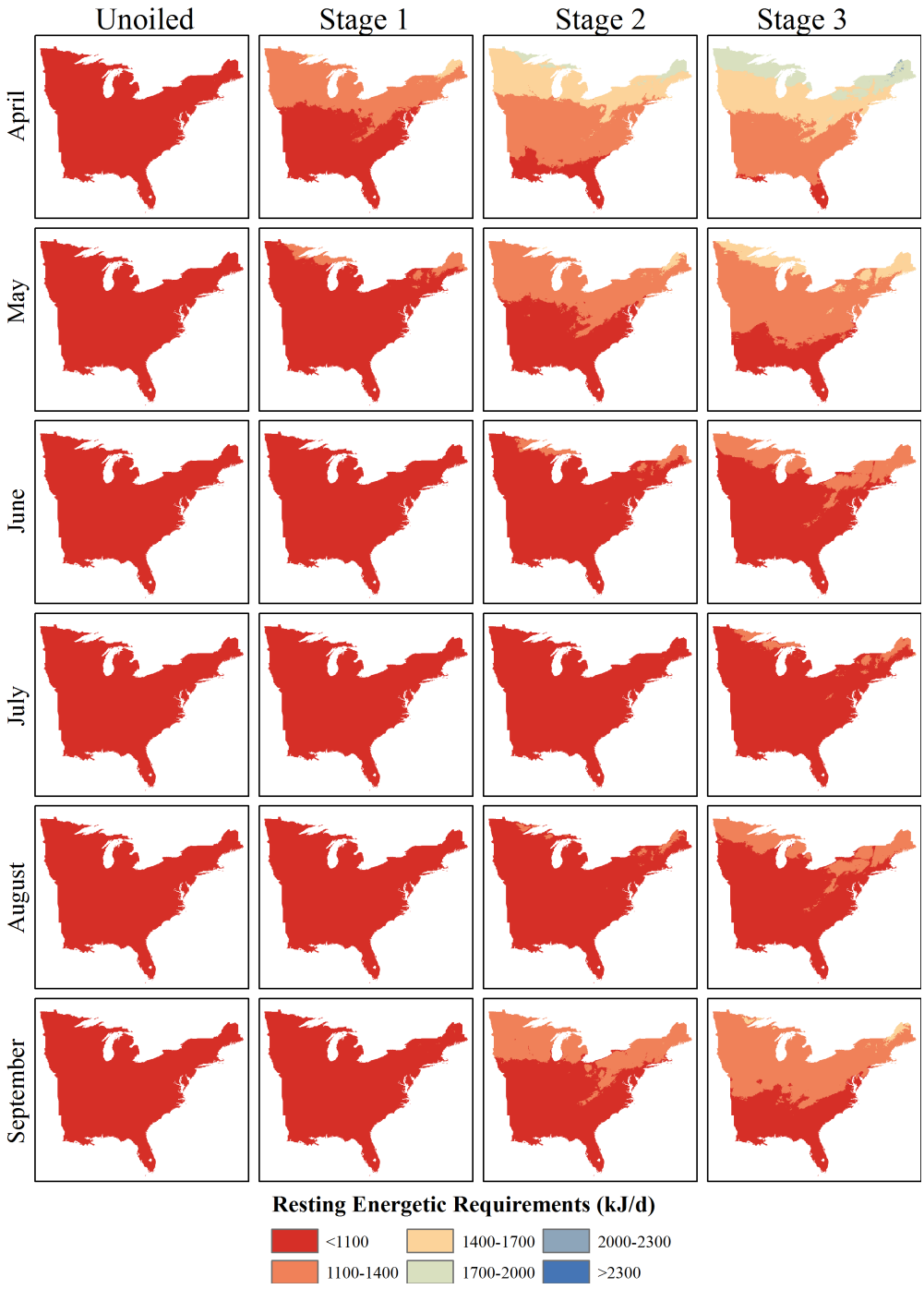


**Figure A1.** Resting energetic requirements (kJ/d) predicted by Niche Mapper for cormorants in warmer months (April-September) across the eastern United States. Results are shown for an unoiled bird and birds in simulated Stage 1 through 3 oil exposure. For reference, the expected daily resting metabolic rate is 833 kJ/d.

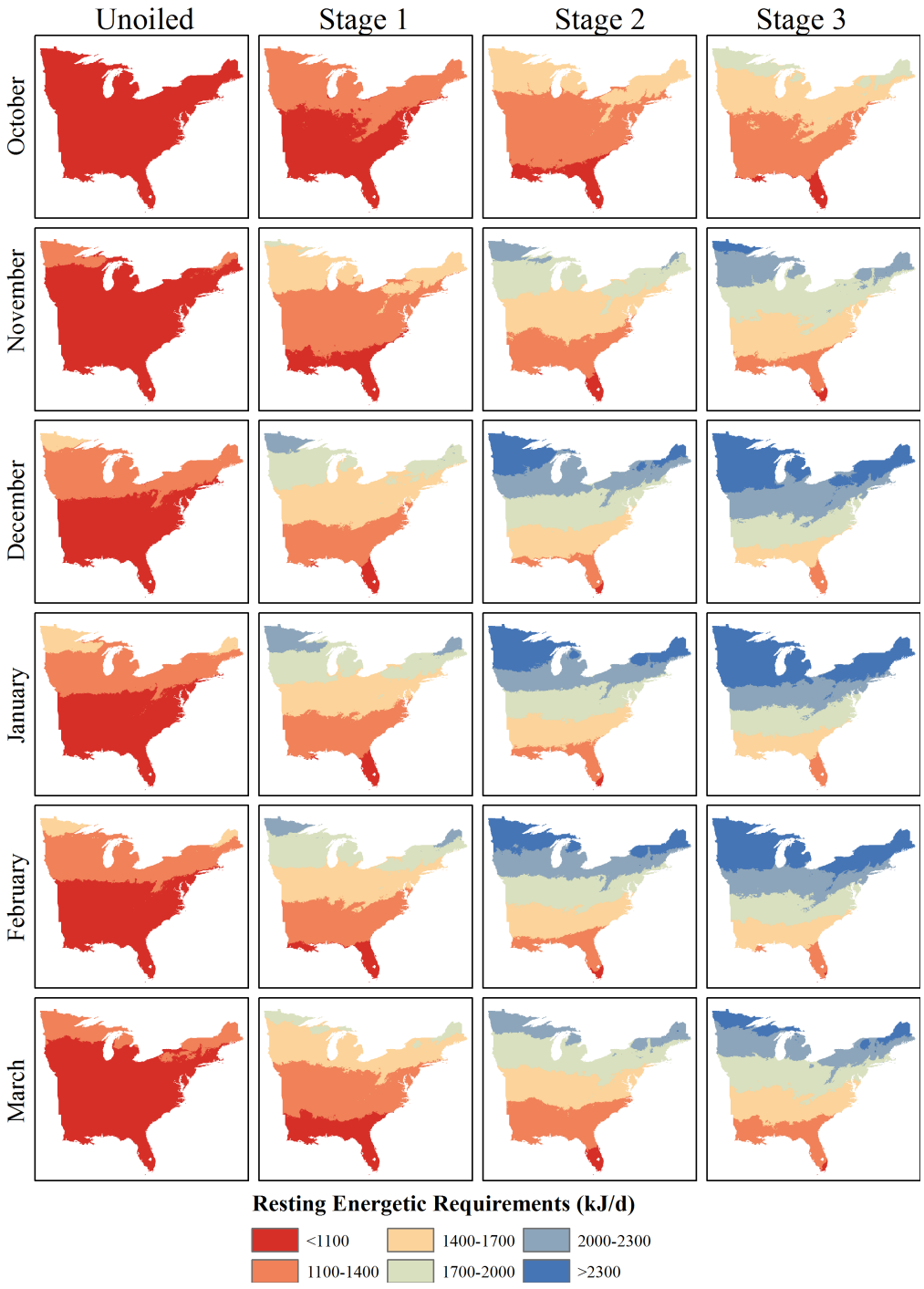


**Figure A2.** Resting energetic requirements (kJ/d) predicted by Niche Mapper for cormorants in cooler months (October-March) across the eastern United States. Results are shown for an unoiled bird and birds in simulated Stage 1 through 3 oil exposure. For reference, the expected daily resting metabolic rate is 833 kJ/d.

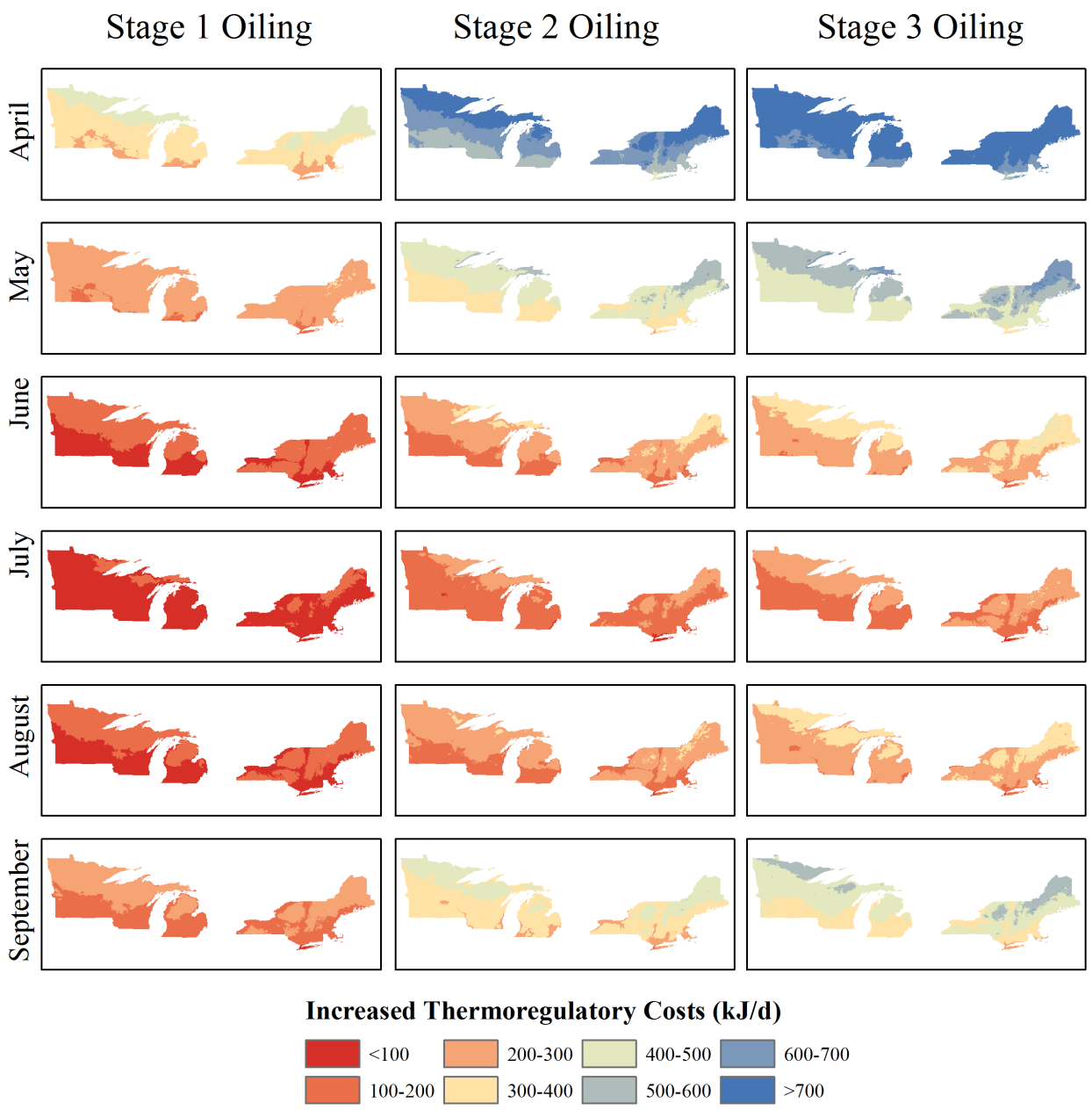


**Figure A3.** Additional thermoregulatory costs predicted by Niche Mapper for cormorants simulated at different oil exposure levels in April-September across their northern breeding range in the United States. For reference, the expected daily resting metabolic rate is 833 kJ/d.

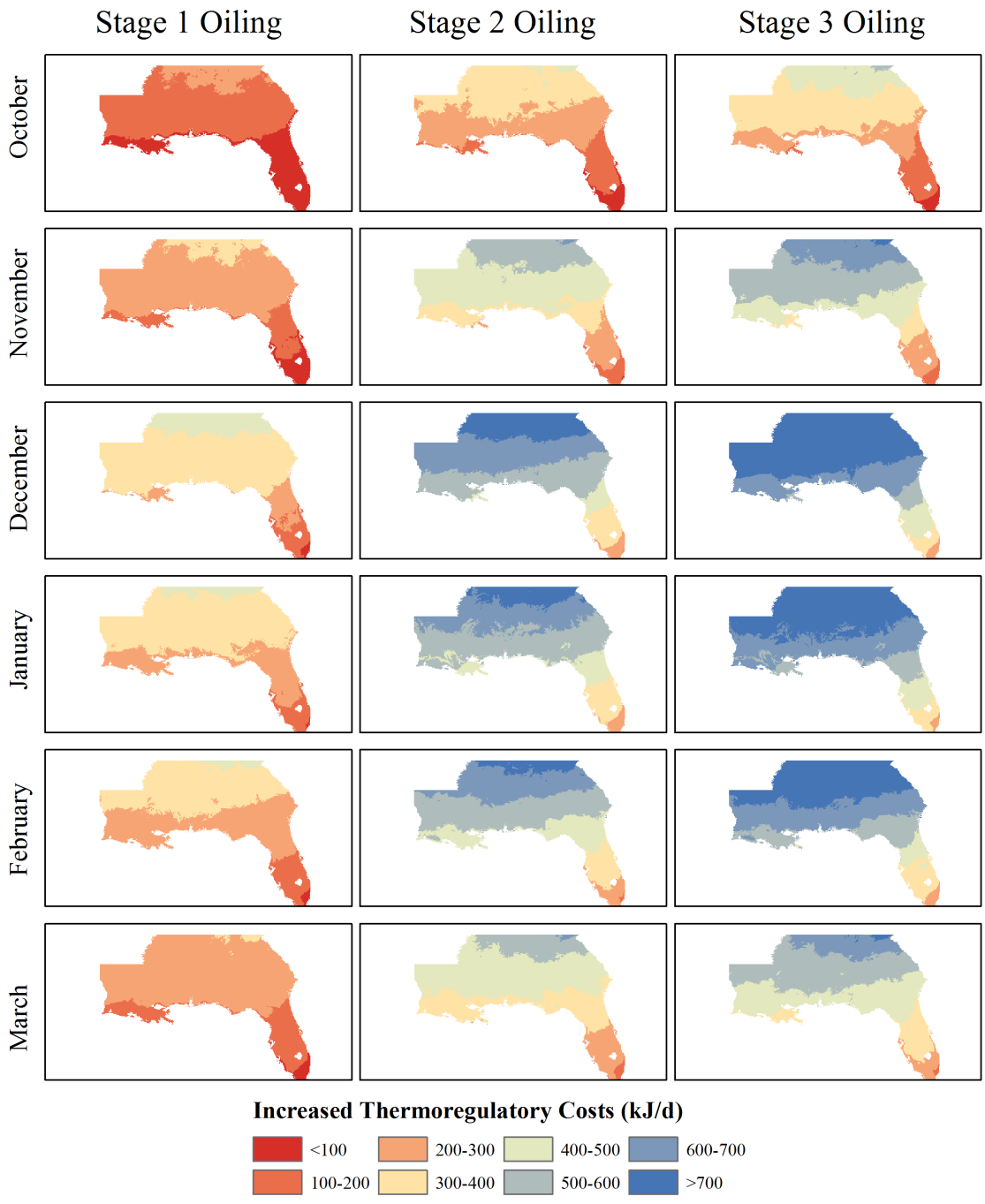


**Figure A4.** Additional thermoregulatory costs predicted by Niche Mapper for cormorants simulated at different oil exposure levels wintering along the Gulf Coast in October through March. For reference, the expected daily resting metabolic rate is 833 kJ/d.

**Table A1.** Predicted total resting energetic costs (kJ/d) for simulated 2.1 kg cormorants in different stages of oiling in selected summer breeding range states and Gulf Coast wintering states. The target resting metabolic rate was 833 kJ/d so any values within 2.5% of that target (812-854) indicate no predicted thermoregulatory costs.

| | Month | No Oil | Stage 1 Oil | Stage 2 Oil | Stage 3 Oil |
|---|---|---|---|---|---|
| **Breeding Range States** | April | 956±31 | 1278±78 | 1583±100 | 1750±110 |
| | May | 870±19 | 1069±40 | 1260±72 | 1383±85 |
| | June | 833±4 | 932±31 | 1053±47 | 1141±55 |
| | July | 831±2 | 884±25 | 981±38 | 1058±44 |
| | August | 833±2 | 922±29 | 1042±41 | 1126±46 |
| | September | 848±12 | 1020±35 | 1185±53 | 1295±64 |
| **Wintering Range States** | October | 835±4 | 948±61 | 1086±81 | 1179±92 |
| | November | 859±21 | 1064±76 | 1254±109 | 1376±127 |
| | December | 908±40 | 1204±104 | 1472±154 | 1628±177 |
| | January | 915±41 | 1188±95 | 1442±147 | 1598±170 |
| | February | 897±36 | 1157±94 | 1406±145 | 1553±166 |
| | March | 857±20 | 1057±62 | 1240±93 | 1358±110 |

**Table A2.** Predicted thermoregulatory costs (kJ/d) for simulated 2.1 kg cormorants in different stages of oiling in selected summer breeding range states and Gulf Coast wintering states. Percent of costs incurred during nighttime hours is noted in parentheses. Thermoregulatory costs are calculated as target resting metabolic rate (833 kJ/d) subtracted from total predicted resting metabolic rate.

| | Month | No Oil | Stage 1 Oil | Stage 2 Oil | Stage 3 Oil |
|---|---|---|---|---|---|
| **Breeding Ground States** | April | 102±31 (99%) | 465±78 (83%) | 770±100 (73%) | 896±110 (72%) |
| | May | 18±18 (100%) | 256±40 (100%) | 447±72 (95%) | 529±85 (92%) |
| | June | 0 (NA) | 119±31 (100%) | 240±47 (100%) | 288±55 (99%) |
| | July | 0 (NA) | 71±25 (100%) | 168±38 (100%) | 205±44 (100%) |
| | August | 0 (NA) | 109±29 (100%) | 229±41 (100%) | 273±46 (100%) |
| | September | 3±5 (100%) | 207±35 (100%) | 372±53 (99%) | 441±64 (97%) |
| **Wintering Ground States** | October | 0 (NA) | 135±59 (100%) | 273±81 (100% | 325±92 (100%) |
| | November | 11±16 (100%) | 251±76 (100%) | 441±109 (98%) | 522±127 (97%) |
| | December | 56±37 (100%) | 391±104 (98%) | 659±154 (92%) | 774±177 (90%) |
| | January | 63±38 (100%) | 375±95 (97%) | 629±147 (89%) | 745±170 (86%) |
| | February | 46±33 (100%) | 344±94 (97%) | 593±145 (88%) | 699±166 (86%) |
| | March | 9±15 (100%) | 244±62 (100%) | 427±93 (99%) | 505±110 (98%) |

ADDENDUM: ABSTRACTS FROM ADDITIONAL PUBLICATIONS

**Wang Y, Porter W, Mathewson PD, Miller PA, Graham R, Williams JW. 2018. Mechanistic modeling of environmental drivers of woolly mammoth carrying capacity declines on St. Paul Island. Ecology 99: 2721-2730.**

On St. Paul Island, a remnant of the Bering Land Bridge, woolly mammoths persisted until 5,600 yr BP with no known predators or competitors, providing a natural system for studying hypothesized environmental drivers of extinction. These include overheating due to rising temperatures, starvation, and drought. Here, we test these hypotheses using Niche Mapper and LPJ-GUESS to mechanistically estimate mammoth metabolic rates and dietary and freshwater requirements and, from these, estimate variations in island carrying capacity on St. Paul for the last 17,000 yr. Population carrying capacity may have been several hundred individuals at the time of initial isolation from the mainland. Adult mammoths could have fasted for two to three months, indicating a necessary ability to access snow-buried forage. During the Holocene, vegetation net primary productivity increased, but shrinking island area overrode increased net primary productivity (NPP), lowering carrying capacity to ~100 individuals. NPP and freshwater availability alternated as critical limiting factors for this island population during the environmental changes of the late Pleistocene and Holocene. Only two or three individuals could have been sustained by the freshwater surplus in crater lakes (up to 18 individuals under the most optimistic parameter sensitivity experiments), suggesting that the St. Paul mammoth population was highly dependent on coastal freshwater sources. The simulations are consistent with the available proxy data, while highlighting the need to retrieve new paleohydrological proxy records from the coastal lagoons to test model predictions. More broadly, these findings

reinforce the vulnerability of island megaherbivore populations to resource limitation and extinction.

**Amélineau F, Fort J, Mathewson PD, Speirs DC, Courbin N, Perret S, Porter WP, Wilson RJ, Grémillet D. 2018. Energyscapes and prey fields shape a North Atlantic seabird wintering hotspot under climate change. Royal Society Open Science 5: 171883**

There is an urgent need for a better understanding of animal migratory ecology under the influence of climate change. Most current analyses require long-term monitoring of populations on the move, and shorter-term approaches are needed. Here, we analysed the ecological drivers of seabird migration within the framework of the energyscape concept, which we defined as the variations in the energy requirements of an organism across geographical space as a function of environmental conditions. We compared the winter location of seabirds with their modelled energy requirements and prey fields throughout the North Atlantic. Across six winters, we tracked the migration of 94 little auks (*Alle alle*), a key sentinel Arctic species, between their East Greenland breeding site and wintering areas off Newfoundland. Winter energyscapes were modelled with Niche Mapper™, a mechanistic tool which takes into account local climate and bird ecophysiology. Subsequently, we used a resource selection function to explain seabird distributions through modelled energyscapes and winter surface distribution of one of their main prey, *Calanus finmarchicus*. Finally, future energyscapes were calculated according to IPCC climate change scenarios. We found that little auks targeted areas with high prey densities and moderately elevated energyscapes. Predicted energyscapes for 2050 and 2095 showed a decrease in winter energy requirements under the high emission scenario, which may be beneficial if prey

availability is maintained. Overall, our study demonstrates the great potential of the energyscape concept for the study of animal spatial ecology, in particular in the context of global change.

**Zhang Y, Mathewson PD, Zhang Q, Porter WP, Ran J. 2018. An ecophysiological perspective on likely giant panda habitat responses to climate change. Global Change Biology 24: 1804-1816.**

Threatened and endangered species are more vulnerable to climate change due to small population and specific geographical distribution. Therefore, identifying and incorporating the biological processes underlying a species' adaptation to its environment are important for determining whether they can persist in situ. Correlative models are widely used to predict species' distribution changes, but generally fail to capture the buffering capacity of organisms. Giant pandas (*Ailuropoda melanoleuca*) live in topographically complex mountains and are known to avoid heat stress. Although many studies have found that climate change will lead to severe habitat loss and threaten previous conservation efforts, the mechanisms underlying panda's responses to climate change have not been explored. Here, we present a case study in Daxiangling Mountains, one of the six Mountain Systems that giant panda distributes. We used a mechanistic model, Niche Mapper, to explore what are likely panda habitat response to climate change taking physiological, behavioral and ecological responses into account, through which we map panda's climatic suitable activity area (SAA) for the first time. We combined SAA with bamboo forest distribution to yield highly suitable habitat (HSH) and seasonal suitable habitat (SSH), and their temporal dynamics under climate change were predicted. In general, SAA in the hottest month (July) would reduce 11.7%–52.2% by 2070, which is more moderate than predicted bamboo habitat loss (45.6%–86.9%). Limited by the availability of bamboo and forest,

panda's suitable climate space loss increases, and only 15.5%–68.8% of current HSH would remain in 2070. Our method of mechanistic modeling can help to distinguish whether habitat loss is caused by thermal environmental deterioration or food loss under climate change. Furthermore, mechanistic models can produce robust predictions by incorporating ecophysiological feedbacks and minimizing extrapolation into novel environments. We suggest that a mechanistic approach should be incorporated into distribution predictions and conservation planning.

**Fitzpatrick, M., P. Mathewson, and W. Porter. 2018. Ecological Energetics of Whooping Cranes in the Eastern Migratory Population. Pages 239-257 *in* J. French, S. Converse, and J. Austin, editors. Whooping Cranes: Biology and Conservation. Academic Press, San Diego, CA.**

This chapter focuses on the ecological energetics of Whooping Cranes in the Eastern Migratory Population (EMP) (French et al., Chapter 1, this volume). Energetics refers to the energy costs of the various behavioral and physiological aspects of survival and reproduction (Tomlinson et al., 2014) and the ways that animals meet those costs. Ecological energetics refers to the study of energetics within the context of environmental constraints (Tomlinson et al., 2014). In this chapter, we review ecological energetics in EMP Whooping Cranes and provide a new analysis of energy requirements of cranes in the EMP across their wintering range.

**Long RA, Bowyer RT, Porter WP, Mathewson P, Monte KL, Findholt SL, Dick B, Kie JG. 2015. Linking habitat selection to fitness-related traits in herbivores: the role of the energy landscape. Oecologia 181: 709-720.**

Animals may partially overcome environmental constraints on fitness by behaviorally adjusting their exposure to costs and supplies of energy. Few studies, however, have linked spatiotemporal variation in the energy landscape to behaviorally mediated measures of performance that ostensibly influence individual fitness. We hypothesized that strength of selection by North American elk (Cervus elaphus) for areas that reduced costs of thermoregulation and activity, and increased access to high-quality forage, would influence four energetically mediated traits related to fitness: birth mass of young, nutritional condition of adult females at the onset of winter, change in nutritional condition of females between spring and winter, and neonatal survival. We used a biophysical model to map spatiotemporally explicit costs of thermoregulation and activity experienced by elk in a heterogeneous landscape. We then combined model predictions with data on forage characteristics, animal locations, nutritional condition, and mass and survival of young to evaluate behaviorally mediated effects of the energy landscape on fitness-related traits. During spring, when high-quality forage was abundant, female elk that consistently selected low-cost areas before parturition gave birth to larger young than less-selective individuals, and birth mass had a strong, positive influence on probability of survival. As forage quality declined during autumn, however, lactating females that consistently selected the highest quality forage available accrued more fat and entered winter in better condition than less-selective individuals. Results of our study highlight the importance of understanding the dynamic nature of energy landscapes experienced by free-ranging animals.

**Fitzpatrick MJ, Mathewson PD, Porter WP. 2015. Validation of a Mechanistic Model for Non-Invasive Study of Ecological Energetics in an Endangered Wading Bird with Counter-Current Heat Exchange in its Legs. PLoS ONE 10: e0136677. doi:10.1371/journal.pone.0136677**

Mechanistic models provide a powerful, minimally invasive tool for gaining a deeper understanding of the ecology of animals across geographic space and time. In this paper, we modified and validated the accuracy of the mechanistic model Niche Mapper for simulating heat exchanges of animals with counter-current heat exchange mechanisms in their legs and animals that wade in water. We then used Niche Mapper to explore the effects of wading and counter-current heat exchange on the energy expenditures of Whooping Cranes, a long-legged wading bird. We validated model accuracy against the energy expenditure of two captive Whooping Cranes measured using the doubly-labeled water method and time energy budgets. Energy expenditure values modeled by Niche Mapper were similar to values measured by the doubly-labeled water method and values estimated from time-energy budgets. Future studies will be able to use Niche Mapper as a non-invasive tool to explore energy-based limits to the fundamental niche of Whooping Cranes and apply this knowledge to management decisions. Basic questions about the importance of counter-current exchange and wading to animal physiological tolerances can also now be explored with the model.

**Moyer-Horner L, Mathewson PD, Kearney MR, Porter WP. 2015. Modeling behavioral thermoregulation in a climate change sentinel. Ecology and Evolution 5: 5810-5822.**

When possible, many species will shift in elevation or latitude in response to rising temperatures. However, before such shifts occur, individuals will first tolerate environmental change and then modify their behavior to maintain heat balance. Behavioral thermoregulation allows animals a range of climatic tolerances and makes predicting geographic responses under future warming scenarios challenging. Because behavioral modification may reduce an individual's fecundity by, for example, limiting foraging time and thus caloric intake, we must consider the range of behavioral options available for thermoregulation to accurately predict climate change impacts on individual species. To date, few studies have identified mechanistic links between an organism's daily activities and the need to thermoregulate. We used a biophysical model, Niche Mapper, to mechanistically model microclimate conditions and thermoregulatory behavior for a temperature-sensitive mammal, the American pika (*Ochotona princeps*). Niche Mapper accurately simulated microclimate conditions, as well as empirical metabolic chamber data for a range of fur properties, animal sizes, and environmental parameters. Niche Mapper predicted pikas would be behaviorally constrained because of the need to thermoregulate during the hottest times of the day. We also showed that pikas at low elevations could receive energetic benefits by being smaller in size and maintaining summer pelage during longer stretches of the active season under a future warming scenario. We observed pika behavior for 288 h in Glacier National Park, Montana, and thermally characterized their rocky, montane environment. We found that pikas were most active when temperatures were cooler, and at sites characterized by high elevations and north-facing slopes. Pikas became significantly less active across a suite of behaviors in the field when temperatures surpassed 20°C, which supported a metabolic threshold predicted by

Niche Mapper. In general, mechanistic predictions and empirical observations were congruent. This research is unique in providing both an empirical and mechanistic description of the effects of temperature on a mammalian sentinel of climate change, the American pika. Our results suggest that previously underinvestigated characteristics, specifically fur properties and body size, may play critical roles in pika populations' response to climate change. We also demonstrate the potential importance of considering behavioral thermoregulation and microclimate variability when predicting animal responses to climate change.

**Deville, A.S., et al. 2014. Impacts of extreme climatic events on the energetics of long-lived vertebrates: The case of the Greater Flamingo facing cold spells in the Camargue. Journal of Experimental Biology 217: 3700-3707**

Most studies analyzing the effects of global warming on wild populations focus on gradual temperature changes, yet it is also important to understand the impact of extreme climatic events. Here we studied the effect of two cold spells (January 1985 and February 2012) on the energetics of greater flamingos (*Phoenicopterus roseus*) in the Camargue (southern France). To understand the cause of observed flamingo mass mortalities, we first assessed the energy stores of flamingos found dead in February 2012, and compared them with those found in other bird species exposed to cold spells and/or fasting. Second, we evaluated the monthly energy requirements of flamingos across 1980-2012 using the mechanistic model Niche Mapper. Our results show that the body lipids of flamingos found dead in 2012 corresponded to 2.6±0.3% of total body mass, which is close to results found in woodcocks (*Scolopax rusticola*) that died from starvation during a cold spell (1.7±0.1%), and much lower than in woodcocks which were fed throughout this same cold spell (13.0±2%). Further, Niche Mapper predicted that flamingo energy

requirements were highest (+6-7%) during the 1985 and 2012 cold spells compared with 'normal' winters. This increase was primarily driven by cold air temperatures. Overall, our findings strongly suggest that flamingos starved to death during both cold spells. This study demonstrates the relevance of using mechanistic energetics modelling and body condition analyses to understand and predict the impact of extreme climatic events on animal energy balance and winter survival probabilities.

**Long RA, Bowyer RT, Porter WP, Mathewson PD, Monteith KL, Kie JG. 2014. Behavior and nutritional condition buffer a large-bodied endotherm against direct and indirect effects of climate. Ecological Monographs 84: 513-532.**

Temporal changes in net energy balance of animals strongly influence fitness; consequently, natural selection should favor behaviors that increase net energy balance by buffering individuals against negative effects of environmental variation. The relative importance of behavioral responses to climate-induced variation in costs vs. supplies of energy, however, is uncertain, as is the degree to which such responses are mediated by current stores of energy. We evaluated relationships among behavior, nutritional condition (i.e., energy state), and spatiotemporal variation in costs vs. supplies of energy available to a large-bodied endotherm, the North American elk (*Cervus elaphus*), occupying two ecosystems with contrasting climates and energy landscapes: a temperate, montane forest and an arid, high-elevation desert. We hypothesized that during spring through autumn, behavioral responses to the energy landscape would be both context dependent (i.e., would vary as a function of the contrasting environmental conditions experienced by elk in the forest vs. the desert), and state dependent (i.e., would vary as a function of the energy balance of an individual). We tested several predictions derived from that

hypothesis by combining output from a biophysical model of the thermal environment with data on forage quality, animal locations, and nutritional condition of individuals. At the population level, elk in the desert selected areas that reduced costs of thermoregulation over those that provided the highest-quality forage. In the forest, however, costs imposed by the thermal environment were less pronounced, and elk selected areas that increased access to high-quality forage over those that reduced costs of thermoregulation. At the individual level, nutritional condition did not influence strength of selection for low-cost areas or high-quality forage among elk in the forest. In the desert, however, strength of selection for low-cost areas (but not forage quality) was state dependent; individuals in the poorest condition at the end of winter showed the strongest selection for areas that reduced costs of thermoregulation during spring and summer, and also expended the least amount of energy on locomotion. Our results highlight the importance of understanding the roles of behavior and nutritional condition in buffering endotherms against direct and indirect effects of climate on fitness.